



NUI MAYNOOTH
Ollscoil na hÉireann M^o Nuad

A Polypyrrole / Sulfonated Calixarene Modified Electrode for the Electrochemical Detection of Dopamine

by Richard Doyle

A major thesis presented as full requirement for the
degree of

Doctor of Philosophy in Chemistry

National University of Ireland, Maynooth

Department of Chemistry,
Faculty of Science & Engineering

28th February 2011

Head of Department:
Prof John Lowry

Supervisors:
Dr Denise Rooney & Prof. Carmel Breslin

Table of Contents

Acknowledgements	i
------------------------	---

Abstract	ii
----------------	----

(Chapter 1) Introduction: A Polypyrrole / Sulfonated Calixarene Modified Electrode for the Electrochemical Detection of Dopamine

(1.1) Introduction.....	1
(1.2) Conducting Polypyrrole	2
(1.2.1) Structural Properties of Polypyrrole.....	2
(1.2.2) Electronic Properties of Polypyrrole.....	4
(1.2.3) Doping and Redox Behaviour of Polypyrrole.....	6
(1.2.4) Charge Transport in Polypyrrole.....	8
(1.2.5) Synthesis of Polypyrrole	9
(1.2.6) Factors Affecting the Electropolymerisation	12
(1.2.7) Polypyrrole Doped with Sulfonated Calixarenes	14
(1.3) Sulfonated Calixarenes	15
(1.3.1) Structural Properties of Sulfonated Calixarenes	15
(1.3.2) Electrochemical Activity of Sulfonated Calixarenes	17
(1.3.3) Molecular Recognition Properties of Sulfonated Calixarenes	19
(1.3.4) Inclusion of Dopamine into Sulfonated Calixarenes.....	21
(1.4) Dopamine Sensors	22
(1.4.1)The Electrochemical Detection of DA.....	23
(1.4.2) Polymer Modified Electrodes	27
(1.4.3)Applications of Calixarenes in DA Sensors.....	29
(1.5) Bibliography.....	31

(Chapter 2) Experimental: Materials, Methods and Techniques

(2.1) Introduction.....	43
(2.2) Chemicals and Synthesis.....	44
(2.2.1) Synthesis of <i>p</i> -Sulfonatocalix[4]arene (C4S).....	44
(2.3) Experimental Setup	49
(2.3.1) Apparatus	49
(2.3.2) The Electrochemical Cell.....	50
(2.3.3) Electrode Materials and Preparation	51
(2.4) Experimental Procedure	53
(2.4.1) Electrosynthesis of the PPy-C4S Film.....	53
(2.4.2) Characterisation of the PPy-C4S Film	53
(2.4.2i) Cyclic Voltammetry.....	53
(2.4.2ii) Electrochemical Impedance Spectroscopy (EIS).....	54
(2.4.2iii) Scanning Electron Microscopy (SEM) and Energy Dispersive X-Ray Spectroscopy (EDX).....	54
(2.4.2iv) Thickness Measurements for the PPy-C4S Film.....	54

(2.4.3) The Detection of DA at the PPy-C4S Modified Electrode	55
(2.4.3i) Cyclic Voltammetry	55
(2.4.3ii) Constant Potential Amperometry	57
(2.4.4) Interferent Studies.....	57
(2.4.5) NMR Complexation Studies.....	58
(2.4.5i) Job’s Method	58
(2.4.5ii) NMR Titration	59
(2.4.5iii) Rotating-Frame Nuclear Overhauser Effect (ROE) Spectroscopy	59
(2.5) Experimental Techniques	60
(2.5.1) Electrochemistry	60
(2.5.1i) Constant Potential Amperometry	60
(2.5.1ii) Cyclic Voltammetry.....	63
(2.5.1iii) Rotating Disk Voltammetry (RDV)	66
(2.5.1iv) Electrochemical Impedance Spectroscopy (EIS).....	68
(2.5.2) Surface Analysis	72
(2.5.2i) Scanning Electron Microscopy (SEM)	72
(2.5.2ii) Energy Dispersive X-Ray Spectroscopy (EDX)	75
(2.5.3) Nuclear Magnetic Resonance (NMR).....	76
(2.5.3i) Job’s Method	77
(2.5.3ii) NMR Titration	78
(2.5.3iii) Rotating-Frame Nuclear Overhauser Effect (ROE) Spectroscopy	80
(2.6) Bibliography.....	85

(Chapter 3) Sensor Characterisation: A Study of the Physical and Electrochemical Properties of the PPy-C4S Film

(3.1) Introduction.....	88
(3.2) Results and Discussion	90
(3.2.1) Physical Characterisation of the PPy-C4S Film	90
(3.2.1.1) Scanning Electron Microscopy (SEM)	90
(3.2.1.2) Energy Dispersive X-Ray Spectroscopy (EDX)	91
(3.2.1.3) Thickness of the PPy-C4S Film	92
(3.2.2) Electrochemical Characterisation of the PPy-C4S Film	94
(3.2.2.1) Cyclic Voltammetry.....	95
(3.2.2.1i) Oxidation and Reduction Properties of the PPy-C4S Film.....	95
(3.2.2.1ii) Capacitance Measurements for the PPy-C4S Film	97
(3.2.2.1iii) Novel Redox Activity of the PPy-C4S Film – the Generation of Calixquinones within the Polymer Film.....	99
(3.2.2.2) Electrochemical Impedance Spectroscopy (EIS).....	108
(3.2.2.2i) General EIS Discussion for the PPy-C4S Film	108
(3.2.2.2ii) Complex Plane Impedance Analysis of PPy-C4S Films in the Oxidised State	111
(3.2.2.2iii) Complex Plane Impedance Analysis of PPy-C4S Films in the Reduced State ...	117
(3.3) Conclusion	122
(3.4) Bibliography.....	124

(Chapter 4) Sensor Application: Optimising the PPy-C4S Film for the Electrochemical Detection of Dopamine

(4.1) Introduction.....	129
(4.2) Results and Discussion	131
(4.2.1) DA Oxidation at Bare Electrodes	131
(4.2.2) Preliminary Studies on the Interaction between C4S and DA in Solution.....	133
(4.2.3) DA Oxidation at Polypyrrole Modified Electrodes.....	135
(4.2.4) Optimising the DA Signal at the PPy-C4S Modified Electrode	138
(4.2.4i) The Concentration of Pyrrole	138
(4.2.4ii) The Concentration of <i>p</i> -Sulfonatocalix[4]arene (C4S).....	140
(4.2.4iii) The Potential Applied for the Electrosynthesis of the PPy-C4S Film	143
(4.2.4iv) Electropolymerisation to a Set Charge	147
(4.2.4v) The Electrochemical Window	150
(4.2.4vi) The Effect of Scan Rate on the DA Signal.....	154
(4.2.4vii) The Effect of pH	161
(4.2.4viii) Supporting Electrolyte	165
(4.2.4ix) The Influence of Oxygen Levels	169
(4.2.4x) The Optimum Conditions for the Detection of DA.....	170
(4.2.5) Dopamine Calibration Curves.....	171
(4.2.5i) Cyclic Voltammetry.....	171
(4.2.5ii) Constant Potential Amperometry	174
(4.3) Conclusion	178
(4.4) Bibliography.....	179

(Chapter 5) Mode of Sensing: Studies on the Selectivity of the Sensor and the Interaction of Dopamine with the PPy-C4S Film

(5.1) Introduction.....	183
(5.2) Results and Discussion	185
(5.2.1)The Interaction of DA at the PPy-C4S Film	185
(5.2.1i) Evidence for the Adsorption of DA at the PPy-C4S Film	185
(5.2.1ii) Evidence for a Specific Interaction between DA and C4S in the PPy-C4S Film.....	187
(5.2.2)The Interaction of DA with C4S in Solution	189
(5.2.2i) Job's Method and the Stoichiometry of the C4S-DA Complex.....	191
(5.2.2ii) NMR Titration.	192
(5.2.2iii) The Structure of the C4S-DA Complex.....	195
(5.2.2iv) Rotating-Frame Nuclear Overhauser Effect (ROE) Spectroscopy	196
(5.2.2v) Insights into the Mode of Sensing	199
(5.2.3) The Selectivity of the PPy-C4S Film	200
(5.2.3i) Ascorbic Acid (AA).....	200
(5.2.3ii) Uric Acid (UA).....	205
(5.2.3iii) 5-Hydroxytryptamine (Serotonin, 5-HT).....	211
(5.2.3iv) Acetylcholine (Ach)	217
(5.3) Conclusion	222
(5.4) Bibliography.....	224

(Chapter 6) Conclusions

(6.1) Conclusions.....	229
(6.2) Bibliography.....	234

Acknowledgements

Firstly, I thank Dr Denise Rooney, my supervisor, for her dedicated support during this project and in guiding me through to the end. I also thank Prof Carmel Breslin for valued advice and encouragement.

Particular thanks go to Dr Johnny Colleran, whose enthusiasm for electrochemistry has inspired me in this project.

My sincere gratitude goes to my friends and colleagues in the Department of Chemistry for their day to day backing and understanding – especially in the final weeks. In particular, Declan Gavin, Dr Denis Donlon, Dr John Walsh, Dr Eoin Byrne, Dr Gillian Hendy, Dr Claire Harley, Dr Sinead McDermott, Dr Valeria Annibaldi, Dr Enrico Andreoli, Catherine Fox, Dr Linda Doyle, Dr Rob Curran, and Dr Eimear Ryan.

I am indebted to the technical staff, Noel Williams, Dr Ken Maddock, Anne Cleary, Orla Fenelon, Ria Collery-Walsh, Barbara Woods, Orla Joyce, and the Executive Administrator, Niamh Kelly, in the Department of Chemistry, who have all been on hand with practical assistance.

I gratefully acknowledge a Post Graduate Scholarship from the Irish Research Council for Science, Engineering and Technology, and the John and Pat Hume Scholarship from NUI Maynooth.

Grateful thanks also to Prof John Lowry, Head of Department.

I thank my wonderful parents, Kathleen and Larry Doyle, and my brother Anthony, for all their love, kindness and patience – particularly over the past months. I am also grateful to Mary and the late Michael O'Neill for their encouragement over the years. Finally, special thanks to Margaret O'Neill, who has been there from start to finish.

Abstract

In this thesis, the development of a *p*-sulfonatocalix[4]arene (C4S) doped polypyrrole (PPy-C4S) modified electrode for the electrochemical detection of dopamine (DA) is reported. The physical and electrochemical characteristics of the PPy-C4S film are discussed, the oxidation of DA at the PPy-C4S modified electrode is investigated and the mode in which DA is detected at this modified electrode is explored.

The PPy-C4S film was fabricated using a potentiostatic mode of growth and the incorporation of C4S into the PPy matrix was confirmed by EDX analysis. A 'cauliflower' morphology was evident from SEM images obtained for the PPy-C4S film and the surface roughness of the film increased with electropolymerisation potential. Capacitance values of 9.4 mF cm^{-2} and 10.4 mF cm^{-2} were determined for the film using cyclic voltammetry and electrochemical impedance spectroscopy, respectively. In addition, the capacitance was found to increase with film thickness. Electrochemical impedance measurements recorded over a range of potentials indicated that redox switching of the polymer involved the movement of cations, *i.e.* the PPy-C4S film exhibits cation exchange properties.

A novel property of the PPy-C4S film is the generation of calixquinones within the polymer matrix. The cyclic voltammetric profile of the PPy-C4S film is characterised by a calixquinone redox couple centred at 0.230 V vs. SCE. This redox process could only be observed when potentials sufficient to oxidise C4S were applied to the film. It was proposed that the oxidation product of C4S was susceptible to nucleophilic attack from water, resulting in the formation of a calixquinone within the film.

The oxidation of DA at the PPy-C4S modified electrode was optimised by varying the factors affecting the growth of the film and the conditions used for cyclic voltammetry. The optimum conditions were those that could simultaneously maximise DA oxidation and minimise calixquinone generation. Using these optimum conditions a limit of detection of $4.11 \times 10^{-6} \text{ mol dm}^{-3}$ was evaluated using constant potential amperometry.

The selectivity of the PPy-C4S modified electrode toward DA was also investigated. It was found that compounds with the potential to be included into C4S were significant interferents in the electrochemical detection of DA, whereas compounds with little or no affinity for C4S caused much less interference. In particular, 5-hydroxytryptamine caused a 60% reduction in the oxidation currents for DA while ascorbic acid did not interfere at all. From these results, the mode in which the PPy-C4S modified electrode could detect DA was primarily attributed to inclusion interactions.

CHAPTER 1

Introduction:

A Polypyrrole / Sulfonated Calixarene
Modified Electrode for the Electrochemical
Detection of Dopamine

1.1 Introduction

The primary aim of this project was the development of an electrochemical sensor for the neurotransmitter dopamine. Previous work carried out in our laboratory had shown that polypyrrole (PPy) doped with a sulfonated cyclodextrin was a simple, selective sensor for dopamine¹. Furthermore, these studies showed that doping the PPy film with a sulfonated cyclodextrin afforded the sensor a greater sensitivity and selectivity in comparison to PPy films doped with chloride, sulfate or dodecylsulfate anions². These promising studies prompted the current research in which PPy was doped with the sulfonated calixarene, *p*-sulfonatocalix[4]arene (C4S). The molecular recognition properties of sulfonated calixarenes are well known. In particular, C4S has demonstrated a strong affinity for dopamine³. Therefore, by altering the macrocyclic dopant we aimed to improve the sensitivity and selectivity of the sensor. Accordingly, this thesis reports the fabrication and characterization of an electrode modified with a C4S doped PPy film (PPy-C4S), the application of this PPy-C4S modified electrode as an electrochemical sensor for dopamine and the mode in which dopamine is detected at the PPy-C4S film.

In this Chapter, the different concepts central to this work are introduced, namely conducting polypyrrole, sulfonated calixarenes and dopamine sensors. In each section, a general review of the concept is provided and the contribution of the current research is discussed.

1.2 Conducting Polypyrrole

Polypyrrole (PPy, Figure 1.1) belongs to a class of polymers known as conducting polymers. Also called organic polymeric conductors or synthetic metals, these materials have the intrinsic ability to carry electric current and come with a wide variety of structures and properties. Polyacetylene was the first example of a conducting polymer to be fully characterized⁴⁻⁶. However, since then, polymers containing heteroatoms, such as polyaniline, polypyrrole, polythiophene and their derivatives, have become more important⁷⁻¹¹. PPy in particular is one of the most extensively studied and applied conducting polymers. The ease of preparation, high conductivity and relative stability of PPy has led to its application in a diverse range of fields such as chemical sensors^{12, 13}, batteries^{14, 15}, supercapacitors^{16, 17} and corrosion protection^{18, 19}. An additional feature of PPy is that it forms a biologically compatible polymer matrix²⁰. As a result, it has been used in a broad number of biomedical fields such as biosensors^{21, 22}, tissue engineering^{23, 24} and implantable biodevices²⁵. Indeed, the important role that conducting polymers, like PPy, have come to play in modern chemistry was highlighted by the awarding of the 2000 Nobel Prize in Chemistry to Heeger, MacDiarmid and Shirakawa for their initial work on polyacetylene⁴⁻⁶.

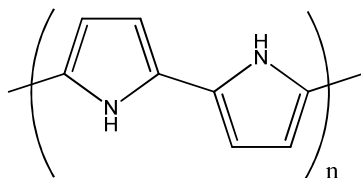


Figure 1.1: Structure of the repeating unit of polypyrrole.

1.2.1 Structural Properties of Polypyrrole

PPy is a black insoluble material consisting of a chain of pyrrole monomer rings connected by carbon-carbon σ bonds (Figure 1.1). Like all conducting polymers, the carbon and nitrogen atoms in PPy are sp^2 hybridised. Each pyrrole monomer contains an aromatic π -system formed from the overlap of the unpaired electrons in

the carbon $2p_z$ orbitals and the lone pair of electrons in the nitrogen $2p_z$ orbital. When the pyrrole rings are coplanar, the π -systems can overlap laterally to form an extended conjugated π -system, allowing the delocalisation of electrons along the polymer chain. Any distortion from the coplanarity of the rings results in a loss of conjugation that has detrimental effects on the conductivity of the polymer.

The preferred bond formation between the pyrrole rings occurs at the carbons in positions 2 and 5 on the ring (Figure 1.2b). This is known as α -coupling and PPy is typically represented in this idealised form (Figure 1.1 and Figure 1.2a-II). However, the bonding in PPy is not necessarily restricted to α -coupling. It is also possible for bonding to occur at positions 3 and 4. This is known as β -coupling (Figure 1.2a-I) and sometimes as many as one pyrrole ring in every three are linked by β -coupling^{26, 27}. The presence of β -coupling is consistent with theoretical calculations showing a diminished difference in reactivity between the α and β positions with increasing degree of conjugation²⁸. This causes a decrease in the conductivity of the polymer, through the formation of branches that break the planarity and linearity of the PPy chains²⁹. Other known defects in PPy are summarised in Figure 1.2a.

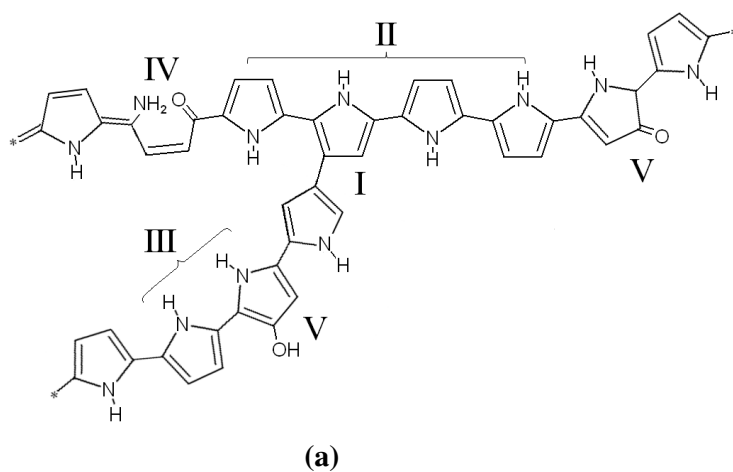


Figure 1.2: (a) Possible structure of PPy chains. (a-I) β -Coupling at the beginning of a polymer branch. (a-II) Sequence of preferred linear α -coupling. (a-III) unrotated α -coupling. (a-IV) Defects generated by the reaction of the oxidized sites in the polymer with water³⁰. (a-V) Functional groups created by secondary oxidation reactions³⁰. (b) Structure of pyrrole with the carbon positions labelled.

1.2.2 Electronic Properties of Polypyrrole

The inherent conductivity of PPy, and conducting polymers in general, stems from their extended conjugated π -system and has been described in terms of the band theory of solids^{31, 32}. The distribution of the energy states of the π orbitals can be evaluated using quantum-mechanics, with the energy (E) of the n^{th} energy level given by³³,

$$E_n = \frac{h^2 n^2}{8ma^2} \quad \text{Eq(1.1)}$$

where m is the mass of an electron, a is the length of a one-dimensional box and h is Planck's constant. For a conducting polymer with a large number (N) of carbon atoms spaced at a distance d from each other, the length of the one dimensional box is approximated as $a = Nd$. Each carbon atom contributes one electron, so for N atoms, contributing a total of N $2p_z$ electrons, the Highest Occupied Molecular Orbital (HOMO) is the $n = N/2$ energy level, the Lowest Unoccupied Molecular Orbital (LUMO) is the $n = \frac{N}{2} + 1$ energy level and the energy difference (ΔE) between the HOMO and the LUMO is given by,

$$\Delta E = E_{LUMO} - E_{HOMO} \cong \frac{(h/d)^2}{8m} \cdot \frac{1}{N} \quad \text{Eq(1.2)}$$

From Equations 1.1 and 1.2 it is clear that the number of energy levels will increase with increasing number of carbon atoms, giving a higher density of states, but ΔE will decrease. If N is very large, the densities of the states for the π -bonding and π^* -antibonding orbitals are sufficiently high for these to be approximated as the conduction band (CB) and the valence band (VB), respectively. In this case, ΔE corresponds to the band gap (Figure 1.3). The band gap is a forbidden energy region where there are no energy states available for the electrons. An electron can only be excited to a higher energy state if it is supplied with an amount of energy at least equal to ΔE . Once it reaches this higher energy state the electron is free to move along the polymer chain. In this way, the conductivity of these polymers can be classed according to the band gap^{31, 32}.

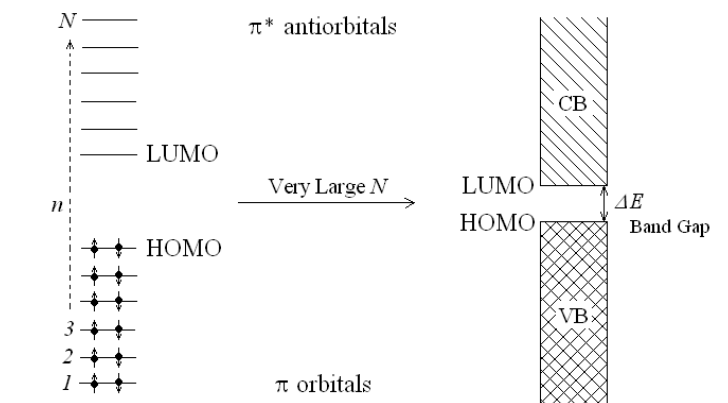


Figure 1.3: Representative energy level diagrams for PPy. The number of energy levels corresponds to the number of carbon atoms, N . For very large N the π -bonding orbitals merge to form the valence band (VB), whereas the π^* -antibonding orbitals merge into a conduction band (CB). All the π electrons are delocalized inside VB. The top level of VB is the HOMO, whereas the bottom level of CB is the LUMO. The band gap, ΔE , of the polymer is given by the energy difference between CB and VB.

In general, materials can be classified as conductors, semiconductors or insulators based on their electrical conductivity (σ), as illustrated in Figure 1.4. In insulators, the electrons in the valence band are separated from the conduction band by a large band gap ($\Delta E > 10$ eV) making it difficult to excite electrons into the conduction band. Consequently insulators do not carry electric current and typical values of σ are below 10^{-6} S m^{-1} . In the case of metals, the valence band and conduction band overlap ($\Delta E = 0$) and form a single diffuse band described as an electron cloud, allowing the free flow of electrons in the crystal lattice of the metal ($\sigma > 10^2$ S m^{-1}). For semiconductors, the conductivity falls in between that of metals and insulators with only those charges that have enough energy to overcome the band gap being able to flow. It can be seen from Figure 1.4 that conducting polymers cover a broad range of conductivities. Typically, the band gap for these polymers is less than 4.0 eV, the band gap for neutral (undoped) PPy is 3.16 eV^{31, 32, 34, 35}. Consequently, they behave like semiconductors. However, when these polymers are doped their conductivity increases significantly. Conductivity values for oxidised (doped) PPy are generally of the order of metals (10^2 to 10^5 S m^{-1})³⁶. This increase in conductivity has been attributed to the formation of mid-gap energy levels, known as polarons and bipolarons, that allow the transport of charge along the polymer backbone. These are discussed in more detail in Sections 1.2.3 and 1.2.4.

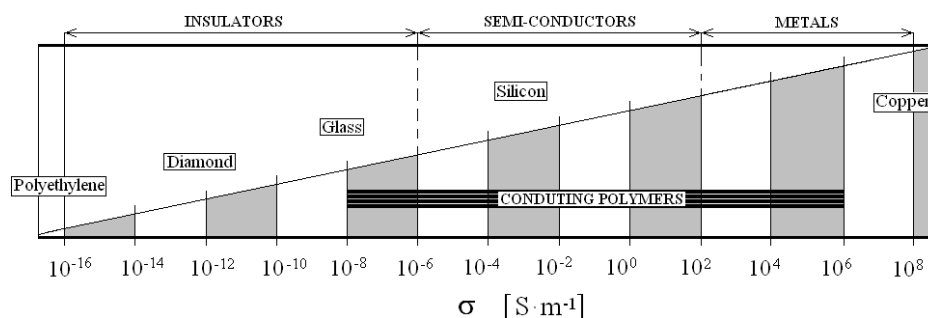


Figure 1.4: Classification of materials in order of electrical conductivity (σ).

1.2.3 Doping and Redox Behaviour of Polypyrrole

A conducting polymer is said to be doped when counterions are taken into the bulk polymer to preserve its charge neutrality. Indeed, conducting polymers are unique in their ability to be doped or undoped based on their oxidation state⁵. PPy becomes doped in its oxidised state by the formation of polarons and bipolarons. A polaron (radical cation) is formed when an electron is removed (oxidised) from the polymer backbone (Figure 1.5a), and a bipolaron (dication) is formed by further oxidising a polaron (Figure 1.5b)^{31, 32}.

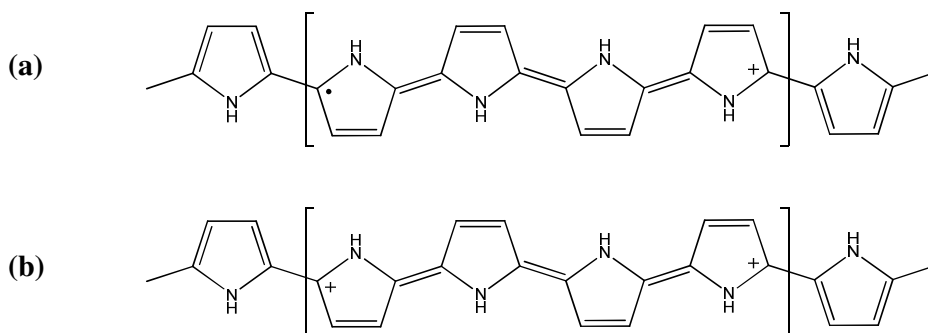


Figure 1.5: Structure of (a) a polaron and (b) a bipolaron for conducting PPy.

The charges left on the polymer by these processes become stabilized by interacting with a dopant, a species of opposite charge introduced into the polymer^{31, 32}. This process is reversible. So the oxidation of PPy is accompanied by an influx of anions, which are then expelled from the polymer when it is reduced back to the neutral state

(Figure 1.6a). This scenario is especially true for small mobile anions such as chlorides. However, larger anions such as *p*-dodecylbenzene sulfonate³⁷ and poly(styrenesulfonate)³⁸ become permanently anchored in the polymer matrix. In this situation, the electroneutrality of the polymer, during reduction, is maintained by the incorporation of mobile cations from the electrolyte solution into the polymer (Figure 1.6b). Thus, PPy can act as an anion or cation exchange polymer based on the size of the dopant. Indeed, the ion-exchange properties of PPy have been examined in detail³⁹⁻⁴⁵. In particular, Shimidzu *et al.*³⁹, studied the ion exchange behaviour of PPy doped with a series of alkyl sulfonate dopants ($C_nH_{n+2}SO_3^-$, $n = 3$ to 10). They found that for small n the sulfonate dopant could move in and out of the polymer during redox switching, whereas for large n , the dopant was trapped inside the polymer and the charge neutrality was maintained by the movement of cations in and out of the film. For intermediate values of n , the polymer displayed mixed anion and cation exchange properties. Similar results were also reported by Khalkhali *et al.*³⁷ for PPy doped with *p*-toluene sulfonate and dodecyl sulfonate.

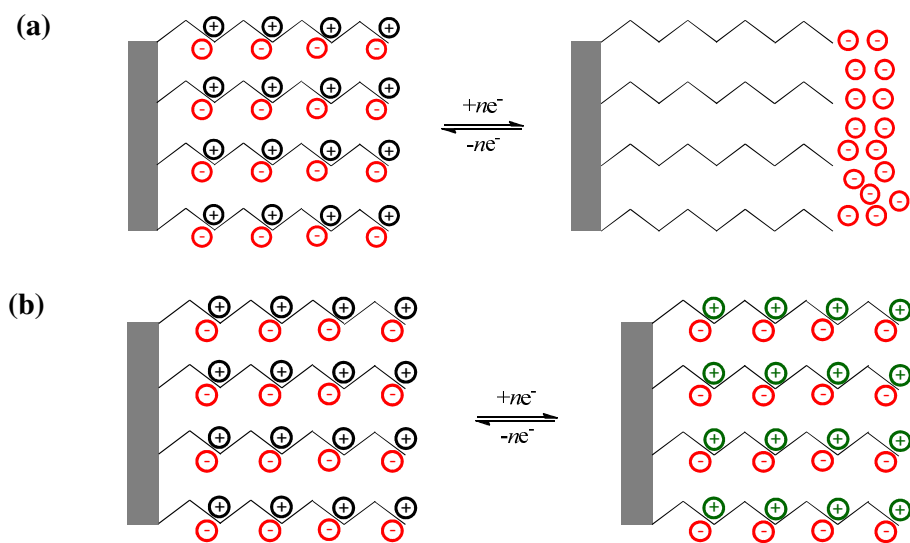


Figure 1.6: Redox switching of PPy coupled with (a) anion exchange and (b) cation exchange.

1.2.4 Charge Transport in Polypyrrole

The increased conductivity observed for doped conducting polymers has been attributed to the formation of mid band gap energy levels, polarons and bipolarons, that allow the transport of charges within the polymer^{31, 32}. When PPy is oxidized to form polarons and bipolarons, the portion of the polymer subjected to this process becomes distorted by the local excess of charge and a corresponding vibration of the polymer lattice (a phonon) is coupled to it⁴⁶. This causes an increase ($+\Delta\varepsilon$) in the energy of the HOMO or VB and a decrease ($-\Delta\varepsilon$) in the energy of the LUMO or CB of the polymer³². In this way, two new localized mid-gap states, corresponding to the energy levels of the polaron (Figure 1.7a) or bipolaron (Figure 1.7c), are formed in the band gap. Electrons are then removed from the lower state to give a polaron (Figure 1.7b) or bipolaron (Figure 1.7d)⁴⁶. It can be seen from Figure 1.7 that the distortion energy for a bipolaron ($\Delta\varepsilon^{bip}$) is larger than that for a polaron ($\Delta\varepsilon^{pol}$). This effect is due to the bipolaron having double the charge of the polaron^{31, 32}.

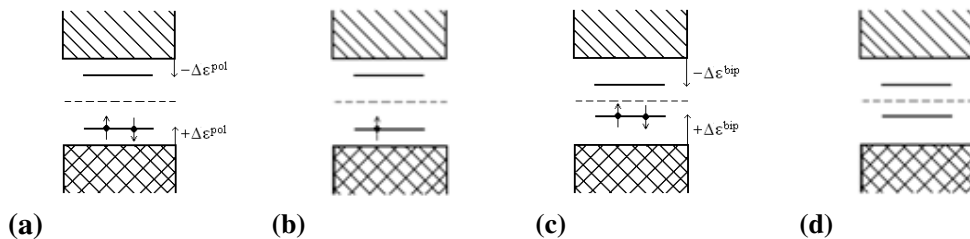


Figure 1.7: Band structure of a polaron and a bipolaron. (a) Polaron - The local distortion in the polymer lattice causes an increase in the VB and a decrease of the CB energies by an amount equal to $\Delta\varepsilon^{pol}$. (b) A positively charged polaron is formed by removing an electron from the lower bounded state. (c) Bipolaron - The local distortion in the polymer lattice causes an increase in the VB and a decrease of the CB energies by an amount equal to $\Delta\varepsilon^{bip}$. (d) A positively charged bipolaron is formed by removing two electrons from the lower bounded state.

These polarons and bipolarons can move along the doped polymer chains (intrachain transfer) or ‘hop’ between the chains (interchain transfer)⁴⁷. The mechanism of intrachain transfer is illustrated in Figure 1.8. In Figure 1.8a, a simple conjugated polymer chain bearing two polarons is shown. The two radical species can recombine to form a double bond, leaving the two positively charged species on the chain (Figure 1.8b). In the presence of a close distribution of anionic dopants, the

positive charges can move along the entire polymer chain by repeated double bond rearrangements (Figure 1.8c-e). The dopant has also been shown to have an important role in the mechanism of interchain ‘hopping’ where it acts as a tunnelling bridge between neighbouring chains⁴⁸. In this way, the strong dependence of the conductivity of PPy, and conducting polymers in general, on the level of doping can be explained by the formation of polarons and bipolarons^{31, 32}.

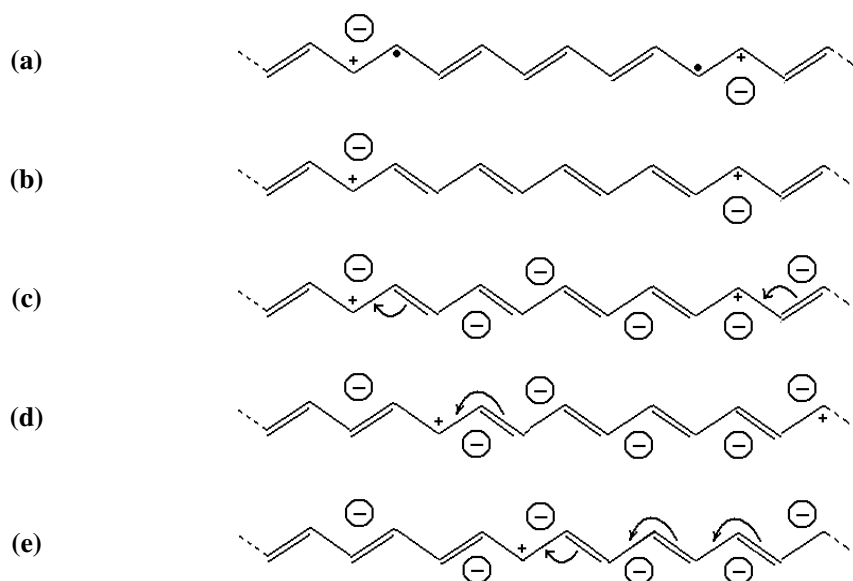


Figure 1.8: Mechanism of intrachain movement of charge carriers inside a conducting polymer. (a) Two hole polarons are localized on the polymer chain. (b) The two radicals have recombined to form a double bond. (c-e) In the presence of a close distribution of anionic dopants the two positive charges can move along the chain⁴⁷.

1.2.5 Synthesis of Polypyrrole

The synthesis of PPy can be performed using either chemical or electrochemical methods^{49, 50}. In both cases, the polymer is formed through oxidative coupling. Generally, the electrochemical route is the preferred method for surface application as the film thickness can be controlled by monitoring the charge passed during electropolymerisation. In addition, it tends to produce purer polymers because harsh oxidising agents are not necessary. That said, the chemical route is quite versatile and is the best choice for the synthesis of large amounts of material.

One of the easiest and most common ways of chemically synthesising PPy is in solution. Polymerisation is initiated by the addition of a strong oxidising agent to a solution of pyrrole, resulting in the precipitation of PPy from solution. The pyrrole monomers are oxidized to radical cations ($Py^{+\cdot}$) which then couple with the monomer to form cation dimers⁵¹. The repeated addition of monomer units to the radical cation and elimination of protons causes the growth of the polymer. The most common oxidising agent employed for the synthesis of PPy is $FeCl_3$, however, salts of other transition metals, such as Cu^{2+} , have also been used^{50, 52}. The anion of the salt is incorporated into the polymer to balance the positive charge carried by the polymer during polymerisation. In this way, it is relatively simple to dope the polymer with different anions.

Electrochemical polymerisation of pyrrole is achieved when an anodic potential is applied to a conducting substrate that has been immersed in a solution containing the pyrrole monomer and a suitable electrolyte. The function of the electrolyte is to allow the flow of current and to provide the anionic dopant. The electropolymerization can be performed using three principle methods, potentiostatic⁵³ (constant potentials), galvanostatic⁵⁴ (constant current) or potentiodynamic⁵⁵ (potential scanning). There is some controversy over the mechanism of pyrrole electropolymerisation and various pathways have been proposed⁵⁶⁻⁶⁶. However, among all the proposed mechanisms, the one proposed by Diaz *et al.* is regarded as the most probable⁶⁷⁻⁶⁹. The main features of this mechanism are outlined in Figure 1.9. This mechanism is based on the assumption that the oxidation of the pyrrole monomer at the electrode surface is faster than the diffusion of the monomer from the bulk solution. In this way, the pyrrole at the electrode surface is predominantly in the form of a radical cation, formed at potential E_i (reaction (1a)). The high concentration of radical cations at the interface drives the coupling of two radical cations to form a dihydromer dication (reaction (1b)). The loss of two protons from the dihydromer dication forms an aromatic dimer (reaction (1c)). This dimer can then be oxidized at the electrode surface (reaction (2a)), couple with a monomer radical cation (reaction (2b)) and deprotonate (reaction (2c)). The continued repetition of these reactions, here shown as the i^{th} step, drives the growth of the polymer chain. The chain growth is terminated by reaction of the polymer

radical cation with water (reaction (t1)), or by stabilization of the delocalized radical cation (reaction (t2))⁶⁷.

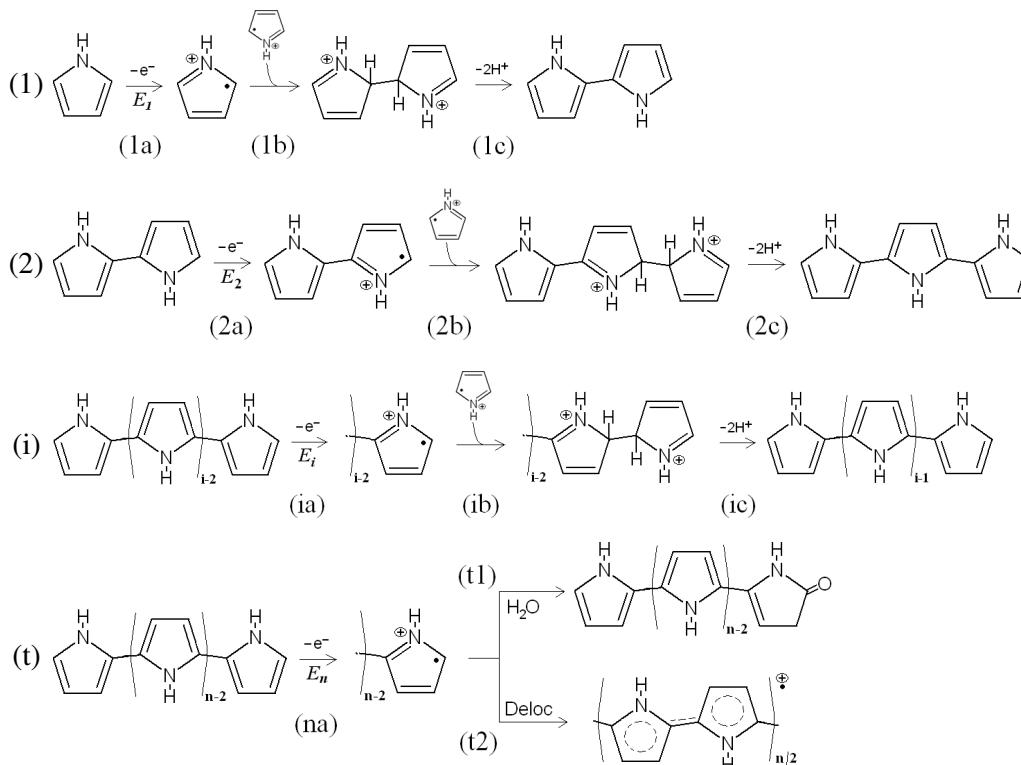


Figure 1.9: The mechanism proposed by Diaz *et al.* for the electropolymerization of Py. (1) Oxidation at potential E_1 of the monomer to radical cation, oxidative coupling of two radical cations and elimination of protons to form a dimer. (2) Oxidation at potential E_2 of the dimer to radical cation, oxidative coupling of dimer and monomer radical cations, and elimination of protons to form a trimer. (i) Chain propagation (i^{th} step) with radical coupling and elimination of protons. (t) Chain termination (n^{th} step) either by water addition or radical delocalization.

It is important to note that the stability of the radical cation increases with increasing number of monomers in the chain. This is due to the improved delocalization of the charge as the π -conjugation is extended. Therefore, the oxidation potentials decrease in the order $E_1 > E_2 > \dots > E_i > \dots > E_n$. As a consequence of this, the polymer chain bears an additional oxidation charge during and after the overall polymerization. This charge is counterbalanced by anions that sit inside the bulk polymer. In this way, PPy is synthesised in the doped (oxidised) state. The number of electrons taken from each monomer is generally taken as $2 + p$, corresponding to two electrons for the polymerization plus p electrons for the oxidation of the polymer chain. For PPy, p is

usually between 0.25 and 0.33, that is, one positive charge delocalized across every 3 to 4 monomeric units^{67, 70}.

1.2.6 Factors Affecting the Electropolymerisation

The electrochemical polymerisation of pyrrole is affected by a wide range of parameters including the potential, solvent, concentration and nature of the supporting electrolyte, temperature, pH and mode of polymerisation. Varying these conditions can have a profound effect on the physical and electrical properties of the PPy films produced.

One of the most important parameters affecting the electropolymerisation process is the supporting electrolyte. The size of the anion incorporated into the polymer can influence various characteristics such as the microstructure and porosity of the film, as well as its ion exchange properties⁶⁷. The nature of the anion also has an impact on the quality of the film produced. Kassim *et al.*⁷¹ showed that conducting polymers doped with large aromatic sulfate anions had better mechanical properties than perchlorate doped polymers. In addition, Warren *et al.*⁷² and Bhattacharya *et al.*⁷³ found that utilising an aromatic dopant increased the conductivity of PPy films. The electrolyte concentration is also important, although its effect is not entirely understood. Li and Yang⁷⁴ have shown that the doping degree, conductivity and tensile strength of a PPy-NO₃ film increases as the electrolyte concentration increases. However, no further increase in these properties was observed for concentrations greater than 2.0 mol dm⁻³.

Another important factor in the electropolymerisation process is the potential. In general, increasing the potential used to prepare the polymer results in an increase in the porosity, surface roughness and conductivity of the films^{75, 76}. However, using potentials that exceed 0.80 V vs. SCE has been shown to cause a decrease in the conductivity of PPy films⁷⁷⁻⁷⁹. This has been attributed to the overoxidation of the film and it is irreversible. The mechanism for overoxidation remains unclear. To date, the most accepted mechanism for the overoxidation of PPy is the nucleophilic attack of PPy by aqueous nucleophiles such as OH⁻, Br⁻ and H₂O⁸⁰. This in turn

causes the formation of carbonyl groups on the α -carbons of the pyrrole ring which breaks the conjugation of the polymeric chain⁸¹.

The solvent and the solution pH also have a strong influence on the electrochemical polymerisation of pyrrole. The main requirement of the solvent is that it has good ionic conductivity and a good electrochemical resistance against decomposition at the monomer oxidation potentials⁸². Aqueous solutions usually require a reasonably high amount of supporting electrolyte to achieve the desired conductivity. Likewise, organic solutions generally need a suitable organic salt. Carquigny *et al.*⁸³ studied the characteristics of PPy grown from aqueous, non aqueous and mixed solutions. They found that thin PPy films were deposited from acetonitrile while the films grown from aqueous and mixed solutions were thicker and more porous. In addition, Ko *et al.*⁸⁴ found that PPy films prepared in acetonitrile were more homogeneous and better conductors than polymers prepared in aqueous solutions. The effect of the solution pH is dependent on a number of variables such as, the buffer species, the supporting electrolyte and the substrate anode material⁸⁵. However, a neutral or weakly acidic pH generally favours the polymerisation of pyrrole^{60, 77}. Excessively alkaline or acidic solutions were found to interfere with the conjugation, resulting in polymers with lower conductivities^{67, 85}.

The electropolymerisation temperature has a substantial effect on the kinetics of polymerisation as well as on the conductivity, redox properties and mechanical characteristics of PPy films⁸⁶. In general, the redox properties and conductivity of PPy films grown at low temperature are superior to those grown at higher temperatures⁷⁹. This is due to increased side reactions, such as nucleophilic attack on polymeric radicals, as the temperature increases, resulting in more structural defects and lower conducting films⁶⁷.

Lastly, the mode of polymerisation can also exert an effect on the electropolymerisation of pyrrole. PPy films are most commonly electrosynthesised *via* galvanostatic (constant current), potentiostatic (constant potential) or potentiodynamic (potential scanning) methods. The films formed from a constant current or constant potential mode of polymerisation are usually more porous and uneven, while the films obtained using cyclic voltammetry are generally smoother and more compact⁸⁷. However, more recent studies carried out by Hernandez-Perez

*et al.*⁸⁸ showed that the potentiostatic mode of growth was better for obtaining reproducible thin films with a smooth surface morphology. Furthermore, they found that PPy film growth was easier to control using this method.

1.2.7 Polypyrrole Doped with Sulfonated Calixarenes

In this work, PPy was doped with a *p*-sulfonatocalix[4]arene during the electropolymerisation process. Several other authors have also incorporated sulfonated calixarenes into PPy films⁸⁹⁻⁹². In particular, Bidan *et al.*⁸⁹ and Mousavi *et al.*⁹¹ reported the synthesis of PPy films doped with C4S. Bidan *et al.*⁸⁹ observed that C4S could be irreversibly incorporated into the PPy matrix. This suggests that the PPy-C4S film could display cation exchange properties. Indeed, a recent paper by Akiehi *et al.*⁹² reported an electrically switchable cation exchange membrane based on PPy doped with a sulfonated calix[6]arene⁹². However, despite these studies no comprehensive characterisation of PPy doped with a sulfonated calixarene has yet been carried out. In light of this, the physical and electrochemical properties of the PPy-C4S film were studied in detail in Chapter 3.

1.3 Sulfonated Calixarenes

Sulfonated calixarenes (*p*-sulfonatocalix[*n*]arenes) are a class of water soluble calixarenes. Calixarenes are macrocyclic compounds consisting of a cyclic array of phenol units connected by methylene bridges. The cavity shape of these molecules has led to their extensive application in the fields of molecular recognition and supramolecular chemistry. Indeed, calixarenes have been referred to as ‘the third generation of supramolecules’, after cyclodextrins and crown ethers⁹³. In particular, water soluble calixarenes have found applications in a range of biological/biomedical fields including biomimetic catalysts, biomimetic receptors, enzyme inhibitors, antiviral agents, antithrombotic agents and ion channel blockers⁹⁴. Water solubility has been conferred on calixarenes using carboxyl groups, amino groups, nitro groups and phosphonate groups⁹⁴. However, the sulfonated calixarenes, first prepared by Shinkai *et al.*^{95, 96}, have the greatest solubilities in water ($> 0.10 \text{ mol dm}^{-3}$)⁹⁴. Figure 1.10 shows the structure of the sulfonated calixarene studied in this work: *p*-sulfonatocalix[4]arene (C4S).

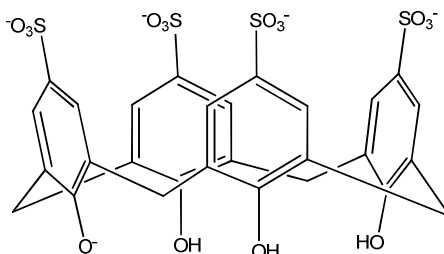
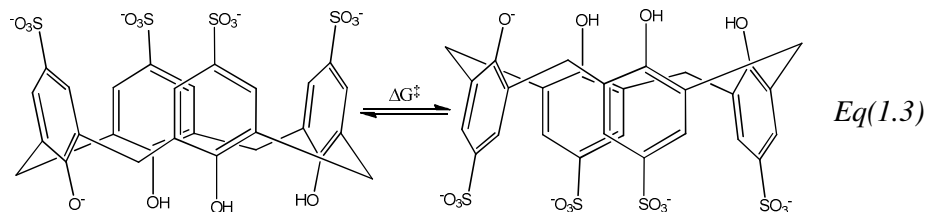


Figure 1.10: Structure of *p*-sulfonatocalix[4]arene (C4S).

1.3.1 Structural Properties of Sulfonated Calixarenes

An important property of calixarenes is their structural flexibility. Each phenol unit can rotate around the axis that passes through the carbon atoms bonded to the bridging methylene groups^{94, 97}. This gives rise to a number of different conformations depending on the number of phenol units. For C4S there are four possible conformers^{94, 97}: cone, partial cone, 1,2-alternate and 1,3-alternate (Figure 1.11). In the solid state, the cone conformation is generally the most stable. In

solution, the calixarene is conformationally mobile resulting in a temperature dependent ring inversion between mirror-image cone conformations (Equation 1.3)^{94, 97}.



The pathway followed for this conformational inversion is not certain however, computational studies provide strong support for a ‘broken chain pathway’ involving a cone \rightarrow partial cone \rightarrow 1,2-alternate/1,3-alternate \rightarrow inverted partial cone \rightarrow inverted cone sequence⁹⁴.

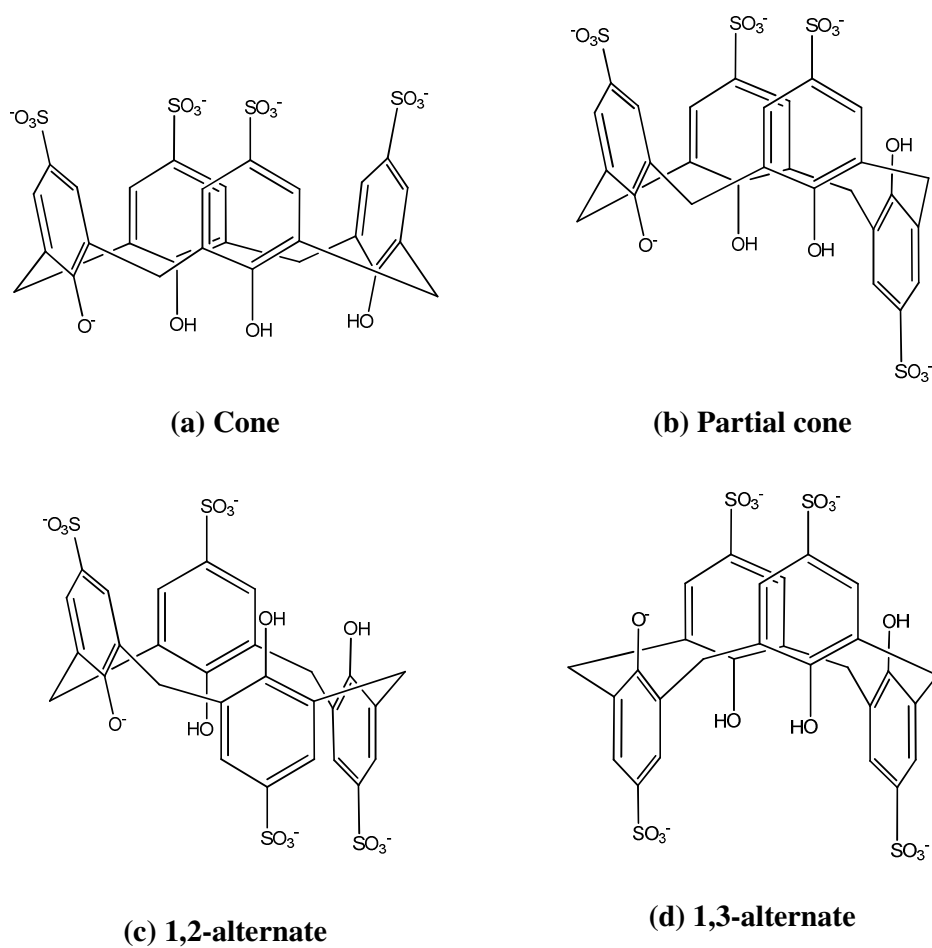


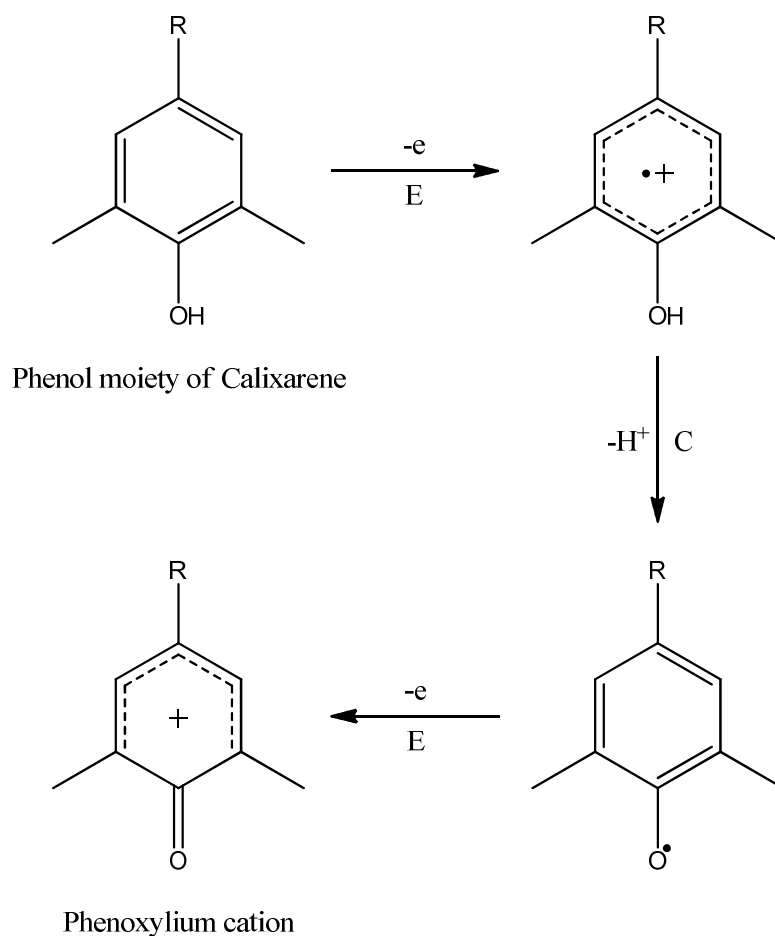
Figure 1.11: The four possible conformations of C4S.

The stabilisation of the cone conformation for calixarenes has been attributed to intramolecular hydrogen bonding interactions among the OH groups⁹⁴. This is especially true for C4S. One of the OH groups of C4S is acidic with a pK_a of approximately 3.27⁹⁸⁻¹⁰⁰. Shinkai *et al.*⁹⁷ studied the conformational inversion of C4S using variable temperature ¹H NMR spectroscopy. The ¹H NMR spectrum of the cone conformation is characterised by a pair of doublets for the methylene protons, when the rate of inversion is slow (low temperature), and a sharp singlet at high temperatures. The coalescence temperature (T_c) is the temperature at which the peaks merge and reflects the rate of conformational inversion. In neutral and basic media, where the acidic OH group would be deprotonated, the authors determined a T_c of 9°C for C4S. However, in acidic media, where the OH group would remain protonated, they could not obtain a value for T_c because the peaks did not split, even at 0°C. From this they concluded that the oxide anion increased the stabilisation of the cone conformation by acting as a stronger acceptor for intramolecular hydrogen bonding than the hydroxyl groups⁹⁷.

1.3.2 Electrochemical Activity of Sulfonated Calixarenes

The electrochemical activity of sulfonated calixarenes has been reported by a number of research groups¹⁰¹⁻¹⁰⁵. Diao *et al.*^{101, 102} and Pailleret *et al.*^{103, 104} found that these calixarenes could be irreversibly oxidised at potentials greater than 0.7 V vs. SCE. In particular, Diao *et al.*¹⁰² determined that the oxidation of C4S was an irreversible two-electron transfer reaction. To the best of our knowledge no reaction mechanism has yet been proposed for this oxidation reaction. However, it is likely that the oxidation of C4S proceeds *via* a similar reaction mechanism to the one proposed by Louati *et al.*¹⁰⁶ for the oxidation of calix[4]arenes (Scheme 1.1). This mechanism comprises an electrochemical step (E), involving the transfer of one-electron, followed by a chemical step (C), involving the loss of a proton, and a final electrochemical step (E) involving the transfer of a second electron. This ECE mechanism was originally proposed by Ronlan *et al.*¹⁰⁷ for the oxidation of sterically hindered phenols and is commonly accepted for non macrocyclic phenolic compounds. Later, Louati and Vataj^{106, 108, 109} adopted this mechanism for the oxidation of the phenol moiety of several different calix[4]arenes based on the

results obtained from spectroelectrochemical experiments. UV-vis spectra recorded during the oxidation reaction showed an intense band at 510 nm. This band was characteristic of a phenoxylum cation (Scheme 1.1) and increased in intensity as the oxidation reaction proceeded. Considering that this mechanism has been applied to a number of different *para* substituted calix[4]arenes^{106, 108, 109}, it is reasonable to apply it to C4S. Especially, since the results obtained by Diao *et al.*¹⁰² indicate that the oxidation of C4S involves the transfer of two electrons.



Scheme 1.1: Mechanism for the irreversible electrochemical oxidation of a calixarene phenol moiety to form a phenoxylum cation¹⁰⁶⁻¹⁰⁹.

1.3.3 Molecular Recognition Properties of Sulfonated Calixarenes

The ability of calixarenes to act as host molecules is one of their most intriguing properties and accounts for much of the research interest they have received. The major focus of calixarene complexation has been on solution state complexes, usually with a demonstrated or putative application in mind. In this respect, sulfonated calixarenes are especially interesting due to their high solubility in water and consequently their potential for biological applications.

The interaction between a host and a guest to form a complex can involve one or more of the following features: hydrophobic effects, hydrogen-bonding, electrostatic attraction, π - π stacking, cation- π and CH- π interaction, van der Waals attraction and charge-transfer interactions⁹⁴. From the structure of C4S depicted in Figure 1.10, it is clear that the sulfonated calixarenes can interact in a number of these ways. The negatively charged sulfonate groups on the ‘upper-rim’ of C4S and the oxide anion on the ‘lower-rim’ can partake in electrostatic interactions with cations. In addition, the lower-rim also has the potential for hydrogen-bonding. The cavity of C4S is hydrophobic, leading to the inclusion of non-polar entities. The π -system of C4S, and calixarenes in general, distinguishes it from cyclodextrins and gives it the potential for π - π stacking, cation- π and CH- π interactions. The experimental measure of the magnitude of such interactions is typically expressed in terms of a stability or association constant (K_a) which is essentially an equilibrium constant for the formation of the complex¹¹⁰. However, the enthalpy and entropy changes for complex formation are also informative. If complex formation is entropically favoured, the interaction is most likely driven by the desolvation of the interacting particles, whereas the driving force for enthalpically favoured complexation is the inclusion of the guest into the host *via* one or more of the numerous interactions outlined above¹¹¹. Similarly, the acquisition of the data for determining complexation capabilities employs a variety of experimental techniques. Among the most often used are NMR, UV-vis and fluorescence spectroscopy, and calorimetry. X-ray crystallography is often used for the structural analysis of complexes, however, this involves the assumption that the solid state architecture reflects that of the solution state. This assumption is reasonable but it is not always accurate. In such cases, the solution state structure can be inferred from NMR measurements⁹⁴.

Since their inception, the sulfonated calixarenes have been the subject of many complexation studies involving a wide range of guest molecules. These include neutral organic molecules, inorganic and organic cations¹¹¹. Of these, the interactions of C4S with metal cations and organic ammonium cations have received the most interest. Bonal *et al.*¹¹² and Morel *et al.*¹¹³ carried out a comprehensive study on the binding interactions of C4S with a range of metal cations. They noted significant differences in the binding abilities of the cations, depending on their valency. Monovalent cations formed very weak interactions with C4S ($K_a < 10^2$), whereas the divalent and trivalent cations were bound quite strongly by C4S with K_a values in the range 10^3 to 10^4 M^{-1} . The authors also obtained data on the enthalpy and entropy changes for the formation of these complexes. The complexation of C4S with the monovalent cations was enthalpy driven, indicating that these cations were included into the cavity of C4S due to cation- π interactions. In contrast, the complexation of C4S with divalent and trivalent cations was entropically favoured. These cations were more hydrated than the monovalent ones and so, were not included into the cavity.

C4S is also known to efficiently bind organic ammonium cations^{97, 114-116}. In fact, these complexes are entirely enthalpy favoured¹¹¹. The driving force for inclusion has been attributed to a number of interactions depending on the guest molecule and the charge on C4S. Arena *et al.*¹¹⁷ studied the binding of various aliphatic and aromatic amino acids by C4S. They observed that the amino acids were anchored in the cavity by their apolar tails while the cationic ammonium group interacted electrostatically with the negatively charged sulfonate groups. Alternatively, Shinkai *et al.*^{97, 115} studied a range of aromatic ammonium cations such as trimethylanilinium (TMA). This molecule could be included into the cavity of C4S in two different ways depending on the pH of the solution. In neutral solutions, where the acidic OH group of C4S would be deprotonated, the cationic ammonium group was preferentially included into the cavity, the driving force being attributed to cation- π interactions with the π -system of C4S. Interestingly, in acidic solutions where the OH group of C4S would be protonated, it was the aromatic ring of TMA that was preferentially included. This marked difference in the mode of inclusion was attributed to the π -system of C4S being less electron rich when the lower rim was protonated^{97, 118}. Thus, the cation- π interactions were weakened in the acidic

solutions making the inclusion of the hydrophobic aromatic ring into the hydrophobic cavity the more favourable interaction.

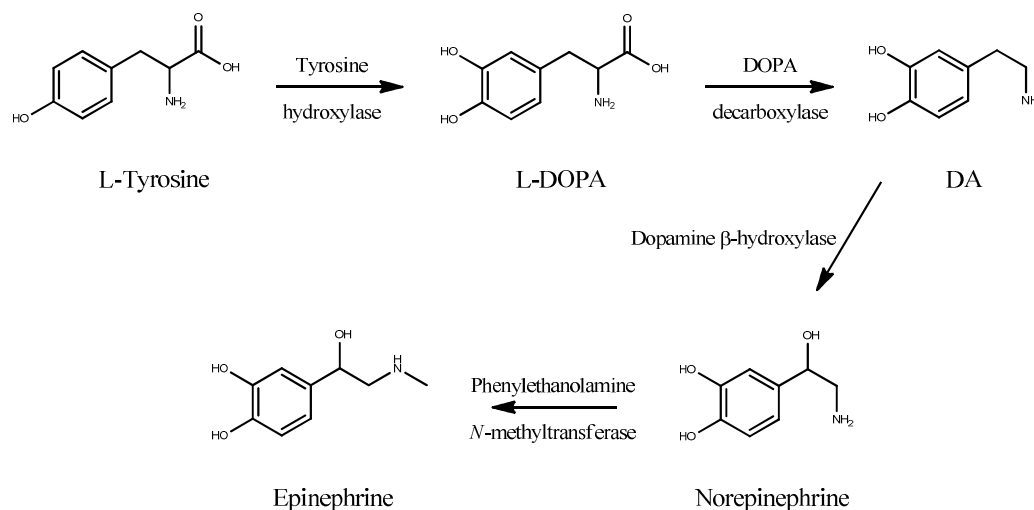
1.3.4 Inclusion of Dopamine into Sulfonated Calixarenes

A final interaction of significance for this work is the inclusion of dopamine into C4S. Using fluorescence spectroscopy, Zhou *et al.*³ studied the inclusion complexes formed between dopamine and sulfonated calix[4] and calix[6]arenes. They found that dopamine formed strong 1:1 inclusion complexes with these calixarenes. In particular, the reported K_a value for the complex formed between C4S and dopamine was 4060 M^{-1} . The authors also proposed a preliminary structure for this complex from the magnitude of the ^1H NMR chemical shifts of dopamine in the presence of C4S. The results suggested that the cationic ammonium group of dopamine was included into the cavity of C4S.

In Chapter 5 of this work, the complex formed between dopamine and C4S was studied in further detail using a range of ^1H NMR techniques and the structure of this complex was determined more conclusively.

1.4 Dopamine Sensors

Dopamine (DA) is one of the most important catecholamine neurotransmitters present in the mammalian central nervous system. DA is produced in the brain, from the naturally occurring amino acid Tyrosine. The synthetic pathway involves the hydroxylation of L-tyrosine to form L-DOPA and the subsequent decarboxylation of this amino acid to form DA (Scheme 1.2). DA itself is a precursor to norepinephrine and epinephrine, however, neurons that are stimulated by DA only contain the necessary enzymes to convert tyrosine as far as DA¹¹⁹.



Scheme 1.2: The biological synthetic pathway of DA¹¹⁹.

Abnormalities in the levels of DA in the brain have been linked to several neurological disorders such as Parkinson's disease, Huntington's disease and schizophrenia. The onset of Parkinson's disease occurs due to deterioration in the DA containing neurons in the brain. Currently, there is no immediate cure for patients with Parkinson's disease. Although the administration of L-DOPA has been found to be helpful, it becomes less effective over time¹²⁰. On the other hand, schizophrenia is believed to be caused by an increase in the number of DA receptors in the brain. Therefore, normal levels of DA in the schizophrenic brain have too

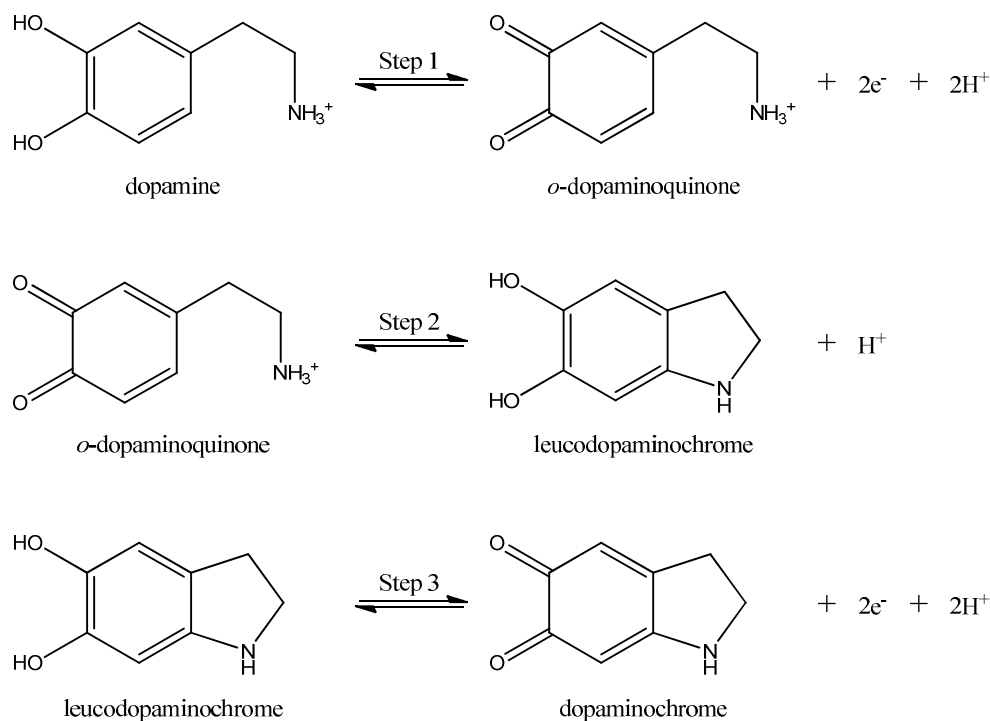
powerful an effect. Again, there is no cure, however, the sensitivity of the system can be reduced by blocking the DA receptors with antipsychotic drugs¹¹⁹. Huntington's disease is a fatal, genetic neurodegenerative movement disorder linked to increased levels of DA. Yet again there is no known cure, though decreasing the release of DA with tetrabenazine has emerged as an effective treatment for the suppression of this disease¹²¹. In addition, DA has also been shown to play an important role in drug addiction¹²² and attention disorders¹²³, and it has even been associated with HIV infection¹²⁴. Consequently, the development of simple analytical methods for the determination of DA concentration is important.

Various techniques have been employed for the determination of DA. In general, these techniques can be divided into electrochemical and non-electrochemical techniques. Non-electrochemical techniques offer excellent sensitivity and usually work by simultaneously detecting DA and a wide range of other compounds. Examples of these techniques include flow injection analysis¹²⁵, microchip capillary electrophoresis¹²⁶, high performance liquid chromatography¹²⁷ and Raman spectroscopy¹²⁸. These techniques can generally be used in conjunction with each other and with electrochemical techniques. Nevertheless, a major disadvantage of these techniques is that they cannot be used as *in vivo* sensors and thus, are unsuitable for real time analysis. In contrast, electrochemical methods provide a relatively simple route for the *in vivo* monitoring of DA levels. The electrodes used in the sensing can be miniaturised and conveniently placed in the living organism for real time analysis. Furthermore, electrochemical sensors are usually inexpensive to manufacture and easy to employ.

1.4.1 The Electrochemical Detection of DA

There has been considerable interest in the development of electrochemical sensors for DA. This interest stems from the fact that DA is electroactive and thus, the oxidation of DA can be followed using electrochemical techniques. The electrochemical oxidation of DA is depicted in Scheme 1.3^{129, 130}. DA is first converted to *o*-dopaminoquinone by a two electron oxidation (Step 1). This molecule can then undergo a 1,4-Michael addition which results in a cyclisation reaction

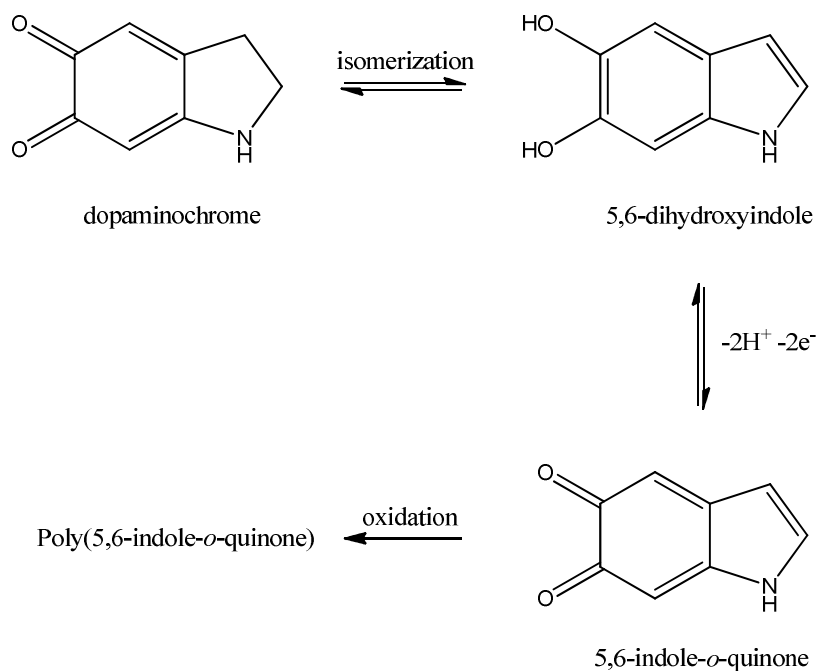
(Step 2). The product of this reaction, leucodopaminochrome, is more easily oxidised than the parent DA and can experience a further two electron oxidation to form dopaminochrome (Step 3).



Scheme 1.3: Steps involved in the electrochemical oxidation of DA^{129, 130}.

Even so, monitoring the concentration of DA using electrochemical methods has proven quite challenging. This is due to a number of reasons. In biological samples, DA co-exists with many other biomolecules that can interfere in the detection of DA. These interfering compounds are usually present at concentrations much higher than DA and several of them can be oxidised at similar potentials to DA at most solid electrodes. This is particularly true of ascorbic acid (AA)¹³¹. Furthermore, the electrochemical detection of DA using solid electrodes can suffer from fouling effects. It is well known that dopaminochrome can be further oxidised to 5,6-indole-*o*-quinone to generate an insoluble melanin polymer (Scheme 1.4)¹³². This polymer can foul the electrode by adhering to its surface. Consequently, an electrochemical sensor for DA should possess a number of important qualities. It should be sensitive

enough to detect the low concentrations of DA typically found in biological samples (10^{-8} to 10^{-6} mol dm $^{-3}$)¹³³. In addition, it should be capable of accurately determining DA in the presence of potential interfering compounds. Finally, it should not be subject to the fouling effects outlined in Scheme 1.4.



Scheme 1.4: The formation of the insoluble melanin polymer responsible for the fouling of solid electrodes¹³².

In evaluating the performance of electrochemical sensors for DA, several different interferent compounds have been used¹³⁴. These include uric acid (UA), 5-hydroxytryptamine (5-HT), epinephrine (EP) and L-DOPA. However, AA is by far the most widely investigated interferent¹³⁴. This is because AA is considered the most problematic interfering compound in the determination of DA. It is oxidised in the same potential region as DA¹³¹ and is present in most biological samples at much higher concentrations than DA¹³³. The maximum physiological concentration of AA in nervous centres is approximately 5.0×10^{-4} mol dm $^{-3}$.¹³⁵ Furthermore, a reaction between the oxidised form of DA (*o*-dopaminoquinone) and AA can occur, which results in the regeneration of DA^{136, 137}. This regenerated DA can then be re-oxidised at the electrode surface leading to a higher DA signal than expected. Accordingly,

AA is used by the majority of researchers as a standard to evaluate the performance of the sensor.

Various different strategies have been employed to overcome these difficulties. One approach is to use non-electrode based sensors. The most common way of doing this is to perform electrochemistry at the interface between two immiscible electrolyte solutions^{138, 139}. Berduque *et al.*¹³⁸ found that a large excess of AA did not affect the electrochemical response of DA and Beni *et al.*¹³⁹ concluded that AA had no influence on the determination of DA. The major drawback of this approach is that it is not suitable for *in vivo* applications.

A more extensively applied approach is to coat the electrode surface with a film of material, producing a 'modified electrode'. The majority of the literature reports for modified electrodes are related to the simultaneous detection of DA and one or more interferents. These electrodes operate by increasing the separation between the signals for DA and the interferents, giving better resolution. The improved resolution is generally attributed to the polymer film exhibiting electrocatalytic behaviour. That is to say, the polymer alters the electrode kinetics of DA, the interferent or both. However, Henstridge *et al.*¹³⁴ have recently pointed out that the increased resolution could also be the result of a change in the mass transport regime. Using a theoretical model, they found that the mass transport regime to a porous electrode could be better described by thin layer diffusion than by planar diffusion. Moreover, they found that increasing the porosity of the electrode led to better resolution, when several oxidation processes were simultaneously occurring at the electrode. Alternatively, some modified electrodes can selectively detect DA in the presence of different interferents. These electrodes operate by inhibiting the oxidation of the interferent, allowing the concentration of DA to be determined more accurately.

The range of modified electrodes that have been developed for the electrochemical detection of DA is truly diverse. Popular strategies include self-assembled monolayer modified electrodes^{11, 140-147}, carbon nanotube modified electrodes^{134, 148-151}, surfactant modified electrodes^{133, 152-154}, DNA/RNA modified electrodes^{155, 156}, metal nanoparticle modified electrodes^{157, 158}, metal oxide modified electrodes¹⁵⁹ and porous carbon modified electrodes¹⁶⁰. However, the development of DA sensors

based on electrodes modified with polymeric materials is the most widely investigated approach.

1.4.2 Polymer Modified Electrodes

Polymer modified electrodes can be prepared in a number of ways. One of the most common routes is the direct electrochemical deposition of a polymer film onto an electrode surface. This method is extremely versatile and has been employed to produce a broad spectrum of polymer modified electrodes^{135, 155, 161-174}. For example, the simultaneous determination of DA, AA and UA was achieved by Lin *et al.*¹⁶⁶, Zhang *et al.*¹⁶⁷ and Li *et al.*¹⁶⁸. A detection limit of 3.0×10^{-7} mol dm⁻³ was established by Lin *et al.*¹⁶⁶ using a poly(*p*-nitrobenzenazo resorcinol) film with differential pulse voltammetry. Zhang *et al.*¹⁶⁷ used a poly(acid chrome blue K) film and differential pulse voltammetry to attain a limit of detection of 5.0×10^{-7} mol dm⁻³ while, Li *et al.*¹⁶⁸ used an overoxidised polypyrrole film with single walled nanotubes to obtain a detection limit of 5.0×10^{-7} mol dm⁻³ with differential pulse voltammetry.

The voltammetric response of DA in the presence of AA was also explored by Hou *et al.*¹⁶³ using a poly(3,5-dihydroxy benzoic acid) film. AA was not calibrated in this study, but varied concentrations of AA were shown to have no effect on the oxidation peak for DA. A limit of detection of 6.0×10^{-8} mol dm⁻³ was subsequently determined in 5.0×10^{-4} mol dm⁻³ AA using differential pulse voltammetry. The selective detection of DA has been reported by Rubianes *et al.*¹³⁵. The authors effectively eliminated the signal for AA using a melanin type polymer obtained by the electropolymerisation of L-DOPA at a glassy carbon electrode. A detection limit of 5.0×10^{-9} mol dm⁻³ was achieved in 5.0×10^{-4} mol dm⁻³ AA using constant potential amperometry and the interference for AA was shown to be less than 9.0%.

Other notable methods used to prepare polymer modified electrodes include Nafion[®] films, Langmuir-Blodgett films and layer-by-layer films. Nafion[®] is a perfluorinated polymer that has been used extensively in DA sensors. Nafion[®] has terminal sulfonate groups that can repel negatively charged anions from the electrode surface. Accordingly, it has been used in a number of modified electrodes¹⁷⁵⁻¹⁷⁹. Zheng *et*

*al.*¹⁷⁶ used an ordered mesoporous carbon / Nafion[®] composite film to simultaneously detect DA, AA and UA. A limit of detection of 5.0×10^{-7} mol dm⁻³ was evaluated using differential pulse voltammetry. A glassy carbon electrode modified with a catechin hydrate / Nafion[®] film was employed by Salimi *et al.*¹⁷⁷ to detect DA in the presence of 1.0×10^{-3} mol dm⁻³ AA. The interference from AA was approximately 5% and a detection limit of 1.1×10^{-8} mol dm⁻³ was achieved using constant potential amperometry. Ferreira *et al.*¹⁸⁰ produced Langmuir-Blodgett films from polyaniline and a ruthenium complex. The oxidation peaks of DA and AA could be separated even when the concentration of AA was three times higher than the concentration of DA. However, when the concentrations of DA and AA were the same the film could not distinguish between them. A detection limit of 4.0×10^{-5} mol dm⁻³ was obtained in the absence of AA using cyclic voltammetry. Interestingly, the authors claim that this limit of detection is sufficient to detect DA in a pharmaceutical product.

Layer-by-layer films have also been developed for the determination of DA. Zucolotto *et al.*¹⁸¹ fabricated layer-by-layer films of nanostructured polyaniline with tetrasulfonated metallic phthalocyanines (TsPc). These films could distinguish between AA and DA, which were present in the solution at concentrations of 6.4×10^{-3} mol dm⁻³ and 6.0×10^{-3} mol dm⁻³, respectively. The DA signal at the polyaniline/iron TsPc film exhibited the most promising results. At this film, the DA signal was more defined and the DA and AA peaks were more resolved. Cyclic voltammetry was the only electrochemical technique employed in this study and a detection limit of 1.0×10^{-5} mol dm⁻³ was achieved in the absence of the AA. A layer-by-layer film of polytyramine and polypyrrole-1-propionic acid was formed by Zhou *et al.*¹⁸². The amperometric response of DA in the presence of UA, L-DOPA and AA was investigated at this electrode. No interference from UA was observed and the interference from L-DOPA was only 11%, when the solution concentrations of DA and L-DOPA were both 2.0×10^{-5} mol dm⁻³. However, the interference from 1.0×10^{-4} mol dm⁻³ AA was 40% when 2.0×10^{-5} mol dm⁻³ DA was present in solution. A limit of detection of 1.0×10^{-7} mol dm⁻³ was determined using constant potential amperometry in the absence of interferents.

1.4.3 Applications of Calixarenes in DA Sensors

Calixarenes have been utilized in the detection of DA using a diverse range of techniques. Wang *et al.*¹⁸³ performed capillary electrophoresis of neurotransmitters using *p*-allylcalix[4]arene coated capillaries. The signals for DA, 5-HT and EP could be separated successfully by the calixarene coated silica columns without any loss in sensitivity compared with bare silica columns. A bilayer lipid membrane incorporated with a calix[4]resorcinarene receptor was developed by Nikolelis *et al.*¹⁸⁴ for the electrochemical detection of DA. The interference from AA was less than 5% when AA and DA were present in a 75:1 molar ratio in solution and the limit of detection was $6.0 \times 10^{-7} \text{ mol dm}^{-3}$. The electrochemical detection of dopamine at a liquidliquid interface was achieved using a homo-oxo-calix[3]arene based ionophore¹⁸⁵. Herzog *et al.*¹⁸⁵ found that the calixarene facilitated the electrochemistry of DA by forming a complex at the interface between water and 1,2-dichloroethane. Square wave voltammetry was used to obtain a limit of detection of $3.8 \times 10^{-6} \text{ mol dm}^{-3}$.

Calixarenes have also been employed in the preparation of modified electrodes. Snedjarkova *et al.*¹⁸⁶ developed a DA sensor based on a 25,26,27,28-tetrakis(11-sulfanylundecyloxy)calix[4]arene self assembled monolayer. The detection of DA was performed using the thickness shear acoustic mode method and it was found that the sensor could discriminate between DA and EP. A highly sensitive detection limit of $5.0 \times 10^{-9} \text{ mol dm}^{-3}$ was achieved. The voltammetric determination of DA was explored by Lai *et al.*¹⁸⁷ using a calix[4]arene crown-4 ether film. The authors prepared the modified electrode by drop casting a solution of the calixarene onto the surface of a glassy carbon electrode. The detection limit using cyclic voltammetry was determined to be $3.4 \times 10^{-6} \text{ mol dm}^{-3}$.

In this work, a PPy-C4S modified electrode was developed for the electrochemical detection of DA. To the best of our knowledge, sulfonated calixarenes have not yet been employed in the detection of DA. However, PPy films doped with a sulfonated calixarene have been shown to be effective cation-selective materials. These modified electrodes have been studied as Ag^+ ion⁹¹, uranyl ion⁹⁰ and trimethyl(ferrocenylmethyl)ammonium ion⁸⁹ sensors, and as electrically switchable cation exchange membranes⁹². Moreover, studies by Bidan and Niel⁸⁹ on the

trimethyl(ferrocenylmethyl)ammonium ion showed that C4S could retain its inclusion properties when immobilized in a polypyrrole film. Therefore, the PPy-C4S film could be selective towards DA due to a combination of both electrostatic interactions and the formation of an inclusion complex. Accordingly, the application of the PPy-C4S modified electrode as an electrochemical sensor for DA was investigated in Chapter 4, and the mode in which the PPy-C4S film could detect DA was explored in Chapter 5.

1.5 Bibliography

- (1) Harley, C. C., NUI Maynooth, **2009**.
- (2) Harley, C. C.; Rooney, A. D.; Breslin, C. B. *Sensors and Actuators B: Chemical* **2010**, *150*, 498-504.
- (3) Zhou, Y.; Liu, C.; Yu, H.; Xu, H.; Lu, Q.; Wang, L. *Spectrosc. Lett.* **2006**, *39*, 409-420.
- (4) Heeger, A. J. *Reviews of Modern Physics* **2001**, *73*, 681-700.
- (5) MacDiarmid, A. G. *Reviews of Modern Physics* **2001**, *73*, 701-712.
- (6) Shirakawa, H. *Reviews of Modern Physics* **2001**, *73*, 713-718.
- (7) Nalwa, H. S. *Handbook of Organic Conductive Molecules and Polymers*, 1st ed.; Wiley, **1997**.
- (8) Chandrasekhar, P. *Conducting polymers, fundamentals and applications: a practical approach*, 1st ed.; Springer, **1999**.
- (9) Skotheim, T. A.; Reynolds, J. R. *Handbook of conducting polymers*, 3rd ed.; CRC Press, **2007**.
- (10) Inzelt, G. *Conducting Polymers: A New Era in Electrochemistry*, 1st ed.; Springer, **2008**.
- (11) Maksymiuk, K. *Electroanalysis* **2006**, *18*, 1537-1551.
- (12) Carquigny, S.; Sanchez, J.-B.; Berger, F.; Lakard, B.; Lallemand, F. *Talanta* **2009**, *78*, 199-206.
- (13) Waghuley, S. A.; Yenorkar, S. M.; Yawale, S. S.; Yawale, S. P. *Sensors and Actuators B: Chemical* **2008**, *128*, 366-373.
- (14) Mermilliod, N.; Tanguy, J.; Petiot, F. *Journal of the Electrochemical Society* **1986**, *133*, 1073-1079.
- (15) Song, H. K.; Palmore, G. T. R. *Advanced Materials* **2006**, *18*, 1764.
- (16) Muthulakshmi, B.; Kalpana, D.; Pitchumani, S.; Renganathan, N. G. *Journal of Power Sources* **2006**, *158*, 1533-1537.
- (17) Ingram, M. D.; Staesche, H.; Ryder, K. S. *Solid State Ionics* **2004**, *169*, 51-57.
- (18) Fenelon, A. M.; Breslin, C. B. *Electrochimica Acta* **2002**, *47*, 4467-4476.
- (19) Zhu, R.; Li, G.; Huang, G. *Materials and Corrosion-Werkstoffe Und Korrosion* **2009**, *60*, 34-39.

- (20) Geetha, S.; Rao, C. R. K.; Vijayan, M.; Trivedi, D. C. *Analytica Chimica Acta* **2006**, *568*, 119-125.
- (21) Wang, J.; Musameh, M. *Analytica Chimica Acta* **2005**, *539*, 209-213.
- (22) Ghanbari, K.; Bathaie, S. Z.; Mousavi, M. F. *Biosensors and Bioelectronics* **2008**, *23*, 1825-1831.
- (23) Collier, J. H.; Camp, J. P.; Hudson, T. W.; Schmidt, C. E. *Journal of Biomedical Materials Research* **2000**, *50*, 574-584.
- (24) Martina, M.; Hutmacher, D. W. *Polymer International* **2007**, *56*, 145-157.
- (25) George, P. M.; Lyckman, A. W.; LaVan, D. A.; Hegde, A.; Leung, Y.; Avasare, R.; Testa, C.; Alexander, P. M.; Langer, R.; Sur, M. *Biomaterials* **2005**, *26*, 3511-3519.
- (26) Pfluger, P.; Street, G. B. *Journal of Chemical Physics* **1984**, *80*, 544-553.
- (27) Pfluger, P.; Krounbi, M.; Street, G. B.; Weiser, G. *Journal of Chemical Physics* **1983**, *78*, 3212-3218.
- (28) Waltman, R. J.; Diaz, A. F.; Bargon, J. *Journal of Physical Chemistry* **1984**, *88*, 4343-4346.
- (29) Jang, J.; Oh, J. H.; Li, X. L. *Journal of Materials Chemistry* **2004**, *14*, 2872-2880.
- (30) Otero, T. F.; Tejada, R.; Elola, A. S. *Polymer* **1987**, *28*, 651-658.
- (31) Bredas, J. L.; Scott, J. C.; Yakushi, K.; Street, G. B. *Phys. Rev. B: Condens. Matter* **1984**, *30*, 1023-1025.
- (32) Bredas, J. L.; Street, G. B. *Acc. Chem. Res.* **1985**, *18*, 309-315.
- (33) McQuarrie, D. A. *Quantum chemistry*, 2nd ed.; University Science Books, **2007**.
- (34) Yang, S. J.; Olishovski, P.; Kertesz, M. *Synthetic Metals* **2004**, *141*, 171-177.
- (35) Bredas, J. L.; Scott, J. C.; Yakushi, K.; Street, G. B. *Physical Review B* **1984**, *30*, 1023-1025.
- (36) Kaiser, A. B. *Advanced Materials* **2001**, *13*, 927-+.
- (37) Ansari Khalkhali, R.; Price, W. E.; Wallace, G. G. *Reactive and Functional Polymers* **2003**, *56*, 141-146.
- (38) Baker, C. K.; Qiu, Y. J.; Reynolds, J. R. *Journal of Physical Chemistry* **1991**, *95*, 4446-4452.
- (39) Shimidzu, T.; Ohtani, A.; Honda, K. *Bulletin of the Chemical Society of Japan* **1988**, *61*, 2885-2890.

- (40) Lim, J. Y.; Paik, W. K.; Yeo, I. H. *Synthetic Metals* **1995**, *69*, 451-454.
- (41) Inzelt, G.; Kertesz, V.; Nyback, A. S. *Journal of Solid State Electrochemistry* **1999**, *3*, 251-257.
- (42) Lisowska-Oleksiak, A.; Zalewska, T. *Solid State Ionics* **1999**, *119*, 97-101.
- (43) Skaarup, S.; Bay, L.; Vidanapathirana, K.; Thybo, S.; Tofte, P.; West, K. *Solid State Ionics* **2003**, *159*, 143-147.
- (44) Syritski, V.; Opik, A.; Forsen, O. *Electrochimica Acta* **2003**, *48*, 1409-1417.
- (45) Weidlich, C.; Mangold, K. M.; Juttner, K. *Electrochimica Acta* **2005**, *50*, 1547-1552.
- (46) Heeger, A. J.; Kivelson, S.; Schrieffer, J. R.; Su, W. P. *Reviews of Modern Physics* **1988**, *60*, 781-850.
- (47) Nordén, B. In (*Advanced Information*) *The Nobel Prize in Chemistry, 2000: Conductive polymers*, **2000**.
- (48) Zuppiroli, L.; Bussac, M. N.; Paschen, S.; Chauvet, O.; Forro, L. *Phys. Rev. B: Condens. Matter* **1994**, *50*, 5196-5203.
- (49) Feast, W. J.; Tsibouklis, J.; Pouwer, K. L.; Groenendaal, L.; Meijer, E. W. *Polymer* **1996**, *37*, 5017-5047.
- (50) Toshima, N.; Hara, S. *Progress in Polymer Science* **1995**, *20*, 155-183.
- (51) Chandrasekhar, P. *Conducting Polymers, Fundamentals and Applications: A Practical Approach*, 1st ed.; Kluwer Academic Publishers, **1999**.
- (52) Nalwa, H. S. *Advanced Functional Molecules and Polymers: Volume 3: Electronic and Photonic Properties*; Taylor & Francis, **2001**.
- (53) Prissanaroon-Ouajai, W.; Pigram, P. J.; Jones, R.; Sirivat, A. *Sensors and Actuators B: Chemical* **2008**, *135*, 366-374.
- (54) Liu, A. S.; Oliveira, M. A. S. *Materials Research* **2007**, *10*, 205-209.
- (55) Tietje-Girault, J.; Ponce de León, C.; Walsh, F. C. *Surface and Coatings Technology* **2007**, *201*, 6025-6034.
- (56) Sayyah, S. M.; Abd El-Rehim, S. S.; El-Deeb, M. M. *Journal of Applied Polymer Science* **2003**, *90*, 1783-1792.
- (57) Zhou, M.; Pagels, M.; Geschke, B.; Heinze, J. *Journal of Physical Chemistry B* **2002**, *106*, 10065-10073.
- (58) Zhou, M.; Heinze, J. *Electrochimica Acta* **1999**, *44*, 1733-1748.
- (59) Zhou, M.; Heinze, J. *Journal of Physical Chemistry B* **1999**, *103*, 8451-8457.
- (60) Zhou, M.; Heinze, J. *Journal of Physical Chemistry B* **1999**, *103*, 8443-8450.

- (61) Zhou, M.; Rang, V.; Heinze, J. *Acta Chemica Scandinavica* **1999**, *53*, 1059-1062.
- (62) Li, Y. F.; Fan, Y. F. *Synthetic Metals* **1996**, *79*, 225-227.
- (63) Kupila, E. L.; Kankare, J. *Synthetic Metals* **1995**, *74*, 241-249.
- (64) Kupila, E. L.; Kankare, J. *Synthetic Metals* **1993**, *55*, 1402-1405.
- (65) Kim, Y. T.; Collins, R. W.; Vedam, K.; Allara, D. L. *Journal of the Electrochemical Society* **1991**, *138*, 3266-3275.
- (66) Zhong, C. J.; Tian, Z. Q.; Tian, Z. W. *Science in China Series B-Chemistry* **1990**, *33*, 656-662.
- (67) Sadki, S.; Schottland, P.; Brodie, N.; Sabouraud, G. *Chemical Society Reviews* **2000**, *29*, 283-293.
- (68) Genies, E. M.; Bidan, G.; Diaz, A. F. *Journal of Electroanalytical Chemistry* **1983**, *149*, 101-113.
- (69) Funt, B. L.; Diaz, A. F. *Organic Electrochemistry: an Introduction and a Guide*; Marcel Dekker, **1991**.
- (70) Feldberg, S. W. *Journal of the American Chemical Society* **1984**, *106*, 4671-4674.
- (71) Kassim, A.; Davis, F. J.; Mitchell, G. R. *Synth. Met.* **1994**, *62*, 41-47.
- (72) Warren, L. F.; Anderson, D. P. *J. Electrochem. Soc.* **1987**, *134*, 101-105.
- (73) Bhattacharya, A.; De, A.; Das, S. *Polymer* **1996**, *37*, 4375-4382.
- (74) Li, Y. F.; Yang, J. *Journal of Applied Polymer Science* **1997**, *65*, 2739-2744.
- (75) Reyes, D. C. J. I.; Cavalieri, R. P.; Powers, J. R. *Synth. Met.* **2004**, *142*, 71-79.
- (76) Zhu, R. L.; Li, G. X.; Zheng, J. H.; Jiang, J. W.; Zeng, H. B. *Surf. Eng.* **2009**, *25*, 156-162.
- (77) Asavapiriyant, S.; Chandler, G. K.; Gunawardena, G. A.; Pletcher, D. *Journal of Electroanalytical Chemistry* **1984**, *177*, 229-244.
- (78) Yeu, T.; Yin, K. M.; Carbajal, J.; White, R. E. *J. Electrochem. Soc.* **1991**, *138*, 2869-2877.
- (79) Satoh, M.; Kaneto, K.; Yoshino, K. *Synthetic Metals* **1986**, *14*, 289-296.
- (80) Beck, F.; Braun, P.; Oberst, M. *Berichte Der Bunsen-Gesellschaft-Physical Chemistry Chemical Physics* **1987**, *91*, 967-974.
- (81) Ge, H. L.; Qi, G. J.; Kang, E. T.; Neoh, K. G. *Polymer* **1994**, *35*, 504-508.

- (82) Nalwa, H. S. *Handbook of Advanced Electronic and Photonic Materials and Devices*; Academic Press, **2000**.
- (83) Carquigny, S.; Segut, O.; Lakard, B.; Lallemand, F.; Fievet, P. *Synthetic Metals* **2008**, *158*, 453-461.
- (84) Ko, J. M.; Rhee, H. W.; Park, S. M.; Kim, C. Y. *Journal of the Electrochemical Society* **1990**, *137*, 905-909.
- (85) Shimoda, S.; Smela, E. *Electrochimica Acta* **1998**, *44*, 219-238.
- (86) Nalwa, H. S.; Editor *Handbook of Organic Conductive Molecules and Polymers, Volume 4: Conductive Polymers: Transport, Photophysics and Applications*, 1st ed.; Wiley, **1997**.
- (87) Otero, T. F.; Delarreta, E. *Synthetic Metals* **1988**, *26*, 79-88.
- (88) Hernandez-Perez, T.; Morales, M.; Batina, N.; Salmon, M. *Journal of the Electrochemical Society* **2001**, *148*, C369-C375.
- (89) Bidan, G.; Niel, M.-A. *Synth. Met.* **1997**, *85*, 1387-1388.
- (90) Kaneto, K.; Bidan, G. *Thin Solid Films* **1998**, *331*, 272-278.
- (91) Mousavi, Z.; Bobacka, J.; Ivaska, A. *Electroanalysis* **2005**, *17*, 1609-1615.
- (92) Akieh, M. N.; Ralph, S. F.; Bobacka, J.; Ivaska, A. *J. Membr. Sci.* **2010**, *354*, 162-170.
- (93) Shinkai, S. *Tetrahedron* **1993**, *49*, 8933-8968.
- (94) Gutsche, C. D.; Editor *Calixarenes: An Introduction, 2nd Edition*; Royal Society of Chemistry, **2008**.
- (95) Shinkai, S.; Araki, K.; Tsubaki, T.; Arimura, T.; Manabe, O. *J. Chem. Soc., Perkin Trans. 1* **1987**, 2297-2299.
- (96) Shinkai, S.; Mori, S.; Koreishi, H.; Tsubaki, T.; Manabe, O. *J. Am. Chem. Soc.* **1986**, *108*, 2409-2416.
- (97) Shinkai, S.; Araki, K.; Kubota, M.; Arimura, T.; Matsuda, T. *J. Org. Chem.* **1991**, *56*, 295-300.
- (98) Arena, G.; Cali, R.; Lombardo, G. G.; Rizzarelli, E.; Sciotto, D.; Ungaro, R.; Casnati, A. *Supramol. Chem.* **1992**, *1*, 19-24.
- (99) Suga, K.; Ohzono, T.; Negishi, M.; Deuchi, K.; Morita, Y. *Supramol. Sci.* **1998**, *5*, 9-14.
- (100) Yoshida, I.; Yamamoto, N.; Sagara, F.; Ishii, D.; Ueno, K.; Shinkai, S. *Bull. Chem. Soc. Jpn.* **1992**, *65*, 1012-1015.
- (101) Diao, G.; Liu, Y. *Electroanalysis* **2005**, *17*, 1279-1284.

- (102) Diao, G.; Zhou, W. *J. Electroanal. Chem.* **2004**, *567*, 325-330.
- (103) Pailleret, A.; Arrigan, D. W. M. *Langmuir* **2002**, *18*, 9447-9452.
- (104) Pailleret, A.; Magan-Oliva, N.; Ollivier, S.; Arrigan, D. W. M. *J. Electroanal. Chem.* **2001**, *508*, 81-88.
- (105) Chen, M.; Wang, H.-L.; Gu, J.; Diao, G.-W. *J. Appl. Electrochem.* **2007**, *37*, 331-337.
- (106) Louati, A.; Spraula, J.; Gabelica, V.; Kuhn, P.; Matt, D. *Electrochem. Commun.* **2006**, *8*, 761-766.
- (107) Ronlan, A.; Parker, V. D. *J. Chem. Soc. C* **1971**, 3214-3218.
- (108) Vataj, R.; Louati, A.; Jeunesse, C.; Matt, D. *Electrochem. Commun.* **2000**, *2*, 769-775.
- (109) Vataj, R.; Louati, A.; Jeunesse, C.; Matt, D. *J. Electroanal. Chem.* **2004**, *565*, 295-299.
- (110) Tsukube, H.; Furuta, H.; Odani, A.; Takeda, Y.; Kudo, Y.; Inoue, Y.; Liu, Y.; Sakamoto, H.; Kimura, K. **1996**; Elsevier; 425-482.
- (111) Guo, D.-S.; Wang, K.; Liu, Y. *J. Inclusion Phenom. Macrocyclic Chem.* **2008**, *62*, 1-21.
- (112) Bonal, C.; Israeli, Y.; Morel, J.-P.; Morel-Desrosiers, N. *J. Chem. Soc., Perkin Trans. 2* **2001**, 1075-1078.
- (113) Morel, J.-P.; Morel-Desrosiers, N. *Org. Biomol. Chem.* **2006**, *4*, 462-465.
- (114) Lehn, J.-M.; Meric, R.; Vigneron, J.-P.; Cesario, M.; Guilhem, J.; Pascard, C.; Asfari, Z.; Vicens, J. *Supramol. Chem.* **1995**, *5*, 97-103.
- (115) Shinkai, S.; Araki, K.; Matsuda, T.; Nishiyama, N.; Ikeda, H.; Takasu, I.; Iwamoto, M. *J. Am. Chem. Soc.* **1990**, *112*, 9053-9058.
- (116) Wang, L.-H.; Guo, D.-S.; Chen, Y.; Liu, Y. *Thermochim. Acta* **2006**, *443*, 132-135.
- (117) Arena, G.; Casnati, A.; Contino, A.; Magri, A.; Sansone, F.; Sciotto, D.; Ungaro, R. *Org. Biomol. Chem.* **2006**, *4*, 243-249.
- (118) Ma, J. C.; Dougherty, D. A. *Chem. Rev. (Washington, D. C.)* **1997**, *97*, 1303-1324.
- (119) Thompson, R. F. *The Brain: A Neuroscience Primer*, 2 ed.; W. H. Freeman and Company, **1993**.
- (120) Revest, P.; Longstaff, A. *Molecular neuroscience*; Taylor & Francis, **1998**.
- (121) Wilson, G. S.; Johnson, M. A. *Chemical Reviews* **2008**, *108*, 2462-2481.

- (122) Phillips, P. E. M.; Stuber, G. D.; Heien, M.; Wightman, R. M.; Carelli, R. M. *Nature* **2003**, *422*, 614-618.
- (123) O'Neill, R. D. *Sensors* **2005**, *5*, 317-342.
- (124) Koutsilieri, E.; ter Meulen, V.; Riederer, P. *Journal of Neural Transmission* **2001**, *108*, 767-775.
- (125) Leu, H. J.; Lin, M. S. *Electroanalysis* **2006**, *18*, 307-310.
- (126) Fischer, D. J.; Vandaveer, W. R.; Grigsby, R. J.; Lunte, S. M. *Electroanalysis* **2005**, *17*, 1153-1159.
- (127) Wang, Y.; Fice, D. S.; Yeung, P. K. F. *Journal of Pharmaceutical and Biomedical Analysis* **1999**, *21*, 519-525.
- (128) Schulze, H. G.; Greek, L. S.; Barbosa, C. J.; Blades, M. W.; Gorzalka, B. B.; Turner, R. F. B. *Journal of Neuroscience Methods* **1999**, *92*, 15-24.
- (129) Afkhami, A.; Nematollahi, D.; Khalafi, L.; Rafiee, M. *International Journal of Chemical Kinetics* **2005**, *37*, 17-24.
- (130) Luczak, T. *Electroanalysis* **2008**, *20*, 1639-1646.
- (131) Lowry, J. P.; O'Neill, R. D. **2006**; American Scientific Publishers; 501-523.
- (132) Li, Y.; Liu, M.; Xiang, C.; Xie, Q.; Yao, S. *Thin Solid Films* **2006**, *497*, 270-278.
- (133) Zheng, J.; Zhou, X. *Bioelectrochemistry* **2007**, *70*, 408-415.
- (134) Henstridge, M. C.; Dickinson, E. J. F.; Aslanoglu, M.; Batchelor-McAuley, C.; Compton, R. G. *Sensors and Actuators B: Chemical* **2010**, *145*, 417-427.
- (135) Rubianes, M. D.; Rivas, G. A. *Anal. Chim. Acta* **2001**, *440*, 99-108.
- (136) Zhang, L.; Jiang, X. *J. Electroanal. Chem.* **2005**, *583*, 292-299.
- (137) Majewska, U. E.; Chmurski, K.; Biesiada, K.; Olszyna, A. R.; Bilewicz, R. *Electroanalysis* **2006**, *18*, 1463-1470.
- (138) Berduque, A.; Zazpe, R.; Arrigan, D. W. M. *Anal. Chim. Acta* **2008**, *611*, 156-162.
- (139) Beni, V.; Ghita, M.; Arrigan, D. W. M. *Biosens. Bioelectron.* **2005**, *20*, 2097-2103.
- (140) Weng, J.; Xue, J.; Wang, J.; Ye, J.-S.; Cui, H.; Sheu, F.-S.; Zhang, Q. *Advanced Functional Materials* **2005**, *15*, 639-647.
- (141) Shervedani, R. K.; Bagherzadeh, M.; Mozaffari, S. A. *Sens. Actuator B-Chem.* **2006**, *115*, 614-621.
- (142) Zhang, L.; Jia, J.; Zou, X.; Dong, S. *Electroanalysis* **2004**, *16*, 1413-1418.

- (143) Liu, T.; Li, M.; Li, Q. *Talanta* **2004**, *63*, 1053-1059.
- (144) Wang, Q.; Jiang, N.; Li, N. *Microchemical Journal* **2001**, *68*, 77-85.
- (145) Zhang, L.; Jiang, X. *J. Electroanal. Chem.* **2005**, *583*, 292-299.
- (146) Wang, Q.; Dong, D.; Li, N. *Bioelectrochemistry* **2001**, *54*, 169-175.
- (147) Zhang, H.-M.; Li, N.-Q.; Zhu, Z. *Microchem. J.* **2000**, *64*, 277-282.
- (148) Keeley, G. P.; Lyons, M. E. G. *Int. J. Electrochem. Sci.* **2009**, *4*, 794-809.
- (149) Ali, S. R.; Parajuli, R. R.; Balogun, Y.; Ma, Y.; He, H. *Sensors* **2008**, *8*, 8423-8452.
- (150) Wu, K.; Fei, J.; Hu, S. *Anal. Biochem.* **2003**, *318*, 100-106.
- (151) Jo, S.; Jeong, H.; Bae, S. R.; Jeon, S. *Microchem. J.* **2008**, *88*, 1-6.
- (152) Chen, S. M.; Chzo, W. Y. *Journal of Electroanalytical Chemistry* **2006**, *587*, 226-234.
- (153) Shahrokhian, S.; Zare-Mehrjardi, H. R. *Sensors and Actuators B: Chemical* **2007**, *121*, 530-537.
- (154) Hosseinzadeh, R.; Sabzi, R. E.; Ghasemlu, K. *Colloids Surf., B* **2009**, *68*, 213-217.
- (155) Kang, G.; Lin, X. *Electroanalysis* **2006**, *18*, 2458-2466.
- (156) Jiang, X.; Lin, X. *Analytica Chimica Acta* **2005**, *537*, 145-151.
- (157) Thiagarajan, S.; Chen, S.-M. *Talanta* **2007**, *74*, 212-222.
- (158) Huang, J.; Liu, Y.; Hou, H.; You, T. *Biosensors and Bioelectronics* **2008**, *24*, 632-637.
- (159) Shakkthivel, P.; Chen, S.-M. *Biosensors and Bioelectronics* **2007**, *22*, 1680-1687.
- (160) Song, S.; Gao, Q.; Xia, K.; Gao, L. *Electroanalysis* **2008**, *20*, 1159-1166.
- (161) Zhang, Y.; Jin, G.; Wang, Y.; Yang, Z. *Sensors* **2003**, *3*, 443-450.
- (162) Zhao, H.; Zhang, Y.; Yuan, Z. *Anal. Chim. Acta* **2001**, *441*, 117-122.
- (163) Hou, S.; Zheng, N.; Feng, H.; Li, X.; Yuan, Z. *Anal. Biochem.* **2008**, *381*, 179-184.
- (164) Zhou, Y. Z.; Zhang, L. J.; Chen, S. L.; Dong, S. Y.; Zheng, X. H. *Chin. Chem. Lett.* **2009**, *20*, 217-220.
- (165) Raoof, J.-B.; Ojani, R.; Rashid-Nadimi, S. *Electrochim. Acta* **2005**, *50*, 4694-4698.
- (166) Lin, X.; Zhang, Y.; Chen, W.; Wu, P. *Sensors and Actuators B: Chemical* **2007**, *122*, 309-314.

- (167) Zhang, R.; Jin, G.-D.; Chen, D.; Hu, X.-Y. *Sensors and Actuators B: Chemical* **2009**, *138*, 174-181.
- (168) Li, Y.; Wang, P.; Wang, L.; Lin, X. *Biosens. Bioelectron.* **2007**, *22*, 3120-3125.
- (169) Ghita, M.; Arrigan, D. W. M. *Electrochim. Acta* **2004**, *49*, 4743-4751.
- (170) Roy, P. R.; Okajima, T.; Ohsaka, T. *Bioelectrochemistry* **2003**, *59*, 11-19.
- (171) Lin, X.; Zhuang, Q.; Chen, J.; Zhang, S.; Zheng, Y. *Sens. Actuator B-Chem.* **2007**, *125*, 240-245.
- (172) Lin, L.; Chen, J.; Yao, H.; Chen, Y.; Zheng, Y.; Lin, X. *Bioelectrochemistry* **2008**, *73*, 11-17.
- (173) Mathiyarasu, J.; Senthilkumar, S.; Phani, K. L. N.; Yegnaraman, V. *Materials Letters* **2008**, *62*, 571-573.
- (174) Gopalan, A. I.; Lee, K.-P.; Manesh, K. M.; Santhosh, P.; Kim, J. H.; Kang, J. S. *Talanta* **2007**, *71*, 1774-1781.
- (175) Yuan, S.; Chen, W.; Hu, S. *Materials Science and Engineering: C* **2005**, *25*, 479-485.
- (176) Zheng, D.; Ye, J.; Zhou, L.; Zhang, Y.; Yu, C. *Journal of Electroanalytical Chemistry* **2009**, *625*, 82-87.
- (177) Salimi, A.; Abdi, K.; Khayatian, G. R. *Microchim. Acta* **2004**, *144*, 161-169.
- (178) Alpat, S.; Alpat, S. K.; Telefoncu, A. *Anal. Bioanal. Chem.* **2005**, *383*, 695-700.
- (179) Lai, G.-S.; Zhang, H.-L.; Han, D.-Y. *Microchim. Acta* **2008**, *160*, 233-239.
- (180) Ferreira, M.; Dinelli, L. R.; Wohnrath, K.; Batista, A. A.; Oliveira, O. N. *Thin Solid Films* **2004**, *446*, 301-306.
- (181) Zucolotto, V.; Ferreira, M.; Cordeiro, M. R.; Constantino, C. J. L.; Moreira, W. C.; Oliveira, J. O. N. *Sensors and Actuators B: Chemical* **2006**, *113*, 809-815.
- (182) Zhou, L.; Shang, F.; Pravda, M.; Glennon, J. D.; Luong, J. H. T. *Electroanalysis* **2009**, *21*, 797-803.
- (183) Wang, Z.; Chen, Y. *Huaxue Tongbao* **2001**, 243-244, 242.
- (184) Nikolelis, D. P.; Petropoulou, S.-S. E.; Pergel, E.; Toth, K. *Electroanalysis* **2002**, *14*, 783-789.

- (185) Herzog, G.; McMahon, B.; Lefoix, M.; Mullins, N. D.; Collins, C. J.; Moynihan, H. A.; Arrigan, D. W. M. *J. Electroanal. Chem.* **2008**, *622*, 109-114.
- (186) Snejdarkova, M.; Poturnayova, A.; Rybar, P.; Lhotak, P.; Himl, M.; Flidrova, K.; Hianik, T. *Bioelectrochemistry* **2010**, *80*, 55-61.
- (187) Lai, G.-S.; Zhang, H.-L.; Jin, C.-M. *Electroanalysis* **2007**, *19*, 496-501.

CHAPTER 2

Experimental:

Materials, Methods and Techniques

2.1 Introduction

The present research work is concerned with the preparation, characterisation and applications of a conducting polypyrrole modified electrode. Polypyrrole (PPy) was electrochemically deposited on different electrode substrates, the primary substrate being platinum, in the presence of a dopant molecule. The dopant of choice for these PPy films was the water soluble calixarene, *p*-sulfonatocalix[4]arene (C4S). The resulting PPy-C4S films were characterised using electrochemical techniques (cyclic voltammetry and electrochemical impedance spectroscopy) and surface analytical techniques (scanning electron microscopy and energy dispersive x-ray spectroscopy). The PPy-C4S modified electrodes were then optimised for the electrochemical detection of dopamine (DA), and calibration curves were generated using cyclic voltammetry and constant potential amperometry. Lastly, the mode in which the PPy-C4S film could detect DA was investigated. The solution interaction of C4S with DA and several interferent compounds was studied using NMR spectroscopy, and the selectivity of the sensor towards DA, in the presence of these interferent compounds, was explored using cyclic voltammetry.

In this chapter, the various materials and methods used throughout this work are described in detail. A brief description of the theoretical background for each of the different experimental techniques is also provided.

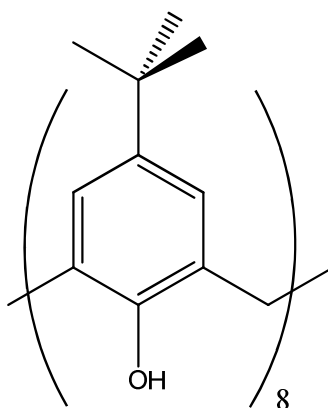
2.2 Chemicals and Synthesis

Unless otherwise stated, all chemicals and solvents used in this work were purchased from Sigma-Aldrich. Pyrrole was distilled under vacuum and stored under nitrogen in the dark at -20°C . Toluene was dried by reflux over sodium wire and stored under nitrogen. High purity nitrogen gas (99.95 %) was supplied by BOC. All other chemicals were of analytical reagent grade and used as received. The electrochemical electrolyte solutions were prepared in distilled water.

2.2.1 Synthesis of *p*-Sulfonatocalix[4]arene (C4S)

The synthesis of C4S was carried out in four steps using the methods outlined by Gutsche¹⁻³ and Shinkai⁴.

Step 1: Synthesis of 5,11,17,23,29,35,41,47-octa-*tert*-butyl-49,50,51,52,53,54,55,56-octahydroxycalix[8]arene¹ (1).



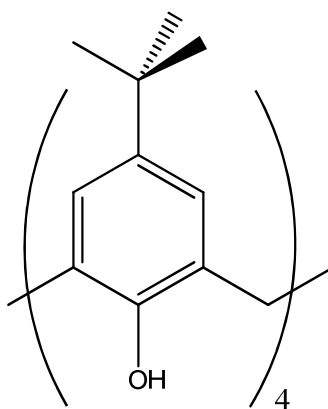
A slurry of *p-tert*-butylphenol (56.0 g, 0.36 mol), *para*formaldehyde (18.0 g, 0.60 mol) and 10 M KOH (0.8 cm³, 8 mmol) in xylene (250 cm³) was refluxed with stirring for 4 h in a 1000 cm³ flask equipped with a Dean Stark water collector. The reaction mixture was then cooled, and the precipitate was isolated by filtration. The solid product was washed in succession with 150 cm³ portions of toluene, ether, acetone, and water and then dried in an oven at 50°C overnight.

Yield: 47.6 g, 81 %

¹H NMR (CDCl₃): (δ ppm)

9.62 (s, 8H, Ar-OH), 7.18 (s, 16H, Ar-H), 4.37 (br d, 8H, CH₂, *J* = 12.9 Hz), 3.50 (br d, 8H, CH₂, *J* = 12.9 Hz), 1.25 (s, 72H, C(CH₃)).

Step 2: Synthesis of 5,11,17,23-tetra-*tert*-butyl-25,26,27,28-tetrahydroxycalix[4]arene² (2).

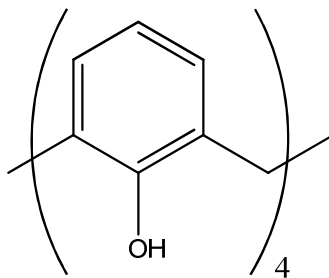


A slurry of **1** (22.0 g, 16.0 mmol) and 10 M NaOH (0.5 cm³, 5.0 mmol) in diphenyl ether (200 cm³) was refluxed for 1.5 h in a 1000 cm³ flask equipped with a Dean Stark water collector. The reaction mixture was cooled and treated with ethyl acetate (200 cm³). The precipitate was isolated by filtration and washed in succession with 100 cm³ portions of toluene, ether, acetone and water, and dried in an oven at 50°C overnight.

Yield: 14.9 g, 68%

¹H NMR (CDCl₃): (δ ppm)

10.34 (s, 4H, Ar-OH), 7.05 (s, 8H, Ar-H), 4.25 (br d, 4H, CH₂, *J* = 12.6 Hz), 3.49 (br d, 4H, CH₂, *J* = 12.6 Hz), 1.21 (s, 36H, C(CH₃)).

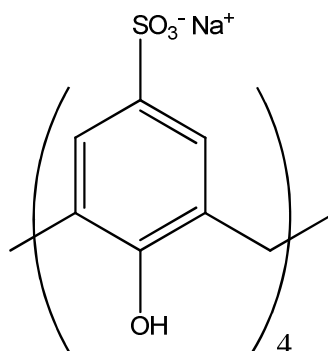
Step 3: Synthesis of 25,26,27,28-tetrahydroxycalix[4]arene³ (3).

A slurry of **2** (5.0 g, 7.5 mmol), phenol (3.4 g, 36.0 mmol) and AlCl_3 (5.3 g, 39.5 mmol) in toluene (50 cm^3) was stirred at room temperature for 4 h in an inert atmosphere. The mixture was poured into 0.2 M HCl (100 cm^3), the organic layer was separated and the toluene was evaporated under reduced pressure. Upon addition of methanol a precipitate formed, which was recovered by filtration. The final product was recrystallised from methanol/chloroform.

Yield: 2.3 g, 70%

^1H NMR (CDCl_3): (δ ppm)

10.20 (s, 4H, Ar-OH), 7.05 (d, 8H, Ar-H, $J = 7.7 \text{ Hz}$), 6.73 (t, 4H, Ar-H, $J = 7.7 \text{ Hz}$), 4.25 (s, 4H, CH_2), 3.55 (s, 4H, CH_2).

Step 4: Synthesis of *p*-sulfonatocalix[4]arene⁴ (C4S).

Compound **3** (1.0 g, 2.4 mmol) was mixed with concentrated H₂SO₄ (10 cm³) and the solution was heated at 60°C for 4 h. An aliquot was withdrawn from the reaction mixture and poured into water to determine the progress of the reaction. The reaction was completed when no water-insoluble material was detected in the aliquot. After cooling, the precipitate was filtered off through a sintered glass filter. The precipitate was dissolved in water and the aqueous solution was neutralised by CaCO₃. Precipitated CaSO₄ was filtered off and washed with hot water. The combined filtrate and washings were evaporated to dryness under reduced pressure. The residue was dissolved in hot water (15 cm³) and the solution was adjusted to pH 8 by addition of Na₂CO₃. After filtration, methanol was added to the filtrate to afford a white precipitate. The product was recovered by filtration and tested for carbonate impurities using infrared spectroscopy. To remove these impurities the product was dissolved in boiling distilled water and any insoluble material was removed by filtration. The product was then precipitated from solution by the addition of methanol, recovered by filtration and retested using infrared spectroscopy. This process was repeated until the carbonate signal in the infrared spectrum was no longer observed.

Yield: 1.3 g, 55%

ν_{\max} / cm⁻¹ (KBr):

(OH) 3447, (SO₃⁻) 1179 and 1048.

^1H NMR (D_2O): (δ ppm)

7.47 (s, 8H, Ar-H), 3.92 (s, 8H, CH_2).

 ^{13}C NMR (D_2O): (δ ppm)

155.7, 133.5, 130.4, 125.9, 31.8.

Microanalysis (C,H,S,Na,Ca):

The analysis of several samples showed a variation in the water content and stoichiometry of the counterions for C4S. Therefore, a general molecular formula, $\text{Ca}_x\text{Na}_{5-2x}\text{C}_{28}\text{H}_{19}\text{O}_{16}\text{S}_4$ ($y\text{H}_2\text{O}$), was proposed. However, the molar concentrations of the C4S solutions used in this work were calculated from the approximated molecular formula $\text{CaNa}_3\text{C}_{28}\text{H}_{19}\text{O}_{16}\text{S}_4 \cdot 9\text{H}_2\text{O}$. The number of water molecules was based on the average literature values⁴⁻⁷.

2.3 Experimental Setup

2.3.1 Apparatus

Most of the electrochemical experiments in this work were carried out using a Solartron potentiostat (Model SI 1285A). Constant potential amperometry was performed on a Chi440 potentiostat (Model EA160). The rotating disk electrode for this experiment was a Pine MRS Rotor System equipped with a platinum E3 Series RDE tip. Electrochemical impedance spectroscopy was carried out with a Solartron potentiostat (Model SI 1287) coupled to a Solartron frequency response analyser (Model SI 1255A). Each potentiostat was controlled by a computer unit and the various software packages used were CorrWare for WindowsTM (Version 2.1), Chi440 software (Version 1.0.0.1) and Zplot (Version 2.1), respectively.

Scanning electron microscopy (SEM) and energy dispersive x-ray spectroscopy (EDX) were performed using two different setups. Most of the analysis was carried out in the Tyndall National Institute at University College Cork, on a Hitachi S-4000 with a cold cathode field emission electron source (FE-SEM), maximum magnification 300,000x and resolution of 1.5 nm. This microscope was equipped with Princeton Gamma Technology Avalon 8000 EDX system with a liquid nitrogen cooled Li(Si) detector. Some analysis was also carried out at NUI Maynooth on a Hitachi S-3200-N with a tungsten filament electron source, maximum magnification of 300,000x and resolution of 3.5 nm. This microscope was equipped with an Oxford Instrument INCAx-act EDX system with a silicon drift detector. In order to obtain high resolution images the samples were sputter coated with gold or gold/palladium ultrathin films with an AGAR Automatic Sputter Coater equipped with an AGAR Terminating Film Thickness Monitor unit.

Thickness measurements for the PPy-C4S films were carried out in the Tyndall National Institute at University College Cork using a KLA Tencor P15 stylus profilometer.

The majority of the NMR spectroscopy experiments were performed at NUI Maynooth using a Shielded Bruker Avance AV 300 high performance digital NMR spectrometer complete with Bruker Avance 300 digital single bay AV NMR console,

Ultrasield 300 MHz magnet and QNP 5 mm probe. However, some of the rotating-frame nuclear Overhauser effect NMR experiments were performed in Trinity College Dublin using a Bruker Avance AV 400 digital NMR spectrometer with an Ultrasield 400 MHz magnet and a QNP 5 mm probe. Both spectrometers were controlled by a computer unit using the software package TopSpin (Version 2.0). In each NMR experiment, the sample was held at 25°C while the spectrum was recorded.

2.3.2 The Electrochemical Cell

All the electrochemical experiments discussed in this work were carried out in a standard three electrode cell at room temperature and pressure. Figure 2.1 shows a schematic of the typical electrochemical setup. This setup consisted of a working electrode (WE), which was a regular (1) or flat disk electrode (2), a reference electrode (RE), and a counter electrode (CE). The electrochemical cell itself was a glass cylinder of 10 or 20 ml volume that had a Teflon lid with openings for the electrodes, a gas inlet and aliquots addition. However, a larger cell was required for experiments involving rotating disk voltammetry. In these experiments, a 50 ml volume of solution was required due to the size of the rotating disk electrode. The three electrodes were immersed in the electrolyte solution and were connected to a potentiostat, which was controlled by a computer unit. When necessary, a micropipette (mp) was used to add known aliquots of certain solutions to the electrolyte solution. In some experiments, a cylinder of nitrogen gas (gc) was required. In cases where the electrolyte solution needed to be stirred a magnetic stirrer (ms) was used.

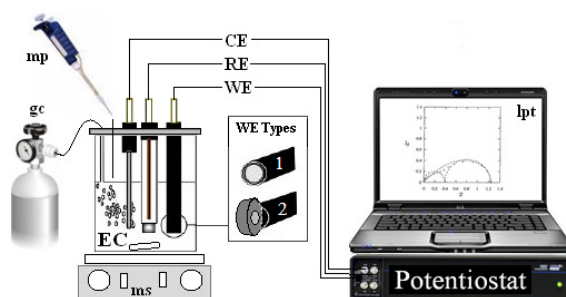
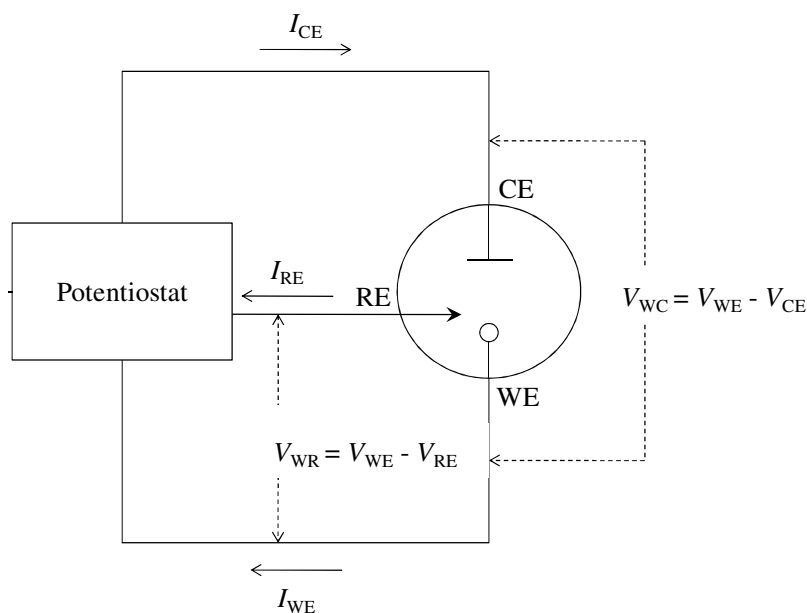


Figure 2.1: The general experimental setup used to record all electrochemical measurements.

The mode of operation of the potentiostat is summarized in Scheme 2.1. The function of the potentiostat was to control the potential, V_{WE} , and the current, I_{WE} , of the WE. V_{WE} could be controlled by monitoring the potential difference between the WE and the RE ($V_{WR} = V_{WE} - V_{RE}$), since V_{RE} was constant. A high input impedance was applied to the RE by the potentiostat resulting in negligible current flow through RE, so I_{RE} is taken as zero. It follows that the current flow in the cell was between WE and CE, $I_{WE} = I_{CE}$. In order to sustain this current, the potential difference between WE and CE ($V_{WC} = V_{WE} - V_{CE}$) needed to be adjusted accordingly. This was only possible by changing V_{CE} since V_{WE} was fixed. Thus, I_{WE} could be controlled by adjusting V_{CE} .



Scheme 2.1: Schematic representation of the mode of operation of the potentiostat.

2.3.3 Electrode Materials and Preparation

The working electrodes (WE), both regular and flat, were prepared from rods of high purity glassy carbon (GC), gold, and platinum (99.99+ %, 4.0 mm in diameter) which were supplied by Goodfellow Cambridge Ltd. To assemble the electrode a piece of rod, approximately half a centimeter in length, was cut and a copper wire was attached to one end of the piece using a highly conducting silver-loaded resin. This formed the electrical contact, the quality of which was checked with a

multimeter to ensure that the resistance between the surface of the electrode and the connection to the potentiostat was lower than 1.0Ω . The wire was then threaded through a Teflon holder and the piece of rod was set in the holder, with epoxy resin, in such a way as to leave the end of the rod exposed. Prior to each experiment, the working electrodes were polished to a mirror finish using, in order, 30, 15, 6 and $1 \mu\text{m}$ diamond suspensions on microcloth supplied by Buehler, sonicated in distilled water and then ethanol, and finally rinsed with distilled water. If the electrode surface was coated in a polymer film, a Buehler METASERV grinder polisher with Buehler SiC grinding paper (Grit P 2500) was used to remove the polymer before the electrode surface was polished.

The reference electrode (RE) was a saturated calomel electrode (SCE). The internal solution of the reference electrode was changed regularly using a saturated solution of super-purum KCl (99.999+ %) supplied by Merck.

The counter electrode (CE) was a high surface area wire of high purity platinum (99.99+ %) supplied by Goodfellow Cambridge Ltd. Before every set of experiments, the counter electrode was brushed with Buehler SiC grinding paper (Grit P 2500), smooth cleaned with a cloth, sonicated in distilled water and finally rinsed with distilled water.

2.4 Experimental Procedure

2.4.1 Electrosynthesis of the PPy-C4S Film

The PPy-C4S films were deposited potentiostatically onto the different substrates. This method involved applying a constant potential to the electrode and recording the current as a function of time. The substrates used were Pt, Au and GC. The standard procedure used to prepare the PPy-C4S films is outlined below. Any variations to this method are given in the relevant sections.

In general, the PPy-C4S films were deposited on a Pt electrode. The polymerization solution consisted of pyrrole, 0.20 mol dm^{-3} , and C4S, 0.01 mol dm^{-3} , dissolved in 10 ml distilled water. The polymer was grown at a constant potential of 0.500 V vs. SCE. The electropolymerisation was stopped once a charge of 0.24 C cm^{-2} was reached. The electrode was then removed from the polymerization solution and rinsed with distilled water.

2.4.2 Characterisation of the PPy-C4S Film.

All electrochemical characterization experiments were carried out in aqueous $0.10 \text{ mol dm}^{-3} \text{ Na}_2\text{SO}_4$ solutions.

2.4.2 (i) Cyclic Voltammetry

PPy-C4S films were prepared using the standard procedure outlined in Section 2.4.1. Cyclic voltammetry profiles for these films were recorded over several potential ranges at varying scan rates. The specific values for these parameters are highlighted in the relevant sections.

Cyclic voltammetry was also used to measure the capacitance of the PPy-C4S film. For these experiments, PPy-C4S films were grown to charges of 0.04, 0.08, 0.12, 0.16, 0.20 and 0.24 C cm^{-2} . The freshly prepared PPy-C4S films were cycled 20 times, between the potentials -0.200 V and 0.800 V vs. SCE, at a scan rate of 100 mV s^{-1} . This was done to obtain a reproducible background current, *i.e.* to ensure the processes within the film had reached a steady state. Then, the polymer films

were cycled 5 times, between the potentials 0.100 V and 0.200 V vs. SCE, at scan rates of, 5, 25, 50, 75, 100, 125, 150 and 200 mV s^{-1} . The current at 0.150 V vs. SCE was recorded and plotted as a function of the scan rate.

2.4.2 (ii) *Electrochemical Impedance Spectroscopy (EIS)*

EIS spectra were recorded at potentials in the range -0.800 V to 0.500 V vs. SCE for PPy-C4S films prepared using the standard procedure outlined in Section 2.4.1. Each impedance measurement was carried out on a freshly prepared PPy-C4S film that had been cycled 20 times, between the potentials -0.200 V and -0.800 V vs. SCE, at a scan rate of 100 mV s^{-1} . Again this ensured a steady state within the polymer. Prior to each impedance measurement the polymer film was equilibrated for 30 min at the applied potential. The frequency response was then recorded between 60 kHz and 10 mHz using a sinusoidal voltage with an amplitude of 10 mV.

2.4.2 (iii) *Scanning Electron Microscopy (SEM) and Energy Dispersive X-ray Spectroscopy (EDX)*

SEM and EDX analysis were performed on PPy-C4S films that had been deposited on a Pt flat disk electrode. The PPy-C4S films were electrosynthesised at 0.500 V and 0.800 V vs. SCE using the standard procedure outlined in Section 2.4.1.

2.4.2 (iv) *Thickness Measurements for the PPy-C4S Film*

PPy-C4S films were deposited on one half of the surface of a flat Pt disk electrode. This was achieved by placing a small piece of electrical tape on the surface of the electrode so that approximately half the surface area was covered. The PPy-C4S films were then electrosynthesised on this electrode, using the standard procedure outlined in Section 2.4.1, until charges of 0.08, 0.16 and 0.24 C cm^{-2} were reached. Two polymer films were grown to each charge and thickness measurements were recorded at three different sites for each film.

2.4.3 The Detection of DA at the PPy-C4S Modified Electrode

The ability of the PPy-C4S modified electrode to sense DA was investigated using cyclic voltammetry and constant potential amperometry. First, cyclic voltammetry was used to optimize the PPy-C4S film for the detection of DA. Then, the PPy-C4S modified electrode was calibrated for the detection of DA using cyclic voltammetry and constant potential amperometry.

2.4.3 (i) Cyclic Voltammetry

All DA solutions were prepared using a supporting electrolyte solution. The electrolyte was either an inorganic salt (sodium sulfate or sodium chloride) or a buffer solution (sodium ethanoate buffer or phosphate buffered saline (PBS)). The sodium ethanoate buffer was prepared by mixing 100 cm³ of a 1.0 mol dm⁻³ sodium ethanoate solution and 62.5 cm³ of 1.0 mol dm⁻³ ethanoic acid and then diluting the mixture to 1000 cm³ with distilled water. The PBS was prepared by dissolving 8.00 g NaCl, 0.20 g KCl, 1.44 g Na₂HPO₄ and 0.24 g KH₂PO₄ in 800 cm³ distilled water, adjusting the pH and then diluting to 1000 cm³ with distilled water. The inorganic salt solutions were prepared in various concentrations which are specified in the relevant sections. The most widely used supporting electrolyte was a 0.10 mol dm⁻³ Na₂SO₄ solution. For the most part, the electrolyte solutions were used as prepared, however, in some cases the pH of the solution was adjusted using 1.0 mol dm⁻³ H₂SO₄ or 1.0 mol dm⁻³ NaOH.

Unless otherwise stated, all DA peak currents have been reported in the form $I_p - I_{Bg}$ where I_p is the observed peak current and I_{Bg} is the background current. The method used to estimate I_{Bg} , is illustrated in Figure 2.2. The current value at the intersection of the two lines gives I_{Bg} and this is then subtracted from I_p to give the background corrected DA peak current.

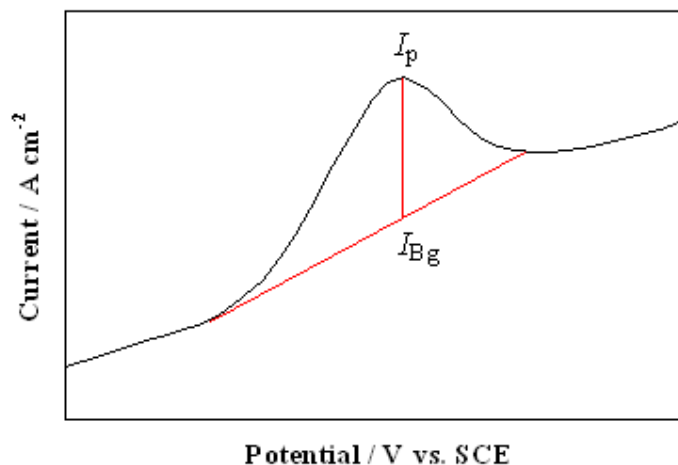


Figure 2.2: Illustration of the method used to determine the background current, I_{Bg} , at the peak potential for DA.

To optimize the PPy-C4S film for the detection of DA, the conditions used to prepare the PPy-C4S film and the parameters for cyclic voltammetry were varied individually. In general, the DA solutions were analysed using the following procedure. The PPy-C4S film was electrosynthesised using the standard procedure outlined in Section 2.4.1. The freshly prepared PPy-C4S modified electrode was cycled 20 times in a $0.10 \text{ mol dm}^{-3} \text{ Na}_2\text{SO}_4$ supporting electrolyte solution, between the potentials -0.200 V and 0.800 V vs. SCE , at a scan rate of 100 mV s^{-1} . This was done to produce a reproducible background current and to ensure that the polymer had reached a steady state. Then, using the same potential window and scan rate, the modified electrode was cycled 50 times in a DA solution of known concentration. Using this number of cycles allowed a steady state current to be reached at each concentration of DA and facilitated the adsorption of DA to the PPy-C4S film, preconcentrating it at the electrode surface. The individual changes to this procedure are specified in the relevant sections.

To calibrate the PPy-C4S film for DA, solutions of DA in the range 2.5×10^{-5} to $1.0 \times 10^{-3} \text{ mol dm}^{-3}$ were prepared. Each solution was analysed using the procedure outlined above. The DA peak currents were then plotted as a function of DA concentration.

2.4.3 (ii) Constant Potential Amperometry

DA calibration was also performed using constant potential amperometry. PPy-C4S films were grown on a Pt rotating disk electrode (RDE) using the standard procedure outlined in Section 2.4.1. The modified electrodes were then immersed in a $0.10 \text{ mol dm}^{-3} \text{ Na}_2\text{SO}_4$ supporting electrolyte solution. A constant potential of 0.650 V vs. SCE was applied to the RDE and the rotation speed was set at 2000 rpm . This rotation speed was at the higher end of the recommended range of rotation speeds for the RDE and was sufficient to obtain a mass-transport limiting current plateau. The corresponding amperometric signal was recorded as a function of time. Once the signal reached a plateau, a series of DA aliquots were added to the solution. At each addition the current step was registered as a response to the introduced DA. The aliquots were added with increasing concentration from 8.0×10^{-6} to $1.0 \times 10^{-3} \text{ mol dm}^{-3}$.

2.4.4 Interferent Studies

The ability of ascorbic acid (AA), uric acid (UA), 5-hydroxytryptamine (5-HT) and acetylcholine (Ach) to interfere in the detection of DA, at the PPy-C4S film, was studied using cyclic voltammetry. The general procedure followed for these studies is outlined below.

The PPy-C4S film was electrosynthesised using the standard procedure outlined in Section 2.4.1. The freshly prepared PPy-C4S modified electrode was cycled 20 times in a $0.10 \text{ mol dm}^{-3} \text{ Na}_2\text{SO}_4$ supporting electrolyte solution, between the potentials -0.200 V and 0.800 V vs. SCE , at a scan rate of 100 mV s^{-1} . Then, using the same potential window and scan rate, the modified electrode was cycled 50 times in the target solution.

The target solution was composed of either, $0.10 \text{ mol dm}^{-3} \text{ Na}_2\text{SO}_4$ and an interferent or $0.10 \text{ mol dm}^{-3} \text{ Na}_2\text{SO}_4$, an interferent and DA. The concentration of the interferent compound was either $1.0 \times 10^{-3} \text{ mol dm}^{-3}$, for AA, 5-HT and Ach, or $1.0 \times 10^{-4} \text{ mol dm}^{-3}$ for UA. The concentration of UA was limited to this value due to

solubility considerations. The concentrations of DA used were 2.5×10^{-5} , 5.0×10^{-5} , 1.0×10^{-4} , 2.5×10^{-4} or 1.0×10^{-3} mol dm⁻³.

2.4.5 NMR Complexation Studies

NMR spectroscopy was used to study the complexation interaction between C4S and DA, 5-HT and Ach. In all cases, the NMR solutions were prepared in deuterium oxide (D₂O) and contained 0.3 mol dm⁻³ KCl. All NMR experiments were carried out at 25°C.

To determine if an inclusion complex could form between C4S and DA the ¹H NMR spectra of DA in the presence and absence of C4S were recorded. The concentration of DA in these solutions was 0.03 mol dm⁻³ and the concentration of C4S used was 0.06 mol dm⁻³. The chemical shifts observed for the DA proton signals in each spectrum were recorded and compared. Similar experiments were carried out for 5-HT and Ach. Further studies on the complex formed between C4S and DA were then performed using Job's method, NMR titration and rotating-frame nuclear Overhauser effect spectroscopy.

2.4.5 (i) Job's Method

Job's method was used to determine the stoichiometry of the complex formed between C4S and DA. A series of solutions containing DA and C4S in varying ratios were prepared, so that a complete range of mole fractions of DA (from 0 to 1) was covered. The total molarity of each solution, that is, the concentration of DA plus the concentration of C4S, remained constant at 0.05 mol dm⁻³. ¹H NMR spectra were then recorded for each solution and the product $X_{DA}\Delta\delta$ was plotted as a function of the mole fraction of DA (X_{DA}) where $\Delta\delta$ was the change in chemical shift observed for the proton signals of DA.

2.4.5 (ii) NMR Titration

An NMR titration was performed to determine the association constant (K_a) for the complex formed between DA and C4S. A series of solutions containing 0.03 mol dm^{-3} DA and varying concentrations of C4S, from zero to 0.15 mol dm^{-3} , were prepared. ^1H NMR spectra were recorded for each of these solutions and $\Delta\delta$ was plotted as a function of the molar ratio of C4S to DA.

2.4.5 (iii) Rotating-Frame Nuclear Overhauser Effect (ROE) Spectroscopy

ROE spectroscopy was used to study the structure of the complex formed between DA and C4S. A ^1H NMR spectrum was recorded for a solution containing 0.06 mol dm^{-3} DA and 0.03 mol dm^{-3} C4S. The resonance frequencies for the DA and C4S proton signals were noted. Each signal was then irradiated individually, using the Selrogp pulse program, and the resulting ROE spectra were recorded. The power level of the ROE spinlock pulse (PL11) was 25 dB and the pulse length (P15) was 0.2 s. The relaxation delay (D1) was 2.0 s.

2.5 Experimental Techniques

2.5.1 Electrochemistry

The two fundamental observables of any electrochemical system are the current (I) and potential (E). The potential is the driving force of the current. A typical electrochemical experiment consists of controlling one of the two observables while recording the time evolution of the other. Notably, the response of the electrochemical system to the external perturbation is influenced by many variables such as the nature and morphology of the materials, the concentration of the species in solution and the temperature. A range of electrochemical techniques were used in this study and brief details on each are provided in the following sections.

2.5.1 (i) Constant Potential Amperometry

Constant potential amperometry consists of applying a fixed potential, E , to an electrode in contact with an electroactive system and recording the current as a function of time, $I = f(t)$. The shape of the current-time response is dependent on several factors such as time, potential, concentration, mass-transfer coefficients, kinetic parameters, and so on⁸. Two specific cases are described here.

In the first case, the redox reaction, $O + ne^- \rightleftharpoons R$, where both species are soluble in solution, is considered. If the potential applied to the electrode is sufficiently large, so that any species O at the electrode surface is instantaneously reduced and its surface concentration goes to zero, the reaction can be said to be under diffusion control. In this situation the current response of the system is given by the *Cottrell* equation⁸,

$$I = \frac{nFAD_O^{1/2} C_O^\infty}{\pi^{1/2} t^{1/2}} \quad \text{Eq(2.1)}$$

where, D_O is the diffusion coefficient ($\text{cm}^2 \text{s}^{-1}$) and C_O^∞ is the bulk concentration (mol cm^{-3}) of the oxidized species (O), n is the number of electrons involved in the redox process, F is Faraday's constant and A is the electrode area (cm^2). The same considerations are also valid for the oxidation of R .

The potential step profile for this experiment is shown in Figure 2.3a. E_1 is a potential at which no electrode reaction occurs. At time $t = 0$, a potential (E_2) in the diffusion controlled region is applied to the electrode. The corresponding current response, Figure 2.3b, decays asymptotically to zero with the square root of time due to progressive thickening of the diffusion layer. This relationship holds over relatively short time periods when the process is dominated by planar diffusion. However, at longer times the diffusion layer can be disrupted by the build up of density gradients and vibrations resulting in currents larger than those predicted by the *Cottrell* equation, Equation 2.1.

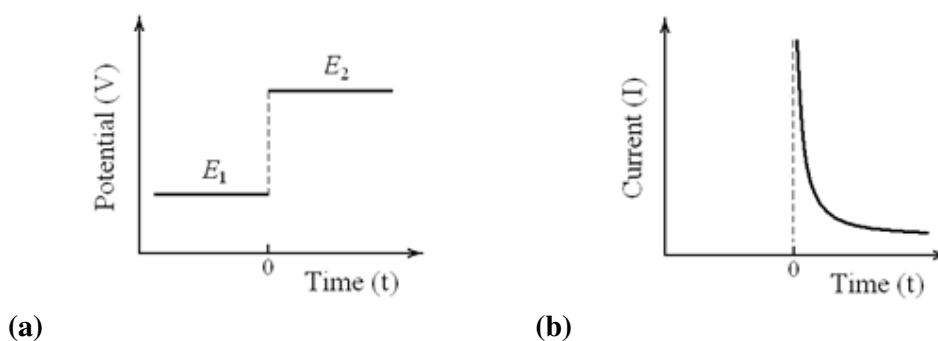


Figure 2.3: Chronoamperometric response of a redox couple following a potential step perturbation. (a) The potential is applied at time $t = 0$, the redox couple is active only at potential E_2 not at E_1 . (b) Diffusion controlled amperometric decay displaying the increasing thickness of the diffusion layer.

In the second case, potentiostatic electropolymerisation onto an electrode surface is considered. The shape of the current-time response for this process is dependent on the type of nucleation involved, the geometry of phase growth, and the rate determining step in phase formation⁹. In particular, Scharifker and Hills¹⁰ modelled the current-time transient for three-dimensional nucleation at multiple sites with diffusion controlled growth. They derived two theoretical diagnostic relationships to determine the type of nucleation process. For instantaneous nucleation, where all the nuclei are formed at the beginning of the pulse,

$$\left(\frac{I}{I_m}\right)^2 = \frac{1.9542}{t/t_m} \left\{1 - \exp\left[-1.2564\left(\frac{t}{t_m}\right)\right]\right\}^2 \quad Eq(2.2)$$

whereas for progressive nucleation, where nuclei are generated continuously during the growth period,

$$\left(\frac{I}{I_m}\right)^2 = \frac{1.2254}{t/t_m} \left\{1 - \exp\left[-2.3367\left(\frac{t}{t_m}\right)\right]\right\}^2 \quad \text{Eq(2.3)}$$

Here, I_m and t_m are the current and time, respectively, corresponding to the maximum in each transient.

The potential step profile for this experiment is shown in Figure 2.4a. The potential E_2 is sufficient to start the electropolymerisation process whereas no reaction occurs at E_1 . In practice, an incubation period is often observed in the current-time transients for potentiostatic polymer growth¹¹. This is illustrated in Figure 2.4b where the current falls to a minimum value after a short time. The incubation period arises because of the initial oxidation of the monomer. Following this period, the current-time transient takes on the typical shape for nucleation and growth. In their analysis, Scharifker and Hills¹⁰ took into account the effect of overlapping nuclei on the current response. At short times, the transients approach those predicted for non-overlapping nuclei. I_{free} increases linearly with $t^{1/2}$ in the case of instantaneous nucleation, and with $t^{3/2}$ in the case of progressive nucleation. For longer times, overlapping effects become more significant causing the current to go through a maximum with a following decrease, I_{overlap} .

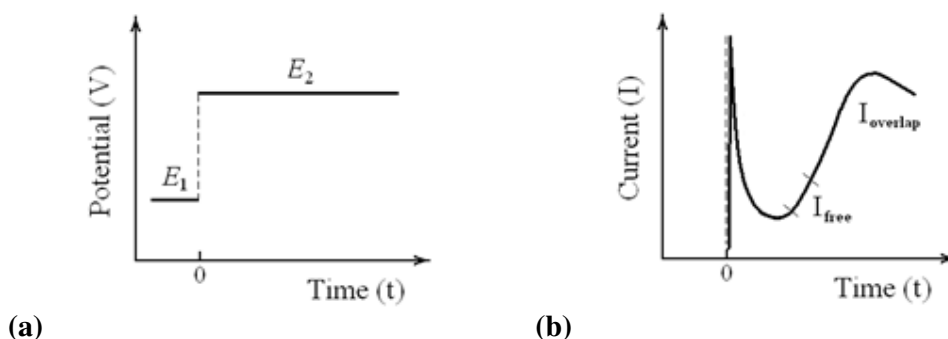


Figure 2.4: Chronoamperometric response of electropolymerisation following a potential step perturbation. (a) The potential is applied at time $t = 0$, the nucleation and growth are active only at potential E_2 not at E_1 . (b) Diffusion controlled amperometric response displaying the current of nucleation and growth without overlapping effects, I_{free} , and the current going through a maximum followed by a decrease due to the nuclei overlapping, I_{overlap} .

2.5.1 (ii) Cyclic Voltammetry

Cyclic voltammetry (CV) involves scanning the potential applied to the working electrode between two potential limits and recording the current as a function of the applied potential⁸. The potential is scanned linearly with time, from the initial potential, E_1 , to a potential, E_2 , at which point the scan is reversed. The scan rate (v) for conventional experiments ranges from mV to $V\ s^{-1}$. The resulting current-potential responses are useful for performing preliminary mechanistic investigations on a system⁹. The shape and scan rate dependence of these responses are characteristic of the reversibility of the redox process and whether the redox species are solution based or adsorbed on the electrode surface. For these reasons, cyclic voltammetry is the most popular technique for the initial study of an electrochemical system.

Typical current-potential curves for the four main CV responses are shown in Table 2.1. It can be seen from Table 2.1 that each response exhibits a peaked shape. This can be attributed to the formation and thickening of the diffusion layer^{8, 9}. Consider the forward (oxidation) scan of each response, as the potential is scanned in the positive direction, towards the standard potential of the redox process ($E^{0'}$), the current increases. This is due to an increase in oxidation of the reduced species. As the potential grows more positive, the surface concentration of the reduced species drops, causing a flux of this species to the electrode surface and a further increase in current. At potentials more positive than $E^{0'}$, the surface concentration of the reduced species goes to zero, and diffusion reaches a maximum. This results in a progressive thickening of the diffusion layer and a subsequent decline in the rate of diffusion. Consequently, the current also declines and a peaked current-potential curve is observed.

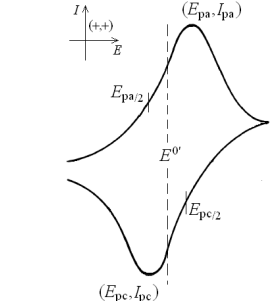
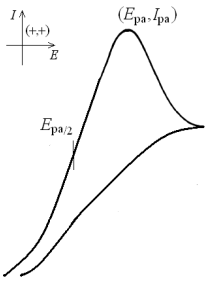
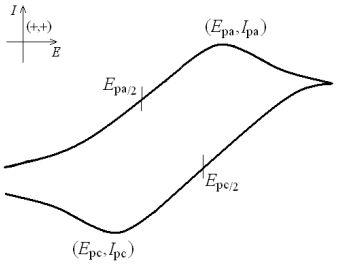
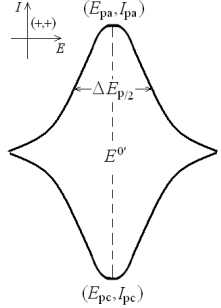
Each CV response in Table 2.1 can be described by three important parameters, the peak current (I_p), the peak potential (E_p) and the quantity $|E_p - E_{p/2}|$ where $E_{p/2}$ is the potential at half the height of the peak, otherwise known as the half-wave potential. Using these parameters, a series of diagnostic tests can be performed to characterise the electrochemical system⁹, some of which are summarised in Table 2.1. Of

particular interest is the dependence of I_p on the potential scan rate. For reversible systems, I_p varies linearly with $v^{1/2}$ according to the Randles-Sevcik equation⁸,

$$I_p = 2.69 \times 10^5 n^{3/2} A D^{1/2} c_0^\infty v^{1/2} \quad \text{Eq(2.4)}$$

where, n is the number of electrons transferred per mole of electroactive species, A is the area of the electrode (cm^2), D is the diffusion coefficient ($\text{cm}^2 \text{s}^{-1}$), c_0^∞ is the bulk concentration of the electroactive species (mol cm^{-3}) and v is the scan rate (V s^{-1}). Thus, if the experimental data fits Equation 2.4, the electrode reaction is under diffusion control and D can be obtained from the slope of a plot of I_p vs. $v^{1/2}$. A linear relationship between I_p and $v^{1/2}$ is also observed for irreversible systems, and, between I_p and v for reversible adsorbed species. For quasi-reversible systems, I_p increases with $v^{1/2}$ but is not proportional to it. The exact equations governing these relationships will not be dealt with here, see references^{8,9}.

Table 2.1: Cyclic voltammograms with their respective peak current (I_p) and peak potential (E_p) characteristics. The integer, n , is the number of electrons involved in the redox process, and α is the corresponding transfer coefficient. The factor $\Delta(\Lambda, \alpha)$ is a function of α and $\Lambda = k^0/(vDF/RT)^{1/2}$, where D is the diffusion coefficient of the electroactive species and k^0 is the standard heterogeneous rate constant. The values of this factor are available in the literature⁸.

Reversible	Irreversible
 <p style="text-align: center;">$I_p \propto v^{1/2}$</p> <p style="text-align: center;">E_p independent of v</p> <p style="text-align: center;">$E_p - E_{p/2} = 59/n \text{ mV}$</p>	 <p style="text-align: center;">$I_p \propto v^{1/2}$</p> <p style="text-align: center;">E_p increases as v increases</p> <p style="text-align: center;">$E_p - E_{p/2} = 48/\alpha n \text{ mV}^{12}$</p>
Quasi-reversible	Reversible Adsorption
 <p style="text-align: center;">I_p not proportional to $v^{1/2}$ as v increases</p> <p style="text-align: center;">E_p increases as v increases</p> <p style="text-align: center;">$E_p - E_{p/2} = 26\Delta(\Lambda, \alpha) \text{ mV}$</p>	 <p style="text-align: center;">$I_p \propto v$</p> <p style="text-align: center;">E_p independent of v</p> <p style="text-align: center;">$\Delta E_{p/2} = 90/n \text{ mV}$</p>

2.5.1 (iii) Rotating Disk Voltammetry (RDV)

The rotating disk electrode (RDE) is a disk electrode that is rotated in solution at a controlled angular speed, ω . This action establishes a well defined flow pattern of solution to the electrode surface (Figure 2.5). Effectively, the RDE acts as a pump, pulling the solution in a perpendicular direction towards the electrode surface and then distributing it radially and evenly on the disk⁹. An important conclusion of the mathematical description of these flow patterns is that the perpendicular flux of solution falls to zero at the electrode surface. In the Nernst diffusion layer model, this trend is described by the assumption of a boundary layer, close to the electrode surface, wherein the solution is totally stagnant and transport is only by diffusion⁹. The thickness, δ , of this layer is inversely proportional to $\omega^{1/2}$ according to Equation,

$$\delta = \frac{1.61\nu^{1/6}D^{1/3}}{\omega^{1/2}} \quad \text{Eq(2.5)}$$

where, ν is the kinematic viscosity of the solvent ($\text{cm}^2 \text{s}^{-1}$), D is the diffusion coefficient of the electroactive species ($\text{cm}^2 \text{s}^{-1}$) and ω is the angular velocity (rad s^{-1}). In this way, the thickness of the diffusion layer can be controlled by changing the rotation speed of the electrode.

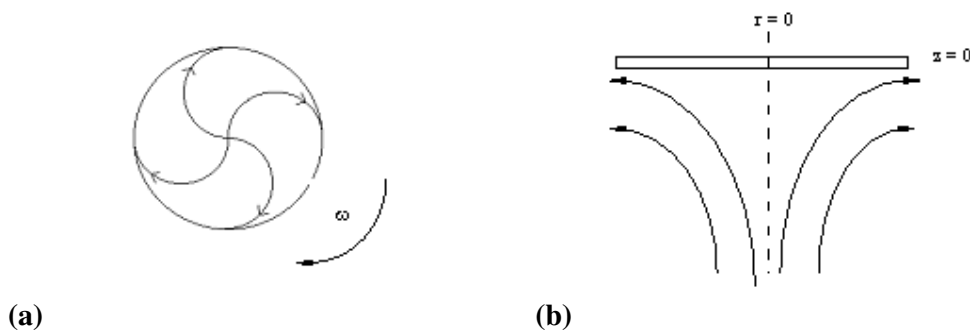


Figure 2.5: Flow patterns to the rotating disk electrode (RDE). (a) The electrode surface viewed from below. (b) The solution flow perpendicular to the electrode.

In a classical RDV experiment, a linear sweep voltammogram is performed at a slow scan rate, 1 to 10 mV s^{-1} , and the current is recorded as a function of the applied potential. Figure 2.6 illustrates the potential-time profile for this experiment and the

typical sigmoidal current-potential wave obtained. At potentials where the rate of electron transfer is high, the current becomes limited by the rate of mass transport and a plateau is observed. This mass-transport limited current, I_L , is given by the Levich equation⁸,

$$I_L = 0.62nFAD^{2/3}\nu^{-1/6}c^\infty\omega^{1/2} \quad \text{Eq(2.6)}$$

where, n is the number of electrons transferred per mole of electroactive species, F is Faraday's constant, A is the area of the electrode (cm^2) D is the diffusion coefficient ($\text{cm}^2 \text{s}^{-1}$) and c^∞ is the bulk concentration of electroactive species (mol cm^{-3}). It is clear from Equation 2.6 that I_L should increase linearly with $\omega^{1/2}$. Indeed, this is a useful test to determine if the current is entirely mass transport controlled⁹.

In this work, the RDE was used to provide a highly controlled mass transport regime for the amperometric detection of DA. This approach leads to higher currents, greater sensitivity and improved reproducibility due to the increased transport of electroactive species to the electrode surface⁹.

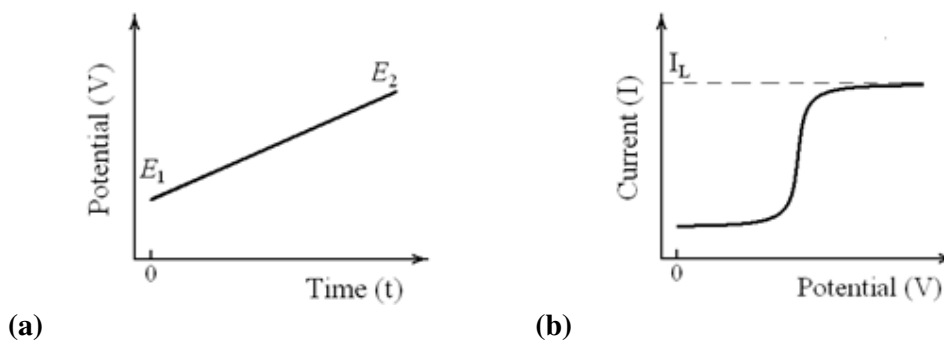


Figure 2.6: Voltammetric response of a potential sweep at a rotating disk electrode (RDE). (a) The potential sweep is applied at time $t = 0$, the potential rises linearly between the starting and ending potentials, E_1 and E_2 . (b) Voltammetric response under totally mass-transfer-limiting condition. The redox current starts in the middle of the potential scan and levels off at a limiting value I_L .

2.5.1 (iv) Electrochemical Impedance Spectroscopy (EIS)

Impedance (Z) is a measure of a circuit's ability to resist the flow of electrical current. It is defined by the ratio between the voltage (V) and the current (I) according to Equation 2.7,

$$Z = \frac{V}{I} \quad \text{Eq(2.7)}$$

where, V and I are sinusoidal signals. To measure the impedance of an electrochemical cell, a sinusoidal excitation voltage is applied to the system, over a range of frequencies, and the current response of the system is measured. The excitation voltage can be represented as follows,

$$V = V_0 \cos(\omega t) \quad \text{Eq(2.8)}$$

where, V_0 is the amplitude of the signal, ω is the frequency (rad s^{-1}) and t is time. Typically, the current response will also be sinusoidal and of the same frequency but different in amplitude and phase from the voltage,

$$I = I_0 \cos(\omega t - \phi) \quad \text{Eq(2.9)}$$

where, I_0 is the amplitude of the current and ϕ is the phase angle between the phasors representing the voltage and the current⁹.

In circuit analysis, it is advantageous to express the voltage and current as complex functions. This can be accomplished using Euler's relationship, giving the following expressions for V and I ,

$$V = V_0 e^{i\omega t} \quad \text{Eq(2.10)}$$

$$I = I_0 e^{i\omega t - i\phi} \quad \text{Eq(2.11)}$$

where, $i = \sqrt{-1}$. By substituting these expressions into Equation 2.7, the impedance can then be represented as a complex number^{9, 13},

$$Z = \frac{V_0 e^{i\omega t}}{I_0 e^{i\omega t - i\phi}} = |Z| e^{i\phi} = |Z| (\cos \phi + i \sin \phi) \quad \text{Eq(2.12)}$$

Therefore, the complex impedance is expressed in terms of a magnitude, $|Z|$, and a phase angle, ϕ . Two common methods of plotting electrochemical impedance data, the Nyquist and Bode plots, arise from this representation of impedance. If the real and imaginary parts of the impedance, at each frequency, are plotted on the x- and y-axis, respectively, a Nyquist plot is generated. In the Bode representation, $|Z|$ and ϕ , at each frequency, are plotted on the y-axis and $\log \omega$ is plotted on the x-axis.

EIS data is commonly analysed by fitting to an equivalent electrical circuit model. The circuit elements in these models are usually simple electrical elements such as resistors and capacitors. Each element in the circuit exhibits a characteristic response to the applied sinusoidal voltage and its complex impedance can be obtained from its current-voltage relationship. For a simple resistor, the current and voltage are related through the resistance, R , as follows,

$$I = \frac{V}{R} = \frac{V_0 e^{i\omega t}}{R} \quad \text{Eq(2.13)}$$

Using the definition of impedance, given by Equation 2.7, the complex impedance of a resistor, Z_R , can be represented as,

$$Z_R = \frac{V}{I} = \frac{R(V_0 e^{i\omega t})}{V_0 e^{i\omega t}} = R \quad \text{Eq(2.14)}$$

So, the current is in phase with the voltage, that is, the resistor allows the current to follow the potential without delay. The impedance corresponds to the resistance and is independent of frequency¹³.

The current-voltage relationship for a capacitor is obtained by applying the definition of capacitance (C),

$$C = \frac{Q}{V} \quad \text{Eq(2.15)}$$

where, Q is the charge. Thus, the current is related to the voltage as follows,

$$I = \frac{dQ}{dt} = C \frac{dV}{dt} = C \frac{d(V_0 e^{i\omega t})}{dt} = i\omega C V_0 e^{i\omega t} \quad \text{Eq(2.16)}$$

and the impedance of the capacitor, Z_C , is given by¹³,

$$Z_C = \frac{V}{I} = \frac{V_0 e^{i\omega t}}{i\omega C V_0 e^{i\omega t}} = \frac{1}{i\omega C} = \frac{1}{\omega C} e^{-i\frac{\pi}{2}} \quad \text{Eq(2.17)}$$

From Equation 2.17, it can be seen that the phase angle is $\phi = -\pi/2$, implying that the current is 90° ahead of the voltage. In other words, the voltage across the capacitor lags behind the current. The impedance of the capacitor is frequency dependent with a magnitude of $|Z| = 1/\omega C$.

To analyse the impedance data of electrochemical systems it is often necessary to include elements of a more general nature in the equivalent circuit. Two such elements were applied in this work, the constant phase element (CPE) and the Warburg element. A CPE is a frequency dependent element, whose complex impedance is described by,

$$Z_{CPE} = \frac{1}{A\omega^n} e^{-i\frac{\pi}{2}n} \quad \text{Eq(2.18)}$$

where, A and n are constants. The inclusion of a CPE is associated with the non-ideal capacitive, conductive and diffusion behaviour typically found in electrochemical systems.¹⁴ This non-ideal behaviour has been described with reference to the inhomogeneous or fractal nature of electrode materials^{15, 16}. It can be seen from Equation 2.18, that the CPE can describe a resistor ($n = 0$ and $A = R^{-1}$), or a capacitor ($n = 1$ and $A = C$). A general expression for the complex impedance of the Warburg element can also be obtained from Equation 2.18, when $n = 0.5$,

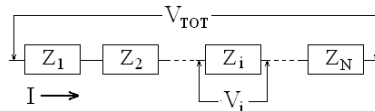
$$Z_W = \frac{1}{A\sqrt{\omega}} e^{-i\frac{\pi}{4}} = \frac{\sigma}{\sqrt{\omega}} - i \frac{\sigma}{\sqrt{\omega}} \quad \text{Eq(2.19)}$$

Here, σ is the Warburg coefficient and is defined as,

$$\sigma = \frac{RT}{F^2 C_D \sqrt{2D}} \quad \text{Eq(2.20)}$$

where, R is the gas constant, T is the temperature, F is Faraday's constant, C_D is a concentration term and D is the diffusion coefficient of the species described by the concentration term¹⁴. The inclusion of a Warburg element in an equivalent circuit is used to model semi-infinite diffusion behaviour.

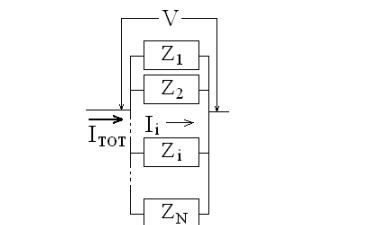
In general, electrochemical systems are too complex to be modelled using a single circuit element. Instead, equivalent circuit models usually consist of a number of elements combined in series or parallel. The total impedance of the system, Z_{TOT} , can then be calculated from the impedances of the individual elements, Z_i , using the following formulas¹³,



The diagram shows a series circuit with N impedance elements $Z_1, Z_2, \dots, Z_i, \dots, Z_N$ connected in a single path. A total voltage V_{TOT} is applied across the entire series combination, and a current I flows through it. The voltage across the i -th element is labeled V_i .

$$Z_{TOT} = \frac{V_{TOT}}{I} = \sum_{i=1}^N Z_i \quad \text{Eq(2.21)}$$

$$V_{TOT} = \sum_{i=1}^N V_i = I \sum_{i=1}^N Z_i$$



The diagram shows a parallel circuit with N impedance elements $Z_1, Z_2, \dots, Z_i, \dots, Z_N$ connected between two common nodes. A total voltage V is applied across the parallel combination, and a total current I_{TOT} flows from the source. The current through the i -th element is labeled I_i .

$$\frac{1}{Z_{TOT}} = \frac{I_{TOT}}{V} = \sum_{i=1}^N \frac{1}{Z_i} \quad \text{Eq(2.22)}$$

$$I_{TOT} = \sum_{i=1}^N I_i = V \sum_{i=1}^N \frac{1}{Z_i}$$

where, N is the total number of impedance elements in series, Equation 2.21, or parallel, Equation 2.22. However, these formulas are only applicable to systems that

behave linearly in a steady state. Electrochemical systems are not linear, but, a pseudo-linear condition can be achieved if the applied voltage signal is small enough to keep the overall state of the system unchanged. For this reason, the input voltage signal is typically 10 mV or less.

When analysing EIS data for a particular electrochemical system, it is common to find that several different equivalent circuit models can describe the electrical behaviour of the system. In these cases, two important criteria should be followed. Firstly, the elements in the model should have a rational basis in the electrochemistry of the system. Secondly, the theoretical model should not deviate greatly from the experimental data. In this work, the quality of the fit was assessed using chi-square (χ^2) values.

2.5.2 Surface Analysis

2.5.2 (i) Scanning Electron Microscopy (SEM)

SEM is performed by focusing a beam of high-energy electrons onto a sample and scanning the beam across its surface. The interaction of the high-energy electrons with the sample generates different signals which are collected ‘point by point’ and used to form the image. These signals can be categorized into two groups depending on whether they are generated by elastic or inelastic interactions¹⁷. The elastic scattering results from the deflection of incident electrons by atomic nuclei or shell electrons with similar energy. This produces backscattered electrons (BSE) with negligible energy loss and scattering angles larger than 90°. The inelastic scattering results from the deep interaction of the incident electrons with the nuclei and core electrons of the material. Signals with substantial energy loss, such as secondary electrons (SE), Auger electrons, X-ray emission and cathodo-luminescence, are generated in this way.

The incident beam has a characteristic penetration volume in the sample and each type of signal originates from a different part of it. This is illustrated in Figure 2.7. The BSE electrons have high enough energy (> 50 eV) to emerge from underneath

the sample surface. Images made from BSE electrons are characterized by Z contrast. The brightness of the element is proportional to its atomic number, Z , as the backscattering yield increases with increasing Z . The resolution of these images is of the order of $1\ \mu\text{m}$ because of the high energy of the BSE electrons. The SE electrons have low energy ($< 50\ \text{eV}$) and consequently carry topographical information about the sample surface. The low energy of SE electrons allows a resolution of about $10\ \text{nm}$. Auger electrons are emitted from atoms ionized by the incident electron beam. Their energy is characteristic of the element, thus, supplying chemical information about the sample. The energy of Auger electrons is very low and their resultant escape depth is only a few nanometers. Cathodo-luminescence results from the emission of photons of infrared, visible and ultraviolet light, due to electron relaxation. Signals of this type allow a resolution of $50\ \text{nm}$. The characteristic X-ray signal is used to perform chemical microanalysis of the sample surface. This technique is called energy dispersive X-ray (EDX) spectroscopy and is discussed separately.

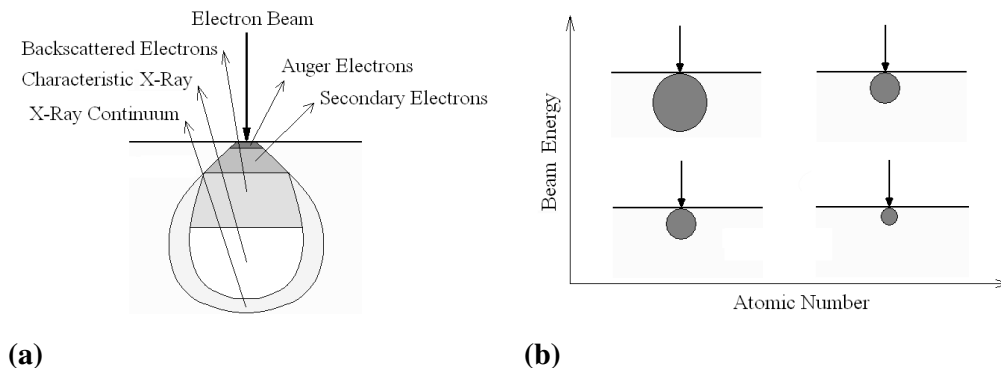


Figure 2.7: Schematic representation of the electron-material interaction in scanning electron microscopy (SEM). (a) Section of the volume of interaction of the electron beam with the sample surface and corresponding areas from which all the different signals are originating. (b) Size of the interaction volume as a function of the atomic number of the elements in the sample and the energy of the electron beam.

The SEM itself consists of an electron-optical column mounted in a vacuum chamber¹⁸. The electron gun placed on top of the column is typically a tungsten thermoionic cathode. The electrons are forced down into the column by an accelerating voltage ranging from 1 to $30\ \text{kV}$. The electron beam is focused on the sample and scanned across its surface using magnetic lenses and scan coils. The

pressure in the vacuum chamber where the sample is placed is 10^{-3} - 10^{-5} Pa ($\sim 10^{-7}$ mmHg). The sample is placed on a stage that can move with nanometric precision along the x, y and z axis. The SEM image is formed using a device consisting of a scintillator, a light pipe and a photomultiplier tube. The scintillator converts the signal into light. The vast majority of SEM images are generated from the SE electrons. The light pipe collects the light and conveys it into a photomultiplier tube where it is converted back into electrons. The electrons are then converted to a visual signal displayed on a cathode ray tube.

The brightness and contrast of the image generated is directly dependent on the surface topography. Figure 2.8a shows the effect of surface roughness on the intensity of the collected signal. If an obscuring feature is positioned between the spot where the beam is focused and the detector (Figure 2.8a), the SE electrons emitted behind the feature are gradually absorbed, giving the image its 3D appearance. Figure 2.8b shows the effect of the emission region on the intensity of the collected signal. When the beam is focused on the top of the feature it has a higher exposure and consequently a more intense signal is generated. The yield of the SE electron emission from the specimen is also dependent on the atomic number of the component in the sample; elements with a low atomic number naturally emit low yields of SE electrons. Charging phenomena at the surface of non conductive samples can interfere with the emission of SE electrons. In order to improve the yield of SE emission and the surface conductivity, samples are often sputter coated with a thin layer of noble metals, *e.g.*, Au (10 nm).

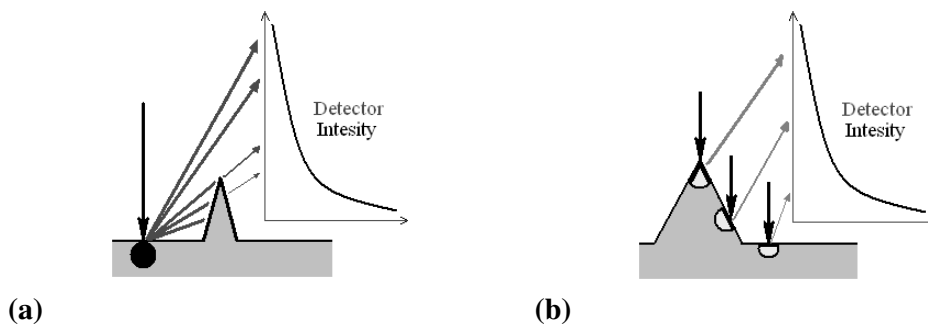


Figure 2.8: Schematic illustration of the effect of surface topography and detector position on the detection of secondary electrons (SE). (a) Effect of surface roughness on the intensity of the collected signal. (b) Effect of the emission region on the intensity of the collected signal.

2.5.2 (ii) Energy Dispersive X-ray Spectroscopy (EDX)

EDX allows the localized micro-elemental analysis of the top few micrometers of a sample. An EDX spectrum is obtained from the X-ray signals generated when the high-energy electron beam hits the sample surface. These X-ray signals are produced from the interaction of the beam electrons with inner shell electrons of the sample. An inner electron is ejected from the sample and replaced by an outer shell electron resulting in the emission of X-rays with energies specific to the energy separation between the levels involved. These electronic transitions are labelled K, L, M and N, after the electronic shells from which the electron is ejected and α , β or γ depending on which outer shell electrons make the transition to fill the vacancy. Transitions from levels immediately after the emptied level are labelled α , with subsequent transitions being labelled β and γ , in order of increasing energy. For example, $K\beta$ denotes the electronic transition $M \rightarrow K$. Since the orbital energies of each element are characteristic, the X-rays emitted by the sample are linked to its chemical composition. Thus, an EDX spectrum consists of a series of peaks at specific energies corresponding to the electronic transitions of the different elements present in the sample. A broad background signal is also present in all EDX spectra. This signal, referred to as Bremsstrahlung, is generated through deceleration of the beam electrons and has a much lower intensity than the elemental peaks. The intensity of the elemental peaks is proportional to the number of counts which, in turn, is proportional to both the amount of chemical element in the sample and to the energy carried by the associated X-ray signal. X-rays of higher energy give more intense peaks.

From the above discussion it is clear that both qualitative and quantitative information about the chemical composition of a sample can be obtained using EDX. However, the quality of this analysis can be affected by the surface roughness of the sample^{19, 20}. The BSE electrons generated by the electron beam can interact with zones surrounding the beam spot (Figure 2.9), causing the emission of X-rays that add to the signal generated at the point of analysis. The extent of such interference depends on the surface roughness of the sample and is a major limitation for quantitative analysis. In practice, quantitative EDX analysis is only sensible for high-quality flat-polished surfaces, and it must be performed against a known standard

prepared and analyzed in the same way. Quantitative analysis is also possible by comparing the relative peak heights of the sample with a standard of known composition measured in the same conditions. However, various correction factors due to matrix effects must be taken into account in order to obtain reliable data^{19, 20}. These factors are related to atomic number (Z), absorption (A) and fluorescence (F) effects and are corrected by using a characteristic ZAF factor which correlates the intensity of the peak to the concentration of the element.

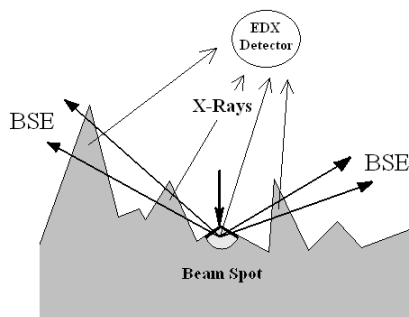


Figure 2.9: Schematic illustration of the effect of the surface roughness on the detection of the X-ray signal. The interaction of the backscattered electrons (BSE) with the surrounding roughness causes the acquisition of a mixed signal by the EDX detector.

2.5.3 Nuclear Magnetic Resonance (NMR)

During the course of this project, proton (^1H) NMR spectroscopy was employed in various ways to study the inclusion complexes of C4S. In this section, the general concept of NMR spectroscopy is discussed briefly and then, the theoretical backgrounds of the different experimental techniques used in this work are covered in more detail.

The fundamental observable parameter in NMR spectroscopy is termed the Larmor frequency (ω). This measurable frequency arises from the interaction between a nucleus with spin and a static magnetic field. Each nucleus with spin has an associated magnetic moment which, when placed in an external, static magnetic field (B_0), aligns itself relative to the field in a discrete number of orientations or spin states. For a spin-1/2 nucleus, such as the proton, there are two possible spin states denoted α , where the nucleus is aligned with the static field (lower energy), or β , where the nucleus is aligned against the static field (higher energy). Nuclear

magnetic resonance occurs when the nucleus changes its spin state due to the absorption of a quantum of energy. The energy required to induce this change in spin state is the Larmor frequency, which is the rate of precession of the nuclear magnetic moment about B_0 . Therefore, the resonance signal for a particular nucleus is observed at its Larmor frequency²¹.

Theoretically, the Larmor frequency of a proton is expected to be constant²¹. However, experimentally, this frequency is observed to vary due to differences in the electronic structure local to the proton. It is this phenomenon that makes NMR spectroscopy such an invaluable tool for the determination of molecular structure. The resonance frequency of each proton in a system is recorded in terms of chemical shift (δ),

$$\delta = \left(\frac{\omega - \omega_{ref}}{\omega_{ref}} \right) \times 10^6 \quad Eq(2.23)$$

where, ω is the Larmor frequency of the nucleus of interest, ω_{ref} is the Larmor frequency of a reference nucleus, typically one that resonates at the operational frequency of the spectrometer, and δ is expressed in parts per million (ppm). In this way, only the variations in the Larmor frequency are observed. Information about the relative chemical environments of each proton can then be easily discerned from the spectrum.

2.5.3 (i) Job's Method

Before any structural or associative investigations can be performed on a complexation interaction, it is important to construct a plausible binding model. Determining the stoichiometry of the complex is very helpful in this regard. This is readily achieved from NMR data by means of the continuous variations or Job's method^{22, 23}.

Consider the formation of a complex between a host (H) and a guest (G), the equilibrium for the formation of this complex (HG) can be represented as follows,



where m and n are the stoichiometric ratios of H and G , respectively. In the Job's method, a series of solutions are prepared where the total molar concentration, $[H] + [G]$, of each solution is kept constant while the molar ratio of $[H]$ to $[G]$ is varied. Under these conditions it has been shown that the concentration of the complex $[H_mG_n]$ reaches a maximum for a molar ratio $[H]/[G] = m/n$. Consequently, a plot of any property that is a linear function of $[H_mG_n]$ against the mole fraction,

$$X = \frac{[G]}{[H] + [G]} \quad \text{Eq(2.25)}$$

results in a curve with zero values at $X = 0$ and $X = 1$, and a maximum at²³,

$$X = \frac{n}{m + n} = \frac{1}{(m/n) + 1} \quad \text{Eq(2.26)}$$

2.5.3 (ii) NMR Titration

The formation of a 1:1 complex between a host molecule (H) and a guest molecule (G) can be represented by the following equilibrium,



The strength of this complexation is measured by the equilibrium constant (K), which is given by,

$$K = \frac{[HG]}{[H][G]} \quad \text{Eq(2.28)}$$

where $[HG]$, $[H]$ and $[G]$ are the equilibrium concentrations of the complex, host and guest, respectively.

The method used to determine K from NMR data depends on the rate of exchange between the uncomplexed and complexed forms of the host and guest. Suppose the

NMR signal for a guest proton is sensitive to complex formation. Under slow exchange conditions, two signals would be observed for this proton signal, one for the uncomplexed guest at δ_G and one for the complexed guest at δ_{HG} . The equilibrium concentration of the complex $[HG]$ can then be obtained from the relative integrals (I) of these signals as follows,

$$\frac{I_{HG}}{I_G + I_{HG}} = X_{HG} = \frac{[HG]}{[G]_0} \quad Eq(2.29)$$

where X_{HG} is the mole fraction of the complex and $[G]_0$ is the initial concentration of the guest. Thus, Equation 2.28 can be rewritten as,

$$K = \frac{[HG]}{([H]_0 - [HG])([G]_0 - [HG])} = \frac{X_{HG}/[G]_0}{(1 - X_{HG})(R - X_{HG})} \quad Eq(2.30)$$

where $[H]_0$ is the initial concentration of host and $R = [H]_0/[G]_0$. This allows the calculation of the equilibrium constant directly from the NMR data²⁴.

For a fast exchange system, only a single signal would be observed for the guest proton. The observed chemical shift of this signal (δ_{obs}) is given by,

$$\delta_{obs} = X_G \delta_G + X_{HG} \delta_{HG} \quad Eq(2.31)$$

In this case, it is not possible to obtain K , as defined by Equation 2.30, directly from the NMR data. Instead, Equation 2.30 is rearranged to give the following quadratic equation,

$$(X_{HG})^2 - \left(1 + R + \frac{1}{K[G]_0}\right) X_{HG} + R = 0 \quad Eq(2.32)$$

with the real root,

$$X_{HG} = \frac{b - \sqrt{b^2 - 4R}}{2} \quad Eq(2.33)$$

where

$$b = 1 + R + \frac{1}{K[G]_0} \quad Eq(2.34)$$

If Equation 2.31 is then rearranged to form,

$$\delta_{obs} = (1 - X_{HG})\delta_G + X_{HG}\delta_{HG} = \delta_G - X_{HG}\Delta_0 \quad Eq(2.35)$$

where

$$\Delta_0 = \delta_G - \delta_{HG} \quad Eq(2.36)$$

and X_{HG} is substituted by Equation 2.33, the following relationship between δ_{obs} and K is achieved²⁴,

$$\Delta\delta = \delta_G - \delta_{obs} = \left(\frac{\Delta_0}{2}\right)\left(b - \sqrt{b^2 - 4R}\right) \quad Eq(2.37)$$

Thus, a value for K can be obtained from nonlinear curve fitting of Equation 2.37 to a plot of $\Delta\delta$ as a function of R . To generate such a plot, a series of NMR spectra are recorded for solutions where the concentration of guest remains constant and the concentration of host is varied so that a broad range of molar ratios (R) are sampled. This experiment is known as an NMR titration.

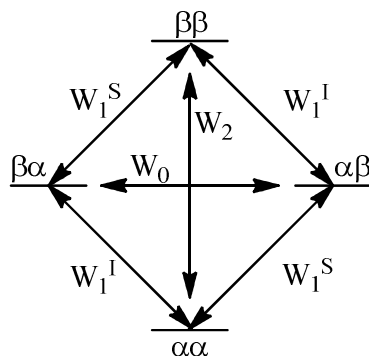
2.5.3 (iii) Rotating-Frame Nuclear Overhauser Effect (ROE) Spectroscopy

The nuclear Overhauser effect (NOE) arises from direct through space magnetic interactions (dipolar couplings) between nuclear spins^{21, 25}. The magnitude of dipolar coupling is acutely sensitive to the internuclear separation and so the NOE is ultimately distance dependent. In practice, significant NOE's will only develop between protons that are within approximately 5 Å of each other^{21, 25}. In this way, NOE spectroscopy has the ability to provide valuable information on three-dimensional molecular geometry.

The NOE itself may be defined as the change in intensity of one resonance when the spin transitions of another are perturbed from their equilibrium populations^{21, 25}. In order to explain this phenomenon, let us first consider a system containing only two homonuclear spin-1/2 nuclei, I and S, which are present in the same molecule and are sufficiently close to share a dipolar coupling. The energy level diagram for 4N such molecules is illustrated in Figure 2.10a. As the system is homonuclear, the energies

associated with the I and S spin transitions are essentially identical. From this, the equilibrium populations of the $\alpha\beta$ and $\beta\alpha$ states can be assumed to be equal. Accordingly, the Boltzmann distribution predicts an excess of nuclei in the lower energy $\alpha\alpha$ state and a deficit in the higher energy $\beta\beta$ state. Therefore, in the absence of any perturbation, the spectrum contains two singlet resonances of equal intensity.

Now let us consider the effect of perturbing this system from its state of equilibrium. This is best illustrated using the example of the steady-state NOE. In the steady-state NOE, the perturbation is brought about by saturating the spin transitions of a resonance, in this case S, by the application of weak radiofrequency irradiation to the resonance. This forces the population differences across the associated spin transitions to zero (Figure 2.10b), perturbing them from their equilibrium state. The system then seeks to regain the equilibrium population differences across the S transitions by altering its spin populations. This occurs through longitudinal spin relaxation processes. For a two spin system, there are six possible longitudinal spin relaxation pathways (Scheme 2.2). However, only two of these processes, W_2 and W_0 , are responsible for the NOE itself. The W_2 process acts to recover the population differences across the S transitions by transferring spins from the $\beta\beta$ state to the $\alpha\alpha$ state (Figure 2.10c). This increases the population difference across the two I transitions, resulting in a net increase in the I-spin resonance intensities in the spectrum, a positive NOE. Similarly, the W_0 process also acts to recover the population differences across the S transitions by transferring spins from the $\alpha\beta$ state to the $\beta\alpha$ state (Figure 2.10d). This results in a decrease in the population difference across the two I transitions, causing a net reduction in the I-spin resonance intensities in the spectrum, a negative NOE. Clearly, these two processes will compete with each other to form the NOE. On the other hand, as soon as the NOE begins to develop, the W_1^1 pathways will act to re-establish the equilibrium population differences across the I-spin transitions, reducing the NOE. In practice, if the S transitions are saturated for a period of time that is long relative to these competing relaxation times, a new steady-state of populations arises from this competition, and it is these that give rise to the observed NOE^{21, 25}.



Scheme 2.2: Schematic showing the six possible longitudinal spin relaxation pathways for a two spin homonuclear system.

Longitudinal spin relaxation processes do not occur spontaneously but require stimulation by a suitable fluctuating field to induce the necessary spin transitions. For the NOE, the field of relevance is the local field experienced by a spin as a result of dipolar interactions with neighbouring magnetic nuclei. Here is the origin of the dipole-dipole dependence of the NOE. This field fluctuates as the molecule tumbles in solution. To induce the relevant spin transitions, the molecule must tumble at the appropriate frequency. As a result, the rate of relaxation and therefore the sign and magnitude of the NOE is dependent on the rate of molecular tumbling. The rate at which a molecule tumbles or rotates in solution is typically defined by the rotational correlation time, τ_c , with rapidly tumbling molecules possessing small correlation times whilst slowly tumbling molecules have large correlation times. In general, the NOE can be shown to vary as a function of $\omega_0\tau_c$ where, ω_0 is the spectrometer observation frequency. The curve generated from this relationship contains three distinct regions. For $\omega_0\tau_c < 1.12$, corresponding to a short τ_c , the NOE is positive with a maximum intensity of 50%. This situation arises for small molecules in low viscosity solvents. For $\omega_0\tau_c > 1.12$, where τ_c is long, the NOE is negative with a maximum intensity of -100%. Large molecules or high viscosity solvents produce NOEs of this type. Between these two extremes, in the vicinity of $\omega_0\tau_c = 1.12$, the NOE approaches zero, making it difficult to measure the NOE for medium sized molecules. In practice, the ROE is the preferred technique for molecules with a mass in the range 700 to 1500 Daltons^{21, 25}.

The advantage of the rotating frame NOE (ROE) is that it is always non-zero and positive. This fact is a consequence of the slightly different experimental approach used to measure the ROE. In the NOE, the spin systems are perturbed using the static magnetic field of the spectrometer, B_0 , and the NOE develops through cross-relaxation in the longitudinal plane. For the ROE, B_0 is replaced as the perturbation signal by a far smaller radiofrequency field, B_1 , applied in the transverse plane. As a result, the ROE develops through cross-relaxation in the transverse plane or 'rotating-frame'. Thus, the intensity of the ROE varies as a function of $\omega_1 \tau_c$ where ω_1 is the rotating-frame frequency. Since $\omega \propto B$, it is clear that ω_1 will be much lower than ω_0 . In fact, the frequency of ω_1 is usually only a few kiloHertz whereas ω_0 typically corresponds to a few hundred megaHertz. Consequently, $\omega_1 \tau_c \ll 1$ for all realistic values of τ_c and the ROE is always positive^{21, 25}.

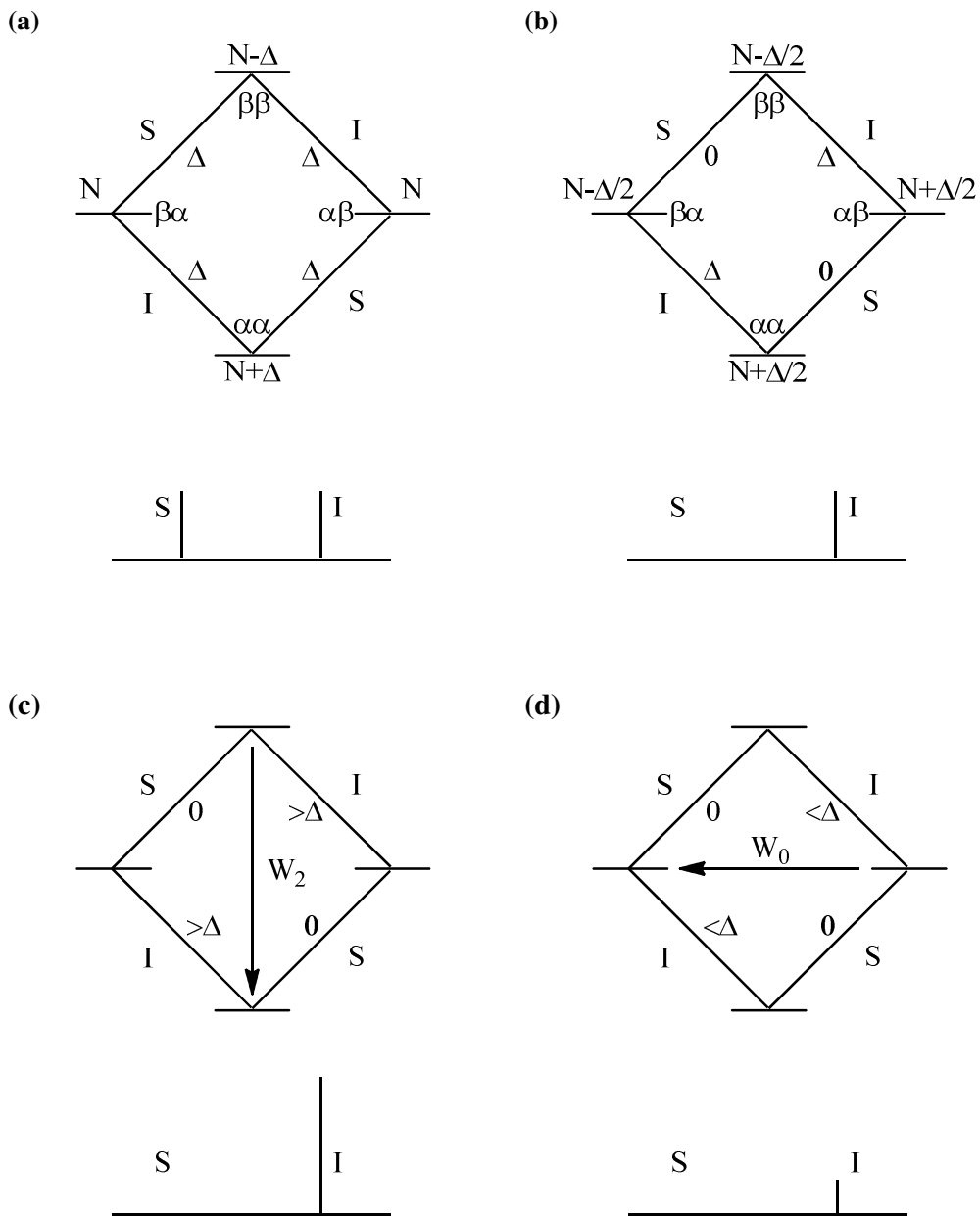


Figure 2.10: The energy level diagrams and population differences for two homonuclear spins (S and I) which share a dipolar coupling, (a) at equilibrium, (b) after saturation of the S-spins, (c) after relaxation via W_2 processes, and (d) after relaxation via W_0 processes. Below each energy level diagram are the corresponding spectra.

2.6 Bibliography

- (1) Gutsche, C. D.; Dhawan, B.; No, K. H.; Muthukrishnan, R. *J. Am. Chem. Soc.* **1981**, *103*, 3782-3792.
- (2) Gutsche, C. D.; Johnston, D. E., Jr.; Stewart, D. R. *J. Org. Chem.* **1999**, *64*, 3747-3750.
- (3) Gutsche, C. D.; Lin, L. G. *Tetrahedron* **1986**, *42*, 1633-1640.
- (4) Shinkai, S.; Araki, K.; Tsubaki, T.; Arimura, T.; Manabe, O. *J. Chem. Soc., Perkin Trans. 1* **1987**, 2297-2299.
- (5) Arena, G.; Cali, R.; Lombardo, G. G.; Rizzarelli, E.; Sciotto, D.; Ungaro, R.; Casnati, A. *Supramol. Chem.* **1992**, *1*, 19-24.
- (6) Suga, K.; Ohzono, T.; Negishi, M.; Deuchi, K.; Morita, Y. *Supramol. Sci.* **1998**, *5*, 9-14.
- (7) Yoshida, I.; Yamamoto, N.; Sagara, F.; Ishii, D.; Ueno, K.; Shinkai, S. *Bull. Chem. Soc. Jpn.* **1992**, *65*, 1012-1015.
- (8) Bard, A. J.; Faulkner, L. R. *Electrochemical Methods: Fundamentals and Applications*, 2nd ed.; Wiley, **2000**.
- (9) Pletcher, D.; Greef, R.; Peat, R.; Peter, L. M.; Robinson, J. *Instrumental Methods in Electrochemistry*, 1st ed.; Ellis Horwood Ltd., **1985**.
- (10) Scharifker, B.; Hill, G. *Electrochim. Acta* **1983**, *28*, 879-889.
- (11) Wang, Y.; Northwood, D. O. *Thin Solid Films* **2008**, *516*, 7427-7432.
- (12) Bard, A. J.; Faulkner, L. R. *Electrochemical methods: fundamentals and applications*, 2nd ed.; Wiley, **2000**.
- (13) Barsoukov, E.; MacDonald, R. *Impedance Spectroscopy: Theory, Experiment, and Applications, 2nd Edition*; John Wiley & Sons, **2005**.
- (14) Rubinson, J. F.; Kayinamura, Y. P. *Chem. Soc. Rev.* **2009**, *38*, 3339-3347.
- (15) Nyikos, L.; Pajkossy, T. *Electrochim. Acta* **1985**, *30*, 1533-1540.
- (16) Nyikos, L.; Pajkossy, T. *Electrochim. Acta* **1986**, *31*, 1347-1350.

- (17) Zhou, W.; Wang, Z. L. *Scanning Microscopy for Nanotechnology: Techniques and Applications*, 1st ed.; Springer, **2006**.
- (18) Szykowska, M. *Scanning Electron Microscopy*; Elsevier, **2005**.
- (19) Goldstein, J.; Newbury, D. E.; Joy, D. C.; Lyman, C. E.; Echlin, P.; Lifshin, E.; Sawyer, L.; Michael, J. R. *Scanning Electron Microscopy and X-ray Microanalysis*, 3rd ed.; Springer, **2003**.
- (20) Kanani, N. *Electroplating: Basic Principles, Processes and Practice*; Elsevier Science, **2005**.
- (21) Claridge, T.; Editor *High-Resolution NMR Techniques in Organic Chemistry*, 1st ed.; Pergamon, **2000**.
- (22) Fielding, L. *Tetrahedron* **2000**, *56*, 6151-6170.
- (23) Tsukube, H.; Furuta, H.; Odani, A.; Takeda, Y.; Kudo, Y.; Inoue, Y.; Liu, Y.; Sakamoto, H.; Kimura, K. **1996**; Elsevier; 425-482.
- (24) Macomber, R. S. *J. Chem. Educ.* **1992**, *69*, 375-378.
- (25) Neuhaus, D.; Williamson, M. P. *The Nuclear Overhauser Effect in Structural and Conformational Analysis*, 2nd ed.; Wiley-VCH, **2000**.

CHAPTER 3

Sensor

Characterisation:

A Study of the Physical and Electrochemical
Properties of the PPy-C4S Film

3.1 Introduction

Electrochemically prepared polypyrrole (PPy) films have been the subject of many characterisation studies¹⁻²⁵. The physical and electrochemical properties of these films are greatly influenced by the variety of processing parameters involved in their formation, such as the electrochemical method, electropolymerisation potential and charge, the concentration of the monomer and electrolyte, the nature of the dopant anion, and temperature. Of these parameters, the nature of the dopant anion is one of the most significant. Depending on the dopant used, the PPy film can behave as an anion exchange or cation exchange polymer, or display characteristics of both²³⁻³³. PPy films doped with large bulky anions generally behave as cation exchange polymers, due to the dopant being irreversibly incorporated into the film^{25-28, 31-33}. Interestingly, the films formed using these bulky anions, especially large aromatic sulfates, have been shown to be more stable and possess better electrochemical and mechanical properties than the films formed using smaller anions³³⁻³⁷. In particular, Ingram³⁴ and Suematsu³³ found that the capacitance of PPy films doped with sulfonated naphthalenes increased as the number of sulfonates per aromatic compound increased.

The PPy films studied here were doped with *p*-sulfonatocalix[4]arene (C4S), the structure of which is shown in Figure 3.1. PPy films doped with sulfonated calixarenes have been reported by several authors³⁸⁻⁴¹. Bidan *et al.* observed that a sulfonated calix[4]arene could be irreversibly incorporated into the PPy matrix³⁸. Moreover, a recent paper by Akieh *et al.* reported an electrically switchable cation exchange membrane based on PPy doped with a sulfonated calix[6]arene⁴¹. However, to the best of our knowledge, no comprehensive characterisation of PPy doped with a sulfonated calixarene has been carried out yet.

Therefore, in this chapter, the physical and electrochemical properties of PPy films doped with C4S (PPy-C4S) were studied using a variety of techniques including: scanning electron microscopy, energy dispersive X-ray spectroscopy, Tencor profilometry, cyclic voltammetry and electrochemical impedance spectroscopy.

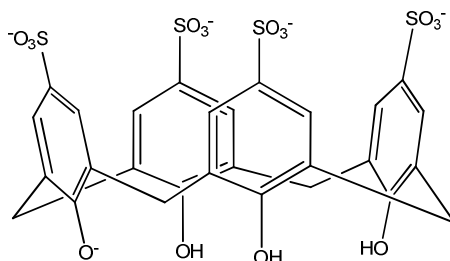


Figure 3.1: Structure of the anionic dopant, *p*-sulfonatocalix[4]arene (C4S), used during pyrrole electropolymerisation.

3.2 Results and Discussion

3.2.1 Physical Characterisation of the PPy-C4S Film

The physical properties of the PPy-C4S film were examined using the techniques of scanning electron microscopy, energy dispersive x-ray spectroscopy and profilometry. Scanning electron microscopy was used to examine the surface morphology of the PPy-C4S film and to investigate the influence of the electropolymerisation potential on the morphology of the film. Energy dispersive X-ray spectroscopy was used to determine the elemental composition of the film. Profilometry was used to measure the thickness of the PPy-C4S film and to ascertain how the thickness related to the electropolymerisation charge.

3.2.1.1 Scanning Electron Microscopy (SEM)

The surface morphology of the PPy-C4S film was examined using the SEM facilities in the Tyndall National Institute at University College Cork. Figure 3.2 shows an SEM image of a PPy-C4S film that had been electropolymerised at a potential of 0.500 V vs. SCE. It can be seen from Figure 3.2a that the PPy-C4S film displayed the typical ‘cauliflower’ morphology commonly observed for PPy films⁴².

SEM measurements were also performed on a PPy-C4S film that had been electropolymerised at 0.800 V vs. SCE. This was to investigate the influence of the electropolymerisation potential on the surface morphology of the film. It can be seen from Figure 3.2b that this polymer also displayed the ‘cauliflower’ morphology. However, its surface was less homogeneous than the polymer grown at 0.500 V vs. SCE. In fact, using a higher applied potential to grow the PPy-C4S film seemed to cause a significant increase in the surface roughness of the film. Similar observations to these have been reported by other authors^{21, 43, 44}.

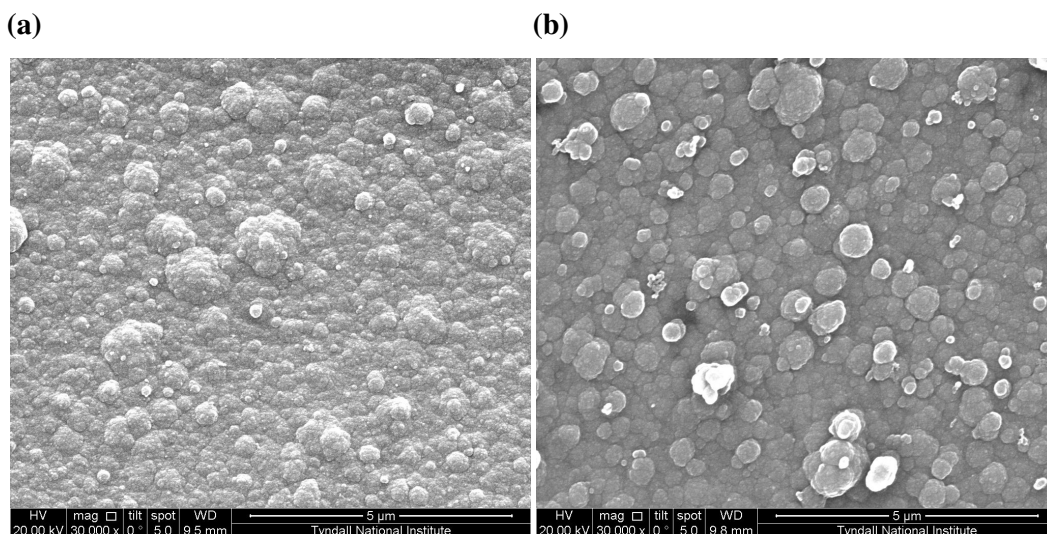


Figure 3.2: SEM image of a PPy-C4S film electropolymerised (a) at 0.500 V vs. SCE and (b) at 0.800 V vs. SCE on a Pt electrode from a solution containing 0.20 mol dm^{-3} pyrrole and 0.01 mol dm^{-3} C4S until a charge of 0.24 C cm^{-2} had been reached.

3.2.1.2 Energy Dispersive X-ray Spectroscopy (EDX)

The elemental composition of the PPy-C4S film was examined using the EDX facilities in the Tyndall National Institute at University College Cork. EDX measurements were carried out on a PPy-C4S film that had been electropolymerised at 0.500 V vs. SCE until a charge of 0.24 C cm^{-2} was reached. The resulting EDX spectrum is shown in Figure 3.3. The presence of the peak for sulfur, $K_{\alpha} = 2.3075 \text{ keV}$, indicated that the calixarene had been successfully incorporated into the film.

The C4S used in the synthesis of the PPy-C4S film had been determined to have a general chemical formula of $\text{Ca}_x\text{Na}_{5-2x}\text{C}_{28}\text{H}_{19}\text{O}_{16}\text{S}_4 (y\text{H}_2\text{O})$. Interestingly, the EDX spectra showed no evidence of Ca^{2+} ions being present in the film. EDX measurements were carried out at several locations on the PPy-C4S film but no peaks were observed in the region characteristic of Ca^{2+} , $K_{\alpha} = 3.6905 \text{ keV}$. This was surprising given that Ca^{2+} is known to form an outer sphere complex, involving a strong electrostatic interaction, with C4S⁴⁵. As such, it was likely that some of the C4S incorporated into the film would have been in the form of a Ca^{2+} complex. However, these results suggest that any complexes that had formed, became

dissociated during the incorporation of the calixarene into the PPy film. In this way, it seems probable that the PPy film was simply doped with the anionic C4S.

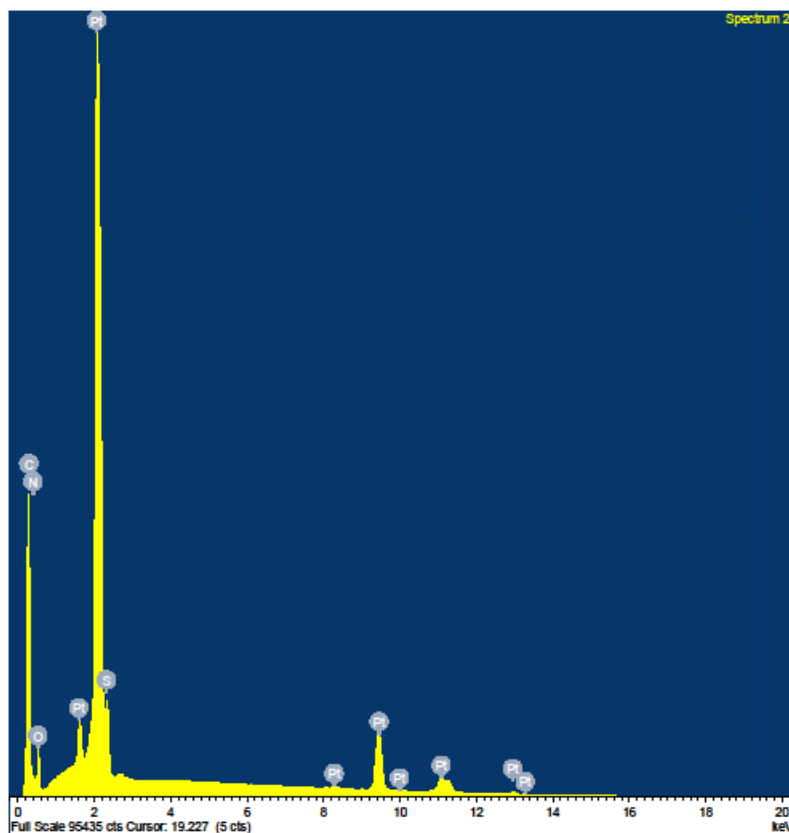


Figure 3.3: EDX spectrum of a PPy-C4S film electropolymerised on a Pt electrode at 0.500 V vs. SCE from a solution containing 0.20 mol dm^{-3} pyrrole and 0.01 mol dm^{-3} C4S until a charge of 0.24 C cm^{-2} had been reached.

3.2.1.3 Thickness of the PPy-C4S Film

The thickness of the PPy-C4S film was measured using a Tencor profilometer in the Tyndall National Institute at University College Cork. PPy-C4S films were electrosynthesised on a Pt disk electrode at 0.500 V vs. SCE until charges of 0.08, 0.16 and 0.24 C cm^{-2} were reached. The films were grown so that only one half of the electrode surface was covered, hence, the film thickness could be obtained by scanning across the electrode surface and measuring the step height. Two separate

measurements were carried out for each electropolymerisation charge and the results are presented in Table 3.1.

Firstly, it can be seen from Table 3.1 that the measurements were not reproducible for two of the films. The thicknesses obtained for the films grown to 0.08 C cm^{-2} were reasonably reproducible, with measured thicknesses of 283 and 209 nm, and an average thickness of $246 \pm 37 \text{ nm}$, but the reproducibility of the measurements decreased as the charge was increased. The measurements obtained for the films grown to 0.16 and 0.24 C cm^{-2} differed by more than 300 and 400 nm, respectively. The reason for this poor reproducibility is not certain. Likely, it is due in part to experimental error. In order to grow the PPy-C4S films on only one half of the electrode surface, it was necessary to cover the other half with tape to prevent any polymerisation occurring. This was done by eye and as such was prone to error. But it is unlikely that this error would have produced discrepancies as large as those observed here. Another possible explanation was an increase in the surface roughness of the film. It has been shown that the surface roughness of PPy films is dependent on the thickness of the film^{12, 20}. Silk¹² and Fonner²⁰ found that PPy films doped with sulfate and tosylate anions became rougher with increasing film thickness. Also, Ingram *et al.* observed that at a given thickness, PPy films doped with polysulfonated aromatic compounds became 'fluffier' with increasing number of sulfates per aromatic anion³⁴. So, it seemed reasonable to assume that the surface roughness of the PPy-C4S film would increase with increasing film thickness. Although Fonner *et al.* obtained their film thicknesses using profilometry, this technique is more suited to homogeneous surfaces, thus, it is possible that increasing surface roughness of the film could account for the discrepancies in the observed thicknesses. However, further studies need to be carried out to fully explain these results.

Despite these difficulties, the thickness of the PPy-C4S film was still observed to increase as the electropolymerisation charge was increased. This was in accordance with theoretical predictions for PPy films. Diaz *et al.* derived a relationship that assumes 1 C cm^{-2} of charge will be passed for each $2.5 \mu\text{m}$ of polymer growth⁴⁶. Using this relationship the thicknesses of the PPy-C4S films grown to 0.08, 0.16 and 0.24 C cm^{-2} were predicted to be 200, 400 and 600 nm, respectively. By comparing these values with those in Table 3.1, it can be seen that the measurements obtained

for the PPy-C4S films grown to 0.08 C cm^{-2} , 283 and 209 nm, were in relatively good agreement with the predicted thickness for this charge, 200 nm. However, as the charge, and consequently the film thickness, increased the predicted thicknesses became less accurate. This deviation with increasing thickness can be explained by the fact that Diaz *et al.* derived their relationship for PPy films doped with chloride anions whereas a much bulkier dopant, C4S, was used here. AFM studies by Silk *et al.* showed that the nature of the dopant anion influenced the thickness of PPy films and that this influence became more significant as the thickness of the film increased¹². As a result, the extent to which the thicknesses of PPy films doped with different anions differ from each other is expected to increase with increasing film thickness. This observation is in agreement with the results obtained here, where Diaz's relationship became less applicable for the PPy-C4S film as the thickness increased.

Table 3.1: Film thickness measurements for PPy-C4S films grown at 0.500 V vs. SCE to various electropolymerisation charges. Measurements were obtained for two separate films grown to each charge.

Charge / C cm^{-2}	Thickness 1 / nm	Thickness 2 / nm
0.08	283 ± 70	209 ± 16
0.16	583 ± 12	268 ± 10
0.24	1125 ± 63	706 ± 101

3.2.2 Electrochemical Characterisation of the PPy-C4S Film

The electrochemical properties of the PPy-C4S film were examined using two techniques; cyclic voltammetry and electrochemical impedance spectroscopy. The electrochemical activity and capacitance of the film were investigated using cyclic voltammetry and the charge transport processes occurring within the film were studied using electrochemical impedance spectroscopy. The capacitance of the PPy-C4S film was also determined using impedance measurements.

3.2.2.1 Cyclic Voltammetry

Cyclic voltammetry has been widely employed to study the electroactivity and electrochemical properties of PPy films. Using this technique allows the electrochemical switching behaviour of PPy, between conducting and insulating states, to be described easily. Typically, cyclic voltammograms of PPy films are characterised by two main features; a well defined redox process, corresponding to the oxidation and reduction of the PPy backbone, and a large capacitance effect, resulting from the redox process and the porous nature of the film³.

In this Section, the redox and capacitive properties of the PPy-C4S film are examined in detail. These studies also revealed some novel redox chemistry associated with the presence of C4S in the film. The factors influencing this redox behaviour are investigated and a suggested origin for this novel redox chemistry is proposed.

3.2.2.1 (i) Oxidation and Reduction Properties of the PPy-C4S Film

A PPy-C4S film was grown on a Pt disk electrode at a potential of 0.500 V vs. SCE until a charge of 0.24 C cm⁻² was reached. The resulting film was cycled in a 0.10 mol dm⁻³ Na₂SO₄ solution at a scan rate of 5 mV s⁻¹ between -0.800 V and 0.200 V vs. SCE. These specific values for the electropolymerisation potential and charge, and the supporting electrolyte, were chosen because they had been determined to be optimal for the detection of dopamine. This is discussed in detail in Chapter 4. The oxidation and reduction properties of the PPy-C4S film can be seen clearly from Figure 3.4. A single oxidation wave was observed at -0.214 V vs. SCE and a corresponding reduction wave was observed at -0.455 V vs. SCE. The peak separation of 0.241 V was indicative of a *quasi*-reversible process which is typical of PPy films^{3,23-25}.

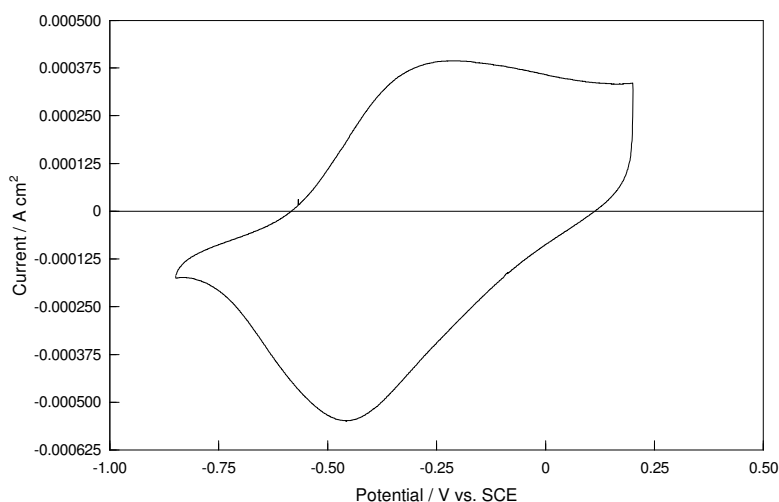
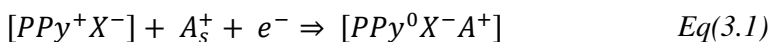


Figure 3.4: A cyclic voltammogram recorded in a $0.10 \text{ mol dm}^{-3} \text{ Na}_2\text{SO}_4$ solution at a scan rate of 5 mV s^{-1} for a PPY-C4S film electropolymerised on a Pt electrode from a solution containing 0.20 mol dm^{-3} pyrrole / 0.01 mol dm^{-3} C4S at 0.500 V vs. SCE until a charge of 0.24 C cm^{-2} was reached.

The relative shape of the oxidation and reduction waves gives some insight into the kinetics of these two processes. From Figure 3.4, the reduction peak can be seen to be sharper than the oxidation peak indicating that the rate of reduction was faster than the rate of oxidation. This observation was suggestive of a cation exchange polymer³². For PPy films doped with small anions the oxidation wave is usually sharper than the reduction wave. This can be explained as follows. When the film is being oxidised, the layer next to the electrode surface is oxidised first. This creates a conducting layer which facilitates the oxidation of the next layer and so on until the conducting layer encompasses the whole film. Upon reduction of the film, the layer adjacent to the electrode surface is again the first to be switched. But this time, an insulating layer is created which makes the overall reduction process less efficient than the oxidation process. A sharper reduction wave, such as that observed here, is often observed for PPy films doped with large anions that are irreversibly incorporated into the film^{25, 32}. In these cases, reduction of the film is accompanied by an influx of cations and can be represented as follows,



where *PPy* represents a segment of the polypyrrole chain, usually between 3-4 monomer units, A^+ are cations, Na^+ in this case, the subscript *s* indicates the cations are in the solution phase and X^- are the dopant anions, C4S in this case. The sharper appearance of the reduction wave for these films has been attributed to the high mobility of the cations³². As a result, the reduction of the PPy-C4S film, which involves the incorporation of Na^+ from the solution phase into the film, is a relatively fast and efficient process, whereas oxidation of the polymer is slower due to the slow release of Na^+ .

3.2.2.1 (ii) Capacitance Measurements for the PPy-C4S Film

It can be seen from Figure 3.4, that the voltammetric current remained high after the oxidation of the PPy-C4S film indicating that the background current for the oxidised film was significant. These high background currents are typical of PPy films and can be attributed to the high capacitance of the film. Through theoretical modelling, Yeu *et al.* determined that the currents observed after the decay in the Faradaic currents, due to oxidation of the PPy backbone, represent predominantly capacitive components³. The currents observed in this potential region generally show a linear relationship with scan rate and the capacitance of the film can be obtained using the following expression^{3, 47},

$$C = \frac{I}{\nu} \quad Eq(3.2)$$

where *C* is the capacitance, *I* is the current in $A\ cm^{-2}$, and ν is the scan rate in $V\ s^{-1}$.

The PPy-C4S film was grown until a charge of $0.24\ C\ cm^{-2}$ was reached. The resulting film was then cycled in a $0.10\ mol\ dm^{-3}\ Na_2SO_4$ solution at various scan rates between potentials of 0.100 and 0.200 V vs. SCE. This narrow potential window was used in an effort to avoid any faradaic contributions to the current. At each scan rate, the current was measured at 0.150 V vs. SCE and these currents were plotted as a function of the scan rate. It is clear from Figure 3.5 that the current showed a linear relationship with scan rate. Accordingly, the capacitance of the

PPy-C4S film could be obtained from the slope of this plot according to Equation 3.2. A capacitance measurement of 9.4 mF cm^{-2} was obtained for the PPy-C4S film which was in agreement with the high capacitance expected for a polypyrrole film^{1-3, 48, 49}.

The capacitance was also measured for PPy-C4S films grown to charges of 0.04, 0.08, 0.12, 0.16 and 0.20 C cm^{-2} . Figure 3.6 shows a plot of capacitance against electropolymerisation charge. It can be seen that the capacitance increased linearly with charge. In Section 3.2.1.3 the relationship between film thickness and charge was discussed and it was found that the film thickness increased as the electropolymerisation charge was increased. Therefore, from the results obtained here, it can be inferred that the capacitance of the PPy-C4S film increased with film thickness. This observation was typical of polypyrrole films^{1, 2} and was consistent with the idea that the capacitance of a polypyrrole film is related to its faradaic process⁵⁰. That is, the capacitance of the film mainly arises from the charge separation between the oxidised polypyrrole backbone and the doping counteranions, in this case the calixarene^{29, 49}. As such, it is reasonable for the film capacitance to increase with increasing film thickness.

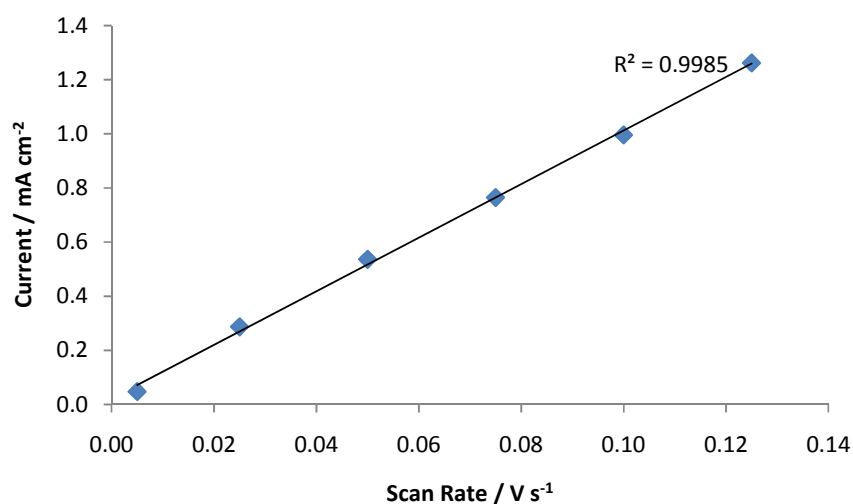


Figure 3.5: A plot of current, measured at 0.150 V vs. SCE, as a function of scan rate for a PPy-C4S film cycled at various scan rates between 0.100 V and 0.200 V vs. SCE in a $0.10 \text{ mol dm}^{-3} \text{ Na}_2\text{SO}_4$ solution. The PPy-C4S film was electropolymerised on a Pt electrode from a solution containing 0.20 mol dm^{-3} pyrrole / 0.01 mol dm^{-3} C4S at 0.500 V vs. SCE until a charge of 0.24 C cm^{-2} was reached.

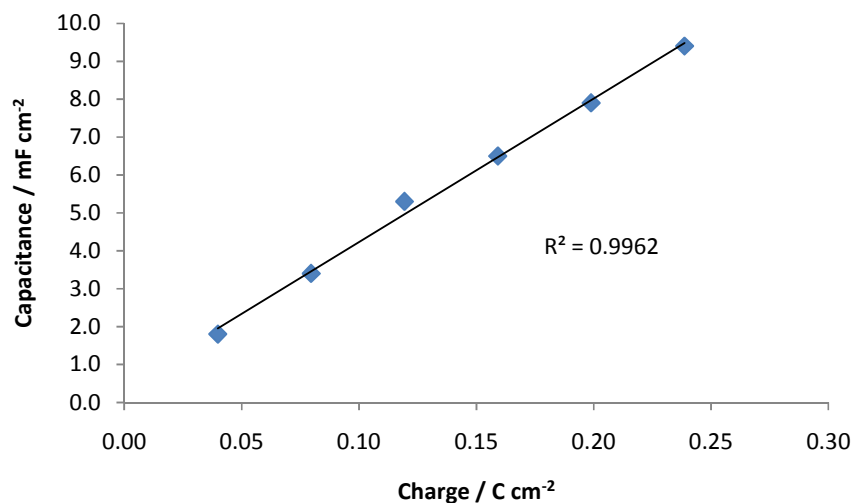


Figure 3.6: A plot of the capacitance of the PPy-C4S film against electropolymerisation charge. The PPy-C4S films were electropolymerised on a Pt electrode from a solution containing 0.20 mol dm^{-3} pyrrole / 0.01 mol dm^{-3} C4S at 0.500 V vs. SCE until charges of 0.04 , 0.08 , 0.12 , 0.16 , 0.20 and 0.24 C cm^{-2} were reached.

3.2.2.1 (iii) Novel Redox Activity of the PPy-C4S Film – the Generation of Calixquinones within the Polymer Film

The cyclic voltammograms discussed so far were all carried out at potentials below 0.200 V vs. SCE. However, the overall aim of this project was to produce an electrochemical sensor for dopamine. Considering the electroactivity of dopamine is generally observed at potentials greater than 0.200 V vs. SCE, the electrochemical behaviour of the PPy-C4S film needed to be investigated at these higher potentials. With this in mind, cyclic voltammetry was performed on the PPy-C4S film over a wider range of potentials. The cyclic voltammetric response of the film, between -0.800 and 0.800 V vs. SCE, is shown in Figure 3.7. Initially, the electrochemical activity of the film was typical of a PPy film. Only the redox behaviour of the PPy backbone, centred at -0.380 V vs. SCE, was observed on the first few scans. However, it quickly became obvious that the film possessed more complex electroactivity than first thought. A second redox couple, centred at 0.230 V vs. SCE, began to develop with further cycling (Figure 3.7). This result was quite unexpected. PPy-C4S modified electrodes had been prepared previously by Bidan and Mousavi but neither had reported any secondary electrochemical activity for the film^{38, 40}. Yet,

several repetitions of the experiment, using separate monomer solutions, verified this result was, in fact, real. Consequently, a series of experiments were carried out in an effort to determine the origin of this redox couple.

Given that sulfonated calixarenes are known to be electroactive⁵¹⁻⁵⁴, it seemed reasonable that the new redox activity could be due to the presence of C4S in the film. To check if this was the case, PPy-Cl and PPy-SO₄ films were prepared, under the same conditions used to prepare the PPy-C4S film, except that 0.10 mol dm⁻³ NaCl and Na₂SO₄ solutions were used as the supporting electrolytes, respectively. Figure 3.8 shows typical cyclic voltammograms obtained for these films. Both films exhibited a single redox couple corresponding to the oxidation and reduction of PPy. Moreover, all scans examined exhibited the same redox behaviour. This result confirmed that the calixarene was responsible for the second redox couple associated with the PPy-C4S film. In this respect, the new redox activity could be considered characteristic of the PPy-C4S film and is offered here as further proof that the calixarene was successfully incorporated into the PPy film.

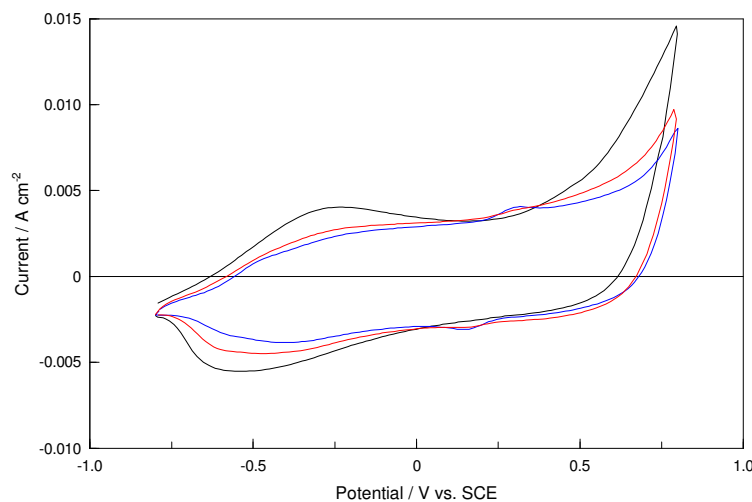


Figure 3.7: Cyclic voltammograms recorded in a 0.10 mol dm⁻³ Na₂SO₄ solution for a PPy-C4S film electropolymerised on a Pt electrode from a solution containing 0.20 mol dm⁻³ pyrrole / 0.01 mol dm⁻³ C4S at 0.500 V vs. SCE until a charge of 0.24 C cm⁻² was reached. Cycles 1 (—), 5 (—) and 10 (—) are shown. The scan rate was 100 mV s⁻¹.

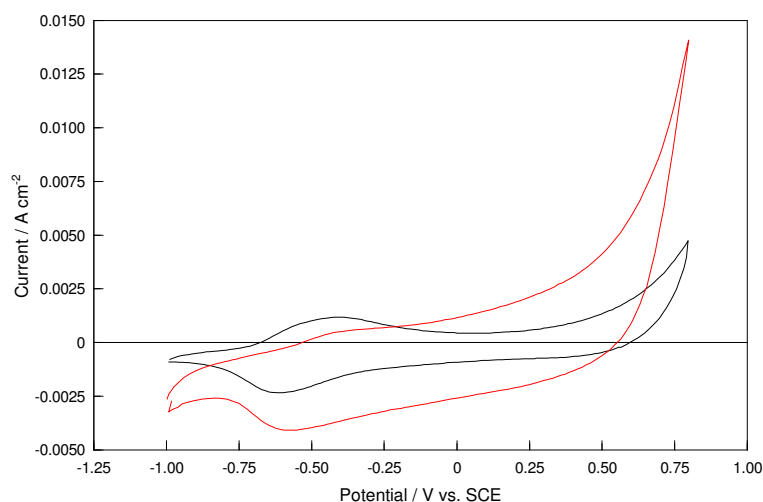
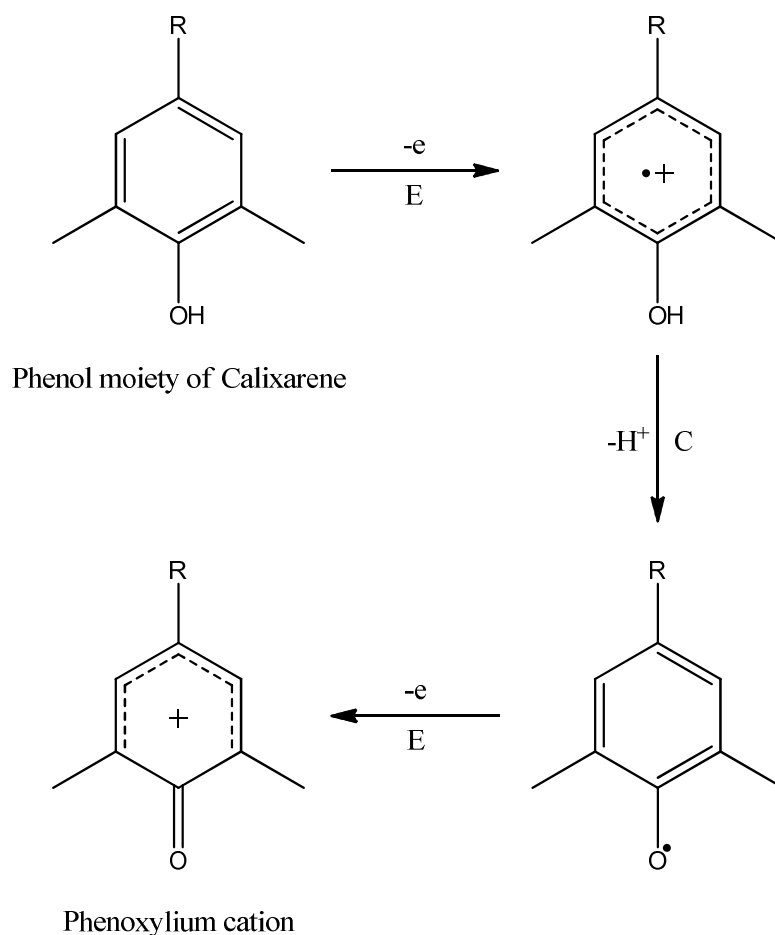


Figure 3.8: Cyclic voltammograms recorded in a $0.10 \text{ mol dm}^{-3} \text{ Na}_2\text{SO}_4$ solution for a PPy-Cl film (—) and a PPy-SO₄ film (—) electropolymerised on a Pt electrode from solutions containing 0.20 mol dm^{-3} pyrrole / 0.10 mol dm^{-3} NaCl and 0.20 mol dm^{-3} pyrrole / 0.10 mol dm^{-3} Na₂SO₄, respectively, at 0.800 V vs. SCE until a charge of 0.24 C cm^{-2} was reached. The scan rate was 100 mV s^{-1} .

However, knowing that the calixarene was responsible for the redox couple did not completely solve the matter. It was unlikely that the reaction being observed was simply the electrochemistry of the calixarene. The reason being that the signal in question was a well defined redox couple whereas the oxidation of the calixarene is known to be irreversible⁵¹⁻⁵⁴. The proposed solution electrochemistry of C4S is shown in Scheme 3.1. Additionally, the redox couple did not become apparent for several cycles suggesting that the species involved was not initially present in the film. In an effort to clarify this situation, both the factors affecting the redox couple and the electrochemistry of C4S needed to be studied in more detail.



Scheme 3.1: Mechanism for the irreversible electrochemical oxidation of a calixarene phenol moiety to form a phenoxylium cation⁵⁵⁻⁵⁸.

Firstly, the potential window for cyclic voltammetry was narrowed in order to focus solely on the redox couple. Figure 3.9 shows several successive cycles for the PPy-C4S film between -0.500 V and 0.800 V vs. SCE in a 0.10 mol dm⁻³ Na₂SO₄ solution. The redox couple was absent for the first few scans but then the Faradaic current could be seen to increase steadily reaching an eventual steady state. This type of behaviour was consistent with the formation of a new electroactive species. What is more, the fact that the current reached a steady state indicated that the new species was not free to diffuse away from the electrode surface but was instead trapped within the polymer film. Further support for this idea, that the redox couple was due to a new species being generated electrochemically within the PPy film, was provided by a study on the effect of potential on the redox couple. It was found that the upper potential limit had a significant influence on the magnitude of the redox

couple. Figure 3.10 shows cyclic voltammograms where the lower potential limit was fixed at -0.500 V vs. SCE and the upper potential limit was 0.500, 0.700, and 0.800 V vs. SCE. Each potential window should have been wide enough to observe the redox couple but as can be seen from Figure 3.10 this was not the case. A well defined redox couple was observed when the potential was scanned to 0.800 V vs. SCE but this redox couple was absent or only present as a small shoulder when the upper potential was 0.500 V and 0.700 V vs. SCE, respectively. This result clearly indicated that a threshold potential, required to generate the redox couple, existed. Thus, the redox couple could be assigned to a new electroactive species, formed within the PPy-C4S film, once this minimum potential was surpassed.

The significance of this threshold potential became clear upon investigation into the electrochemical activity of C4S. Figure 3.11 shows a cyclic voltammogram for the oxidation of C4S at a bare glassy carbon (GC) electrode. A single oxidation peak, observed at 0.900 V vs. SCE, with no corresponding reduction peak, confirmed the irreversibility of the oxidation of C4S, consistent with literature results⁵¹. However, a small redox couple, centred at 0.050 V vs. SCE, became apparent on the second scan (Figure 3.12). On further inspection of these cyclic voltammograms, the reduction peak for this redox couple, observed at -0.130 V vs. SCE, was also present on the first cycle. These observations pointed to the formation of a new electrochemically active species subsequent to the oxidation of C4S. Assuming this process could also occur when C4S was incorporated into the PPy-C4S film, it seemed likely that the redox couple observed for the PPy-C4S film could be attributed to the same process. Indeed, a comparison of the potentials required to generate both these species supported this assumption. The fact that a potential of 0.800 V vs. SCE was required to properly observe the PPy-C4S redox couple and that $E_{1/2}$ for the oxidation of C4S in solution was 0.780 V vs. SCE suggested that the PPy-C4S redox couple was connected to the oxidation of the calixarene. Therefore, it was proposed that the new redox couple, observed for the PPy-C4S film, was due to the formation of a new electrochemically active species within the film, following the oxidation of C4S.

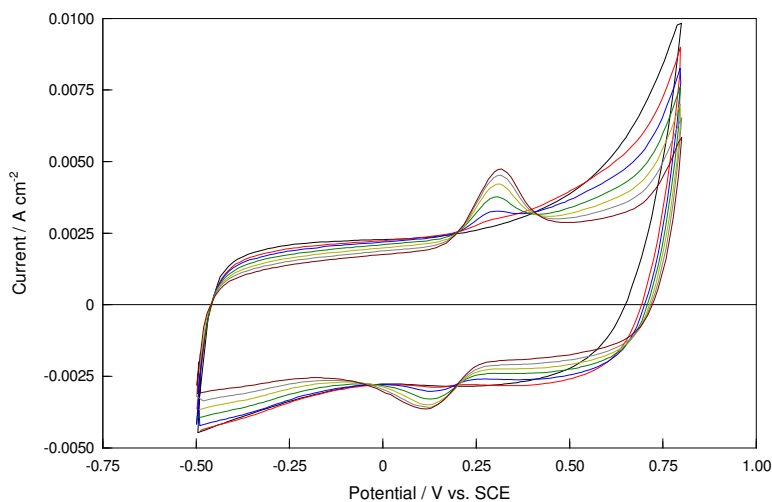


Figure 3.9: Cyclic voltammograms recorded in a $0.10 \text{ mol dm}^{-3} \text{ Na}_2\text{SO}_4$ solution for a PPy-C4S film electropolymerised on a Pt electrode from a solution containing 0.20 mol dm^{-3} pyrrole / 0.01 mol dm^{-3} C4S at 0.500 V vs. SCE until a charge of 0.24 C cm^{-2} was reached. Cycles 1 (—), 5 (—), 10 (—), 15 (—), 20 (—), 25 (—) and 30 (—) are shown. The scan rate was 100 mV s^{-1} .

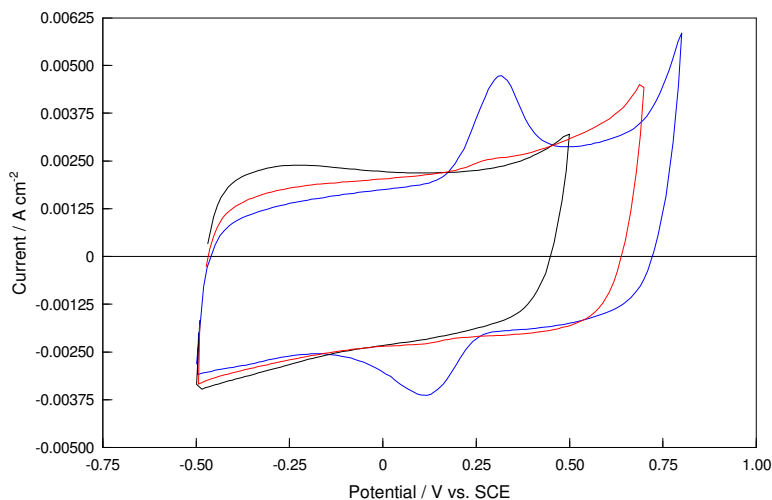


Figure 3.10: Cyclic voltammograms recorded in a $0.10 \text{ mol dm}^{-3} \text{ Na}_2\text{SO}_4$ solution from -0.500 V vs. SCE to 0.500 V (—), 0.700 V (—) and 0.800 V vs. SCE (—) for PPy-C4S films electropolymerised on a Pt electrode from a solution containing 0.20 mol dm^{-3} pyrrole / 0.01 mol dm^{-3} C4S at 0.500 V vs. SCE until a charge of 0.24 C cm^{-2} was reached. The scan rate was 100 mV s^{-1} .

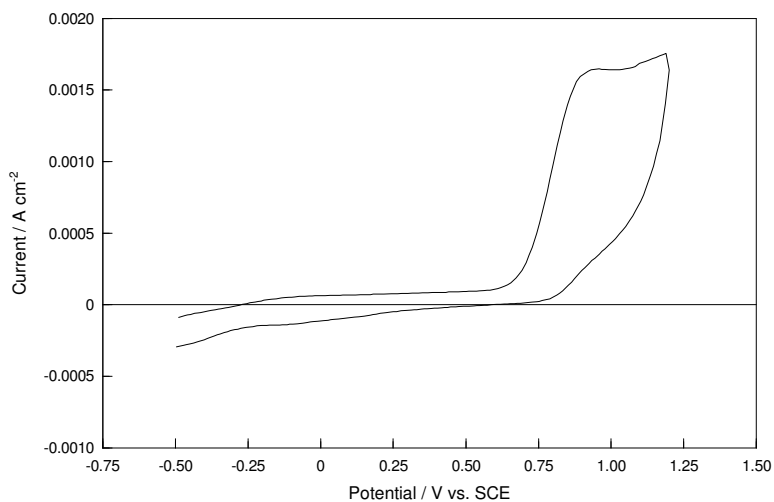


Figure 3.11: Cyclic voltammogram recorded in a 0.01 mol dm^{-3} C4S solution for a GC electrode at a scan rate of 100 mV s^{-1} .

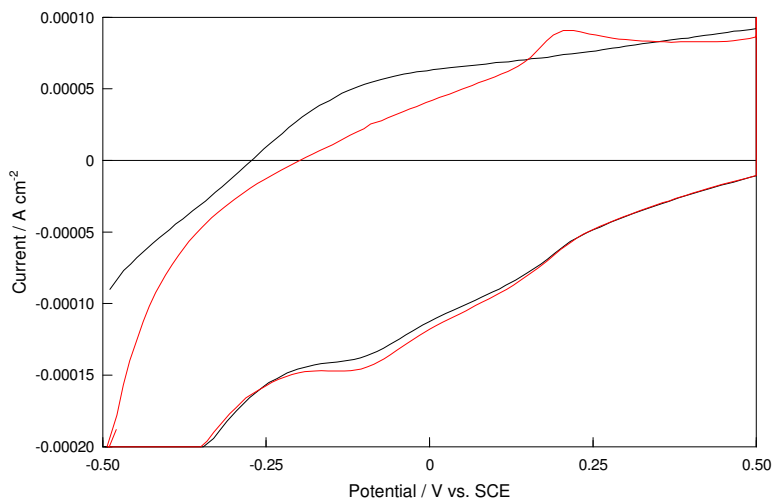


Figure 3.12: Cyclic voltammograms recorded in a 0.01 mol dm^{-3} C4S solution for a GC electrode at a scan rate of 100 mV s^{-1} . Cycles 1 (—) and 2 (—) are shown.

To the best of our knowledge, such a mechanism had not been reported previously for the sulfonated calixarenes. But there was a precedent. Louati and co-workers reported the electro-synthesis of calixquinones from several calix[4]arene and *p*-tert-butylcalix[4]arene derivatives^{55, 57, 58}. They too observed the appearance of new redox couples following the oxidation of the calixarene. Using preparative coulometry, with a fixed potential sufficient to fully oxidise the calixarene, they were able to synthesise and isolate mono- and di- calixquinones depending on the number of free phenolic hydroxyl groups present on the calixarene. Figure 3.13 shows one of the tert-butyl calixarene derivatives studied by Louati and co-workers and the calixdiquinone they successfully synthesised from it. They proposed a mechanism for this reaction similar to that put forward by Ronlan *et al.* for the synthesis of quinones from sterically hindered phenols^{55, 56}. The free phenol moieties of the calixarene were oxidised via a two electron ECE mechanism to form a phenoxylium cation (Scheme 3.1). This species was susceptible to nucleophilic attack, from residual water in the organic solvents used, resulting in the formation of a quinone at each free phenol moiety. Hence, it was proposed that the new redox couple, which appeared following the oxidation of C4S in solution, could be accounted for by the formation of a calixquinone.

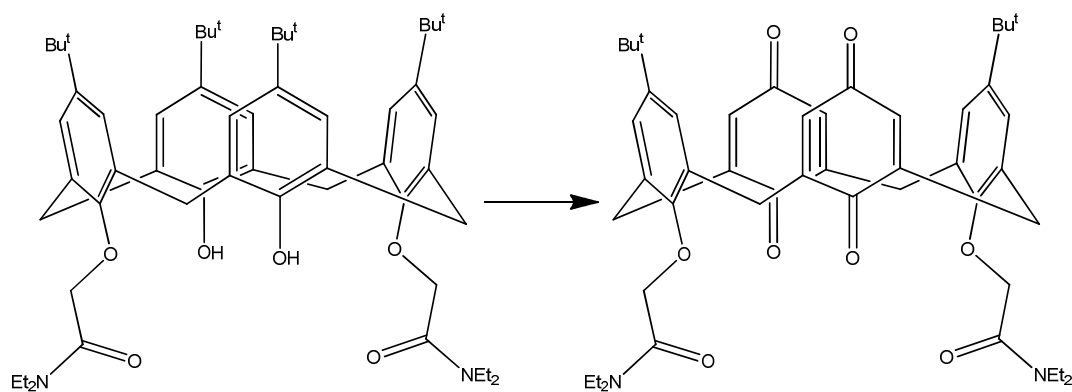


Figure 3.13: *p*-tert-butylcalix[4]arene-(OH)₂-(OCH₂CONEt₂)₂ and the calixdiquinone synthesised from it.

Although this proposal was not proven definitively, several factors suggested that the mechanism put forward by Louati could also be applied to C4S. Firstly, the oxidation of C4S is known to involve two electrons⁵¹ and so is likely to follow the same ECE mechanism reported by Ronlan and Louati. Secondly, the sulfonate group

of C4S would be expected to possess better leaving group abilities than the tert-butyl group of the *p*-tert-butylcalix[4]arene derivatives studied by Louati. The leaving group ability of a group is related to its stability when dissociated from the parent molecule. The more stable the group is, when free, the more likely it is to act as a leaving group. The leaving groups in this case were SO_3^{2-} , for C4S, and $(\text{CH}_3)_3\text{C}^-$, for Louati's calixarenes. The stability of these groups could be predicted by the pK_a of their conjugate acids. The lower the pK_a of the conjugate acid the more stable the base form of that species will be. The corresponding conjugate acids were HSO_3^- and $(\text{CH}_3)_3\text{CH}$, with pK_a values of 7.21 and 51 respectively. Clearly, the sulfonate was the more stable anion which implied a better ability to act as a leaving group. Thirdly, the nucleophile in both Louati and Ronlan's work was water, residual water in the solvent in Louati's case, whereas in this work the solvent itself was water. This meant that the concentration of nucleophile was significantly higher in this work making the nucleophilic substitution reaction more favourable. Taking these factors into consideration it was reasonable to assume that the new redox couple, which appeared subsequent to the oxidation of C4S, could be attributed to a calixquinone.

In light of these findings it seemed likely that the unexplained redox couple observed for the PPy-C4S film could also be attributed to a calixquinone. However, a comparison of the electrochemical response of the calixquinone in solution (Figure 3.12) and in the PPy-C4S film (Figure 3.9) showed some significant differences. Firstly, the peak separation for the calixquinone redox couple was reduced from 0.360 V, in solution, to 0.200 V, in the polymer. Such increases in reversibility are not unusual for redox systems within a polymer film. Raouf *et al.* reported a 630 mV reduction in peak separation for $\text{Fe}(\text{CN})_6^{3-}$ incorporated in a PPy film, and can be accounted for by the close proximity of these species to the electrode surface⁵⁹. Secondly, the currents observed for the calixquinone in the polymer were considerably higher than those observed for the calixquinone in solution. This was most likely due to the fact that the calixquinone and the calixarene were trapped within the polymer film. The calixquinone produced in solution could diffuse away from the electrode surface before it was reduced but the calixquinone produced in the film would be concentrated at the electrode surface. Also a greater proportion of calixarene would be expected to be oxidised when incorporated in the polymer film,

due to its preconcentration at the electrode surface, leading to larger quantities of calixquinone being produced. As a result of these factors higher currents were expected for the calixquinone in the PPy-C4S film than in solution.

3.2.2.2 Electrochemical Impedance Spectroscopy (EIS)

EIS is a powerful technique that can be used to characterise different electrochemical processes occurring simultaneously in a conducting polymer modified electrode. Electrochemical processes such as charge transfer, ion diffusion and capacitance are separated on the basis of their frequency dependent response and can be evaluated individually if their time constants differ enough, with fast processes being observed at high frequencies while slower processes are observed at lower frequencies. Fitting of equivalent circuit models, where each element in the circuit is assumed to represent a real process, can be used to elucidate the contribution of each of these processes to the overall impedance of the modified electrode. When the correct model is applied it can help to understand both the electronic and physicochemical properties of the conducting polymer modified electrode.

3.2.2.2 (i) General EIS Discussion for the PPy-C4S Film

PPy-C4S films were electrosynthesised on a platinum electrode at 0.500 V vs. SCE until a charge of 0.24 C cm^{-2} was reached. Impedance measurements were carried out over a range of frequencies, from 60 kHz to 10 mHz, and the frequency dependent response of the PPy-C4S modified electrode was studied at bias potentials from 0.500 V to -0.800 V vs. SCE. Prior to each frequency scan the films were allowed to equilibrate at the bias potential for 30 minutes. The complex plane impedance plots obtained for the film at 0.200 V and -0.800 V vs. SCE, by scanning the frequency from high to low and then in the reverse direction, are shown in Figure 3.14. The frequency response of the modified electrode was found to be independent of the direction the frequency was scanned. This observation indicated that the 30 minute equilibration time was sufficient for the polymer to reach a steady

state. Thus, possible hysteresis effects on the impedance results could be disregarded.

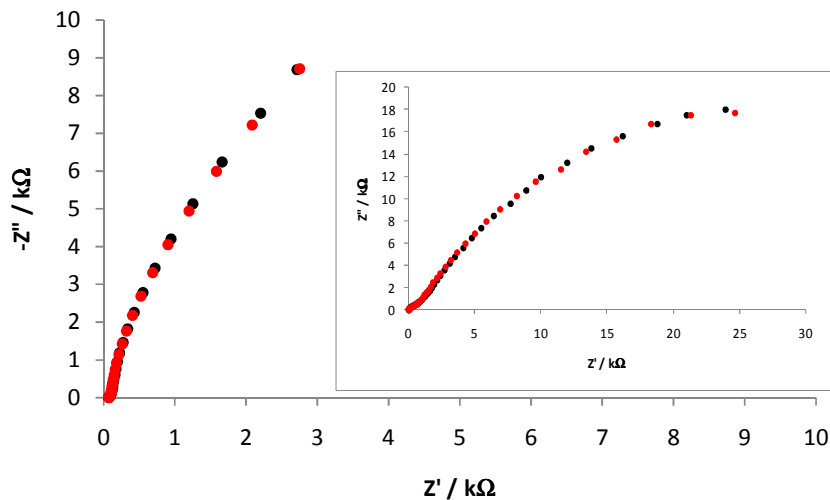


Figure 3.14: Complex plane impedance plots obtained for the PPy-C4S film at 0.200 V and -0.800 V vs. SCE (Inset). The frequency was scanned first from 60 kHz to 10 mHz (●) and then in the reverse direction, from 10 mHz to 60 kHz (●).

To the best of our knowledge this is the first EIS characterisation study of a PPy-C4S film. However, polypyrrole films in general have been studied extensively using EIS. A dual rail transmission line circuit (Figure 3.15) has been used by several groups to explain the impedance data observed for these films⁶⁰⁻⁶⁵. In this model, first proposed by Albery and co-workers⁶⁰, two parallel resistances are used to represent the transport of electrons (R_e) and counterions (R_{ion}) within the polymer film. A distributed capacitance (C_f), representing the faradaic capacitance of the film, connects the two film resistances and a third resistance (R_s) is used to represent the resistance of the electrolyte solution. In practice, it was found that a simpler transmission line in which one resistance rail was considered negligible could usually describe the system adequately⁶³. In particular, Pickup determined that the electronic resistance (R_e) of polypyrrole was generally too low to contribute significantly to the impedance of the film^{27, 66}. This was due to the high conductivity of polypyrrole films when even slightly oxidised. Only at high reduction potentials

was the contribution of R_e to the overall impedance substantial^{64, 67}. Similar results were obtained for the PPy-C4S films studied here.

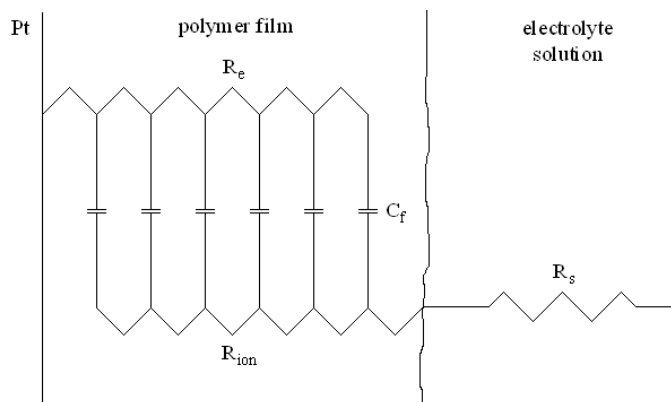


Figure 3.15: The dual rail transmission line circuit used to model the electrochemistry of polypyrrole films.

The complex plane impedance plots obtained for the PPy-C4S modified electrode exhibited two forms over the potential range 0.500 V to -0.800 V vs. SCE. These forms were dependent on the degree of oxidation of the film. It can be seen from Figure 3.16 that a significant portion of the film was oxidised at -0.400 V vs. SCE whereas at -0.600 V vs. SCE the film was predominantly reduced and at -0.800 V vs. SCE the film was completely reduced. Consequently, the complex plane impedance plots obtained at -0.400 V vs. SCE and above, where the film was largely in the oxidised state, were of one form and below this potential, where the film was reduced, the impedance plots were of a different form. Several equivalent circuits were fitted to the experimental data and the quality of fit obtained was estimated by the chi-square (χ^2) value. Two different circuits were required to explain the frequency response of the PPy-C4S film over the entire potential range studied and these circuits are now discussed separately.

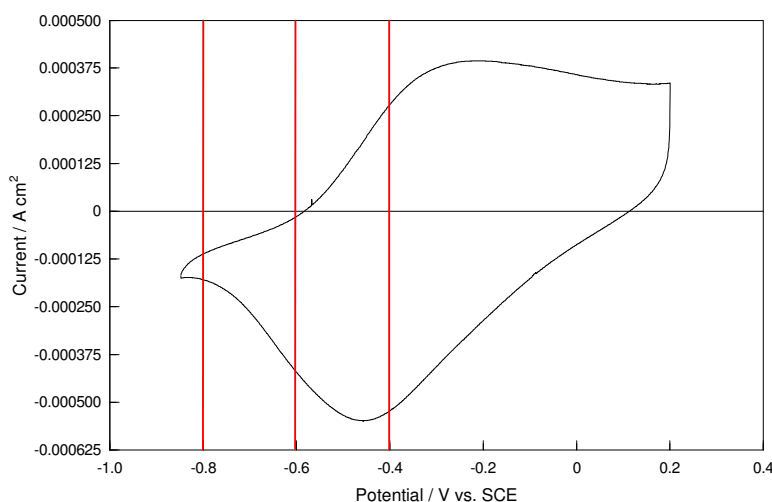


Figure 3.16: Cyclic voltammogram recorded in a $0.10 \text{ mol dm}^{-3} \text{ Na}_2\text{SO}_4$ solution for a PPy-C4S film electropolymerised on a Pt electrode from a solution containing 0.20 mol dm^{-3} pyrrole / 0.01 mol dm^{-3} C4S at 0.500 V vs. SCE until a charge of 0.24 C cm^{-2} was reached. The potentials of -0.400 V , -0.600 V and -0.800 V vs. SCE are highlighted. The scan rate was 5 mV s^{-1} .

3.2.2.2 (ii) Complex Plane Impedance Analysis of PPy-C4S Films in the Oxidised State.

Typical complex plane impedance plots for the oxidised films are shown in Figure 3.17. For clarity only the plots obtained at 0.200 V , 0 V , -0.200 V and -0.400 V vs. SCE are given. The circuit shown in Figure 3.18 was found to give the best fit over the potential range 0.500 V to -0.400 V vs. SCE with an average χ^2 value of 3.1×10^{-4} . The quality of the fit can be seen from the close agreement between the experimental and theoretical impedance plots in Figure 3.17. The equivalent circuit was composed of two resistors (R_s and R_p), a constant phase element (CPE_p) and a Warburg element (W_i). The values obtained for these circuit parameters are listed in Table 3.2.

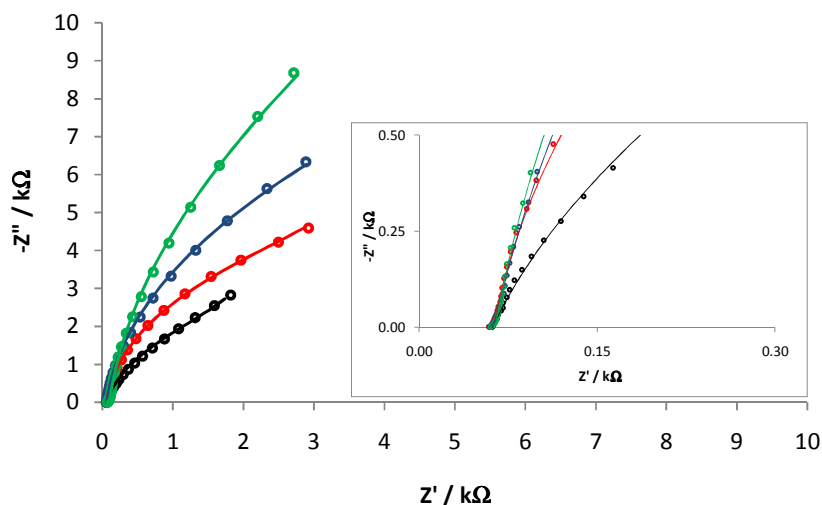


Figure 3.17: Experimental (●) and theoretical (—) complex plane impedance plots for the PPy-C4S film at -0.400 V (●), -0.200 V (●), 0 V (●) and 0.200 V vs. SCE (●). The high frequency region is expanded in the inset. The equivalent circuit used to fit the experimental data is also shown.

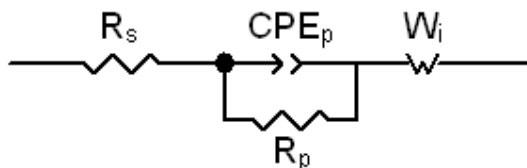


Figure 3.18: The equivalent electrical circuit used to model the electrochemical impedance data for the oxidised PPy-C4S films.

Table 3.2: The equivalent circuit fitting parameters and faradaic capacitance values, C_f , for the PPy-C4S film at potentials between 0.500 V and -0.400 V vs. SCE.

$E /$ V vs. SCE	R_s / Ω	CPE_p -A / $mF\ cm^{-2}$	n	$C_f /$ $mF\ cm^{-2}$	R_p / Ω	W_i $B / s^{0.5}$
0.5	60.72	9.5	($n=0.91$)	9.4	8145	0.85
0.3	59.83	9.5	($n=0.89$)	9.1	7369	0.82
0.2	61.41	11.1	($n=0.94$)	10.4	7773	0.50
0.0	59.72	13.5	($n=0.93$)	12.6	7228	0.25
-0.2	59.95	17.5	($n=0.90$)	15.8	3653	0.12
-0.3	57.89	19.9	($n=0.89$)	18.4	2516	0.09
-0.4	59.83	19.0	($n=0.89$)	17.0	1873	0.06

As discussed previously, R_e was negligible in this potential region due to oxidation of the film^{27, 66}. This is clear from the relatively constant value obtained for R_s . The value for R_s was determined from the high frequency intercept of the impedance plot with the real axis. Using the transmission line model^{60, 62} outlined above, the high frequency intercept gives $R_{soln} + R_\infty$, where R_{soln} is the uncompensated solution resistance and

$$\frac{1}{R_\infty} = \frac{1}{R_e} + \frac{1}{R_{ion}} \quad Eq(3.3)$$

It can be seen from Table 3.2 and the inset in Figure 3.17 that R_s was independent of potential for all data considered here. This situation occurs because R_∞ approaches zero when either R_e or R_{ion} , in this case R_e , is negligible compared to the solution resistance. Therefore, R_s could be attributed to the uncompensated solution resistance^{60, 62}.

The parallel combination of a constant phase element, CPE_p , and a resistance, R_p , was used to represent the pseudo-capacitance and resistance of the film, respectively. A CPE is commonly used to compensate for the non-ideal capacitive, conductive and diffusion behaviour typically displayed by conducting polymer modified electrodes⁶⁸. This non-ideal behaviour has been attributed to the inhomogeneous, ie. rough or porous, nature of these materials⁶⁸. The impedance of the constant phase element is defined by,

$$Z_{CPE} = \frac{1}{A(j\omega)^n} \quad Eq(3.4)$$

where A and n are constants, n having values between 0 and 1, $j = \sqrt{-1}$ and $\omega = 2\pi f$ is the angular frequency. For $n = 1$, the CPE describes an ideal capacitor and $A = C$ where C is capacitance. For $n = 0$, the CPE describes an ideal resistor and for $n = 0.5$ it describes semi-infinite diffusion. It can be seen from the n values listed in Table 3.2 that CPE_p represented a slightly distorted capacitance. Therefore, the pseudo-capacitance C_f of the film could be approximated by the CPE constant (A). The pseudo-capacitance of the film was also obtained directly from the impedance data by plotting the imaginary impedance (Z'') as a function of $1/\omega$. Figure 3.19 shows the plot obtained using the impedance data measured at 0.200 V vs. SCE. The plots obtained for all potentials were linear at intermediate frequencies with a slope

equal to $1/C_f$. The CPE- A and C_f values are presented in Table 3.2 and ranged from 9.5 and 9.3 mF cm^{-2} to 19.9 and 18.4 mF cm^{-2} , respectively. The good agreement observed between these two sets of measurements indicated that the equivalent circuit in Figure 3.18 was a good model for the oxidised PPy-C4S film. Furthermore, the capacitance value of 9.4 mF cm^{-2} , measured using cyclic voltammetry for the PPy-C4S film at 0.150 V vs. SCE (Section 3.2.2.1 (ii)), compares well with the capacitance values reported here.

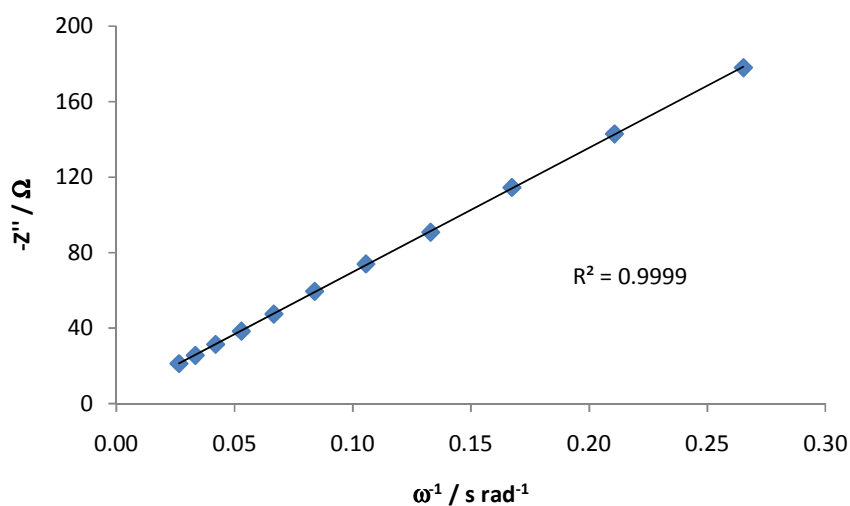


Figure 3.19: A plot of the imaginary impedance as a function of $1/\omega$ for the PPy-C4S film at 0.200 V vs. SCE.

High capacitance values were obtained using both methods outlined above. These results were consistent with the high charge storage capacity typically displayed by polypyrrole films^{1-3, 27, 48, 49}. Polypyrrole films are generally found to have volumetric capacitances in excess of 100 F cm^{-3} . In this case, a direct comparison was difficult due to the fact that a consistent measurement of the film thickness was not achieved. However, if the film thickness is said to be $1 \mu\text{m}$, approximately the largest thickness measurement obtained in Section 3.2.1.3, then an estimation of the volumetric capacitance of the PPy-C4S film can be made. Using the average C_f value obtained over the potential range 0.200 V to 0.500 V vs. SCE gives a volumetric capacitance of at least 97 F cm^{-3} for the oxidised PPy-C4S film. Again this value is merely for

the sake of comparison, and is likely an underestimate, but it shows that the capacitance of the film is in the range expected for a polypyrrole film.

The capacitance of conducting polymers arises from oxidation and reduction of the polymer backbone and can be regarded as being due to the charge separation between positively charged sites of the polymer chain and doping anions^{29, 49, 68}. As such, a potential dependence for the capacitance would be expected. The relationship between the capacitance (C_f) and the potential applied to the PPy-C4S film is shown in Figure 3.20. For the sake of completeness, the capacitance values of the reduced PPy-C4S films, -0.600 V and -0.800 V vs. SCE, are also shown. The capacitance was indeed dependent on potential. In the reduced state, -0.800 V vs. SCE, the capacitance of the film was at its lowest (1.1 mF cm⁻²). As the potential was increased, the capacitance increased sharply due to oxidation of the film. The capacitance of the PPy-C4S film reached a maximum near the peak oxidation potential of film and then decreased slightly as the film was becoming fully oxidised. Similar trends in capacitance have been observed for both chemically^{49, 69} and electrochemically^{27, 29, 67, 70} synthesised polypyrrole.

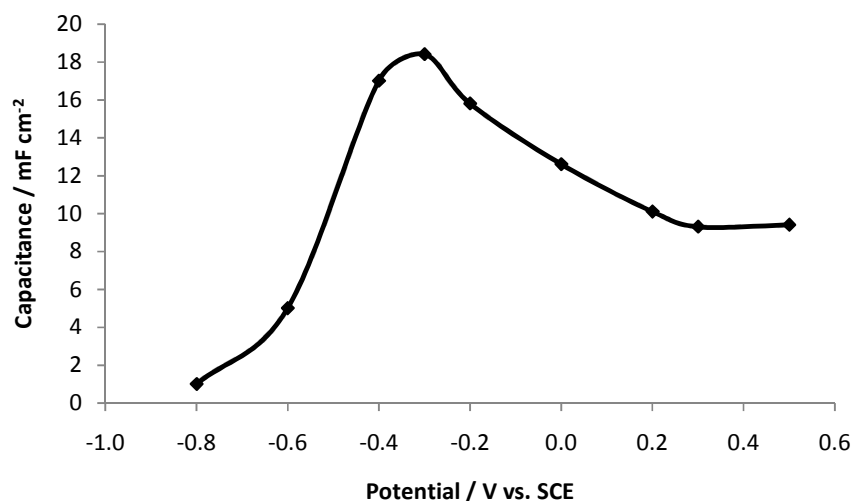


Figure 3.20: A plot of the capacitance, C_f , of the PPy-C4S film, obtained from the inverse slopes of plots of Z'' vs. $1/\omega$, as a function of the potential applied to the polymer.

The resistor, R_p , represented the resistance of the PPy-C4S film. As R_e was negligible in this potential region, R_p was related to the ionic resistance of the film. The values of R_p obtained from fitting of the equivalent circuit to the impedance data are presented in Table 3.2. The resistance values ranged from 8145 to 1873 Ω and were of a comparable magnitude ($k\Omega$ range) to ionic resistances reported in the literature for polypyrrole films^{28, 29, 48, 62, 70}. From Table 3.2 it can be seen that the resistance decreased as the potential decreased. This form of relationship between ionic resistance and potential is typical of cation exchange polymers. Ren and Pickup measured the ionic resistance of polypyrrole films doped with polystyrenesulfonate (PSS)^{27, 28}. They too observed a decrease in ionic resistance with decreasing potential. This trend can be explained by considering the nature of the ionic charge carriers in the film. In contrast to polypyrrole films doped with small anions, where the anions move during the electrochemical switching of the polymer, the electrochemistry of polypyrrole films doped with large polyanions, such as PSS and C4S, involves cation transport. Consequently, their ionic resistance is governed by the concentration of cations in the film. In the oxidised state, the electroneutrality of the film is maintained by the immobile counteranion (C4S or PSS). As such, there is a lack of mobile ionic charge carriers in the film so its ionic resistance is high. As the potential is lowered, the film starts to be reduced and Na^+ cations enter the film to balance the negative charges on the calixarene, causing an increase in the concentration of mobile charge carriers in the film. Hence, the ionic resistance is observed to decrease as the potential decreases. Thus, the results outlined here can be regarded as further evidence that C4S is irreversibly incorporated into the polypyrrole matrix.

The final element in the circuit is the Warburg impedance. Warburg behaviour, as it applies to conducting polymers, has been attributed to the slow motion of ions within a porous polymer film. In this case, W_i describes the movement of Na^+ ions in the PPy-C4S film. The Warburg impedance can be represented by,

$$Z_W = \frac{B^2 \coth(B\sqrt{j\omega})}{C B\sqrt{j\omega}} \quad Eq(3.5)$$

where j and ω have been defined previously, C is the distributed charge capacity of the film and B is a diffusional time constant defined by,

$$B = \sqrt{\frac{L^2}{D}} \quad \text{Eq(3.6)}$$

where L is the diffusion length and D is the ionic diffusion coefficient^{29, 70-72}.

The values for the Warburg time constant (B) were determined from fitting of the equivalent circuit to the impedance data and are listed in Table 3.2. A decrease in the values of B was observed as the potential decreased. From Equation 3.6 it can be seen that $D \propto 1/B^2$. Assuming the length of the diffusion pathway remained constant, as L is usually approximated as the dry film thickness, a general increase in the diffusion coefficient, with decreasing potential, could be inferred. This finding was consistent with the increasing permeability of the film to Na^+ cations, due to reduction of the film, as the potential was decreased. A similar but opposite trend is typically observed for polypyrrole doped with small anions. In these cases anions are expelled upon reduction of the film and so the diffusion coefficient decreases with decreasing potential^{68, 70-72}.

3.2.2.2 (iii) Complex Plane Impedance Analysis of PPy-C4S Films in the Reduced State

The complex plane impedance plots for the reduced PPy-C4S film, measured at -0.600 V and -0.800 V vs. SCE, are shown in Figure 3.21. The inset of Figure 3.21 shows the expanded high frequency region. The equivalent circuit in Figure 3.22 was found to give the best fit with an average χ^2 value of 3.0×10^{-4} . The parameters determined from fitting of this equivalent circuit to the impedance data are given in Table 3.3.

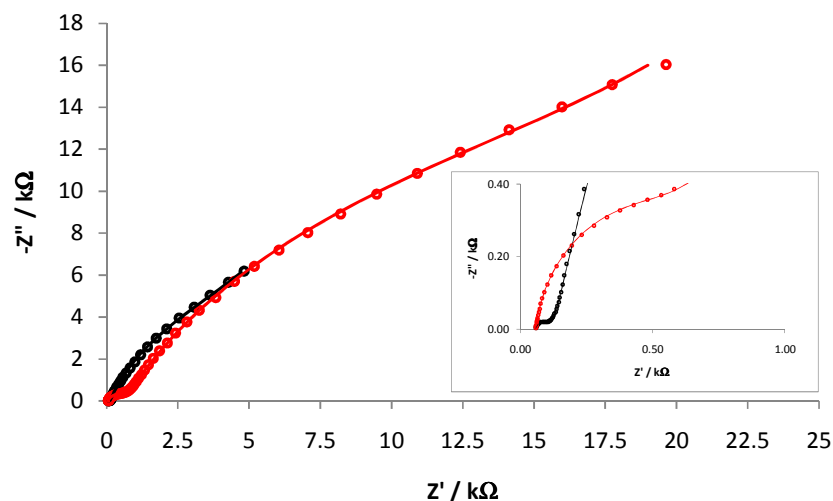


Figure 3.21: Experimental (●) and theoretical (—) complex plane impedance plots for the PPy-C4S film at -0.600 V (●), -0.800 V vs. SCE (●). The high frequency region is expanded in the inset.

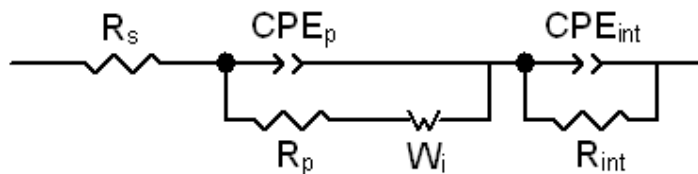


Figure 3.22: The equivalent electrical circuit used to model the electrochemical impedance data for the reduced PPy-C4S films.

Table 3.3: The equivalent circuit fitting parameters and faradaic capacitance values, C_f , for the PPy-C4S film at potentials of -0.600 V and -0.800 V vs. SCE.

E / V	R_s / Ω	$CPE_p \cdot A / \text{mF cm}^{-2}$	$C_f / \text{mF cm}^{-2}$	R_p / Ω	W_i $B / \text{s}^{0.5}$	$CPE_{int} \cdot A / \mu\text{F cm}^{-2}$	R_{int} / Ω
-0.6	58.90	6.4 ($n=0.78$)	5.0	9612	0.26	294 ($n=0.77$)	69.51
-0.8	61.31	1.3 ($n=0.80$)	1.1	23053	0.51	95 ($n=0.67$)	806.9

The equivalent circuit was composed of the solution resistance (R_s), a Warburg element (W_i), and two parallel combinations of a constant phase element (CPE_p and CPE_{int}) and a resistor (R_p and R_{int}). A comparison between the R_s values in Table 3.3 and those obtained for the oxidised film (Table 3.2) shows this resistance remained independent of potential. Therefore, it represented the uncompensated resistance of the electrolyte solution, as outlined in Section 3.2.2.2 (ii).

The complex plane impedance plots were characterised by two semicircular regions which were modelled using two CPE-R circuits in series. Similar impedance plots consisting of two semi-circular regions have been observed for polypyrrole by many groups^{18, 29, 64, 73-76}. Typically the impedance of the bulk polymer is represented by one semi-circle and the impedance at either the polymer/electrolyte or polymer|Pt interface is represented by the other. In this case, the low frequency semicircle was attributed to the impedance of the PPy-C4S film, and the high frequency semicircle represented the impedance at the polymer|Pt interface.

The capacitance of the PPy-C4S film was represented by the constant phase element, CPE_p . Comparing the n values listed in Table 3.2 and Table 3.3 it is clear that the capacitance was more distorted for the reduced films. This suggested that the film became less homogeneous as it was reduced. A possible explanation for this may be the ingress of Na^+ cations associated with the reduction of the film. At the potentials studied here the film was predominantly, -0.600 V vs. SCE, or completely, -0.800 V vs. SCE, reduced. Consequently, the concentration of Na^+ in the film would be highest at these potentials. The pseudo-capacitance of the reduced PPy-C4S film was estimated in the same way as described for the oxidised films. The capacitance, being related to the degree of oxidation of the film, was expected to decrease with decreasing potential. This was reflected in the decreasing CPE-A and C_f values given in Table 3.3.

The resistance R_p represented the resistance of the PPy-C4S film. It is clear from Table 3.3 and the relative magnitude of the low frequency semicircles (Figure 3.21) that R_p increased as the potential was decreased. This trend can be explained by considering the contributions of both R_{ion} and R_e to the resistance of the film. Ren and Pickup observed that R_e becomes significant for reduced polypyrrole films^{64, 67}. In particular, they found that the resistance of reduced cation exchange polymers,

such as PPy-PSS and PPy-C4S films, can be adequately described by a single resistance, R_e . At potentials where these films are reduced and R_e is significant, the ionic resistance tends to be low due to the high concentration of ionic charge carriers within the film. Thus, R_p could be attributed to the electronic resistance of the PPy-C4S film. As such, the increase in R_p with decreasing potential was in accordance with the increased reduction of the film. In fact, the values obtained for R_e by Ren and Pickup⁶⁴ for a reduced PPy-PSS film (approx 10 k Ω) are comparable to the R_p values reported here.

As was the case for the oxidised films, the inclusion of a Warburg element in the circuit represented the movement of Na^+ in the PPy-C4S film. The values obtained for the diffusional time constant (B) are presented in Table 3.3. These values were expected to decrease with decreasing potential, just like the oxidised films in Section 3.2.2.2 (ii), due to additional ingress of Na^+ as the film was further reduced. However, the opposite trend was observed. The B value obtained at -0.600 V vs. SCE (Table 3.3) was considerably larger than at -0.400 V vs. SCE (Table 3.2) and it increased further when the potential was lowered to -0.800 V vs. SCE. This trend was consistently observed for these potentials and, from examination of Equation 3.6, suggested that the ionic diffusion coefficient decreased as the polymer was reduced. A possible explanation for this was the 'ladder doped' structure proposed by Ingram *et al.* for PPy films doped with polysulfonated aromatic compounds³⁴. In this model the dopants act as cross linkers at the positive positions along neighbouring oxidized PPy chains. In this way, the anions create open channels, within the oxidized polymer, in which fast ionic movement can occur. However, upon reduction of the polymer the anions would be free to bind with the incoming cations causing the open structure to collapse and thereby hindering ionic movement. As a result, the ionic diffusion coefficient would be expected to decrease. Assuming the PPy-C4S film has a similar structure, this could account for the trend in B values observed for the reduced films.

The emergence of a high frequency semi-circle suggested that an interfacial charge transfer process had become slow enough to be observed. This feature was assigned to the polymer|Pt interface as observed and supported by the impedance analysis of Ren and Pickup⁶⁴. The constant phase element, CPE_{int} , represents the capacitance or

charging of the double layer formed at this interface. From the n values presented in Table 3.3, it can be seen that CPE_{int} represented a considerably distorted capacitance. Due to this degree of distortion, the CPE-A values could not be used to approximate the capacitance at this interface however the magnitude of these values ($\mu F\ cm^{-2}$) was of the order expected for a double layer capacitance^{64, 75, 76}. The resistor, R_{int} , represented the charge transfer resistance at this interface. The increase in this value with decreasing potential was in accordance with the increased reduction and electronic resistance of the PPy-C4S film.

3.3 Conclusion

The work presented in this chapter represents the first systematic characterisation of a conducting polypyrrole (PPy) film doped with a sulfonated calixarene. Pyrrole was electropolymerised on a platinum substrate from an aqueous solution containing *p*-sulfonatocalix[4]arene (C4S). The physical and electrochemical properties of the resulting PPy-C4S films were then studied using a variety of different techniques.

EDX analysis performed on the PPy-C4S film showed that C4S had been successfully incorporated into the PPy matrix. Moreover, this analysis indicated that the film was doped solely by the penta-anionic calixarene. SEM images recorded for these films exhibited the typical ‘cauliflower’ morphology widely observed for PPy films. In addition, a noticeable increase in the surface roughness of the PPy-C4S film was observed when the electropolymerisation potential was increased. Although the thickness of the PPy-C4S film could not be measured accurately, it was found that increasing the charge consumed during the growth of the film caused a definite increase in the thickness of the film.

Cyclic voltammetry carried out in the region of PPy oxidation and reduction suggested that the PPy-C4S film could act as a cation exchange polymer. The sharper appearance of the reduction wave, relative to the oxidation wave, indicated that this process was accompanied by an influx of high mobility cations (Na^+) rather than the expulsion of bulky C4S anions. EIS studies on the charge transport processes occurring in the PPy-C4S film supported this deduction. A decrease in the ionic resistance (R_{ion}) of the film was observed when the polymer was switched from the oxidised to the reduced state. Again, this could be explained by an influx of mobile cations into the film during reduction. The electronic resistance (R_e) was determined to be negligible for the PPy-C4S film, in accordance with the high electronic conductivity of oxidised PPy films, only becoming significant when the film was highly reduced.

Capacitance measurements for the PPy-C4S film were performed using cyclic voltammetry and EIS. These measurements were in good agreement giving capacitance values of 9.4 and 10.4 mF cm^{-2} , respectively, for the fully oxidised film. The results from both of these studies suggested that the capacitance of the PPy-C4S

film was predominantly due to the charge separation between positively charged sites along the PPy chains and the anionic C4S. Using cyclic voltammetry, the capacitance was found to increase with film thickness, and from the EIS studies, the capacitance was observed to increase with potential, reaching a maximum near the peak oxidation potential of the film.

Finally, cyclic voltammetry studies of the PPy-C4S film also revealed a second redox couple, centred at 0.230 V vs. SCE, which was independent of the electrochemistry of PPy. This novel electrochemical activity was attributed to the oxidation and reduction of a calixquinone. Calixquinones could be generated within the PPy-C4S film at potentials sufficient to oxidise C4S. We propose that the oxidation product of C4S was susceptible to nucleophilic attack from water, resulting in the formation of a calixquinone. Thus, this novel electrochemistry arose from the presence of C4S within the film and could be considered characteristic of the PPy-C4S film.

3.4 Bibliography

- (1) Bull, R. A.; Fan, F. R. F.; Bard, A. J. *J. Electrochem. Soc.* **1982**, *129*, 1009-1015.
- (2) Ko, J. M.; Rhee, H. W.; Park, S. M.; Kim, C. Y. *J. Electrochem. Soc.* **1990**, *137*, 905-909.
- (3) Yeu, T.; Yin, K. M.; Carbajal, J.; White, R. E. *J. Electrochem. Soc.* **1991**, *138*, 2869-2877.
- (4) Kaplin, D. A.; Qutubuddin, S. *Polymer* **1995**, *36*, 1275-1286.
- (5) Wood, G. A.; Iroh, J. O. *Synth. Met.* **1996**, *80*, 73-82.
- (6) Wood, G. A.; Iroh, J. O. *Polym. Eng. Sci.* **1996**, *36*, 2389-2395.
- (7) Wood, G. A.; Iroh, J. O. *J. Appl. Polym. Sci.* **1996**, *61*, 519-528.
- (8) Iroh, J. O.; Wood, G. A. *J. Appl. Polym. Sci.* **1996**, *62*, 1761-1769.
- (9) Iroh, J. O.; Wood, G. A. *Eur. Polym. J.* **1997**, *33*, 107-114.
- (10) Li, Y.; Yang, J. *J. Appl. Polym. Sci.* **1997**, *65*, 2739-2744.
- (11) Su, W.; Iroh, J. O. *Electrochim. Acta* **1997**, *42*, 2685-2694.
- (12) Silk, T.; Hong, Q.; Tamm, J.; Compton, R. G. *Synth. Met.* **1998**, *93*, 59-64.
- (13) Otero, T. F.; Cantero, I. *J. Electrochem. Soc.* **1999**, *146*, 4118-4123.
- (14) Arrigan, D. W. M.; Lowens, M. J. *Electroanalysis* **1999**, *11*, 647-652.
- (15) Hernandez-Perez, T.; Morales, M.; Batina, N.; Salmon, M. *J. Electrochem. Soc.* **2001**, *148*, C369-C375.
- (16) Xing, S.; Zhao, G. *Polym. Bull. (Heidelberg, Ger.)* **2006**, *57*, 933-943.
- (17) Tietje-Girault, J.; Ponce, d. L. C.; Walsh, F. C. *Surf. Coat. Technol.* **2007**, *201*, 6025-6034.
- (18) Akinyeye, R. O.; Michira, I.; Sekota, M.; Al, A. A.; Tito, D.; Baker, P. G. L.; Brett, C. M. A.; Kalaji, M.; Iwuoha, E. *Electroanalysis* **2007**, *19*, 303-309.
- (19) Wang, Y.; Northwood, D. O. *Thin Solid Films* **2008**, *516*, 7427-7432.
- (20) Fonner, J. M.; Forciniti, L.; Nguyen, H.; Byrne, J. D.; Kou, Y.-F.; Syeda-Nawaz, J.; Schmidt, C. E. *Biomed Mater* **2008**, *3*, 034124.
- (21) Zhu, R. L.; Li, G. X.; Zheng, J. H.; Jiang, J. W.; Zeng, H. B. *Surf. Eng.* **2009**, *25*, 156-162.
- (22) Bhattacharya, A.; De, A.; Das, S. *Polymer* **1996**, *37*, 4375-4382.

- (23) Yuan, Y. J.; Adeloju, S. B.; Wallace, G. G. *Eur. Polym. J.* **1999**, *35*, 1761-1772.
- (24) Saidman, S. B.; Quinzani, O. V. *Electrochim. Acta* **2004**, *50*, 127-134.
- (25) Ansari, K. R. *Russ. J. Electrochem.* **2005**, *41*, 950-955.
- (26) Baker, C. K.; Qiu, Y. J.; Reynolds, J. R. *J. Phys. Chem.* **1991**, *95*, 4446-4452.
- (27) Ren, X.; Pickup, P. G. *J. Phys. Chem.* **1993**, *97*, 5356-5362.
- (28) Ren, X.; Pickup, P. G. *Electrochim. Acta* **1996**, *41*, 1877-1882.
- (29) Grzeszczuk, M.; Zabinska-Olszak, G. *J. Electroanal. Chem.* **1997**, *427*, 169-177.
- (30) Inzelt, G.; Kertesz, V.; Nyback, A.-S. *J. Solid State Electrochem.* **1999**, *3*, 251-257.
- (31) Salzer, C. A.; Elliott, C. M.; Hendrickson, S. M. *Anal. Chem.* **1999**, *71*, 3677-3683.
- (32) Raudsepp, T.; Marandi, M.; Tamm, T.; Sammelseg, V.; Tamm, J. *Electrochim. Acta* **2008**, *53*, 3828-3835.
- (33) Suematsu, S.; Oura, Y.; Tsujimoto, H.; Kanno, H.; Naoi, K. *Electrochim. Acta* **2000**, *45*, 3813-3821.
- (34) Ingram, M. D.; Staesche, H.; Ryder, K. S. *J. Power Sources* **2004**, *129*, 107-112.
- (35) De Paoli, M. A.; Panero, S.; Paserini, S.; Scrosati, B. *Adv. Mater. (Weinheim, Fed. Repub. Ger.)* **1990**, *2*, 480-482.
- (36) Kassim, A.; Davis, F. J.; Mitchell, G. R. *Synth. Met.* **1994**, *62*, 41-47.
- (37) Kupila, E.-L.; Kankare, J. *Synth. Met.* **1995**, *74*, 241-249.
- (38) Bidan, G.; Niel, M.-A. *Synth. Met.* **1997**, *85*, 1387-1388.
- (39) Kaneto, K.; Bidan, G. *Thin Solid Films* **1998**, *331*, 272-278.
- (40) Mousavi, Z.; Bobacka, J.; Ivaska, A. *Electroanalysis* **2005**, *17*, 1609-1615.
- (41) Akieh, M. N.; Ralph, S. F.; Bobacka, J.; Ivaska, A. *J. Membr. Sci.* **2010**, *354*, 162-170.
- (42) Wallace, G. G.; Spinks, G. M.; Kane-Maguire, L. A. P. *Conductive Electroactive Polymers: Intelligent Materials Systems, Second Edition*; CRC Press, 2002.
- (43) Ingram, M. D.; Staesche, H.; Ryder, K. S. *Solid State Ionics* **2004**, *169*, 51-57.

- (44) Reyes, D. C. J. I.; Cavalieri, R. P.; Powers, J. R. *Synth. Met.* **2004**, *142*, 71-79.
- (45) Guo, D.-S.; Wang, K.; Liu, Y. *J. Inclusion Phenom. Macrocyclic Chem.* **2008**, *62*, 1-21.
- (46) Diaz, A. F.; Castillo, J. I.; Logan, J. A.; Lee, W. Y. *J. Electroanal. Chem. Interfacial Electrochem.* **1981**, *129*, 115-132.
- (47) Bard, A. J.; Faulkner, L. R. *Electrochemical Methods: Fundamentals and Applications*, 2nd ed.; Wiley, 2006.
- (48) Duffitt, G. L.; Pickup, P. G. *J. Chem. Soc., Faraday Trans.* **1992**, *88*, 1417-1423.
- (49) Tanguy, J.; Mermilliod, N.; Hoclet, M. *J. Electrochem. Soc.* **1987**, *134*, 795-802.
- (50) Patake, V. D.; Joshi, S. S.; Lokhande, C. D.; Joo, O.-S. *Mater. Chem. Phys.* **2009**, *114*, 6-9.
- (51) Diao, G.; Zhou, W. *J. Electroanal. Chem.* **2004**, *567*, 325-330.
- (52) Pailleret, A.; Magan-Oliva, N.; Ollivier, S.; Arrigan, D. W. M. *J. Electroanal. Chem.* **2001**, *508*, 81-88.
- (53) Pailleret, A.; Arrigan, D. W. M. *Langmuir* **2002**, *18*, 9447-9452.
- (54) Diao, G.; Liu, Y. *Electroanalysis* **2005**, *17*, 1279-1284.
- (55) Louati, A.; Spraula, J.; Gabelica, V.; Kuhn, P.; Matt, D. *Electrochem. Commun.* **2006**, *8*, 761-766.
- (56) Ronlan, A.; Parker, V. D. *J. Chem. Soc. C* **1971**, 3214-3218.
- (57) Vataj, R.; Louati, A.; Jeunesse, C.; Matt, D. *Electrochem. Commun.* **2000**, *2*, 769-775.
- (58) Vataj, R.; Louati, A.; Jeunesse, C.; Matt, D. *J. Electroanal. Chem.* **2004**, *565*, 295-299.
- (59) Raoof, J.-B.; Ojani, R.; Rashid-Nadimi, S. *Electrochim. Acta* **2004**, *49*, 271-280.
- (60) Albery, W. J.; Chen, Z.; Horrocks, B. R.; Mount, A. R.; Wilson, P. J.; Bloor, D.; Monkman, A. T.; Elliott, C. M. *Faraday Discuss. Chem. Soc.* **1989**, *88*, 247-259.
- (61) Albery, W. J.; Mount, A. R. *J. Chem. Soc., Faraday Trans.* **1994**, *90*, 1115-1119.
- (62) Pickup, P. G. *J. Chem. Soc., Faraday Trans.* **1990**, *86*, 3631-3636.

- (63) Ren, X.; Pickup, P. G. *J. Chem. Soc., Faraday Trans.* **1993**, *89*, 321-326.
- (64) Ren, X.; Pickup, P. G. *Journal of Electroanalytical Chemistry* **1997**, *420*, 251-257.
- (65) Garcia-Belmonte, G.; Bisquert, J. *Electrochim. Acta* **2002**, *47*, 4263-4272.
- (66) Mao, H.; Pickup, P. G. *J. Am. Chem. Soc.* **1990**, *112*, 1776-1782.
- (67) Ren, X.; Pickup, P. G. *J. Electrochem. Soc.* **1992**, *139*, 2097-2105.
- (68) Rubinson, J. F.; Kayinamura, Y. P. *Chem. Soc. Rev.* **2009**, *38*, 3339-3347.
- (69) Mermilliod, N.; Tanguy, J. *J. Electrochem. Soc.* **1986**, *133*, 1073-1079.
- (70) Mostany, J.; Scharifker, B. R. *Synth. Met.* **1997**, *87*, 179-185.
- (71) Bobacka, J.; Lewenstam, A.; Ivaska, A. *J. Electroanal. Chem.* **2000**, *489*, 17-27.
- (72) Amemiya, T.; Hashimoto, K.; Fujishima, A. *J. Phys. Chem.* **1993**, *97*, 4187-4191.
- (73) Ye, S.; Girard, F.; Belanger, D. *J. Phys. Chem.* **1993**, *97*, 12373-12378.
- (74) Hallik, A.; Alumaa, A.; Tamm, J.; Sammelselg, V.; Vaeaertnou, M.; Jaenes, A.; Lust, E. *Synth. Met.* **2006**, *156*, 488-494.
- (75) Waller, A. M.; Compton, R. G. *J. Chem. Soc., Faraday Trans. 1* **1989**, *85*, 977-990.
- (76) Waller, A. M.; Nicholas, A.; Hampton, S.; Compton, R. G. *J. Chem. Soc., Faraday Trans. 1* **1989**, *85*, 773-781.

CHAPTER 4

Sensor Application:

Optimising the PPy-C4S Film for the
Electrochemical Detection of Dopamine

4.1 Introduction

The dopamine sensor developed during my Ph.D. studies is an electrode that has been modified using a polypyrrole (PPy) film doped with a *p*-sulfonatocalix[4]arene (C4S) during the electropolymerization process. Previous work carried out in our laboratory had shown that PPy doped with a sulfonated cyclodextrin was a simple, selective sensor for dopamine¹. Furthermore, these studies showed that doping the PPy film with a sulfonated cyclodextrin afforded the sensor a greater sensitivity and selectivity when compared with PPy films doped with chloride, sulfate or dodecylsulfate anions². As an extension of this work we aimed to further improve the sensitivity of the sensor by altering the macrocyclic dopant. Sulfonated calixarenes were chosen for the following reasons. Firstly, PPy films doped with a sulfonated calixarene have been shown to be effective cation-selective materials. These modified electrodes have been studied as Ag⁺ ion³, uranyl ion⁴ and trimethyl(ferrocenylmethyl)ammonium ion⁵ sensors, and as electrically switchable cation exchange membranes⁶. Secondly, C4S has been shown to form a strong inclusion complex with dopamine (DA)⁷. Moreover, studies by Bidan and Niel on the trimethyl(ferrocenylmethyl)ammonium ion showed that C4S can retain its inclusion properties when immobilized in a polypyrrole film⁵. Therefore, the PPy-C4S film could be selective towards DA due to a combination of both electrostatic interactions and the formation of an inclusion complex.

However, C4S is electroactive and this led to some complications concerning the application of the film as an electrochemical sensor for DA. At a bare electrode, C4S undergoes an irreversible oxidation beginning at approximately 0.70 V vs. SCE⁸. The products of this oxidation can undergo a nucleophilic substitution reaction to form calixquinones⁹⁻¹³ (Section 3.2.2.1 (iii)). These species are electroactive and when present in the PPy-C4S film produce a redox couple centred at 0.230 V vs. SCE. It was shown in Chapter 2 that the size of this redox couple is potential dependent. Using higher upper potential limits for cyclic voltammetry leads to increased oxidation of C4S and consequently a larger redox couple for the calixquinone species. This can hinder the detection of DA due to overlap of the oxidation peaks: the oxidation peak associated with the calixquinone species, occurring at approximately 0.30 V vs. SCE, is close to that of DA, at approximately

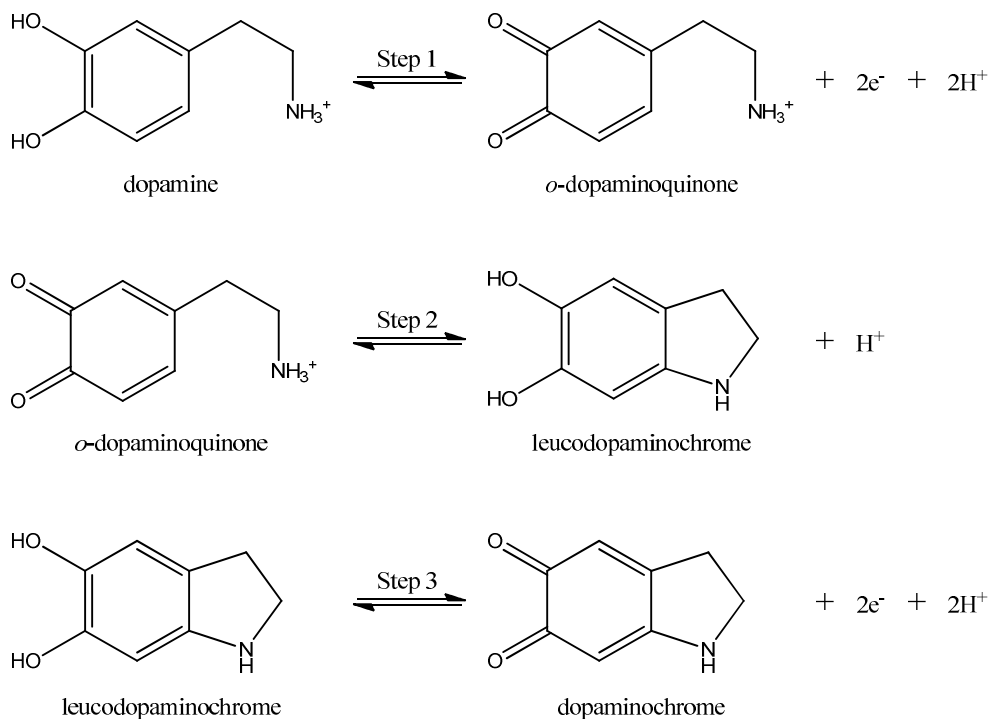
0.45 V vs. SCE. Therefore, it was necessary to minimise the oxidation of the calixarene as much as possible.

In this chapter, the response of DA at the PPy-C4S film was examined using cyclic voltammetry. The parameters for cyclic voltammetry and the factors affecting the growth of the polymer were varied in order to simultaneously optimise the signal for DA oxidation and minimise the production of the calixquinone species. When these optimum conditions were determined a calibration curve for the sensing of DA at the PPy-C4S film was generated using both cyclic voltammetry and constant potential amperometry.

4.2 Results and Discussion

4.2.1 DA Oxidation at Bare Electrodes

The electrochemical oxidation of DA is known to follow an ECE mechanism^{14, 15}. An ECE mechanism involves an initial electrochemical step (E), the product of which can undergo a chemical reaction (C) to produce a new electroactive species. This new species can then react electrochemically itself (E). The electrochemical oxidation of DA is depicted in Scheme 4.1. DA is first converted to *o*-dopaminoquinone (DOQ) by a two electron oxidation (Step 1, E). This molecule can then undergo a 1,4-Michael addition which results in a cyclisation reaction (Step 2, C). The product of this reaction, leucodopaminochrome (LDC), is more easily oxidized than the parent DA and can experience a further two electron oxidation to form dopaminochrome (DC) (Step 3, E). DC can be oxidized further and, through a series of reactions, go on to form melanin polymers^{16, 17}. These polymers are known to passivate the electrode by depositing on its surface.



Scheme 4.1: Steps involved in the electrochemical oxidation of DA.

Three common electrode materials, platinum, gold and glassy carbon (GC), were investigated in this study. The cyclic voltammetric response of DA at a bare Pt, Au and GC electrode is shown in Figure 4.1. It is clear from this figure that two redox couples were observed at each electrode. The larger redox couple, centred at approximately 0.4 V vs. SCE, corresponds to the process in Step 1 of Scheme 4.1. The smaller redox couple, centred at about 0.05 V vs. SCE, corresponds to the process in Step 3 of Scheme 4.1. This redox couple was only observed after the first cycle at each electrode, consistent with an ECE mechanism. The presence of this redox couple indicates that these electrodes will be subject to fouling by the melanin polymers discussed above, making them unsuitable as electrochemical sensors for DA.

The peak currents and potentials for the oxidation of DA at each electrode are presented in Table 4.1. The peak current ratios and the peak separations are also given and these were indicative of a *quasi-reversible* process with typical ΔE values in the range 0.3 to 0.4 V. This is in agreement with literature reports¹⁸⁻²⁷.

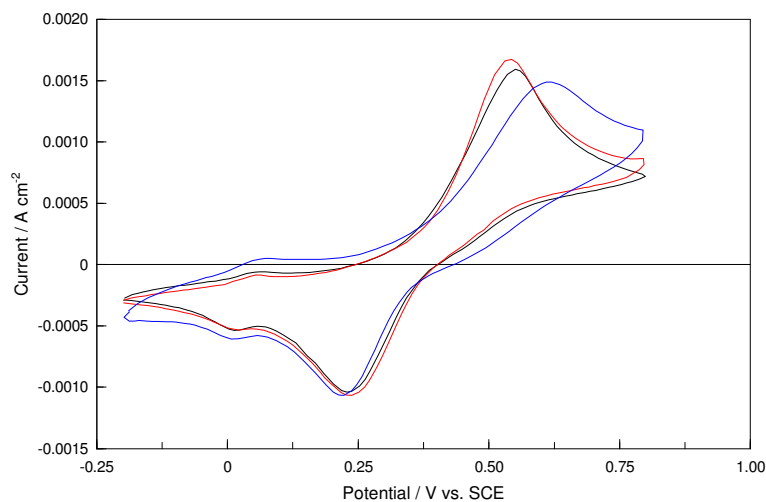


Figure 4.1: Cyclic voltammograms of bare GC (—), Au (—) and Pt (—) electrodes in a $5.0 \times 10^{-3} \text{ mol dm}^{-3}$ DA / 0.10 mol dm^{-3} Na_2SO_4 solution. The scan rate used was 100 mV s^{-1} .

Table 4.1: Peak currents and potentials observed for the redox pair corresponding to the oxidation of DA and the reduction of DOQ at bare electrodes.

Electrode	I_p^A A cm ⁻²	I_p^C A cm ⁻²	I_p^A/I_p^C	E_p^A / V vs. SCE	ΔE / V
GC	0.001591	0.001306	1.22	0.5501	0.3220
Au	0.001674	0.001340	1.25	0.5434	0.3067
Pt	0.001487	0.001341	1.11	0.6101	0.3877

4.2.2 Preliminary Studies on the Interaction between C4S and DA in Solution

The C4S used in this research was synthesized according to literature procedures and carefully purified by crystallization. The material formed was characterized by ¹H and ¹³C NMR, and IR spectroscopy and the results compared well with literature values²⁸. Microanalysis was performed on the material formed from a number of different syntheses and a chemical formula of Ca_xNa_{5-2x}C₂₈H₁₉O₁₆S₄ (yH₂O) was assigned.

One concern, which arose from the presence of Ca²⁺ ions in the material, was the possible interaction of Ca²⁺ with the calixarene. Ca²⁺ is known to form an outer sphere complex with C4S, involving a strong electrostatic interaction²⁹. This complexation could compete with the interaction of DA with C4S. As a result, the ability of the PPy-C4S film to detect DA could be hindered. Therefore, it was necessary to investigate if the C4S containing Ca²⁺ ions could still interact with DA in solution.

NMR titration was used to examine the interaction of C4S with DA. The ¹H chemical shifts for a fixed concentration of DA were monitored while the concentration of calixarene was increased. Figure 4.2 shows the results obtained for the methylene protons in the α -position to the amine group. The signal for these protons shifted upfield by more than 1 ppm (300 Hz) when approximately one molar

equivalent of C4S was present in solution. This shielding of the DA protons by the calixarene is indicative of inclusion complex formation. Clearly, the presence of Ca^{2+} ions did not prevent C4S from interacting with DA in solution. The nature of this interaction is discussed in more detail in Chapter 5. Additionally, the EDX analysis of the PPy-C4S film showed no evidence of Ca^{2+} within the film. Figure 4.3 shows an EDX spectrum recorded for the PPy-C4S film. No peaks were observed in the region characteristic of Ca^{2+} ($K_{\alpha} = 3.6905 \text{ keV}$). Thus, it was concluded that the presence of Ca^{2+} ions in the C4S material should not hinder the detection of DA at the PPy-C4S film.

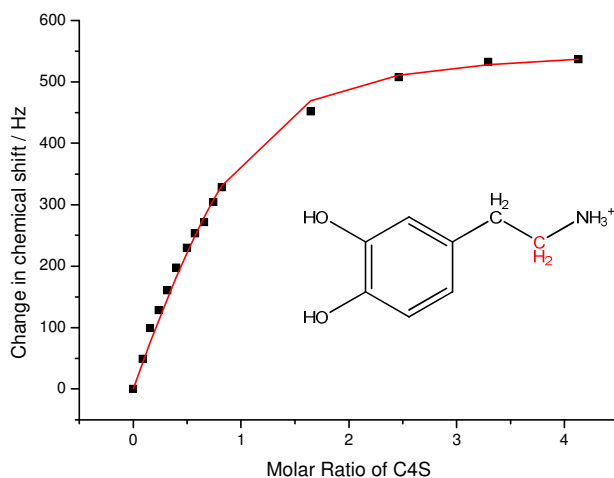


Figure 4.2: A plot of the ^1H NMR chemical shift value, for the methylene protons in the α -position to the amine group, as a function of the molar ratio of C4S to DA. The structure of DA is also shown with the α -methylene group highlighted in red.

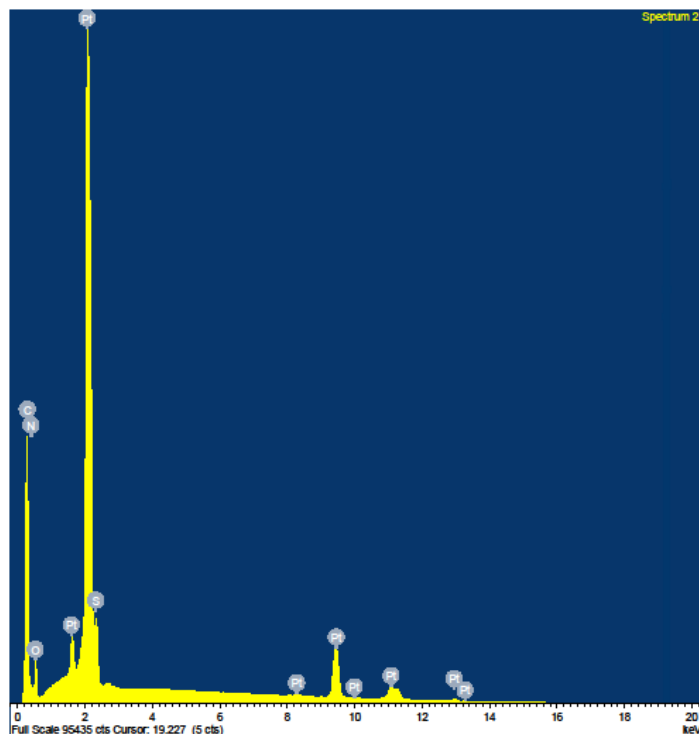


Figure 4.3: EDX spectrum of a PPy-C4S film electropolymerised on a Pt electrode at 0.500 V vs. SCE from a solution containing 0.20 mol dm^{-3} pyrrole and 0.01 mol dm^{-3} C4S until a charge of 0.24 C cm^{-2} had been reached.

4.2.3 DA Oxidation at Polypyrrole Modified Electrodes

To ensure that DA was being oxidized at the polymer surface and not diffusing through the polymer and reacting at the underlying substrate, the PPy-C4S films were electropolymerised on the three substrates (Pt, Au and GC) investigated in Section 4.2.1. The films were electropolymerised at a potential of 0.500 V vs. SCE until a charge of 0.24 C cm^{-2} was reached and the response of DA at each of these electrodes was examined using cyclic voltammetry (Figure 4.4), under similar conditions to those used for the bare electrodes (Section 4.2.1). In contrast to the results for the bare electrodes, it is clear from Figure 4.4 that the electrochemical behavior of DA at each modified electrode was very similar. The peak currents, peak potentials and peak separations for the oxidation of DA at each modified electrode are presented in Table 4.2. The oxidation currents observed for DA were the same at each electrode and considerably higher than those observed at the bare electrodes. This increase in current was even more substantial considering the concentration of DA studied for the modified electrodes was lower, $1.0 \times 10^{-3} \text{ mol dm}^{-3}$, than for the

bare electrodes, $5.0 \times 10^{-3} \text{ mol dm}^{-3}$. The peak oxidation potentials varied slightly, from 0.450 V to 0.464 V vs. SCE, but the difference in the potential between electrodes was less than 14 mV and the difference in peak separation at each electrode was less than 19 mV. Between the bare electrodes, the variation in the electrochemical behavior of DA was much greater. In particular, between the Au and Pt electrodes, the peak oxidation potentials differed by 67 mV and the peak separations by 81 mV, thus, it can be concluded that DA was being oxidised at the polymer film and not at the underlying electrode substrate.

The PPy-C4S modified electrodes were also compared with electrodes modified by sulfate and dodecylsulfate doped PPy films. The oxidation of $1.0 \times 10^{-3} \text{ mol dm}^{-3}$ DA at these films has been studied previously in our laboratory¹ and peak currents of 8.0×10^{-4} and $3.0 \times 10^{-4} \text{ A cm}^{-2}$ were reported, respectively. These currents were much lower than those observed at the PPy-C4S films, approximately $2.0 \times 10^{-3} \text{ A cm}^{-2}$, indicating that a superior response was obtained at the PPy-C4S modified electrode.

It should also be noted from Figure 4.4 that the redox couple corresponding to Step 3 of Scheme 4.1 was not observed at the PPy-C4S polymer film, even after 50 cycles. However, this process was observed at the bare electrodes after the first cycle. Moreover, the oxidation currents observed for DA at the PPy-C4S films increased steadily with successive cycling, eventually reaching a steady state, whereas those for the bare electrodes were observed to decrease after the first cycle. This implied that the PPy-C4S coated electrodes were not subject to passivation by the melanin polymers that can foul the bare electrodes.

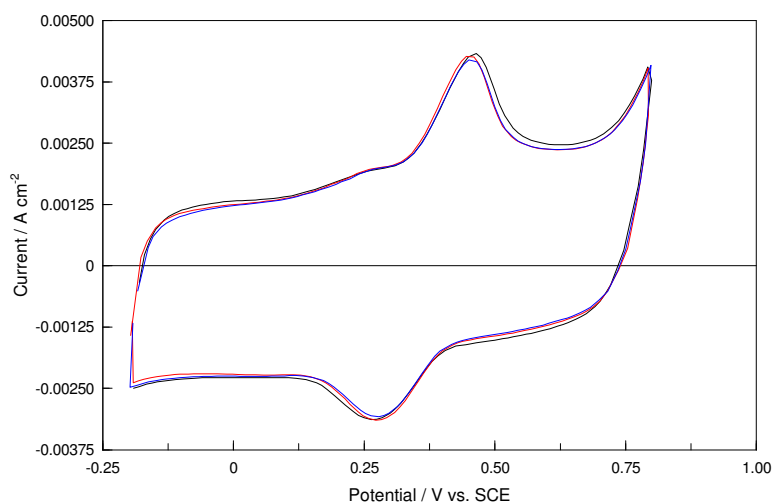


Figure 4.4: Cyclic voltammograms recorded in a $1.0 \times 10^{-3} \text{ mol dm}^{-3} \text{ DA} / 0.10 \text{ mol dm}^{-3} \text{ Na}_2\text{SO}_4$ solution at a scan rate of 100 mV s^{-1} for PPy-C4S films electrosynthesised at 0.500 V vs. SCE on GC (—), Au (—) and Pt (—) electrodes from 0.20 mol dm^{-3} pyrrole / 0.01 mol dm^{-3} C4S.

Table 4.2: Peak currents and potentials for the oxidation of $1.0 \times 10^{-3} \text{ mol dm}^{-3} \text{ DA}$ at the PPy-C4S film grown on various working electrodes.

Electrode	$I_p^A / \text{A cm}^{-2}$	$E_p^A / \text{V vs. SCE}$	$\Delta E / \text{V}$
GC	0.002075	0.4640	0.1905
Au	0.002073	0.4600	0.1876
Pt	0.002068	0.4504	0.1723

4.2.4 Optimising the DA Signal at the PPy-C4S Modified Electrode

The PPy-C4S modified electrode has, thus far, been shown to be a viable sensor for the detection of DA, displaying significant improvements over the unmodified electrodes in terms of sensitivity and reduction in fouling. In this section, the effects of varying the factors influencing the growth of the polymer and the conditions used to detect DA were investigated. In an effort to optimise the performance of the sensor, the most favorable parameters for the detection of DA were determined.

4.2.4 (i) The Concentration of Pyrrole

The concentration of pyrrole in the monomer solution was varied in order to determine its effect on the ability of the modified electrode to sense DA. In each case the PPy-C4S films were electropolymerised onto a Pt electrode under identical conditions, except that the pyrrole concentration was varied from 0.02 to 0.30 mol dm⁻³. It is clear from Figure 4.5 and Table 4.3 that DA was oxidized at the same potential at each PPy-C4S film. However, the peak oxidation currents for DA were found to increase as the concentration of pyrrole in the monomer solution increased from 0.02 to 0.20 mol dm⁻³. No further increase in peak oxidation current was observed for pyrrole concentrations greater than 0.20 mol dm⁻³.

There are two effects associated with an increase in the concentration of pyrrole in the monomer solution that can account for this increase in current. Firstly, Su *et al.* examined the surface morphology of polypyrrole films grown from solutions containing various concentrations of pyrrole³⁰. They found that smooth compact films were formed from low concentrations of pyrrole (0.05 mol dm⁻³) whereas rougher, more porous films were formed when the concentration of pyrrole in the monomer solution was increased. Thus, the increase in DA current, observed when higher concentrations of pyrrole were used, can be explained by an increase in the surface area due to the rougher morphology of the film. The second effect associated with an increase in pyrrole concentration is a possible increase in the doping level of the film. It can be seen from Figure 4.5 that the capacitive background current of the PPy-C4S film increased with increasing pyrrole concentration. This indicates an increase in the conductivity of the film as the concentration of pyrrole in the

monomer solution was increased. It may be that lower concentrations of pyrrole lead to the formation of shorter polymer chains, which will be less conducting and have lower doping levels. Yuan *et al.* observed a similar trend in the conductivity of polypyrrole films due to increasing concentrations of pyrrole³¹. They explained this observation using the concept of electroneutrality coupling. The more PPy⁺ sites produced for internal charge compensation in higher pyrrole concentrations, the more efficiently the anions will compensate the positive charge of the resulting PPy⁺. As a result more sites for DA to interact with will be incorporated into the film leading to increased oxidation currents.

A 0.20 mol dm⁻³ solution of pyrrole was chosen for the monomer solution for subsequent studies, as higher concentrations of pyrrole provided no further increase in current.

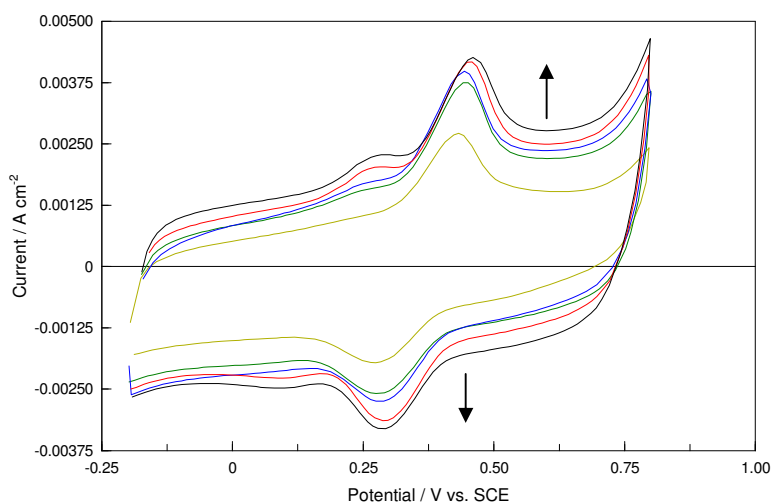


Figure 4.5: Cyclic voltammograms recorded in a 1.0×10^{-3} mol dm⁻³ DA / 0.10 mol dm⁻³ Na₂SO₄ solution for PPy-C4S films electrosynthesised on a Pt electrode at 0.500 V vs. SCE to a charge of 0.24 C cm⁻² from solutions containing 0.01 mol dm⁻³ C4S and 0.30 mol dm⁻³ (—), 0.20 mol dm⁻³ (—), 0.10 mol dm⁻³ (—), 0.05 mol dm⁻³ (—) and 0.02 mol dm⁻³ (—) pyrrole. The scan rate used was 100 mV s⁻¹.

Table 4.3: The peak currents and potentials for the oxidation of 1.0×10^{-3} mol dm⁻³ DA at PPy-C4S films electrosynthesised on a Pt electrode from solutions containing various concentrations of pyrrole.

Pyrrole concentration / mol dm ⁻³	$I_p^A / A\ cm^{-2}$	$E_p^A / V\ vs.\ SCE$
0.02	0.001472	0.4610
0.05	0.001963	0.4599
0.10	0.002037	0.4608
0.20	0.002240	0.4617
0.30	0.002246	0.4608

4.2.4 (ii) The Concentration of *p*-Sulfonatocalix[4]arene (C4S)

The concentration of C4S in the monomer solution was varied in order to determine its effect on the ability of the modified electrode to sense DA. In each case the PPy-C4S films were electropolymerised onto a Pt electrode under identical conditions except that the C4S concentration was varied from 5.0×10^{-4} to 1.0×10^{-2} mol dm⁻³. From Figure 4.6 and Table 4.4 it can be seen that DA was oxidised at the same potential at each PPy-C4S film. However, the oxidation currents for DA were found to increase as the concentration of C4S in the monomer solution was increased.

Increasing the electrolyte concentration in the monomer solution can affect the properties of the PPy film in two ways that can account for the observed increase in currents. The first is a change in the surface morphology of the film. Su *et al.* examined the surface morphology of polypyrrole films grown from solutions containing various concentrations of electrolyte³⁰. They found that the porosity and roughness of the films increased as the concentration of electrolyte in the monomer solution increased. Therefore, when higher concentrations of C4S were used, the PPy film would be formed with an increased surface area, leading to an increase in sites for DA to react with and, consequently, an increase in current. Also, the increased

porosity of the film would make it easier for DA to diffuse into the polymer, again resulting in an increase in current. The second effect associated with an increase in electrolyte concentration is an increase in the doping level of the film. Li *et al.* observed an increase in the Near Infra-Red (NIR) absorption of polypyrrole films when the concentration of electrolyte in the monomer solution was increased³². This absorption band is related to the doping state of the polypyrrole film and so, the stronger NIR absorption indicated a higher counteranion doping degree. Hence, an increased concentration of C4S in the monomer solution will lead to more recognition sites for DA being incorporated into the film and consequently increased DA oxidation currents will be observed.

The increase in DA oxidation current observed upon increasing the concentration of C4S in the monomer solution from 7.5×10^{-3} to 1.0×10^{-2} mol dm⁻³ was negligible. This suggested that further increases in the concentration of C4S would not have any significant effect on the doping level or morphology of the film. Li *et al.*³² observed a similar trend for PPy-NO₃ films. The doping levels of these films increased with increasing NaNO₃ concentration until a concentration of 2.0 mol dm⁻³ was reached. No further increase in the doping levels of these films was observed for electrolyte concentrations greater than 2.0 mol dm⁻³. The fact that this concentration is considerably higher than the maximum effective electrolyte concentration determined for the PPy-C4S film (1.0×10^{-2} mol dm⁻³) can be attributed to the difference in the thickness of the films. The PPy-NO₃ films studied by Li *et al.*³² were between 6.0 and 9.0 μm in thickness whereas the thickness of the PPy-C4S film was approximately 1 μm (Section 3.2.1.3). Therefore, a 1.0×10^{-2} mol dm⁻³ solution of C4S was chosen for the monomer solution for subsequent studies.

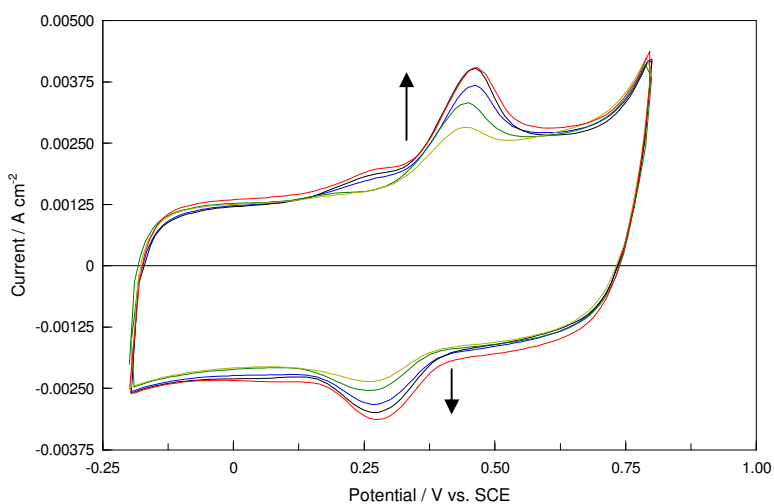


Figure 4.6: Cyclic voltammograms recorded in a $1.0 \times 10^{-3} \text{ mol dm}^{-3}$ DA / 0.10 mol dm^{-3} Na_2SO_4 solution for PPy-C4S films electrosynthesised on a Pt electrode at 0.500 V vs. SCE to a charge of 0.24 C cm^{-2} from solutions containing 0.20 mol dm^{-3} pyrrole and $1.0 \times 10^{-2} \text{ mol dm}^{-3}$ (—), $7.5 \times 10^{-3} \text{ mol dm}^{-3}$ (—), $5.0 \times 10^{-3} \text{ mol dm}^{-3}$ (—), $1.0 \times 10^{-3} \text{ mol dm}^{-3}$ (—) and $5.0 \times 10^{-4} \text{ mol dm}^{-3}$ (—) C4S. The scan rate used was 100 mV s^{-1} .

Table 4.4: The peak currents and peak potentials for the oxidation of $1.0 \times 10^{-3} \text{ mol dm}^{-3}$ DA at PPy-C4S films electrosynthesised on a Pt electrode from solutions containing various concentrations of C4S.

C4S concentration / mol dm^{-3}	$I_P^A / \text{A cm}^{-2}$	$E_P^A / \text{V vs. SCE}$
5.0×10^{-4}	0.001518	0.4670
1.0×10^{-3}	0.001841	0.4623
5.0×10^{-3}	0.002089	0.4636
7.5×10^{-3}	0.002299	0.4578
1.0×10^{-2}	0.002327	0.4642

4.2.4 (iii) *The Potential Applied for the Electrosynthesis of the PPy-C4S Film.*

Increasing the applied potential used to prepare the PPy-C4S film can have two major effects on the growth of the polymer. Firstly, it has been widely reported that the morphology of PPy films is influenced by the applied potential³³⁻³⁸. Polymers deposited at low potentials have been shown to be smoother and more homogeneous than those deposited at higher potentials^{36, 38}. Indeed the results from our SEM studies further attest to a rougher polymer surface being formed when the applied potential is increased (Section 3.2.1.1). Accordingly, increasing the potential applied to grow the polymer will provide DA with a larger surface area at which it can react. Secondly, more pyrrole will be oxidised as the applied potential is increased leading to higher amounts of doping by the calixarene. As a consequence of both of these factors, the DA oxidation current was expected to increase with applied potential.

PPy-C4S films were electropolymerised at potentials from 0.450 V to 0.800 V vs. SCE on a Pt electrode until a charge of 0.24 C cm⁻² was reached. Potentials higher than 0.800 V vs. SCE were not investigated because PPy is known to become over-oxidised at these potentials. The result of this is a loss of conductivity and a degradation of the mechanical properties of the film³⁹. The response of DA at each electrode was recorded using cyclic voltammetry (Figure 4.7) and the peak currents and peak potentials for the oxidation of DA at the PPy-C4S films are presented in Table 4.5. A plot of peak oxidation current against applied potential is shown in Figure 4.8. It can be seen from Figure 4.8 that the currents increased with potential, as expected, up to 0.600 V vs. SCE. However, for the potentials higher than 0.600 V vs. SCE used to form the polymer, there was little difference between the observed oxidation currents. The cause of this deviation from the expected trend can be attributed to the calixquinone species. The oxidation peak associated with this species, at 0.300 V vs. SCE, increased with applied potential due to increased oxidation of C4S during the growth of the polymer. It is clear from Figure 4.7 that there was considerable overlap between this peak and the DA oxidation peak, when applied potentials of 0.600 V vs. SCE and above were used. This could have led to inaccurate background current readings for the films grown at the higher potentials, thereby accounting for the unexpected trend in DA oxidation currents. To check if this was indeed the case, the background currents were taken as the lowest current observed after the DA oxidation peak. Estimating the background currents in this

way prevented the overlap with the calixquinone peak from affecting the result. Figure 4.9 shows a plot of the DA peak oxidation currents, obtained by subtracting the new background current, as a function of the applied potential. This time the expected increase of DA oxidation current with applied potential was observed over the whole range, 0.450 to 0.800 V vs. SCE, of potentials studied. So, considering only the DA peak current and ignoring the calixquinone redox couple, the optimum applied potential was 0.800 V vs. SCE.

However, the stability of the PPy-C4S film was also affected by the applied potential. It can be seen from Table 4.5 that the DA current decreased dramatically over 20 cycles when applied potentials greater than 0.500 V vs. SCE were used, whereas the DA current reached a steady state for the polymers grown at 0.500 V and 0.450 V vs. SCE. The instability is most likely due to the presence of the calixarene. PPy films doped with electrochemically inactive anions are known to be stable at the potentials used in these experiments. C4S, on the other hand, is irreversibly oxidised at potentials greater than 0.6 V vs. SCE (Section 3.2.2.1 (iii)). This reaction results in unstable radical and cationic species⁹⁻¹² which could react with the PPy backbone causing it to be over-oxidised at the lower potentials examined here. This would account for the rapid drop in currents observed for the polymers grown at applied potentials greater than 0.500 V vs. SCE.

Therefore, an applied potential of 0.500 V vs. SCE was chosen to grow the PPy-C4S films for subsequent studies. Applying this potential to grow the PPy-C4S film provided the best compromise between maximising the DA signal and ensuring the stability of the film while also minimising the calixquinone redox couple.

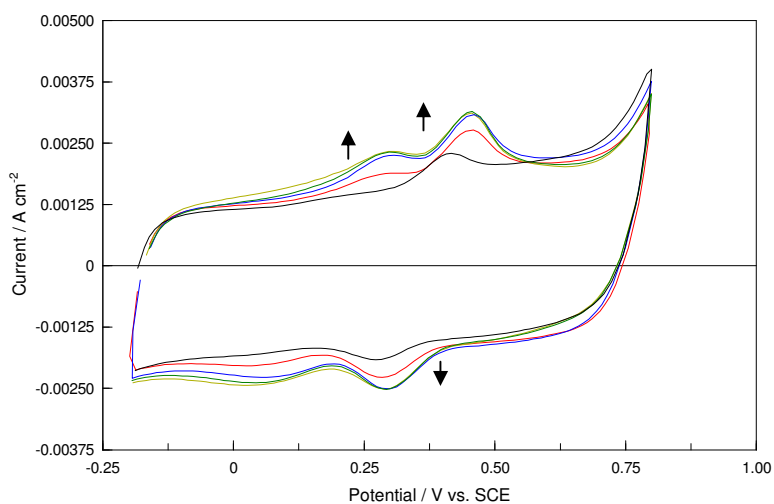


Figure 4.7: Cyclic voltammograms recorded in a $2.0 \times 10^{-4} \text{ mol dm}^{-3} \text{ DA} / 0.10 \text{ mol dm}^{-3} \text{ Na}_2\text{SO}_4$ solution at a scan rate of 100 mV s^{-1} for PPy-C4S films electrosynthesised on a Pt electrode at potentials of 0.450 V (—), 0.500 V (—), 0.600 V (—), 0.700 V (—) and 0.800 V vs. SCE (—) from $0.20 \text{ mol dm}^{-3} \text{ pyrrole} / 0.01 \text{ mol dm}^{-3} \text{ C4S}$.

Table 4.5: Peak oxidation currents, peak potentials and the percentage decrease in peak current over 20 cycles for the oxidation of DA at PPy-C4S films electropolymerised at various potentials.

Applied Potential / V vs SCE	$I_p^A / \text{A cm}^{-2}$	$E_p^A / \text{V vs. SCE}$	% Reduction in I_p after 20 cycles
0.450	0.0006201	0.4097	4
0.500	0.0008368	0.4510	5
0.600	0.0009912	0.4520	33
0.700	0.0010107	0.4546	26
0.800	0.0009567	0.4556	32

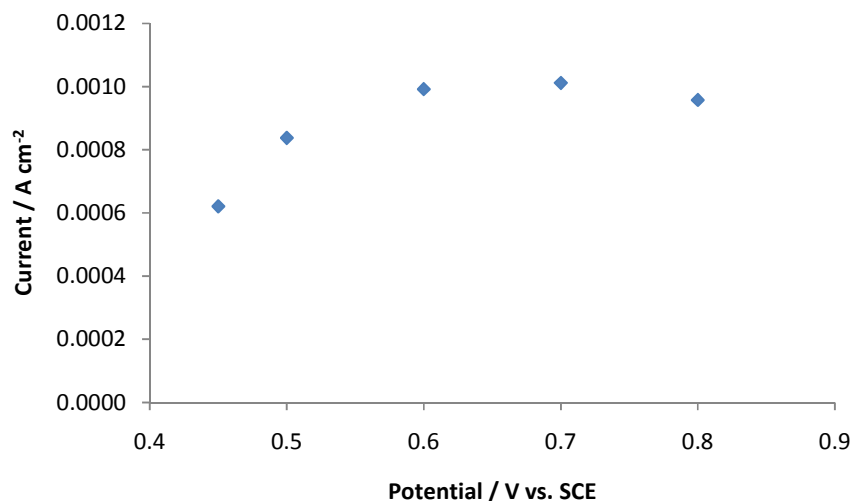


Figure 4.8: Plot of peak oxidation current from the oxidation of 2.0×10^{-4} mol dm⁻³ DA at the PPy-C4S film as a function of the electropolymerisation applied potential. The background was estimated in the standard way.

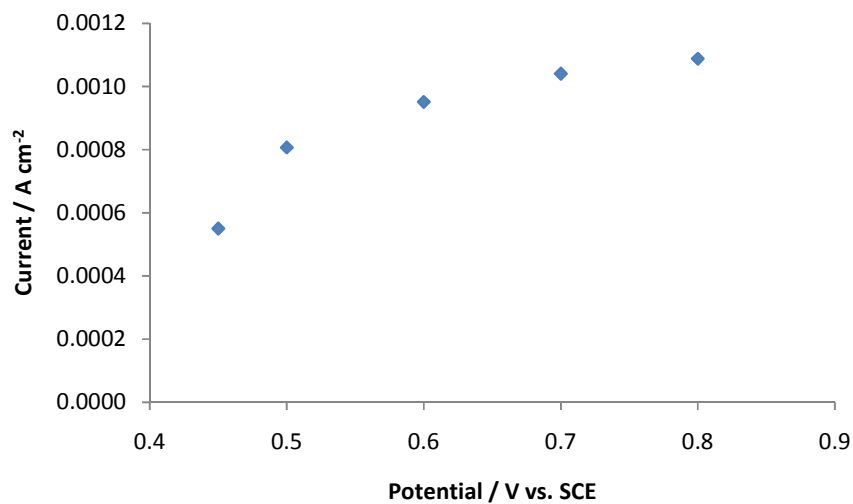


Figure 4.9: Plot of peak oxidation current from the oxidation of 2.0×10^{-4} mol dm⁻³ DA at the PPy-C4S film as a function of the electropolymerisation applied potential. The background current was estimated as the lowest current after the DA oxidation peak.

4.2.4 (iv) Electropolymerisation to a Set Charge

The thickness of the PPy film formed has been shown to be related to the charge passed during electropolymerisation. Diaz *et al.* derived a relationship that assumes 1 C cm^{-2} of charge will be passed for each $2.5 \text{ }\mu\text{m}$ of polymer growth⁴⁰. Equation 4.1 has been derived from the equation given by Stankovic *et al.* to theoretically calculate the thickness of PPy films⁴¹. Here, T is the thickness of the film, $M(\text{Py})$ is the molar mass of the monomer, x is the number of dopant molecules per monomeric unit, $M(\text{C4S})$ is the molar mass of the dopant, d is the density of PPy, F is Faraday's constant and q is the charge passed. It is clear from both of these relationships that the thickness of PPy films is predicted to increase as the charge passed during electrosynthesis is increased. Therefore, the effect of polymer thickness on the oxidation of DA at the PPy-C4S films could be investigated by varying the charge to which the polymer was grown.

$$T = \frac{M(\text{Py}) + xM(\text{C4S})}{d(2 + x)F} q \quad \text{Eq (4.1)}$$

PPy-C4S films were electropolymerised at an applied potential of 0.500 V vs. SCE on a platinum electrode until charges in the range 0.08 C cm^{-2} to 0.64 C cm^{-2} were reached. The response of DA at each electrode was recorded using cyclic voltammetry. For clarity, only the cyclic voltammograms recorded for five of these electrodes are shown in Figure 4.10. It should be noted from Figure 4.10 that the background current increased as the charge, to which the polymer was grown, increased. This can be accounted for by an increase in the capacitance of the film. In Section 3.2.2.1 (ii), the capacitance of the PPy-C4S film was shown to increase, as the charge consumed during the growth of the polymer increased. Therefore, seeing that the background currents were predominantly capacitive in nature⁴², an increase in these currents with increasing electropolymerisation charge was to be expected.

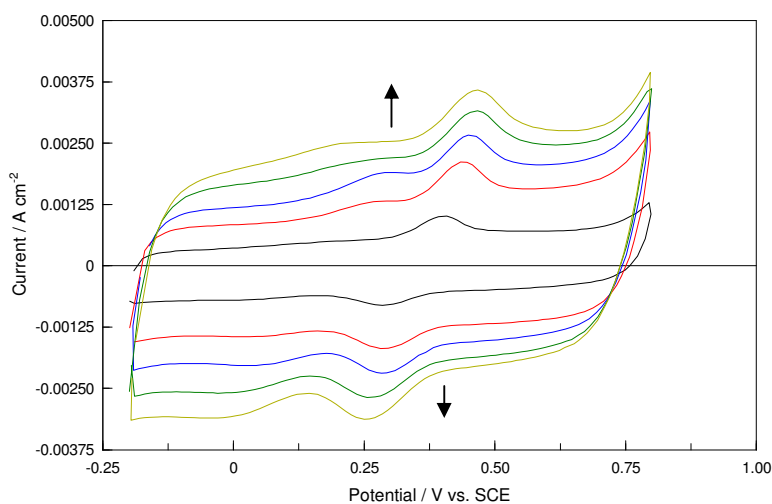


Figure 4.10: Cyclic voltammograms recorded in a $2.0 \times 10^{-4} \text{ mol dm}^{-3}$ DA / 0.10 mol dm^{-3} Na_2SO_4 solution at a scan rate of 100 mV s^{-1} for PPy-C4S films electrosynthesised on a Pt electrode at 0.500 V vs. SCE to charges of 0.08 (—) to 0.64 (—) C cm^{-2} from 0.20 mol dm^{-3} pyrrole / 0.01 mol dm^{-3} C4S.

In Figure 4.11, the DA peak oxidation current is plotted against the electropolymerisation charge and the peak oxidation currents and potentials are presented in Table 4.6. The DA peak oxidation current was found to increase with increasing charge (Figure 4.11). This was likely due to an increase in the porosity of the PPy-C4S film. The porosity of PPy films have been shown to increase with film thickness⁴³. As a result, the polymers grown to a higher charge will be more open, facilitating easier diffusion of DA into the film, and have a larger surface area at which DA can react. Consequently, larger DA oxidation currents can be observed. However, it was also found that the DA peak oxidation potential and peak separation increased with electropolymerisation charge, Table 4.6, indicating the reaction became less reversible as the thickness of the polymer increased.

An electropolymerisation charge of 0.24 C cm^{-2} was chosen as this seemed to offer the best compromise between maximising the DA oxidation signal and the reversibility of the reaction.

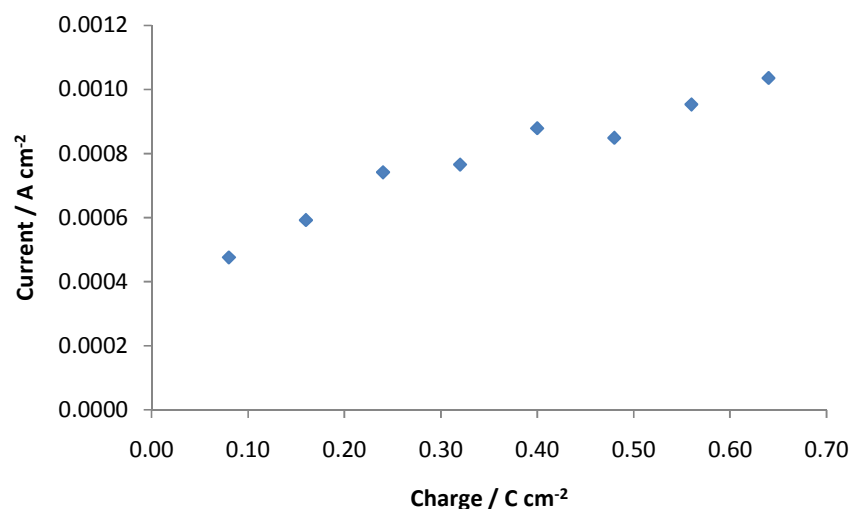


Figure 4.11: Plot of peak oxidation current from the oxidation of 2.0×10^{-4} mol dm⁻³ DA at the PPy-C4S film as a function of the electropolymerisation charge.

Table 4.6: The peak currents, peak potentials and peak separations for the oxidation of DA at PPy-C4S films electropolymerised to various charges.

Charge / C cm ⁻²	I_p^A / A cm ⁻²	E_p^A / V vs. SCE	ΔE_p / V
0.08	0.000476	0.4081	0.1108
0.16	0.000592	0.4343	0.1478
0.24	0.000664	0.4493	0.1607
0.32	0.000765	0.4670	0.1954
0.40	0.000879	0.4679	0.2152
0.48	0.000849	0.4742	0.2267
0.56	0.000953	0.4845	0.2335
0.64	0.001036	0.5040	0.2601

4.2.4 (v) *The Electrochemical Window*

The upper and lower potential limits for cyclic voltammetry were varied in order to optimise the signal for DA. The range over which these potentials could be varied, however, was limited by the electrochemical properties of the PPy-C4S film. PPy begins to become over-oxidised at potentials greater than 0.800 V vs. SCE. This can cause the polymer to breakdown and become more insulating. Figure 4.12 shows the effect of using a potential limit higher than 0.800 V vs. SCE. It is clear that the signal for DA and the background current begin to decay rapidly after only 5 cycles. This rapid decrease in current can be attributed to a decrease in the conductivity of the film due to the over-oxidation of PPy. Conversely, the polymer remains stable, reaching a steady state after 20 cycles (Figure 4.13), when a potential of 0.800 V vs. SCE is not exceeded. The electrochemistry of the calixarene was also a limiting factor for the determination of the optimal upper potential limit. In Section 3.2.2.1 (iii), it was shown that the generation of the calixquinone species was dependent on the upper potential limit. The magnitude of the calixquinone redox couple was found to be highest when an upper potential limit of 0.800 V vs. SCE was used. So, the use of upper potential limits below 0.800 V vs. SCE was investigated. However, it was found that the peak currents for DA oxidation were significantly reduced and the peak separation was significantly increased when the upper potential limit was lower than 0.800 V vs. SCE (Figure 4.14). This was unexpected as reducing the upper potential limit to 0.750 V vs. SCE (Figure 4.14) should not have affected the DA signal in such a significant manner. Unfortunately, no satisfactory explanation can be offered for this observation. For these reasons, the upper potential limit for cyclic voltammetry was chosen to be 0.800 V vs. SCE.

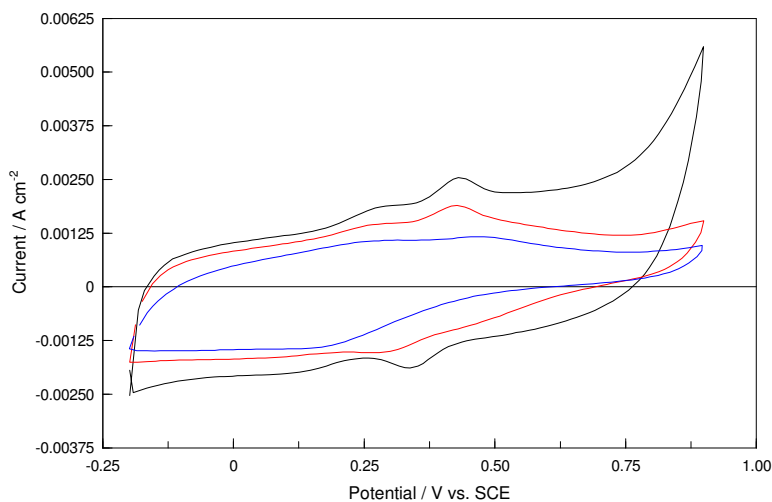


Figure 4.12: Cyclic voltammograms recorded in $2.0 \times 10^{-4} \text{ mol dm}^{-3}$ DA / 0.10 mol dm^{-3} Na_2SO_4 solutions at a scan rate of 100 mV s^{-1} from 0.900 V to -0.200 V vs. SCE for the PPy-C4S film electrosynthesised on a Pt electrode at 0.500 V vs. SCE to a charge of 0.24 C cm^{-2} from 0.20 mol dm^{-3} pyrrole / 0.01 mol dm^{-3} C4S. Cycles shown are 5 (—), 10 (—) and 15 (—).

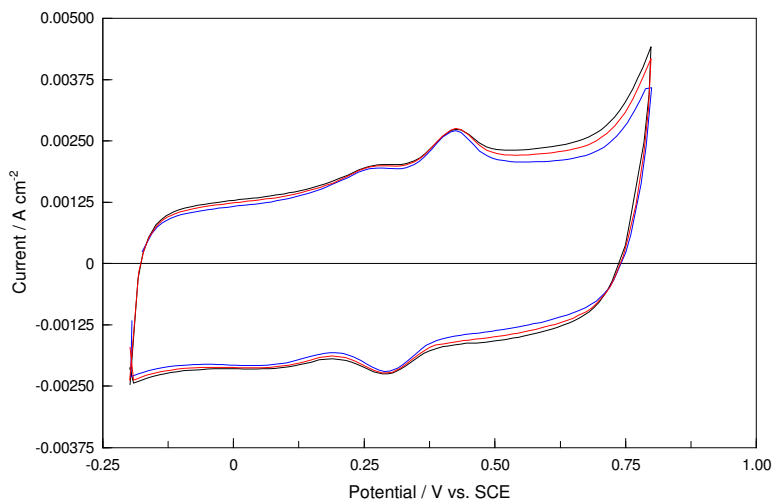


Figure 4.13: Cyclic voltammograms recorded in $2.0 \times 10^{-4} \text{ mol dm}^{-3}$ DA / 0.10 mol dm^{-3} Na_2SO_4 solutions at a scan rate of 100 mV s^{-1} from 0.800 V to -0.200 V vs. SCE for the PPy-C4S film electrosynthesised on a Pt electrode at 0.500 V vs. SCE to a charge of 0.24 C cm^{-2} from 0.20 mol dm^{-3} pyrrole / 0.01 mol dm^{-3} C4S. Cycles shown are 20 (—), 25 (—) and 30 (—).

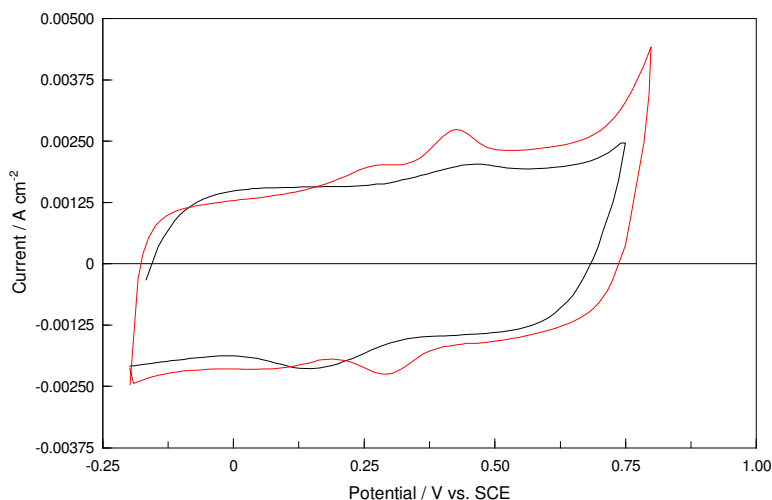


Figure 4.14: Cyclic voltammograms recorded in $2.0 \times 10^{-4} \text{ mol dm}^{-3} \text{ DA} / 0.10 \text{ mol dm}^{-3} \text{ Na}_2\text{SO}_4$ solutions at a scan rate of 100 mV s^{-1} from 0.750 V (—) and 0.800 V (—) to -0.200 V vs. SCE for PPy-C4S films electrosynthesised on a Pt electrode at 0.500 V vs. SCE to a charge of 0.24 C cm^{-2} from 0.20 mol dm^{-3} pyrrole / 0.01 mol dm^{-3} C4S.

The use of 0.800 V vs. SCE as the upper potential limit had implications for the lower potential limit. Again, this was due to the formation of the calixquinone species. In Figure 4.15, it can be seen that the calixquinone redox couple increased as the lower potential limit became more negative. This could be accounted for by more calixquinone being reduced as the potential became more negative. Clearly, the redox couple was substantial when potential limits lower than -0.200 V vs. SCE were used, therefore, these potentials were to be avoided.

A scanning potential not exceeding -0.200 V vs. SCE could also be considered advantageous when the electrochemistry of PPy is considered. The reduction of PPy films doped with large bulky anions, such as C4S, is known to be accompanied by an influx of cations, Na^+ in this case, from solution. This is due to the fact that the calixarene is trapped within the PPy matrix. In order to maintain the charge neutrality of the PPy-C4S film, sodium cations from the electrolyte enter the film when it is reduced. Ingram *et al.* reported that this can negatively affect the mobility of ions within the film by causing a reduction in its porosity⁴⁴. They proposed a ‘ladder doped’ structure for PPy films doped with polysulfonated aromatic compounds. In this model, the dopants act as cross linkers at the positive positions

along neighbouring oxidised PPy chains. In this way, the anions create open channels, within the polymer, in which fast ionic movement can occur. However, upon reduction of the polymer the anions would be free to bind with the incoming cations causing the structure to collapse. Ingram *et al.* suggests that this can be avoided if the polymer is never fully reduced. Assuming the PPy-C4S film has a similar structure, then maintaining the polymer in an oxidised state will facilitate easy access for the DA molecules to the calixarene, due to the open porous structure of the film. This can be achieved by using -0.200 V vs. SCE as the lower potential limit for cyclic voltammetry. On the other hand, cycling to more negative potentials would reduce the polymer, causing the structure to collapse and obstructing access to the calixarene.

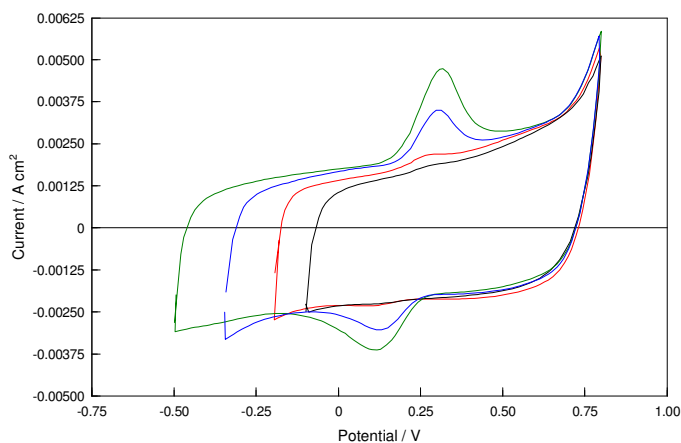


Figure 4.15: Cyclic voltammograms recorded in $0.10 \text{ mol dm}^{-3} \text{ Na}_2\text{SO}_4$ solutions at a scan rate of 100 mV s^{-1} from 0.800 V to -0.100 V (—), -0.200 V (—), -0.350 V (—) and -0.500 V (—) vs. SCE for PPy-C4S films electro synthesised on a Pt electrode at 0.500 V vs. SCE to a charge of 0.24 C cm^{-2} from 0.20 mol dm^{-3} pyrrole / 0.01 mol dm^{-3} C4S.

With these factors in mind, the lower potential limit was varied down to -0.200 V vs. SCE. It was found that the peak currents for the oxidation of DA increased as the lower potential limit was decreased from 0 V to -0.200 V vs. SCE (Figure 4.16). For the reasons outlined above, the lower potential limit for cyclic voltammetry was chosen to be -0.200 V vs. SCE.

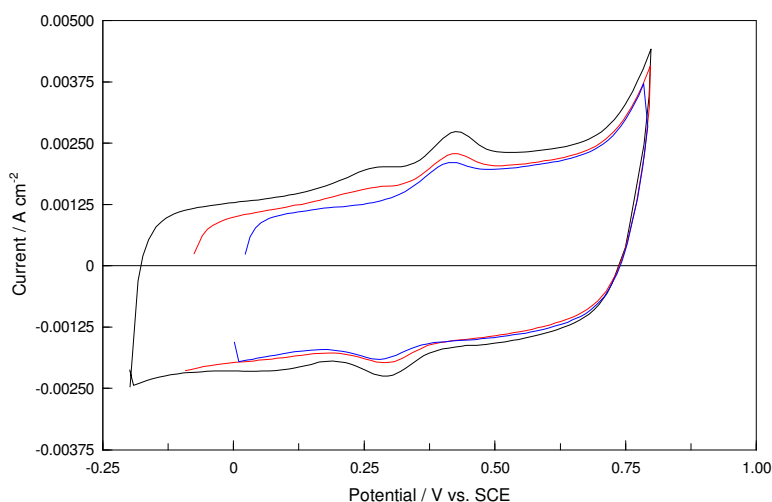


Figure 4.16: Cyclic voltammograms recorded in $2.0 \times 10^{-4} \text{ mol dm}^{-3} \text{ DA} / 0.10 \text{ mol dm}^{-3} \text{ Na}_2\text{SO}_4$ solutions at a scan rate of 100 mV s^{-1} from 0.800 V to -0.200 V (—), -0.100 V (—) and 0 V vs. SCE (—) for PPy-C4S films electrosynthesised on a Pt electrode at 0.500 V vs. SCE to a charge of 0.24 C cm^{-2} from 0.20 mol dm^{-3} pyrrole / 0.01 mol dm^{-3} C4S.

4.2.4 (vi) The Effect of Scan Rate on the DA Signal

The effect of scan rate on the DA signal was studied using cyclic voltammetry. Figure 4.17 shows the response of the PPy-C4S modified electrode to $1.0 \times 10^{-3} \text{ mol dm}^{-3} \text{ DA}$ at scan rates from 5 mV s^{-1} to 200 mV s^{-1} . It is clear from Figure 4.17 that the redox currents increased as the scan rate was increased. The dependence of peak current on scan rate can be described using the following relationship,

$$I_{p,a} = kv^x \quad \text{Eq (4.2)}$$

$$\text{Log}(I_{p,a}) = \text{Log}(k) + x\text{Log}(v) \quad \text{Eq (4.3)}$$

where $I_{p,a}$ is the peak oxidation current (A cm^{-2}), v is the scan rate (V s^{-1}), x is the exponent of scan rate and k is a proportionality constant^{45, 46}. This relationship is useful in determining the nature of the rate limiting process for an electrochemical reaction. If the electrode kinetics satisfies Equation 4.2, then the reaction is controlled by the electron transfer process, when $x = 1.0$, or the reactant diffusion process⁴⁵⁻⁴⁷, when $x = 0.5$.

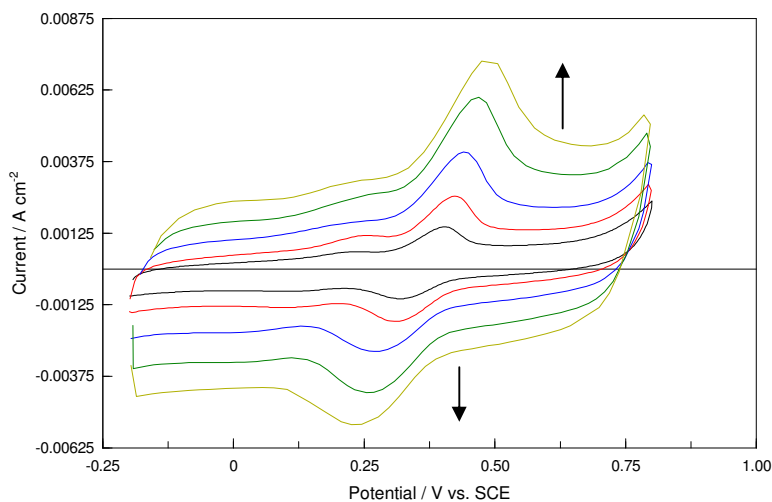


Figure 4.17: Cyclic voltammograms recorded in $1.0 \times 10^{-3} \text{ mol dm}^{-3} \text{ DA} / 0.10 \text{ mol dm}^{-3} \text{ Na}_2\text{SO}_4$ solutions at a scan rate of 25 (—), 50 (—), 100 (—), 150 (—) and 200 (—) mV s^{-1} for PPy-C4S films electrosynthesised on a Pt electrode at 0.500 V vs. SCE to a charge of 0.24 C cm^{-2} from 0.20 mol dm^{-3} pyrrole / 0.01 mol dm^{-3} C4S.

The log of peak oxidation current was plotted against the log of scan rate for the data shown in Figure 4.17. A linear relationship was obtained (Figure 4.18) with a slope of 0.76. This value is larger than expected. Ideally the slope should approach 0.50 under semi-infinite diffusion conditions, where the diffusion of DA from the bulk solution to the electrode surface is rate limiting. However, the larger slope may indicate that the electron transfer process was, to some extent, also a limiting factor. This could be the case if one of two additional processes were occurring. Firstly, it is possible that DA can become adsorbed to the PPy-C4S film through interactions with the calixarene. Secondly, there is evidence in the literature for the presence of thin layer diffusion in conducting porous films⁴⁷⁻⁵⁰. Both of these processes are characterized by a change in the peak current response from a square root to a linear dependence on scan rate. Indeed, a linear relationship was obtained when the DA peak oxidation current was plotted as a linear function of scan rate (Figure 4.19). This indicated that one or both of these processes were contributing to the observed DA oxidation current.

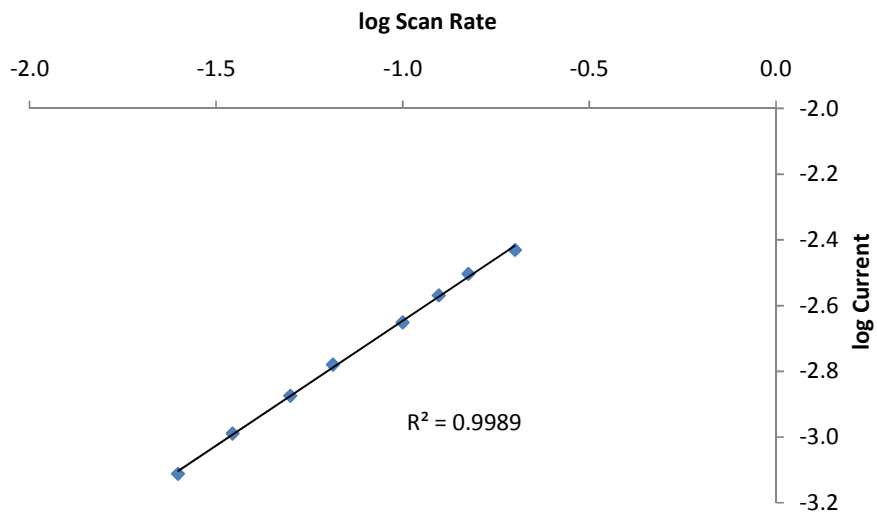


Figure 4.18: Plot of the logarithm of peak current for the oxidation of DA at the PPy-C4S modified electrode as a function of the logarithm of scan rate.

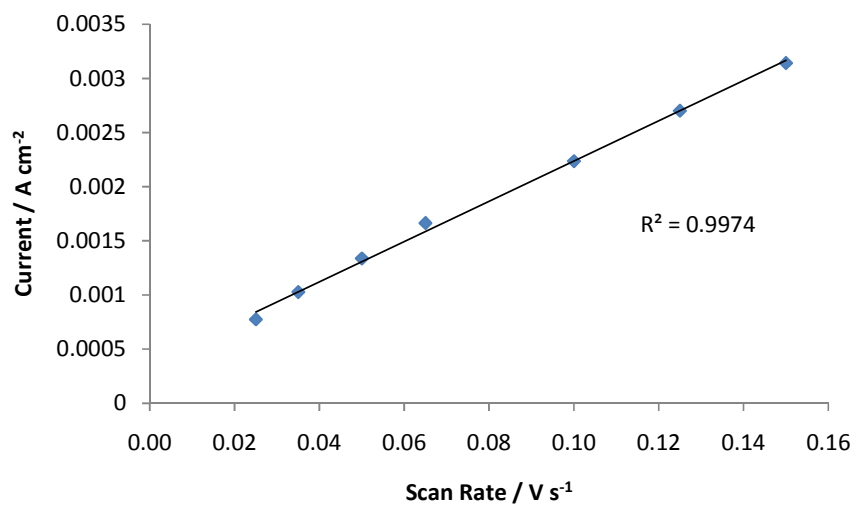


Figure 4.19: Plot of peak current for the oxidation of DA at the PPy-C4S modified electrode as a function of the scan rate.

Distinguishing between thin layer diffusion and adsorption effects is not easy as the case of adsorption might be seen as the ultimate limit of thin layer diffusion⁵⁰. However, there are certain characteristics that could imply one over the other. Adsorption effects may be inferred if the signal for DA increases steadily over a period of time rather than being observed immediately upon exposure of the PPy-C4S electrode to the solution. Figure 4.20 shows a range of scans, from the first to the twentieth, for the PPy-C4S modified electrode in a 1.0×10^{-3} mol dm⁻³ solution of DA. While a voltammetric signal for DA was observed on the first scan, indicating that diffusional processes were present, this signal increased steadily with subsequent cycles, reaching a steady state by the twentieth. This suggested that adsorption of DA was taking place. Adsorption effects may also be inferred if, after exposure to a solution of DA, the PPy-C4S electrode is transferred to a solution of background electrolyte and a signal for DA is observed. With this in mind a freshly prepared PPy-C4S modified electrode was cycled 20 times in a 0.10 mol dm⁻³ Na₂SO₄ solution, between -0.200 V and 0.800 V vs. SCE, and then immersed in a 1.0×10^{-3} mol dm⁻³ solution of DA for 10 min. After rinsing thoroughly with deionised water, the electrode was cycled again in a 0.10 mol dm⁻³ Na₂SO₄ solution. The resulting cyclic voltammogram is presented in Figure 4.21, along with a cyclic voltammogram recorded in a solution containing DA for comparison. Clearly, the PPy-C4S film had been modified during its immersion in the DA solution. This, in conjunction with the fact that the signal observed for DA remained relatively constant over 20 cycles, implied that DA was not free to diffuse away but was adsorbed to the PPy-C4S film. However, it can also be seen from Figure 4.21 that the current observed was much lower than when DA was present in solution. This indicated that diffusional processes played a more important role in the reaction. To investigate this further the diffusion coefficient of DA was evaluated.

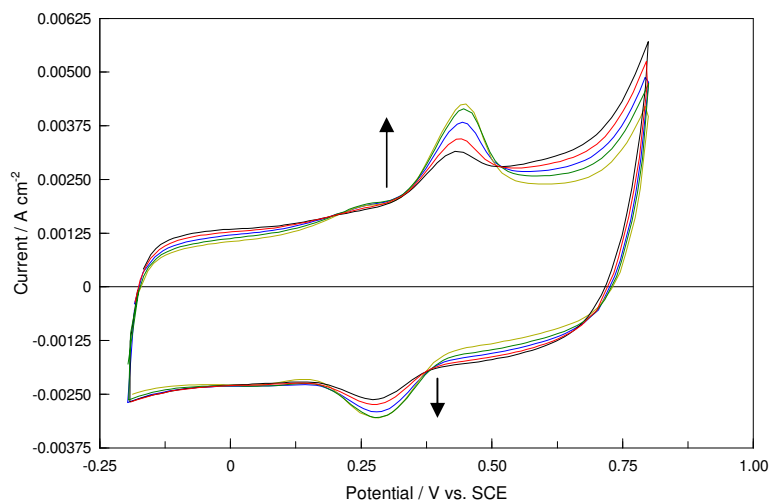


Figure 4.20: Cyclic voltammograms recorded in a $1.0 \times 10^{-3} \text{ mol dm}^{-3} \text{ DA} / 0.10 \text{ mol dm}^{-3} \text{ Na}_2\text{SO}_4$ solution at a scan rate of 100 mV s^{-1} for a PPy-C4S film electrosynthesised on a Pt electrode at 0.500 V vs. SCE to a charge of 0.24 C cm^{-2} from 0.20 mol dm^{-3} pyrrole / 0.01 mol dm^{-3} C4S. Cycles shown are 1 (—), 5 (—), 10 (—), 15 (—) and 20 (—).

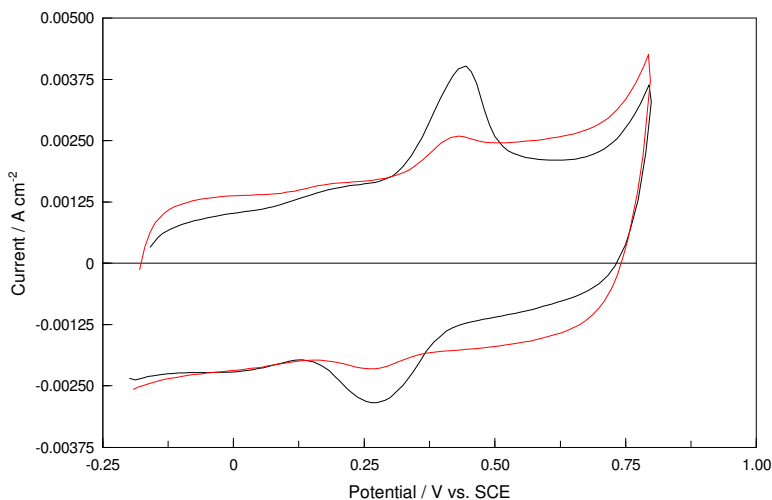


Figure 4.21: Cyclic voltammograms recorded in (—) a $1.0 \times 10^{-3} \text{ mol dm}^{-3} \text{ DA} / 0.10 \text{ mol dm}^{-3} \text{ Na}_2\text{SO}_4$ solution for a PPy-C4S modified electrode and (—) a $0.10 \text{ mol dm}^{-3} \text{ Na}_2\text{SO}_4$ solution for a PPy-C4S modified electrode that had been immersed in a $1.0 \times 10^{-3} \text{ mol dm}^{-3} \text{ DA} / 0.10 \text{ mol dm}^{-3} \text{ Na}_2\text{SO}_4$ solution for 10 min. The scan rate used was 100 mV s^{-1} . All PPy-C4S films were electrosynthesised on a Pt electrode at 0.500 V vs. SCE to a charge of 0.24 C cm^{-2} from 0.20 mol dm^{-3} pyrrole / 0.01 mol dm^{-3} C4S.

Two plots of peak current for the oxidation of DA as a function of the square root of scan rate are shown in Figure 4.22. One is for the total anodic peak current and the second is for the current obtained when the background current was subtracted. Clearly both of these currents increase linearly with the square root of scan rate. From the slope of these plots the diffusion coefficient of DA at the PPy-C4S modified electrode could be estimated using the Randles-Sevcik equation,

$$I_p = (2.69 \times 10^5)n^{3/2}D^{1/2}\nu^{1/2}c_0 \quad \text{Eq (4.4)}$$

where I_p is the peak current (A cm^{-2}), n is the electron stoichiometry, D is the diffusion coefficient ($\text{cm}^2 \text{s}^{-1}$), ν is the scan rate (V s^{-1}) and c_0 is the concentration (mol cm^{-3}). A diffusion coefficient of $1.83 \times 10^{-4} \text{ cm}^2 \text{ s}^{-1}$ was obtained from the plot of the background corrected currents while a diffusion coefficient of $6.70 \times 10^{-4} \text{ cm}^2 \text{ s}^{-1}$ was obtained from the total anodic peak currents. The difference between these two values for the diffusion coefficient of DA can be explained by considering the capacitance of the film. It was shown previously, Section 3.2.2.1 (ii), that the PPy-C4S film has a large capacitance and that its capacitive background current increases linearly with scan rate. The contribution of the capacitance to the total current can be seen clearly in Figure 4.17 where the background current increases significantly with increasing scan rate. This could account for the difference in diffusion coefficients obtained. Secondly, and more importantly, both of these values are considerably higher than the typical range of diffusion coefficients, 10^{-6} to $10^{-5} \text{ cm}^2 \text{ s}^{-1}$, obtained for the solution based diffusion of DA^{20, 50-52}. This suggests that more processes, other than just the diffusion of DA from bulk solution, are occurring at this modified electrode.

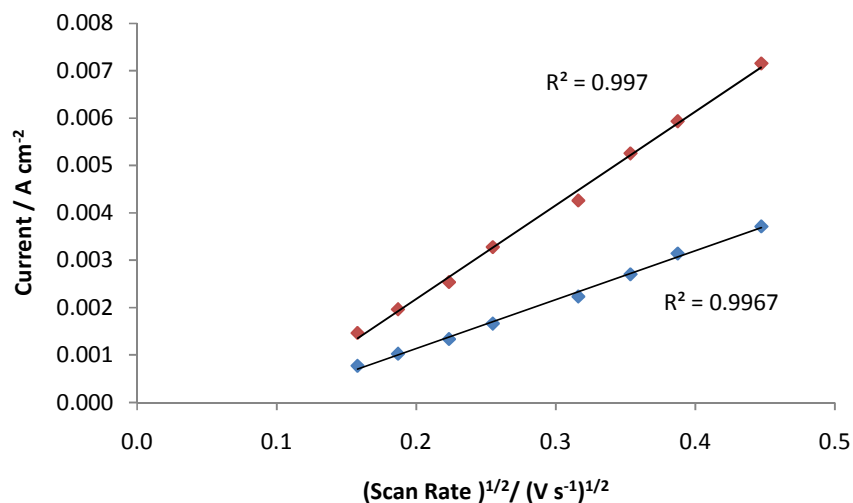


Figure 4.22: Plot of peak current for the oxidation of DA at the PPy-C4S modified electrode as a function of the square root of scan rate where the total anodic current (■) and the current with the background current subtracted (■) are plotted.

The results outlined above suggest that the current observed is not simply due to the oxidation of DA from bulk solution, but that a more complex process is responsible. This possibility is further supported, on a more observational level, by the shape of the cyclic voltammograms in Figure 4.17. While the characteristic diffusive tail remains evident in these cyclic voltammograms, the peaks are more symmetrical than would be expected if the oxidation reaction was controlled solely by the diffusion of DA from bulk. Moreover, the shape of the peaks was barely altered as the scan rate was increased. These observations along with the results outlined above attest to the oxidation of DA at the PPy-C4S modified electrode occurring by a combination of adsorption and diffusion controlled processes.

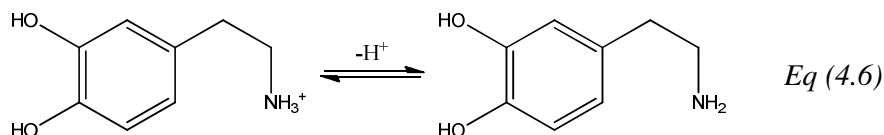
4.2.4 (vii) The Effect of pH

The dependence of peak potential on pH can be described using the Nernst equation. If the Nernst equation is applied to the $2e^-/2H^+$ oxidation of DA Equation 4.5 is obtained. Accordingly, the peak potential for the oxidation of DA is expected to vary linearly with pH to give a slope value of 59.1 mV per pH unit.

$$E = E^o - \frac{0.0591}{2} \log \frac{[DA - o - quinone][H^+]^2}{[DA]} \quad Eq (4.5)$$

Taking this relationship into consideration, the effect of the solution pH on the oxidation of DA at the PPy-C4S modified electrode was studied using cyclic voltammetry. The peak oxidation currents and potentials for DA obtained at pH values in the range 2.0 to 6.0 are presented in Table 4.7. It can be seen from Table 4.7 that the solution pH has essentially no effect on the DA peak oxidation potentials and currents over the pH range of 4.0 to 6.0. Although the oxidation peak potentials do shift to higher values when the pH is decreased below 4.0, this shift is not that significant given that the shift in the oxidation peak potential is only 13.6 mV and 20.7 mV when the pH is lowered to 3.0 and 2.0 respectively.

Clearly, under these experimental conditions the proton participation in the DA oxidation reaction does not follow normal Nernstian behaviour. However, there is substantial evidence in the literature that the oxidation of DA does follow normal Nernstian behaviour at a broad range of modified electrodes^{20, 24, 25, 53}, so the lack of a dependence on pH in this case was unusual. One factor that can be ruled out in this analysis is the concentration of protonated DA in solution as the pH is varied from 2.0 to 6.0. Equation 4.6 shows the conversion of protonated DA to the neutral species. The pK_a for this reaction is 9.05⁵⁴. Given that the solution pH is related to the pK_a by Equation 4.7, then the protonated form of DA will predominate at pH values less than 9.05. Thus, the deprotonation of DA should not be a concern in this analysis as DA will be more or less 100% protonated in the pH region studied.



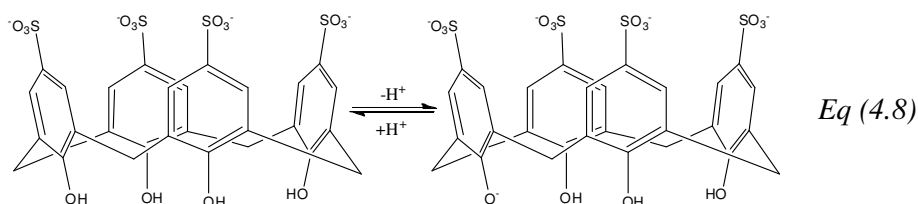
$$pH = pK_a + \log \frac{[DA]}{[\text{protonated DA}]} \quad \text{Eq (4.7)}$$

One possible reason explored for the lack of a pH dependence was the existence of a local pH within the polymer. Due to the porous structure of the polymer it was possible that the internal channels still contained some of the solution (pH 6-7) that the polymer was prepared from. This solution may have been slow, on the timescale of the experiment, to diffuse through the polymer to the bulk solution. As a result, the bulk solution pH would not have been an accurate representation of the pH DA was oxidized at. To investigate this possibility, a freshly prepared PPy-C4S modified electrode was immersed, overnight, in a stirred 0.10 mol dm⁻³ Na₂SO₄ solution, that had been adjusted to pH 3.0. This was to ensure the pH within the polymer and the bulk solution was uniform. The response of DA at the modified electrode was then recorded at pH 3.0. No difference in the peak oxidation potential for DA was observed when the result was compared with the initial experiment. This meant that any possible pH gradients between the internal channels of the polymer and the bulk solution were not the reason for the lack of a dependence of potential on pH.

The reason for the lack of any pH dependence between pH 4.0 and 6.0 is unknown. A similar result was also observed for the sulfonated β-cyclodextrin (SCD) doped PPy film studied previously in our laboratory². In this case, the DA peak oxidation potential was found to be independent of pH between pH 3.0 and 6.0. Again, no satisfactory explanation could be determined.

Still, on further inspection of the initial experimental data it was noticed that the pH at which the oxidation potential of DA began to shift had meaning for the calixarene. C4S is known to have one phenolic proton with a pK_a value of approximately 3.27⁵⁵⁻⁵⁷. Assuming this value is unaffected by the calixarene being immobilized in the PPy film, the calixarene will change from a predominantly penta-anionic state at pH 4.0 and above to a predominantly tetra-anionic state at pH 3.0 and below (Equation 4.8). It was shown in Section 4.2.4 (*vi*) that adsorption effects play a role in the oxidation of DA at the PPy-C4S modified electrode. This adsorption is likely to involve complex formation with the calixarene. Protonation of C4S would alter this complexation in two ways. One probable type of interaction is the electrostatic

attraction of DA to the negatively charged lower rim, which could not occur if the calixarene was protonated. Also, protonation of the lower rim of C4S would change the size of the cavity. It is known that the negatively charged O^- stabilises the cone conformation of C4S, through intramolecular hydrogen bonding interactions with the other OH groups on the lower rim⁵⁸. The loss of this stabilising effect would make the calixarene more conformationally mobile which may disfavor complexation. Therefore, it is reasonable to expect the protonation of the calixarene to inhibit this interaction.



To examine this matter further, the adsorption of DA to the PPy-C4S film was studied at pH 2. A freshly prepared PPy-C4S modified electrode was cycled in a $0.10 \text{ mol dm}^{-3} \text{ Na}_2\text{SO}_4$ solution (pH 2.0) and then immersed in a $1.0 \times 10^{-3} \text{ mol dm}^{-3}$ solution of DA (pH 2.0) for 10 min. After rinsing thoroughly with deionised water, the modified electrode was cycled again in a $0.10 \text{ mol dm}^{-3} \text{ Na}_2\text{SO}_4$ solution (pH 2.0). The resulting cyclic voltammograms are shown in Figure 4.23. It is clear from the voltammetric signal observed in Figure 4.23 that DA was present. However, the signal that was observed declined steadily, suggesting that DA was free to diffuse away from the electrode. This made it unlikely that DA was adsorbing to the surface of the PPy-C4S film. In this case, the signal observed was probably due to DA that had become trapped within the pores of the film during the immersion of the modified electrode. Conversely, the results in Section 4.2.4 (vi) show that at pH 6.0, when the calixarene was in the penta-anionic state, DA was not free to diffuse away from the film.

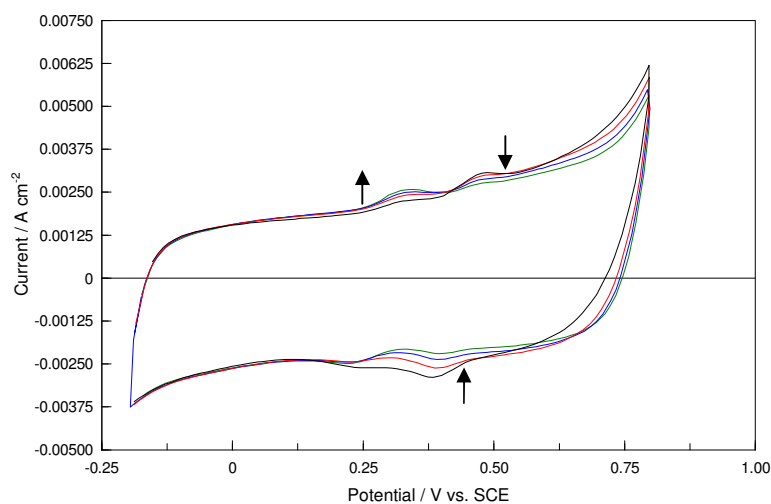


Figure 4.23: Cyclic voltammograms recorded in a $0.10 \text{ mol dm}^{-3} \text{ Na}_2\text{SO}_4$ solution for a PPy-C4S modified electrode that had been immersed in a $1.0 \times 10^{-3} \text{ mol dm}^{-3} \text{ DA} / 0.10 \text{ mol dm}^{-3} \text{ Na}_2\text{SO}_4$ solution for 10 min. Cycles shown are 5 (—), 10 (—), 15 (—) and 20 (—). The scan rate used was 100 mV s^{-1} . The PPy-C4S film was electrosynthesised on a Pt electrode at 0.500 V vs. SCE to a charge of 0.24 C cm^{-2} from $0.20 \text{ mol dm}^{-3} \text{ pyrrole} / 0.01 \text{ mol dm}^{-3} \text{ C4S}$.

Clearly, the protonation of the calixarene affected the adsorption of DA to the PPy-C4S modified electrode. But, whether the adsorption was prevented completely or just weakened is not certain. Nonetheless, it is obvious that the oxidation of DA at the PPy-C4S modified electrode became a more diffusion controlled process when the calixarene was protonated. This may account for the emerging pH dependence observed for the oxidation of DA at pH 3.0 and 2.0.

Table 4.7: The peak currents and peak potentials for the oxidation of 1.0×10^{-3} mol dm⁻³ DA solutions at various pH values at the PPy-C4S film.

Solution pH	$I_p^A / A\ cm^{-2}$	$E_p^A / V\ vs\ SCE$	$\Delta E / V$
2.0	0.001893	0.4961	0.1387
3.0	0.001890	0.4754	0.1677
4.0	0.002085	0.4618	0.1790
5.0	0.002089	0.4657	0.1819
6.0	0.002076	0.4694	0.1906

4.2.4 (viii) Supporting Electrolyte

The decision to use C4S as the dopant for the PPy film was based on its known ability to form a strong inclusion complex with DA⁷. However, C4S has also demonstrated an affinity, to varying degrees, for metal cations²⁹. Consequently, depending on the strength of this attraction, the detection of DA at the PPy-C4S modified electrode could be hindered by metal cations in the electrolyte solution. Hence, the binding affinity of the calixarene for the metal cation had to be considered when choosing potential electrolytes for studying the sensor. Guo *et al.* carried out a comprehensive study on the binding of metal cations by sulfonated calixarenes²⁹. They observed that the affinity of C4S was weakest for monovalent metal cations. Moreover, they reported no detectable affinity of C4S for Na⁺. For this reason, all electrolytes studied were in the form of sodium salts.

The oxidation of DA at the PPy-C4S film in several different electrolyte solutions was investigated using cyclic voltammetry. The peak currents, peak potentials and peak separations for the oxidation of DA in each electrolyte are presented in Table 4.8. Ideally, we would have liked to study the sensor in a buffer solution as this would eliminate the pH effects associated with adding excess amounts of interferent compounds such as ascorbic and uric acid. However, it is clear from Table 4.8 that the buffer solutions tested were less effective than simple salt solutions as supporting electrolytes. The increased peak separation in the acetate buffer, 0.3772 V, indicated a decrease in the reversibility of DA oxidation and the peak currents observed in both of the buffer solutions, 1.34×10^{-3} and 5.73×10^{-4} A cm⁻² for the acetate and saline-phosphate buffers respectively, showed a significant decrease in comparison to the salt solutions. The highest peak current, 2.11×10^{-3} A cm⁻², and the lowest peak separation, 0.2043 V, for the oxidation of DA were observed in sodium sulfate. However, the sodium sulfate solution also had the highest ionic strength. This could have accounted for its increased performance.

In order to investigate the effect ionic strength had on the oxidation of DA, NaCl and Na₂SO₄ solutions of varied ionic strengths were used as supporting electrolytes. Table 4.9 and Table 4.10 show the peak currents, peak potentials and peak separations for the oxidation of DA in Na₂SO₄ and NaCl solutions of varied ionic strength. It is clear that the ionic strength of the supporting electrolyte has an effect on the oxidation of DA. It was found that the peak currents and the peak separations decreased with increasing ionic strength. The peak separations observed in different electrolytes of similar ionic strength were found to be comparable. DA oxidation recorded in NaCl solutions with ionic strengths of 0.10 and 0.30 mol dm⁻³ had peak separations comparable to those in Na₂SO₄ solutions with ionic strengths of 0.15 and 0.30 mol dm⁻³ respectively. This explains the difference in peak separation observed for the Na₂SO₄ and NaCl solutions in Table 4.8. However, the peak currents observed in electrolytes of similar ionic strength were not comparable. In fact, the peak currents observed in Na₂SO₄ were higher than those observed in NaCl for all solutions examined.

Therefore, it was decided to use Na₂SO₄ as the supporting electrolyte. A 0.10 mol dm⁻³ Na₂SO₄ solution was chosen as this gave the best compromise between optimising the reversibility of the DA oxidation – the smallest peak

separation, and optimising the sensitivity of the PPy-C4S electrode for DA detection – the highest peak currents.

Table 4.8: The peak currents, potentials and peak separations for the oxidation of $1.0 \times 10^{-3} \text{ mol dm}^{-3}$ DA, in various electrolyte solutions, at the PPy-C4S film. The ionic strengths of the supporting electrolyte solutions are also shown.

Supporting Electrolyte	$I_p^A / \text{A cm}^{-2}$	$E_p^A / \text{V vs. SCE}$	$\Delta E / \text{V}$	Ionic Strength / mol dm^{-3}
0.10 mol dm⁻³ Na₂SO₄	0.002106	0.4595	0.2043	0.30
0.10 mol dm⁻³ NaCl	0.001922	0.4913	0.2634	0.10
0.10 mol dm⁻³ Acetate Buffer	0.001343	0.4046	0.3772	0.10
0.15 mol dm⁻³ Saline- Phosphate Buffer	0.000573	0.3076	0.2186	0.16

Table 4.9: The peak currents, potentials and peak separations recorded at the PPy-C4S film for the oxidation of 1.0×10^{-3} mol dm⁻³ DA in various Na₂SO₄ solutions and the corresponding ionic strengths.

Concentration of Na ₂ SO ₄ / mol dm ⁻³	$I_p^A / A\ cm^{-2}$	$E_p^A / V\ vs.\ SCE$	$\Delta E / V$	Ionic Strength / mol dm ⁻³
0.05	0.002114	0.4944	0.2710	0.15
0.10	0.002106	0.4595	0.1850	0.30
0.20	0.002020	0.4282	0.1373	0.40
0.30	0.001787	0.4117	0.1184	0.60

Table 4.10: The peak currents, potentials and peak separations recorded at the PPy-C4S film for the oxidation of 1.0×10^{-3} mol dm⁻³ DA in various NaCl solutions and the corresponding ionic strengths.

Concentration of NaCl / mol dm ⁻³	$I_p^A / A\ cm^{-2}$	$E_p^A / V\ vs.\ SCE$	$\Delta E / V$	Ionic Strength / mol dm ⁻³
0.05	0.001362	0.5346	0.4509	0.05
0.10	0.001922	0.4913	0.2634	0.10
0.20	0.001490	0.4574	0.2105	0.20
0.30	0.001252	0.4403	0.1813	0.30

4.2.4 (ix) The Influence of Oxygen Levels

In order to determine if the level of dissolved oxygen in solution had any effect on the performance of the sensor, the levels of dissolved oxygen in the monomer, background electrolyte and DA solutions were reduced prior to experiment. Nitrogen gas was passed through each solution for 20 min before use and the performance of the sensor was recorded. The data obtained from these solutions was then compared with data from solutions that had not had their oxygen levels reduced. As shown in Figure 4.24, the level of dissolved oxygen in the solutions had very little effect on the DA signal. The magnitude and reversibility of the DA signal were unaffected by the deoxygenation process. Typically, the characterisation of sensors is carried out in deoxygenated solutions, but in this case, the reduction of dissolved oxygen from solution was deemed unnecessary for the optimal performance of the sensor.

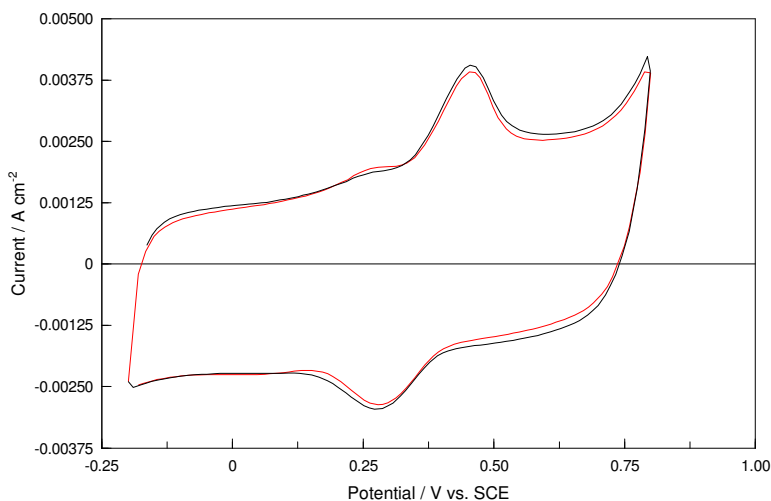


Figure 4.24: Cyclic voltammograms recorded at a (—) PPy-C4S film in a $1.0 \times 10^{-3} \text{ mol dm}^{-3}$ DA / 0.10 mol dm^{-3} Na_2SO_4 solution where the monomer, background electrolyte and DA solutions had not been bubbled with N_2 for 20 mins and a (—) PPy-C4S film in a $1.0 \times 10^{-3} \text{ mol dm}^{-3}$ DA / 0.10 mol dm^{-3} Na_2SO_4 solution where the monomer, background electrolyte and DA solutions had been bubbled with N_2 for 15 mins. The scan rate used was 100 mV s^{-1} . The PPy-C4S films were electrosynthesised on a Pt electrode at 0.500 V vs. SCE to a charge of 0.24 C cm^{-2} from 0.20 mol dm^{-3} pyrrole / 0.01 mol dm^{-3} C4S.

4.2.4 (x) The Optimum Conditions for the Detection of DA

A comprehensive study of the factors affecting the growth of the PPy-C4S film and the conditions used to detect DA has been outlined above. In each case the optimum condition for each parameter was determined in an effort to maximise the cyclic voltammetric signal for DA. A summary of these parameters and their optimum conditions is presented in Table 4.11.

Table 4.11: Summary of the parameters studied and their optimum conditions.

Parameter	Optimum Result
Working Electrode	The substrate the PPy-C4S film is electrosynthesised on is not important. A Pt electrode was chosen.
Concentration of Pyrrole	The increase in DA current was not significant for concentrations of pyrrole greater than 0.20 mol dm^{-3} . A concentration of 0.20 mol dm^{-3} was used.
Concentration of <i>p</i>-Sulfonatocalix[4]arene	The increase in DA current was not significant for concentrations of <i>p</i> -sulfonatocalix[4]arene greater than 0.01 mol dm^{-3} . A concentration of 0.01 mol dm^{-3} was used.
Electropolymerisation Potential	The optimum applied potential for growing the PPy-C4S film was 0.500 V vs. SCE .
Electropolymerisation Charge	The optimum charge was 0.24 C cm^{-2} .
Electrochemical Window	The optimum window was from -0.200 V vs. SCE to 0.800 V vs SCE .
Scan Rate	The scan rate chosen was 100 mV s^{-1} .
Effect of pH	No significant effect on the DA signal. A pH of 6.0 was chosen.
Supporting Electrolyte	The DA signal with the highest peak current was observed in aqueous 0.10 mol dm^{-3} Na_2SO_4 solution.
Effect of Oxygen Levels	Dissolved oxygen in solution had no observed effect on the DA signal. Solutions were not deoxygenated.

4.2.5 Dopamine Calibration Curves

Now, having determined the conditions for the optimal performance of the sensor, it was necessary to assess its sensitivity towards DA. In order to do this, calibration curves for the oxidation of DA at the PPy-C4S modified electrode were generated using the conditions outlined in Table 4.11. Two different techniques were employed to calibrate the sensor: cyclic voltammetry and constant potential amperometry.

4.2.5 (i) Cyclic Voltammetry

The first technique employed was cyclic voltammetry. The oxidation of DA at the PPy-C4S modified electrode was recorded over a range of concentrations. The peak oxidation currents and potentials observed at each of these DA concentrations are presented in Table 4.12. It can be seen from Table 4.12 that the peak oxidation currents increased with increasing concentrations of DA and that the peak oxidation potentials shifted to more positive potentials. Plotting these peak oxidation currents as a function of DA concentration produced a curve (Figure 4.25), with a linear response observed for the lower concentrations (Figure 4.26). This region of the curve was the most important as a linear response provides the simplest way to evaluate the amount of DA in solution. The linear regression equation for this region was $I_p^A = 3.38c_{DA}$, with a correlation coefficient of 0.997. The lowest concentration of DA that could be detected using cyclic voltammetry was $2.5 \times 10^{-5} \text{ mol dm}^{-3}$. This detection limit is too high given that the typical concentrations of DA range from 10^{-8} to $10^{-6} \text{ mol dm}^{-3}$ in most biological samples²⁶. In an effort to increase the sensitivity of the PPy-C4S modified electrode constant potential amperometry was employed.

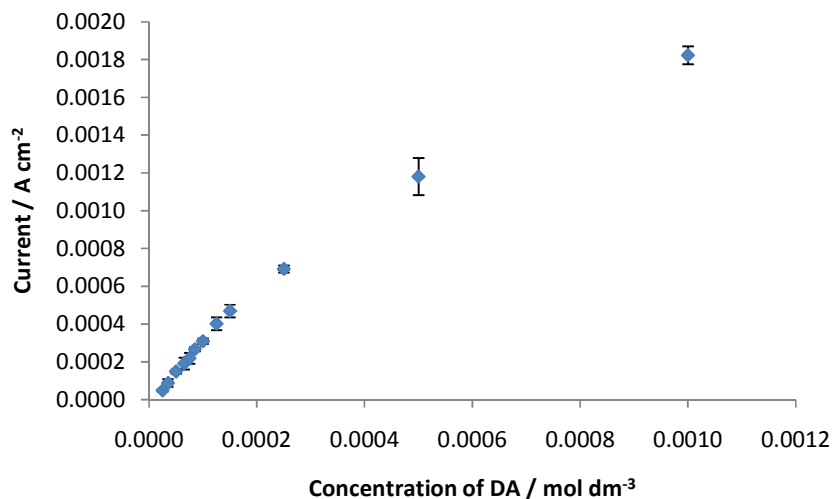


Figure 4.25: Plot of peak current for the oxidation of DA at the PPy-C4S film as a function of DA concentration ($n = 3$). The conditions used to sense DA and to prepare the PPy-C4S film were the optimum conditions outlined in Table 4.11.

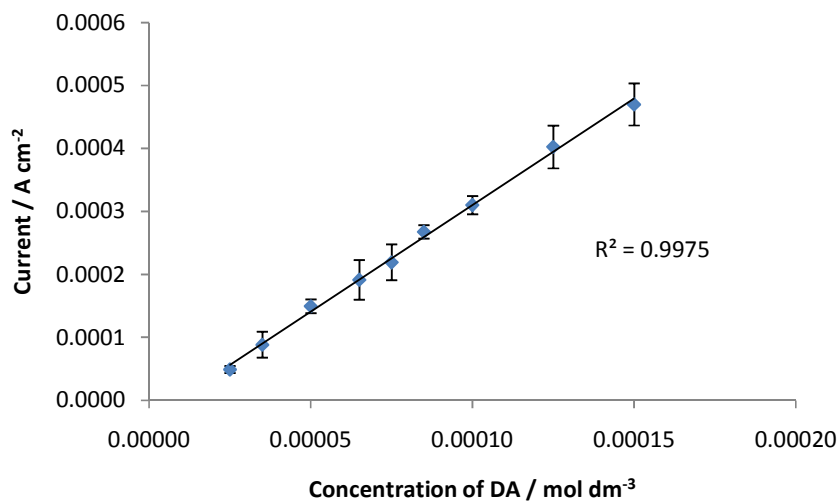


Figure 4.26: Plot of peak current for the oxidation of DA at the PPy-C4S film as a function of DA concentration ($n = 3$). The linear region of the curve is shown. The conditions used to sense DA and to prepare the PPy-C4S film were the optimum conditions outlined in Table 4.11.

Table 4.12: The peak oxidation currents and peak oxidation potentials for various concentrations of DA at the PPy-C4S modified electrode.

Conc. of DA / mol dm ⁻³	I_p^A / A cm ⁻²	E_p^A / V vs. SCE
2.5×10^{-5}	0.000049	0.3854
3.5×10^{-5}	0.000088	0.3894
5.0×10^{-5}	0.000149	0.3900
6.5×10^{-5}	0.000191	0.3895
7.5×10^{-5}	0.000219	0.3908
8.5×10^{-5}	0.000268	0.3926
1.25×10^{-4}	0.000402	0.4011
1.5×10^{-4}	0.000470	0.4132
2.5×10^{-4}	0.000692	0.4219
5.0×10^{-4}	0.001181	0.4251
1.0×10^{-3}	0.001823	0.4473

4.2.5 (ii) Constant Potential Amperometry

Constant potential amperometry was performed using a Pt rotating disk electrode (RDE) that had been modified with a PPy-C4S film. The use of RDE can significantly improve the mass transport of the analyte to the electrode surface allowing for lower concentrations to be detected. In this case, a constant potential of 0.650 V vs. SCE was applied to the modified electrode while it was rotated at a constant speed of 2000 rpm. This potential was high enough to ensure the complete oxidation of DA but low enough to prevent any considerable oxidation of the calixarene. After allowing the electrode to equilibrate at the applied potential for 30 min, the current was recorded while various aliquots of DA were added to the solution containing the modified electrode. The amperometric response of the PPy-C4S film to successive additions of DA is shown in Figure 4.27. The response time, the time taken for the current to reach a steady state after the addition of each aliquot of DA, was 2.3 s. This response time was quite fast⁵⁹, which suggested that the modified electrode displayed reasonably fast kinetics for the oxidation of DA.

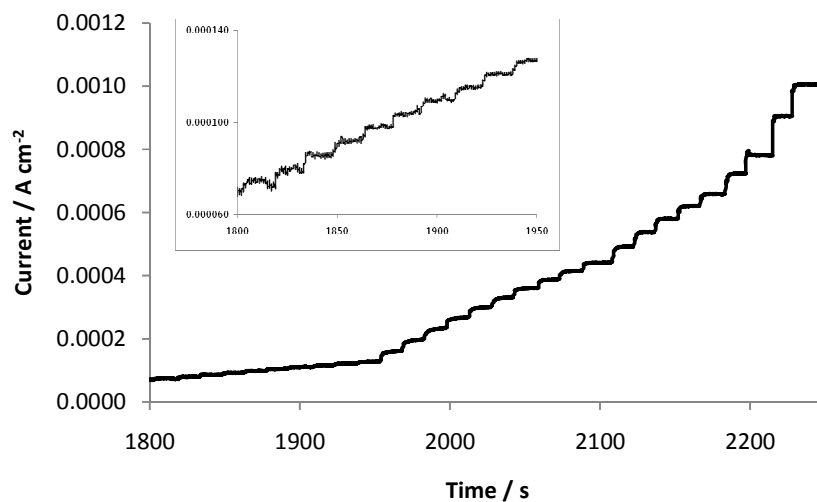


Figure 4.27: Constant potential amperometry, recorded at 0.650 V vs SCE and a rotation speed of 2000 rpm, for the PPy-C4S films. The current steps correspond with successive additions of aliquots of DA ranging from 100 μ L to 5 mL. The region between 1800 and 1950 s is expanded in the inset. The PPy-C4S films were grown using the optimum conditions outlined in Table 4.11 and the supporting electrolyte was 0.10 mol dm⁻³ Na₂SO₄.

The averaged results of four separate amperometric determinations are presented in Figure 4.28. A curve was obtained over the whole concentration range, while a linear relationship was obtained for the lower concentrations (Figure 4.29). The linear regression equation was $I_p^A = 1.074C_{DA}$, with a correlation coefficient of 0.999. The limit of detection could be calculated from the current to concentration ratio of $1.074 \mu\text{A} \mu\text{M}^{-1}$, given by the linear regression equation, and the standard deviation of the signal noise, σ . In order for an increase in current to be considered real, it should be at least 3σ in magnitude. Since σ for the noise in this system was $1.47 \mu\text{A}$ the lowest current that could be accurately distinguished from the noise at the modified electrode was $4.41 \mu\text{A}$. Correlating this value with DA concentration using the current to concentration ratio gave a detection limit of $4.11 \times 10^{-6} \text{ mol dm}^{-3}$ DA. Disappointingly, this value was slightly higher than the detection limit obtained for the polypyrrole-sulfonated β -cyclodextrin (PPy-SCD) modified electrode studied previously in our laboratory¹ ($3.36 \times 10^{-6} \text{ mol dm}^{-3}$), indicating that the calixarene did not increase the sensitivity of the sensor.

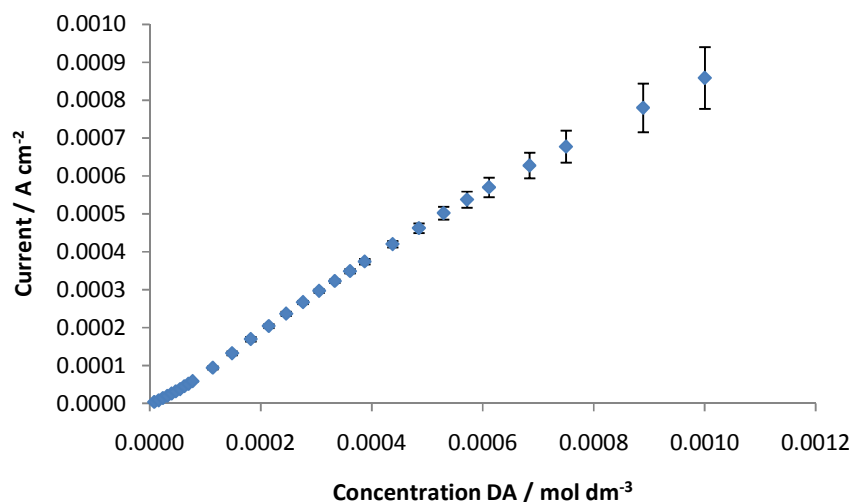


Figure 4.28: Steady-state currents from constant potential amperometry plotted as a function of the DA concentrations ($n = 4$). The PPy-C4S films were grown with the optimum conditions outlined in Table 4.11.

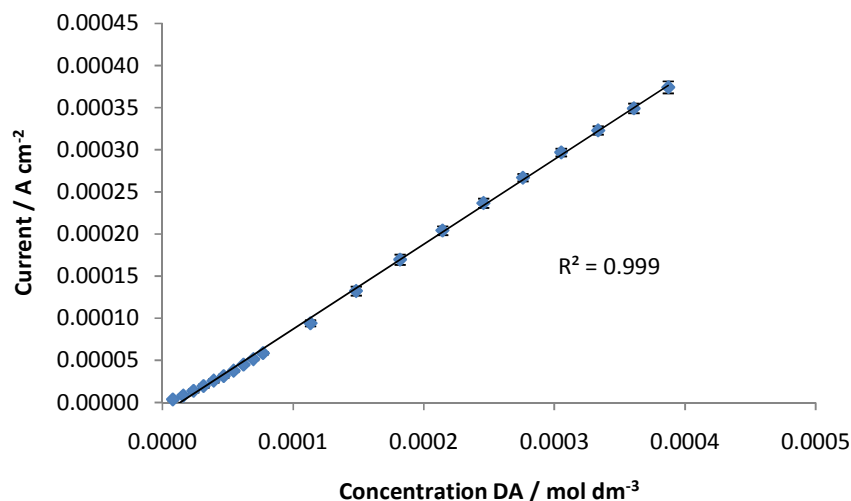


Figure 4.29: Steady-state currents from constant potential amperometry plotted as a function of the linear response of DA at low concentrations ($n = 4$). The PPy-C4S films were grown with the optimum conditions outlined in Table 4.11.

It should also be noted that the reproducibility of the currents, for the oxidation of DA at the modified electrode, was positively affected by constant potential amperometry. Comparing the linear plots for cyclic voltammetry (Figure 4.26) and constant potential amperometry (Figure 4.29) it can be seen that the error bars for the amperometric technique are smaller and more uniform than those for cyclic voltammetry. This increased reproducibility was likely due to two factors. The first was the inherent differences in the techniques. The forced convection method (RDE) used for amperometry increased the mass transport of DA to the electrode surface allowing for greater current sensitivity than cyclic voltammetry. The second was the lower potentials involved in the amperometric determinations. It was possible to carry out the amperometry at a lower potential, 0.650 V vs. SCE, than cyclic voltammetry, upper potential limit of 0.800 V vs. SCE, thereby avoiding any considerable oxidation of the calixarene. This resulted in a more stable PPy-C4S film which increased the reproducibility of its performance.

Clearly, the use of constant potential amperometry had enhanced the sensitivity and performance of the sensor. Although this new limit of detection 4.11×10^{-6} mol dm⁻³ DA was still too high for the modified electrode to be considered a viable *in vivo* DA sensor, it may be possible to reach lower detection limits using pulsed techniques

such as differential pulse voltammetry or square wave voltammetry. Moreover, the narrow potential windows typically used for pulsed techniques would minimise the oxidation of C4S. Thus, these pulsed techniques should make the sensor more reproducible, as was the case for constant potential amperometry.

4.3 Conclusion

In this chapter, the ability of the PPy-C4S modified electrode to sense DA was examined. It was found that DA could indeed be oxidized at the modified electrode and that this reaction occurred at the PPy-C4S film and not at the underlying metal substrate. By comparison with PPy films doped with sulfate and dodecylsulfate anions, the PPy-C4S modified electrode was shown to produce significantly larger currents for the oxidation of DA. This superior performance by the PPy-C4S film indicated that the calixarene played an important role in the sensing of DA. This was confirmed by the fact that DA was found to adsorb to the polymer film and that protonating C4S was shown to have an effect on this adsorption interaction. However, this interaction did not increase the sensitivity of the sensor in comparison to the PPy-SCD modified electrode.

The PPy-C4S modified electrode was optimized for the detection of DA by varying the factors affecting the growth of the polymer and the parameters used for cyclic voltammetry. The optimum conditions were determined based on a compromise between maximizing the oxidation of DA and minimizing the generation of calixquinones within the film. Then, using these optimum conditions, the sensitivity of the sensor was investigated. Calibration curves generated using cyclic voltammetry and constant potential amperometry gave detection limits of 2.50×10^{-5} and $4.11 \times 10^{-6} \text{ mol dm}^{-3}$ DA, respectively.

Even though these detection limits were not low enough for *in vivo* monitoring of DA levels, the results outlined here are promising. Constant potential amperometry not only improved the sensitivity of the sensor but its performance in general. Thus, the easy assembly and excellent reproducibility of this DA sensor, when calixquinone generation is minimized, make it worthy of further study.

4.4 Bibliography

- (1) Harley, C. C. Ph.D Thesis, NUI Maynooth, 2009.
- (2) Harley, C. C.; Rooney, A. D.; Breslin, C. B. *Sensors and Actuators B: Chemical* **2010**, *150*, 498-504.
- (3) Mousavi, Z.; Bobacka, J.; Ivaska, A. *Electroanalysis* **2005**, *17*, 1609-1615.
- (4) Kaneto, K.; Bidan, G. *Thin Solid Films* **1998**, *331*, 272-278.
- (5) Bidan, G.; Niel, M.-A. *Synth. Met.* **1997**, *85*, 1387-1388.
- (6) Akieh, M. N.; Ralph, S. F.; Bobacka, J.; Ivaska, A. *J. Membr. Sci.* **2010**, *354*, 162-170.
- (7) Zhou, Y.; Liu, C.; Yu, H.; Xu, H.; Lu, Q.; Wang, L. *Spectrosc. Lett.* **2006**, *39*, 409-420.
- (8) Diao, G.; Zhou, W. *J. Electroanal. Chem.* **2004**, *567*, 325-330.
- (9) Ronlan, A.; Parker, V. D. *J. Chem. Soc. C* **1971**, 3214-3218.
- (10) Louati, A.; Spraula, J.; Gabelica, V.; Kuhn, P.; Matt, D. *Electrochem. Commun.* **2006**, *8*, 761-766.
- (11) Vataj, R.; Louati, A.; Jeunesse, C.; Matt, D. *Electrochem. Commun.* **2000**, *2*, 769-775.
- (12) Vataj, R.; Louati, A.; Jeunesse, C.; Matt, D. *J. Electroanal. Chem.* **2004**, *565*, 295-299.
- (13) Gomez-Kaifer, M.; Reddy, P. A.; Gutsche, C. D.; Echegoyen, L. *J. Am. Chem. Soc.* **1994**, *116*, 3580-3587.
- (14) Hawley, M. D.; Tatawawadi, S. V.; Piekarski, S.; Adams, R. N. *Journal of the American Chemical Society* **1967**, *89*, 447-450.
- (15) Majewska, U. E.; Chmurski, K.; Biesiada, K.; Olszyna, A. R.; Bilewicz, R. *Electroanalysis* **2006**, *18*, 1463-1470.
- (16) Lane, R. F.; Hubbard, A. T. *Anal. Chem.* **1976**, *48*, 1287-1293.
- (17) Ke, N. J.; Lu, S.-S.; Cheng, S.-H. *Electrochem. Commun.* **2006**, *8*, 1514-1520.
- (18) Rubianes, M. D.; Rivas, G. A. *Anal. Chim. Acta* **2001**, *440*, 99-108.
- (19) Raoof, J.-B.; Ojani, R.; Rashid-Nadimi, S. *Electrochim. Acta* **2005**, *50*, 4694-4698.
- (20) Zhang, H.-M.; Li, N.-Q.; Zhu, Z. *Microchem. J.* **2000**, *64*, 277-282.

- (21) Zhang, Y.; Jin, G.; Wang, Y.; Yang, Z. *Sensors* **2003**, *3*, 443-450.
- (22) Zhao, H.; Zhang, Y.; Yuan, Z. *Anal. Chim. Acta* **2001**, *441*, 117-122.
- (23) Zhou, Y. Z.; Zhang, L. J.; Chen, S. L.; Dong, S. Y.; Zheng, X. H. *Chin. Chem. Lett.* **2009**, *20*, 217-220.
- (24) Wang, Q.; Dong, D.; Li, N. *Bioelectrochemistry* **2001**, *54*, 169-175.
- (25) Lai, G.-S.; Zhang, H.-L.; Han, D.-Y. *Microchim. Acta* **2008**, *160*, 233-239.
- (26) Zheng, J.; Zhou, X. *Bioelectrochemistry* **2007**, *70*, 408-415.
- (27) Liu, T.; Li, M.; Li, Q. *Talanta* **2004**, *63*, 1053-1059.
- (28) Shinkai, S.; Araki, K.; Tsubaki, T.; Arimura, T.; Manabe, O. *J. Chem. Soc., Perkin Trans. 1* **1987**, 2297-2299.
- (29) Guo, D.-S.; Wang, K.; Liu, Y. *J. Inclusion Phenom. Macrocyclic Chem.* **2008**, *62*, 1-21.
- (30) Su, W.; Iroh, J. O. *Electrochim. Acta* **1997**, *42*, 2685-2694.
- (31) Yuan, Y. J.; Adeloju, S. B.; Wallace, G. G. *Eur. Polym. J.* **1999**, *35*, 1761-1772.
- (32) Li, Y.; Yang, J. *J. Appl. Polym. Sci.* **1997**, *65*, 2739-2744.
- (33) Kaplin, D. A.; Qutubuddin, S. *Polymer* **1995**, *36*, 1275-1286.
- (34) Wood, G. A.; Iroh, J. O. *Polym. Eng. Sci.* **1996**, *36*, 2389-2395.
- (35) Hernandez-Perez, T.; Morales, M.; Batina, N.; Salmon, M. *J. Electrochem. Soc.* **2001**, *148*, C369-C375.
- (36) Reyes, D. C. J. I.; Cavalieri, R. P.; Powers, J. R. *Synth. Met.* **2004**, *142*, 71-79.
- (37) Wang, Y.; Northwood, D. O. *Thin Solid Films* **2008**, *516*, 7427-7432.
- (38) Zhu, R. L.; Li, G. X.; Zheng, J. H.; Jiang, J. W.; Zeng, H. B. *Surf. Eng.* **2009**, *25*, 156-162.
- (39) García, M. A. L.; Smit, M. A. *Journal of Power Sources* **2006**, *158*, 397-402.
- (40) Diaz, A. F.; Castillo, J. I.; Logan, J. A.; Lee, W. Y. *J. Electroanal. Chem. Interfacial Electrochem.* **1981**, *129*, 115-132.
- (41) Stankovic, R.; Pavlovic, O.; Vojnovic, M.; Jovanovic, S. *Eur. Polym. J.* **1994**, *30*, 385-393.
- (42) Yeu, T.; Yin, K. M.; Carbajal, J.; White, R. E. *J. Electrochem. Soc.* **1991**, *138*, 2869-2877.
- (43) Carquigny, S.; Segut, O.; Lakard, B.; Lallemand, F.; Fievet, P. *Synth. Met.* **2008**, *158*, 453-461.

- (44) Ingram, M. D.; Staesche, H.; Ryder, K. S. *J. Power Sources* **2004**, *129*, 107-112.
- (45) Kim, Y.; Kwon, Y.; Lee, K.; Park, J.; Seo, H.; Kim, T. *Mol. Cryst. Liq. Cryst.* **2004**, *424*, 153-158.
- (46) Gal, Y.-S.; Lee, W.-C.; Lyoo, W. S.; Jin, S.-H.; Lim, K. T.; Park, Y.-I.; Park, J.-W. *Int. J. Photoenergy* **2008**, No pp. given.
- (47) Ko, J. M.; Rhee, H. W.; Park, S. M.; Kim, C. Y. *J. Electrochem. Soc.* **1990**, *137*, 905-909.
- (48) Keeley, G. P.; Lyons, M. E. G. *Int. J. Electrochem. Sci.* **2009**, *4*, 794-809.
- (49) Streeter, I.; Wildgoose, G. G.; Shao, L.; Compton, R. G. *Sensors and Actuators B: Chemical* **2008**, *133*, 462-466.
- (50) Henstridge, M. C.; Dickinson, E. J. F.; Aslanoglu, M.; Batchelor-McAuley, C.; Compton, R. G. *Sensors and Actuators B: Chemical* **2010**, *145*, 417-427.
- (51) Zou, G.; Liu, Z.; Wang, C. *Analytica Chimica Acta* **1997**, *350*, 359-363.
- (52) Wang, X.; Yang, N.; Wan, Q.; Wang, X. *Sensors and Actuators B: Chemical* **2007**, *128*, 83-90.
- (53) Wu, K.; Fei, J.; Hu, S. *Anal. Biochem.* **2003**, *318*, 100-106.
- (54) Corona-Avendano, S.; Alarcon-Angeles, G.; Rosquete-Pina, G. A.; Rojas-Hernandez, A.; Gutierrez, A.; Ramirez-Silva, M. T.; Romero-Romo, M.; Palomar-Pardave, M. *J. Phys. Chem. B* **2007**, *111*, 1640-1647.
- (55) Arena, G.; Cali, R.; Lombardo, G. G.; Rizzarelli, E.; Sciotto, D.; Ungaro, R.; Casnati, A. *Supramol. Chem.* **1992**, *1*, 19-24.
- (56) Suga, K.; Ohzono, T.; Negishi, M.; Deuchi, K.; Morita, Y. *Supramol. Sci.* **1998**, *5*, 9-14.
- (57) Yoshida, I.; Yamamoto, N.; Sagara, F.; Ishii, D.; Ueno, K.; Shinkai, S. *Bull. Chem. Soc. Jpn.* **1992**, *65*, 1012-1015.
- (58) Shinkai, S.; Araki, K.; Kubota, M.; Arimura, T.; Matsuda, T. *J. Org. Chem.* **1991**, *56*, 295-300.
- (59) Lyons, M. E.; Breen, W.; Cassidy, J. *J. Chem. Soc., Faraday Trans.* **1991**, *87*, 115-123.

CHAPTER 5

Mode of Sensing:

Studies on the Selectivity of the Sensor and
the Interaction of Dopamine with the
PPy-C4S Film

5.1 Introduction

The application of electrochemical methods for the detection of dopamine (DA) has been the subject of many electroanalytical studies¹⁻²⁷. However, the accurate *in vivo* determination of DA is problematic. In a living organism, DA exists in the presence of other biological molecules. Many of these species are electroactive, with oxidation potentials similar to DA. Consequently, the detection of DA can be hindered due to masking of the electrochemical signal. The higher biological concentrations of these species, in comparison to DA, make this problem all the more significant. Additionally, several of these species have been shown to adhere to electrode surfaces, reducing the activity of the sensor. For these reasons, the development of materials that are highly selective for DA, in the presence of other biological molecules, is important for the accurate determination of DA. Therefore, understanding the mode in which DA is sensed by these materials can be helpful for the successful design of more selective sensors.

In Chapter 4, the polypyrrole/*p*-sulfonatocalix[4]arene (PPy-C4S) modified electrode was shown to be capable of sensing DA. A number of interactions could have accounted for the detection of DA at this modified electrode. Firstly, the formation of ion pairs at both the upper and lower rim of C4S has been reported in the literature²⁸⁻³⁰. In this way, DA could have been electrostatically attracted to the C4S incorporated within the PPy-C4S film. Alternatively, DA could have been included into the cavity of C4S. It is known that DA forms a strong inclusion complex with C4S³¹. In addition, previous studies carried out in our laboratory, on a polypyrrole/chloride (PPy-Cl) modified electrode, suggested that some oxidation of DA could also occur at the PPy backbone³. However, these DA oxidation currents were much lower than those observed for PPy doped with a sulfonated β -cyclodextrin (SCD). Accordingly, in this chapter, the mode in which the PPy-C4S film sensed DA was explored.

The mode of sensing of the PPy-C4S film was considered from three perspectives. To begin with, the interaction of DA at the PPy-C4S film was examined to determine if DA was specifically interacting with the C4S incorporated within the film. Next, NMR spectroscopy was used to study the inclusion complex formed between DA and C4S. The structure of this complex provided some insight into the mode of

sensing of the PPy-C4S film. Finally, the selectivity of the PPy-C4S film towards DA was investigated in the presence of ascorbic acid, uric acid, 5-hydroxytryptamine and acetylcholine. The varying degrees to which these compounds could interfere with the electrochemical detection of DA had implications for the mode of sensing of the PPy-C4S film.

5.2 Results and Discussion

5.2.1 The Interaction of DA at the PPy-C4S film.

In Chapter 4, several experiments were carried out with the aim of optimising the PPy-C4S modified electrode for the electrochemical detection of DA. During this process, some interesting results regarding the interaction of DA at the PPy-C4S film came to light. In this section, these results are presented together for clarity and their implications for the mode of sensing are discussed.

5.2.1 (i) Evidence for the Adsorption of DA at the PPy-C4S Film.

In Section 4.2.4 (vi), the kinetics of the oxidation of DA at the PPy-C4S film were studied by varying the scan rate for cyclic voltammetry. While the diffusion of DA from the bulk solution was found to be the major rate limiting process, there was also considerable evidence to suggest that DA could adsorb to the PPy-C4S film. Firstly, the DA peak oxidation current could be plotted as a function of the scan rate to obtain a linear relationship, Figure 5.1. This type of relationship is characteristic of both adsorption and thin layer diffusion, where the electron transfer process is rate limiting^{4, 9, 32-35}. Secondly, the voltammetric behaviour of DA at the PPy-C4S film suggested that adsorption of DA was taking place. Figure 5.2 shows a range of scans, from the first to the twentieth, for the PPy-C4S modified electrode in a 1.0×10^{-3} mol dm⁻³ solution of DA. A voltammetric signal for DA was obtained immediately on exposure of the electrode to the solution, indicating that diffusional processes were present⁴. However, this signal increased steadily with subsequent cycles reaching a steady state by the twentieth. From this it could be inferred that adsorption effects were also present⁴. Thirdly, when a PPy-C4S electrode, which had been immersed in a 1.0×10^{-3} mol dm⁻³ solution of DA for 10 min, was transferred, after rinsing thoroughly with deionised water, to a 0.10 mol dm⁻³ Na₂SO₄ solution, a signal for DA could still be observed, as shown in Figure 5.3. This indicated that the PPy-C4S electrode had been modified during its immersion in the DA solution. Moreover, this signal remained relatively constant over 20 cycles, suggesting that DA was not just trapped within the pores of the film, and free to diffuse away, but was adsorbed to the PPy-C4S film.

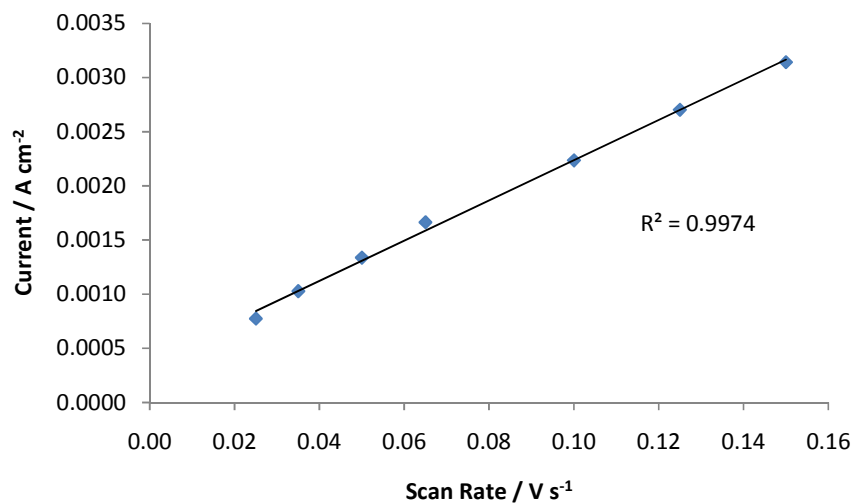


Figure 5.1: Plot of peak current for the oxidation of DA at the PPy-C4S modified electrode as a function of the scan rate.

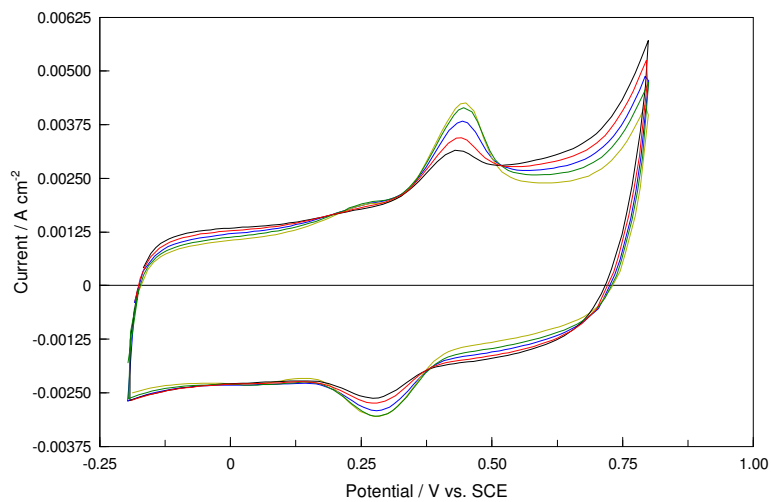


Figure 5.2: Cyclic voltammograms recorded in a $1.0 \times 10^{-3} \text{ mol dm}^{-3}$ DA / 0.10 mol dm^{-3} Na₂SO₄ solution at a scan rate of 100 mV s^{-1} for the PPy-C4S modified electrode. Cycles shown are 1 (—), 5 (—), 10 (—), 15 (—) and 20 (—).

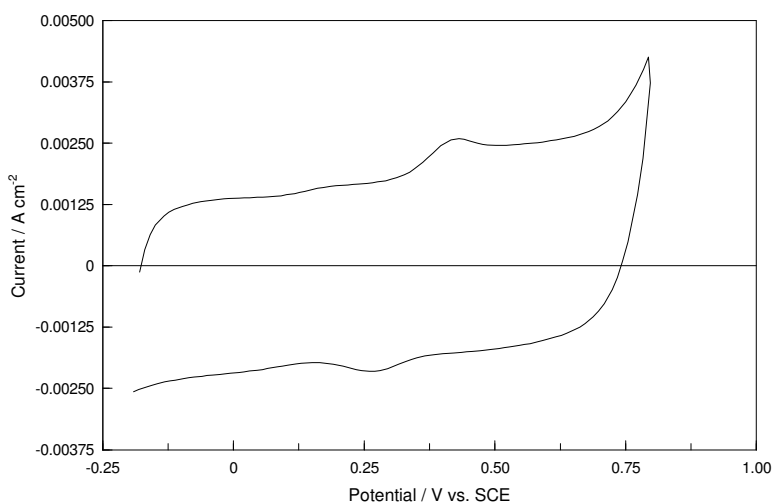


Figure 5.3: Cyclic voltammogram recorded in a $0.10 \text{ mol dm}^{-3} \text{ Na}_2\text{SO}_4$ solution for a PPy-C4S modified electrode that had been immersed in a $1.0 \times 10^{-3} \text{ mol dm}^{-3} \text{ DA} / 0.10 \text{ mol dm}^{-3} \text{ Na}_2\text{SO}_4$ solution for 10 min. The scan rate used was 100 mV s^{-1} .

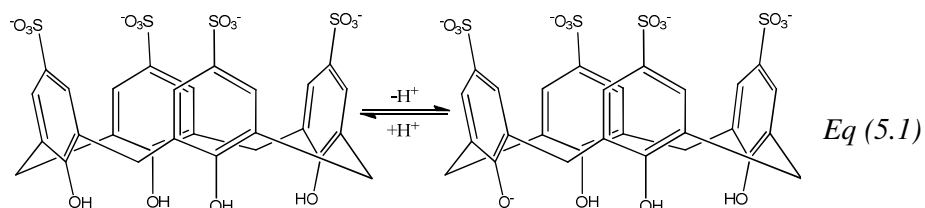
5.2.1 (ii) Evidence for a Specific Interaction between DA and C4S in the PPy-C4S Film.

The results outlined above strongly suggest that it is possible for DA to adsorb to the PPy-C4S film. Considering that DA is positively charged, the most likely site for this adsorption was the anionic C4S. Moreover, the fact that C4S is known to form a strong inclusion complex with DA ($K_a = 4060 \text{ mol}^{-1}$) made this proposal seem even more probable³¹. In a general sense, the results outlined in Section 4.2.3 further support this idea. These studies compared the electrochemical response of DA at the PPy-C4S modified electrode with the response obtained at electrodes modified using sulfate and dodecylsulfate (SDS) doped PPy films. It was found that the oxidation of DA was far superior at the PPy-C4S film. This suggested that the presence of C4S in the film made the interaction of DA more favorable at the PPy-C4S film.

More specifically, a comparison of the adsorption tests carried out in Section 4.2.4 (vi) and Section 4.2.4 (vii), provided some insight into the nature of this interaction between DA and C4S. These experiments were carried out at pH 6 and pH 2 respectively. It was found that the DA signal observed, after immersing the

PPy-C4S electrode in a 1.0×10^{-3} mol dm⁻³ solution of DA for 10 min, had a shorter lifetime at pH 2 than at pH 6. Figure 5.4 shows the cyclic voltammograms obtained for the adsorption test at pH 2. Although a signal for DA was observed, the currents declined steadily with each successive cycle suggesting that DA was free to diffuse away. In contrast, the signal obtained for the same experiment at pH 6 was stable over 20 cycles. This suggested that the adsorption of DA at the PPy-C4S film was either weakened or did not occur at pH 2.

There are two possible contributions to the interaction between C4S and DA that can explain why this interaction becomes weaker at lower pH, both of which arise from the protonation of the calixarene. C4S is known to have one phenolic proton with a pK_a value of approximately 3.27³⁶⁻³⁸. Assuming this pK_a value is unaffected by the incorporation of the calixarene into the PPy film, then C4S was expected to be predominantly penta-anionic at pH 6 and predominantly tetra-anionic at pH 2 (Equation 5.1). As a result, the lower rim of the calixarene would no longer be anionic and capable of interacting electrostatically with DA at pH 2.



Moreover, the inclusion of DA into C4S would also be affected by a reduction in pH. Shinkai *et al.* studied the complexes formed between several organic ammonium cations and C4S^{29, 39}. They found that electrostatic contributions to the binding were significant for these complexes, with the driving force for inclusion being attributed to cation- π interactions between the cationic ammonium group and the calixarene aromatic π -systems²⁹. These interactions were enhanced when the lower rim of the calixarene was ionized, due to the π -system being more electron-rich^{29, 40}. Thus, the inclusion of DA into the tetra-anionic form of C4S was likely to be less favoured. From these results, it was clear that the interaction of DA with the PPy-C4S film was specific to C4S. In an effort to better understand these interactions, the complex formed between DA and C4S was studied in solution.

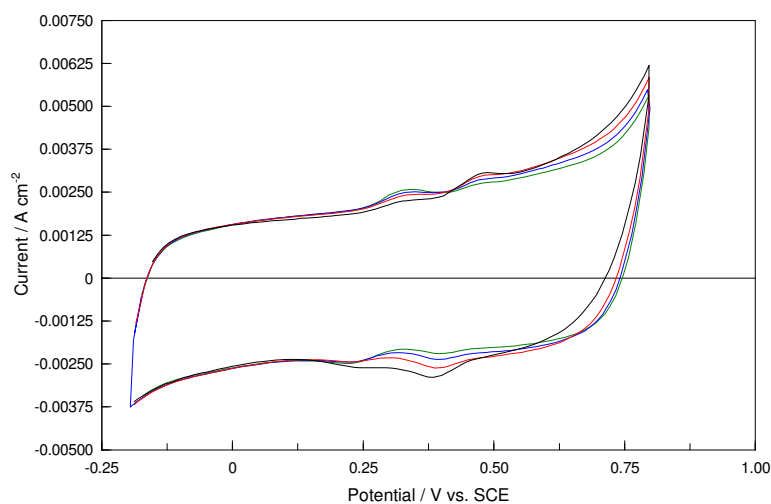


Figure 5.4: Cyclic voltammograms recorded in a $0.10 \text{ mol dm}^{-3} \text{ Na}_2\text{SO}_4$ solution for a PPy-C4S modified electrode that had been immersed in a $1.0 \times 10^{-3} \text{ mol dm}^{-3} \text{ DA} / 0.10 \text{ mol dm}^{-3} \text{ Na}_2\text{SO}_4$ solution for 10 min. Cycles shown are 5 (—), 10 (—), 15 (—) and 20 (—). The scan rate used was 100 mV s^{-1} .

5.2.2 The Interaction of DA with C4S in Solution

The interaction between DA and C4S, in solution, was studied using NMR spectroscopy. Fluorescence spectroscopic studies carried out by Zhou *et al.* showed that DA can form a 1:1 inclusion complex with C4S³¹. The formation of this complex can be represented generally by the following equilibrium,



where m and n are the stoichiometric ratios of C4S and DA, respectively. The association constant, K_a , for this process gives an estimate of the strength of the interaction between DA and C4S. Both of these properties can be easily determined using NMR spectroscopy.

In this section, Job's method was applied to the NMR spectroscopic data to determine the stoichiometry of the complex and the result was used to test the accuracy of the molecular formula assigned to the calixarene. Following this analysis, K_a could be estimated using NMR titration. A structure for the complex was also inferred from the NMR spectroscopic data. This is the advantage of using

NMR spectroscopy for binding studies, as it can provide more microscopic information on complex structures. The structure of the complex was probed further using Rotating frame Nuclear Overhauser Effect (ROE) spectroscopy. Lastly, the implications of these results for the mode of sensing were discussed.

First of all, in order for Job's method and the NMR titration to be applicable, at least one of the proton signals for DA or C4S needed to be sensitive to complex formation. Figure 5.5 shows the ^1H NMR spectra obtained for DA in the absence and presence of a two molar equivalent of C4S. Clearly, each DA proton signal was shifted upfield, to lower ppm, in the presence of C4S. Therefore, the experimentally observed parameters used for the Job's analysis and NMR titration were the chemical shift values and the changes in these values for the DA proton signals. However, proton chemical shift values can be sensitive to changes in the ionic strength of the solution. This was a possible problem for these studies as the high charge on the calixarene and its varied concentration meant that the ionic strength, of the solutions examined, would not be constant. In order to minimise these effects, an excess of KCl (0.30 mol dm^{-3}) was added to each solution.

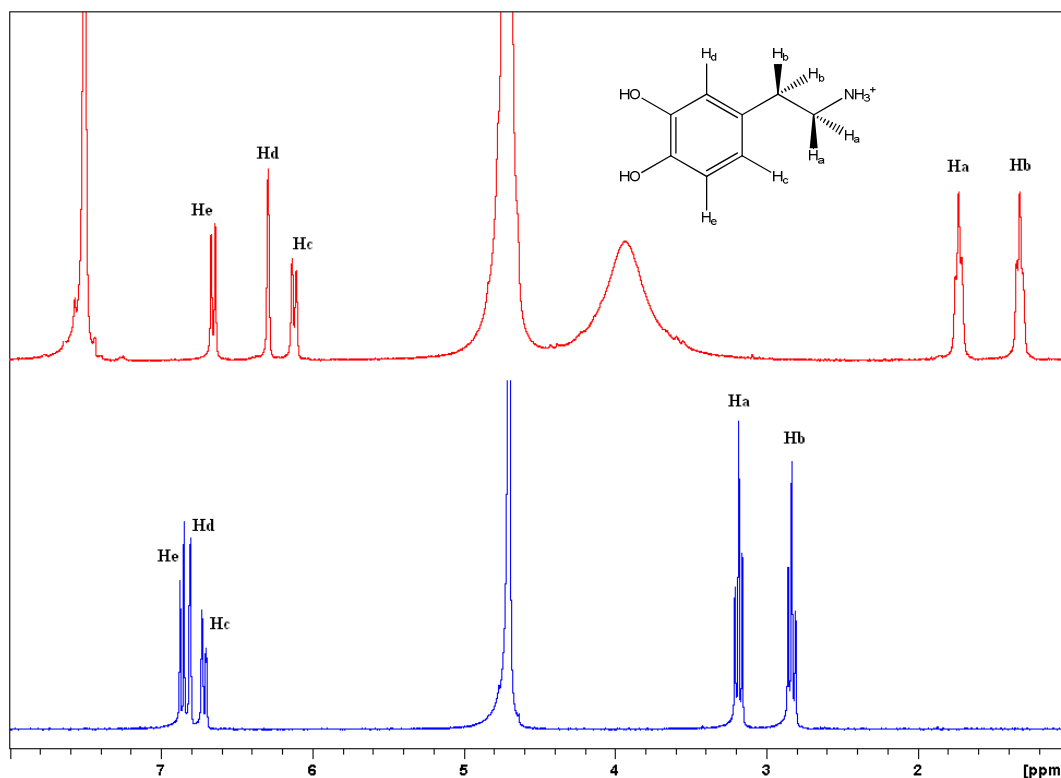


Figure 5.5: ^1H NMR spectra of DA in the absence (—) and presence (—) of a two molar equivalent of C4S. The structure of DA is also shown with the appropriate protons labeled.

It should also be noted from Figure 5.5, that a single signal was observed for each DA proton when C4S was present. This indicated that the exchange between *free* and *complexed* DA was “fast” on the NMR timescale. Under “slow exchange” conditions, the spectrum would have consisted of two signals for each DA proton signal⁴¹: one for uncomplexed DA, at the observed chemical shift position δ_{free} , and one for DA complexed by C4S, at $\delta_{complex}$. In contrast, under “fast exchange” conditions, just one signal, at the weighted-average of δ_{free} and $\delta_{complex}$, is observed. This observation was significant for the NMR titration analysis in Section 5.2.2 (ii).

5.2.2 (i) Job’s Method and the Stoichiometry of the C4S-DA Complex.

The stoichiometry of the complex formed between DA and C4S was determined using Job’s method. This method involved recording ¹H NMR spectra for a series of solutions containing DA and C4S in varying proportions, such that the total molar concentration, $[C4S] + [DA]$, of each solution remained constant^{42, 43}. Under these conditions, a plot of the NMR data in the form $X_{DA}\Delta\delta$ versus X_{DA} where,

$$X_{DA} = \frac{[DA]}{[C4S] + [DA]} \quad Eq(5.3)$$

is the mole fraction of DA in each solution, and

$$\Delta\delta = \delta_{free} - \delta_{obs} \quad Eq(5.4)$$

where $\Delta\delta$ is the change in chemical shift of a particular proton signal, δ_{free} is the chemical shift of the proton signal in the free molecule and δ_{obs} is the observed chemical shift of the proton signal in the spectrum, gives a curve with a maximum value at,

$$X_{DA} = \frac{1}{m/n + 1} \quad Eq(5.5)$$

where m/n is the ratio of C4S to DA in the complex^{42, 43}.

The Job's plots created for each DA proton signal are shown in Figure 5.6. These plots were created using an approximate molar mass for C4S (1010.96). Microanalysis carried out on several different samples of C4S led to the assignment of the general molecular formula, $\text{Ca}_x\text{Na}_{5-2x}\text{C}_{28}\text{H}_{19}\text{O}_{16}\text{S}_4 \cdot (y\text{H}_2\text{O})$. However, an approximate formula was used to calculate the molar mass of C4S ($\text{CaNa}_3\text{C}_{28}\text{H}_{19}\text{O}_{16}\text{S}_4 \cdot (9\text{H}_2\text{O})$, MW = 1010.96). It is clear from Figure 5.6 that a curve, with a maximum at $X_{DA} \cong 0.5$, was obtained for each DA proton signal. Therefore, by applying Equation 5.5, a value of $m/n = 1$ was obtained, indicating the formation of a 1:1 complex between C4S and DA. This result was in agreement with the 1:1 stoichiometry determined by Zhou *et al.*³¹, suggesting that the molecular formula assigned to C4S was reasonably accurate.

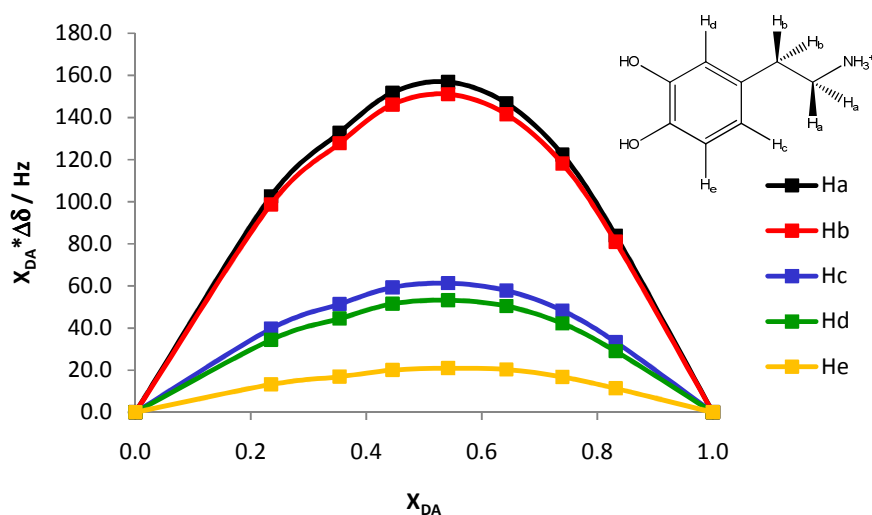


Figure 5.6: The Job's plot obtained for each DA proton signal. The curves are labeled according to which protons they represent and the structure of DA is given with the appropriate protons labeled.

5.2.2 (ii) NMR Titration

NMR titration was used to determine the association constant, K_a , for the formation of the 1:1 complex between DA and C4S,



It was shown previously that the rate of interconversion for this complex was “fast” relative to the NMR timescale. Under these “fast exchange” conditions, the observed change in chemical shift, $\Delta\delta$, for a DA proton signal was expected to vary, as a function of the molar ratio of C4S, $R = [C4S]/[DA]$, according to the following relationship⁴¹,

$$\Delta\delta = \left(\frac{\Delta_0}{2}\right) \left(b - \sqrt{b^2 - 4R}\right) \quad Eq(5.7)$$

where,

$$b = 1 + R + \frac{1}{K_a[DA]} \quad Eq(5.8)$$

and,

$$\Delta_0 = \delta_{free} - \delta_{complex} \quad Eq(5.9)$$

where δ_{free} and $\delta_{complex}$ have their previously defined values. Thus, a value for K_a could be obtained from non-linear curve fitting of Equations 5.7 and 5.8 to a plot of $\Delta\delta$ against the molar ratio of C4S, R , in solution⁴¹.

With this in mind, a series of solutions containing varying ratios of C4S to DA were prepared, where the concentration of DA in each solution remained constant. ¹H NMR spectra were recorded for each of these solutions and $\Delta\delta$, for each DA proton, was plotted as a function of the molar ratio of C4S (R), as shown in Figure 5.7. It can be seen from Figure 5.7, that each proton signal shifted upfield as the concentration of C4S increased. The relationship outlined above was then fitted to each of these curves to obtain a value for K_a . Figure 5.8 shows the experimental and predicted values for $\Delta\delta$ for the DA proton signal H_a. It can be seen from Figure 5.8 that the predicted and experimental values were in good agreement. A good fit was obtained for all the DA proton signals with an average correlation coefficient of 0.995. The average K_a value determined from each of these fittings was $161.0 \pm 28.5 \text{ mol}^{-1}$. This value does not agree well with the value obtained by Zhou *et al.* using fluorescence measurements (4060 mol^{-1}), in fact it is significantly lower³¹. The reason for this is not certain. It could be due to the high concentration of KCl (0.30 mol dm^{-3}) present in the solutions used in the NMR study. Recent studies

carried out in our laboratory found that the ionic strength of the solution can have a significant effect on the value obtained for the binding constant⁴⁴. Using UV-vis spectroscopy, K_a values for the complex formed between C4S and diquat were measured in solutions containing varying concentrations of Na_2SO_4 . The measured K_a value was found to decrease significantly with increasing salt concentration. Given that C4S has been shown to have no binding affinity for Na^+ ,²⁸ this effect was attributed to the increasing ionic strength of the solutions. Zhou *et al.*³¹ carried out their fluorescence measurements in a 0.10 mol dm^{-3} phosphate buffer solution (ionic strength $\sim 0.10 \text{ mol dm}^{-3}$), whereas, a 0.30 mol dm^{-3} KCl solution (ionic strength $\sim 0.30 \text{ mol dm}^{-3}$) was used for these NMR studies. Therefore, the lower K_a value obtained here could be due to the higher ionic strength of the NMR solutions. However, this requires further investigation.

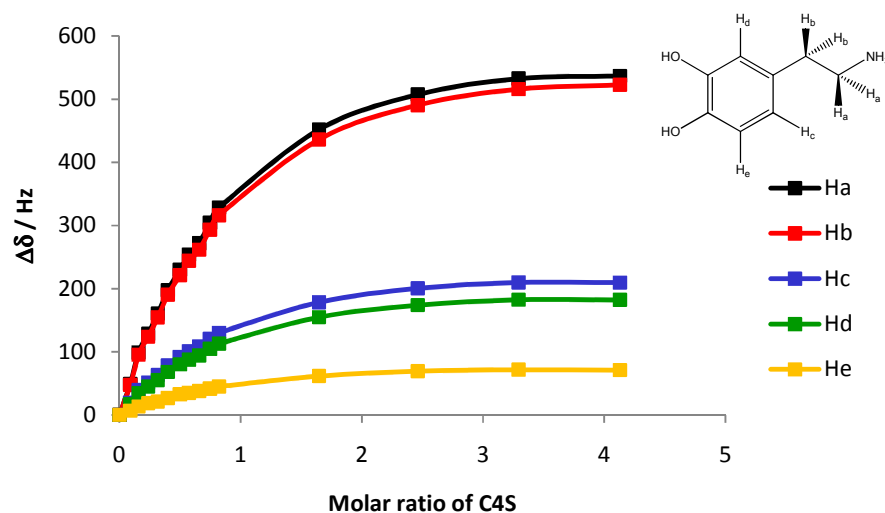


Figure 5.7: The change in chemical shift, $\Delta\delta$, for each DA proton signal plotted as a function of the molar ratio of C4S. The curves are labeled according to which protons they represent and the structure of DA is given with the appropriate protons labeled.

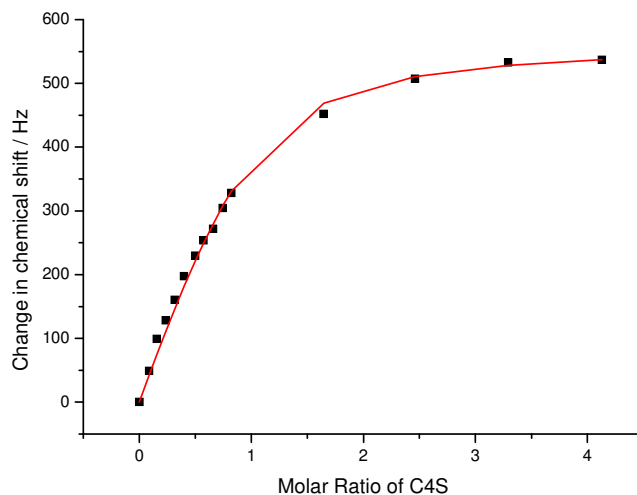


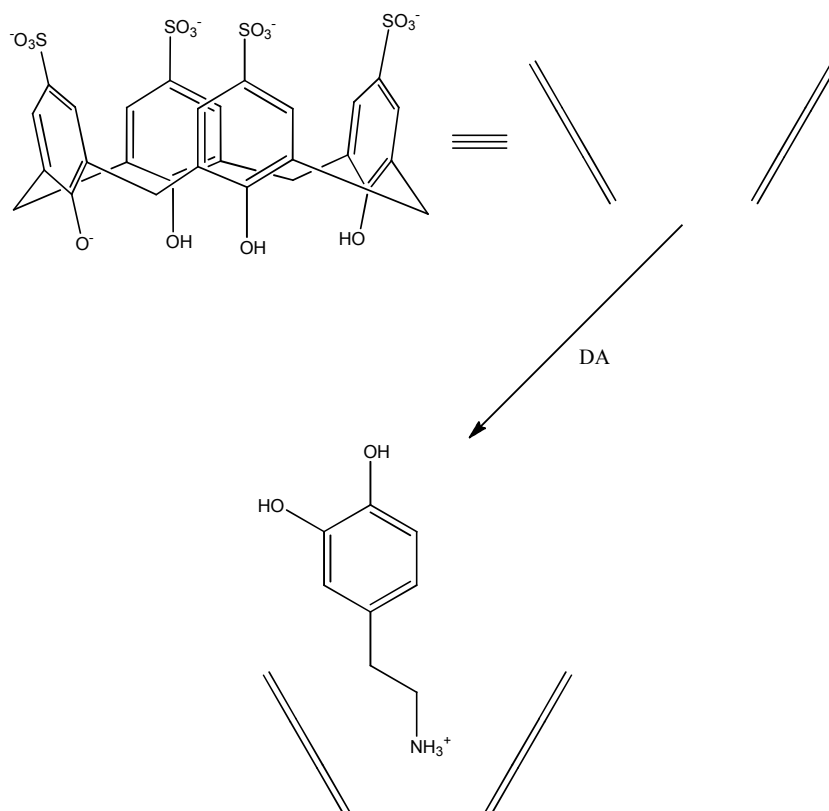
Figure 5.8: A plot of the experimental (■) and theoretical (—) observed changes in chemical shift for the H_a NMR signal as a function of the molar ratio of C4S (R).

5.2.2 (iii) The Structure of the C4S-DA Complex

As mentioned previously, the use of NMR spectroscopy for binding studies has the advantage of providing structural information about the complex. In the Job's and NMR titration experiments outlined above, the effect of complex formation, on the chemical shift values of the DA proton signals, was monitored. The nature and magnitude of these changes can be indicative of the structure of the complex being formed. Firstly, it was found that each DA proton signal was shifted upfield, to a higher magnetic field, in the presence of C4S. This can be seen clearly in Figure 5.5. This upfield shift meant that each proton, in the *complexed* form, was more shielded, from the applied magnetic field, than in the *free* form. A change in chemical shift of this nature indicated that DA was being included into the cavity of C4S^{29, 39, 45, 46}. Within the cavity, the protons of DA would be shielded by the ring currents generated by the aromatic π -electrons. As a result, their NMR signals would be observed at a lower chemical shift position in the spectrum.

Secondly, it is clear from the Job's plots (Figure 5.6) and the NMR titration plots (Figure 5.7) that the magnitude of this shift was different for each DA proton signal. The signals for the aliphatic protons, H_a and H_b , displayed the largest upfield shift

indicating that they experienced the greatest shielding effect. The implication of this was that DA was included into the calixarene cavity *via* its aliphatic amine moiety. This was supported by the fact that $\Delta\delta_{c,d}$ was greater than $\Delta\delta_e$ which indicated that protons H_c and H_d were inserted further into the cavity than H_e. Therefore, the mode of inclusion presented in Scheme 5.1 was proposed for the C4S-DA complex. The validity of this structure was further checked using ROE NMR spectroscopy.



Scheme 5.1: The proposed mode of inclusion of DA by C4S.

5.2.2 (iv) Rotating-Frame Nuclear Overhauser Effect (ROE) Spectroscopy

Nuclear Overhauser effects arise due to through space interactions between protons that are in close proximity to each other. In order for an NOE to be observed between two protons there must be a significant interaction between the magnetic dipoles of the two nuclei. These dipole-dipole interactions are strongly dependent on

distance such that an NOE can only occur between two protons that are less than 5 - 6 Å apart^{47, 48}. Consequently, if DA was being included into the calixarene cavity then specific NOE interactions were expected to occur between the DA and calixarene protons. However, due to the size of the calixarene, it was necessary to use rotating-frame NOE spectroscopy to measure these NOE interactions. NOE signals can be positive or negative depending on the rate of molecular tumbling (correlation time)⁴⁸. This is determined, in large part, by the molecular weight of the molecule. The NOE is positive for small molecules, goes through zero for molecules with a molecular weight in the range 700 - 1500, and becomes negative for large molecules⁴⁷. For medium sized molecules, where the NOE may be theoretically zero, the rotating frame NOE is often preferred since the ROE is always non-zero and positive. Therefore, as the molecular weight of C4S was approximately 1011, the ROE experiment was the most suitable.

Several 1D selective ROE experiments were carried out on a solution containing DA and C4S in the ratio 2:1. Each experiment involved irradiating a specific proton signal and then recording the resulting spectrum. Figure 5.9 shows the spectra obtained when the signals for the DA aliphatic protons, H_a and H_b, and the calixarene aromatic protons, ArH, were irradiated. In each spectrum the irradiated signal is phased down and the ROE signals have positive phase. Before discussing these spectra it is important to note some artifacts that were observed. When H_a was irradiated, a specific ROE should have been observed for H_b. However, it can be seen from Figure 5.9, that both signals show negative phase. This anomaly is most likely due to a ¹H-TOCSY artifact. The pulse sequences for the 1D-selective TOCSY and 1D-selective ROE experiments are very similar⁴⁸. As a result, TOCSY transfer can also be observed in ROE spectra. These signals are identified by having opposite phase to the ROE signals. TOCSY transfer only occurs for protons that are in the same spin system⁴⁷. That is, protons that are *J*-coupled or have a mutual *J*-coupling will exhibit TOCSY signals. Moreover, TOCSY artifacts in ROE spectra are particularly strong for CH₂ groups⁴⁸. Therefore, the negative signal observed for H_b, when H_a was irradiated, could be attributed to TOCSY transfer between these two CH₂ groups. Similarly, the negative signal observed for H_a, when the signal for H_b was irradiated, can also be explained in this way. Due to the presence of these artifacts, the irradiated signal in each spectrum is designated with an arrow.

It is clear from Figure 5.9 that a specific ROE was observed between the calixarene aromatic protons, ArH, and the DA aliphatic protons, H_a and H_b. When H_a and H_b were irradiated, the positive signals observed were for H_c, H_d, and ArH. Thus, protons H_a and H_b had to be in close proximity to the calixarene aromatic protons. This result provided further support for the proposed structure of the complex (Scheme 5.1) where the DA aliphatic amine was included into the calixarene cavity. Correspondingly, when the calixarene ArH signal was irradiated, specific ROEs were observed for each DA proton signal. Again this indicated that DA was close in space to the calixarene aromatic protons. Therefore, the complex structure presented in Scheme 5.1 was assumed to be correct.

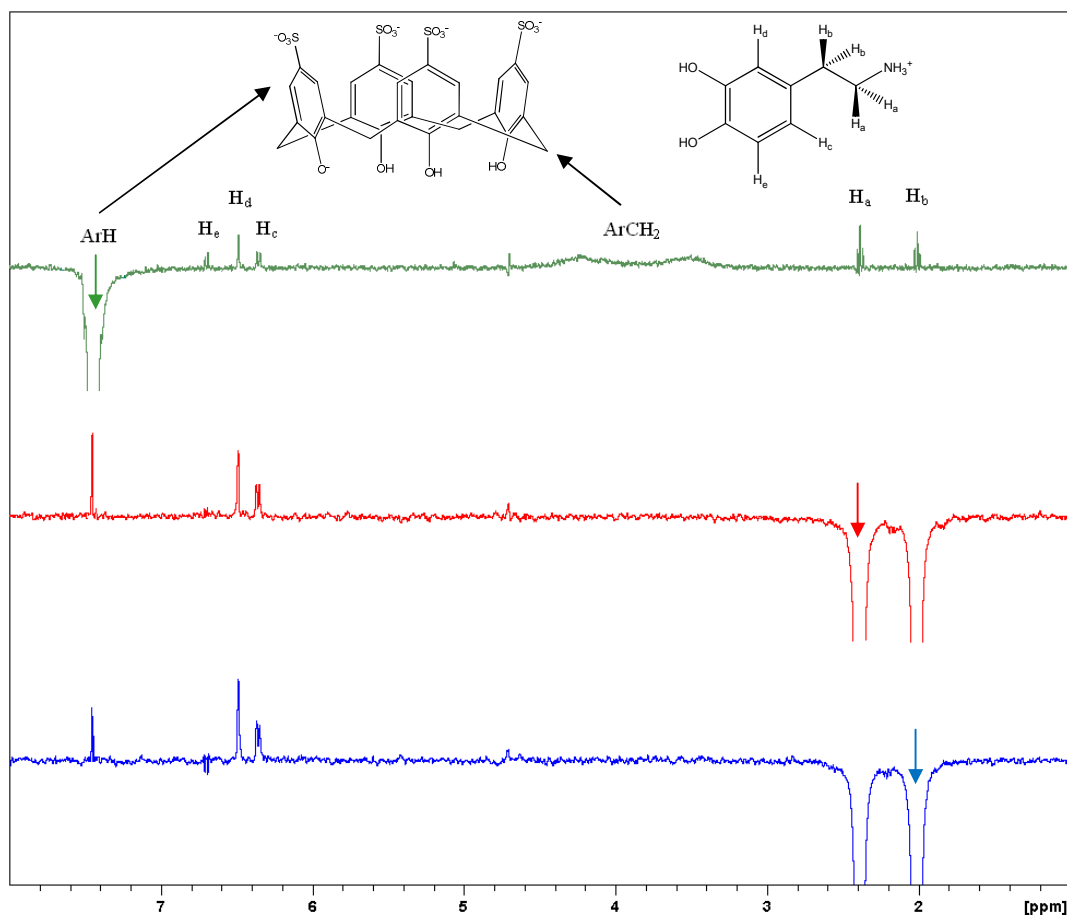


Figure 5.9: 1D-selective ROE spectra for solutions containing DA and C4S in the ratio 2:1 where the DA aliphatic proton signals, H_b (—) and H_a (—), and the calixarene aromatic protons, ArH (—) have been irradiated. The structures of C4S and DA are given and the appropriate protons and NMR signals have been labeled accordingly.

5.2.2 (v) *Insights into the Mode of Sensing*

Based on the NMR results outlined above, it can be concluded that DA and C4S form a 1:1 inclusion complex in solution. Furthermore, the amine moiety of DA can be confidently assigned as the inclusion site of DA. This mode of inclusion is consistent with literature reports that the C4S cavity can efficiently bind organic ammonium cations in a similar manner^{29, 39, 46, 49}. If this interaction is possible when C4S is incorporated into the PPy film, then the formation of such a complex within the film could account for the superior performance of the PPy-C4S film in comparison to the PPy-SO₄ and PPy-SDS films. Of these three dopants, only C4S could form an inclusion complex with DA, making the interaction of DA with the PPy-C4S film more favorable.

Such an interaction could also explain the effect of pH on the adsorption of DA to the PPy-C4S film. It has been shown that the inclusion of cationic amines into C4S is facilitated by cation- π interactions with the calixarene aromatic π -systems²⁹. This interaction is enhanced when the lower rim of the calixarene is ionized, due to the π -system being more electron rich^{29, 40}. In addition, electrostatic interactions between the guest ammonium cation and the negatively charged lower rim of the calixarene have also been shown to be important^{29, 39}. Clearly, both of these interactions would be weakened by protonation of the lower rim O⁻ group. Therefore, the fact that the ability of DA to adsorb to the PPy-C4S film was reduced at pH 2, where the lower rim O⁻ groups would be predominantly protonated, suggested that the adsorption of DA involved inclusion of its amine moiety into the cavity of C4S. While this observation was reasonable, it was not conclusive. Although previous work by Bidan and Niel⁵⁰ suggests that C4S can retain its recognition properties within a polymer film, the actual orientation of C4S within the PPy film was unknown. As such, any information obtained in solution could not be applied with certainty to the film. Accordingly, further studies on the interaction of DA with the PPy-C4S film were necessary. With this in mind, the selectivity of the PPy-C4S film towards the oxidation of DA was investigated.

5.2.3 The Selectivity of the PPy-C4S Film.

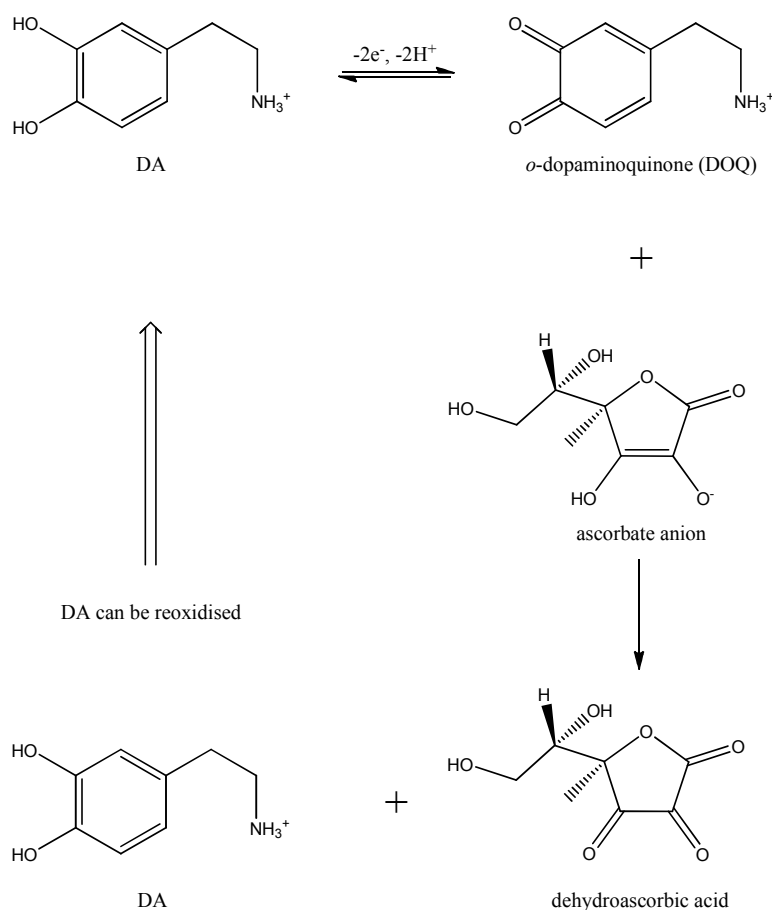
Here, the selectivity of the PPy-C4S film towards the oxidation of DA was explored. Four potential interferents in the electrochemical detection of DA were studied: ascorbic acid, uric acid, serotonin, and acetylcholine. These compounds were chosen based on their charge: positive, negative, or neutral, and their potential to form an inclusion complex with C4S. It was thought that the nature of any interference from these compounds would provide further insight into the mode of sensing of the PPy-C4S film. Therefore, the electrochemical response of each of these compounds at the PPy-C4S film and their ability to interfere with the detection of DA was investigated.

To begin with, it is important to address the effect of pH in these experiments. In Section 4.2.4 (viii) it was shown that buffer solutions were ineffective electrolytes for DA analysis at the PPy-C4S modified electrode. Consequently, the pH of the DA solutions examined in these experiments varied depending on the interferent compound. The experimental pH ranged from pH 4.3, when ascorbic acid was present in solution, to pH 5.5, in the presence of acetylcholine. However, in Section 4.2.4 (vii), the peak currents and peak potentials for the oxidation of DA at the PPy-C4S film were found to be practically independent of pH in the range pH 4.0 to pH 6.0. Thus, the effect of pH on the results of these experiments was assumed to be negligible.

5.2.3 (i) Ascorbic Acid (AA).

Ascorbic acid (AA) is a sugar acid with great biochemical importance. It has been employed for the prevention and treatment of a diverse range of health conditions such as infertility, cancer, AIDS and the common cold²¹. AA is also considered to be the most problematic interferent in the electrochemical detection of DA. This interference occurs in a variety of ways. Firstly, AA is electroactive and can be oxidized at most solid electrodes in the same potential region as DA. $E_{1/2}$ values for AA range between -100 to 400 mV vs. SCE with those for DA falling in the range 100 to 250 mV vs. SCE⁵¹. This is particularly problematic due to the fact that AA

coexists with DA in most biological systems at concentrations that are significantly higher than DA²⁴. Typical concentrations of DA lie in the range 10^{-8} to 10^{-6} mol dm⁻³ while AA concentrations can be as high as 10^{-4} mol dm⁻³. Consequently, the electrochemical response of these systems is dominated by AA. In addition, the oxidation products of AA can foul solid electrode surfaces causing a decrease in the currents observed at these electrodes¹². Still further complications can arise, due to the catalytic regeneration of DA by AA^{12, 52}. The mechanism for this reaction is outlined in Scheme 5.2. AA undergoes a redox reaction with the oxidation product of DA, *o*-dopaminoquinone (DOQ), resulting in the oxidation of AA and the reduction of DOQ back to DA. This regenerated DA can then be oxidized again at the electrode surface. As a result, higher currents than expected, for a given concentration of DA, are generated at the electrode.



Scheme 5.2: The mechanism for the electrocatalytic oxidation of AA by DA^{12, 52}.

The electrochemical response of a 1.0×10^{-3} mol dm⁻³ AA solution at a bare Pt electrode and the PPy-C4S modified electrode are shown in Figure 5.10. It is clear that AA was oxidized at the bare Pt electrode as the currents for the AA solution were higher than the currents for the solution containing no AA. In contrast, no electrochemical signal was observed for AA at the PPy-C4S electrode indicating that AA was not oxidized at the PPy-C4S film. The influence of AA on the oxidation of DA at the PPy-C4S film was also investigated. Figure 5.11 compares the peak currents for the oxidation of DA in the presence and absence of 1.0×10^{-3} mol dm⁻³ AA. It can be seen that the DA signal was not affected by the presence of AA in the solution. In particular, there was no evidence of any increase in the DA oxidation current, irrespective of DA concentration, as a result of the reaction between DOQ and AA. The peak potentials for the oxidation of DA in the presence and absence of AA were also compared, as shown in Figure 5.12. Again, the presence of AA in the solution was found to have no effect on the DA signal. These results show that the PPy-C4S electrode was highly selective towards DA in the presence of excess AA.

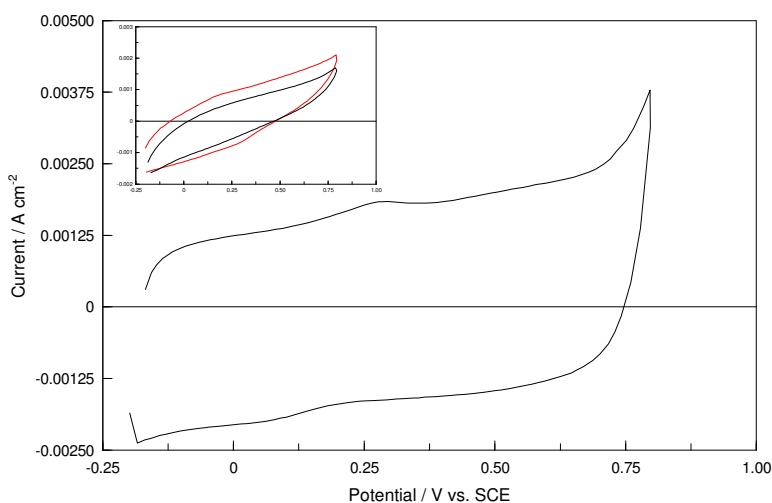


Figure 5.10: Cyclic voltammogram recorded in a 1.0×10^{-3} mol dm⁻³ AA / 0.10 mol dm⁻³ Na₂SO₄ solution for the PPy-C4S modified electrode. The inset shows cyclic voltammograms recorded for a bare Pt electrode in the absence (—) and presence (—) of 1.0×10^{-3} mol dm⁻³ AA.

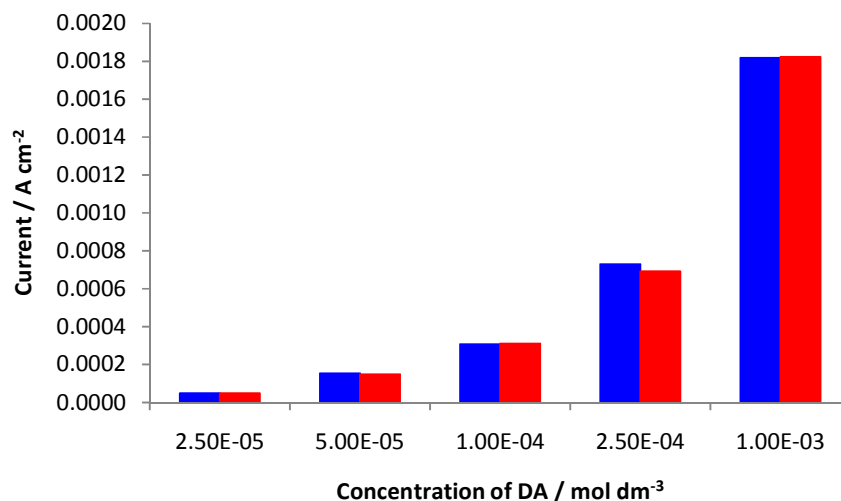


Figure 5.11: Peak oxidation currents for a range of DA concentrations from 2.5×10^{-5} to $1.0 \times 10^{-3} \text{ mol dm}^{-3}$, obtained using cyclic voltammetry, in the absence ■ and presence ■ of $1.0 \times 10^{-3} \text{ mol dm}^{-3}$ AA in a 0.10 mol dm^{-3} Na_2SO_4 solution, pH ~4.3 (n = 3). The currents shown have been corrected for background currents.

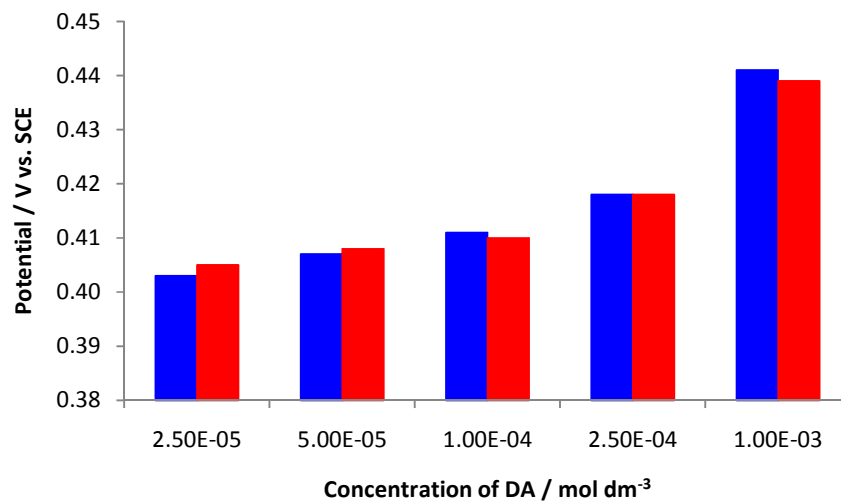
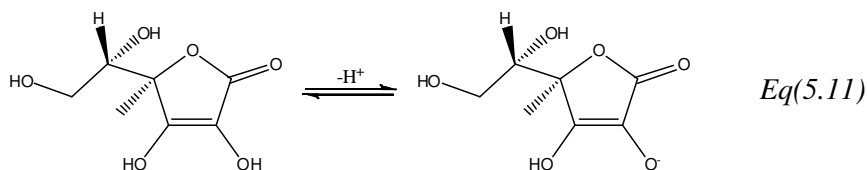


Figure 5.12: Peak oxidation potentials for a range of DA concentrations from 2.5×10^{-5} to $1.0 \times 10^{-3} \text{ mol dm}^{-3}$, obtained using cyclic voltammetry, in the absence ■ and presence ■ of $1.0 \times 10^{-3} \text{ mol dm}^{-3}$ AA in a 0.10 mol dm^{-3} Na_2SO_4 solution, pH ~4.3 (n = 3).

The lack of interference from AA at the PPy-C4S film can be primarily attributed to electrostatic repulsion between AA and C4S. At the pH of the experiment (pH 4.3), AA was predominantly anionic. Equation 5.11 shows the dissociation of AA to form the ascorbate anion. The pK_a for this reaction is 4.10^{23} . Given that the solution pH is related to the pK_a by Equation 5.12, then the ascorbate anion will predominate at pH values greater than 4.10. More specifically, the composition of the AA solution, at the experimental pH of 4.3, can be calculated using Equation 5.13. Accordingly, AA was expected to be 62% dissociated at pH 4.3.



Eq(5.11)

$$pH = pK_a + \log \frac{[AA^-]}{[AA]} \quad Eq(5.12)$$

$$\% \text{ dissociation} = \frac{100}{1 + 10^{pK_a - pH}} \quad Eq(5.13)$$

Therefore, the majority of the AA present would have been repelled by the negative charges in the PPy-C4S film. Overall, the PPy-C4S film can be considered neutral. This is due to the negative charges on the calixarene being balanced by the positively charged PPy backbone (PPy⁺). However, negatively charged local sites will exist due to the individual anionic calixarene molecules. The interaction of these negatively charged sites with the anionic AA could have acted as a barrier to interfacial electron transfer, preventing the oxidation of AA at the PPy-C4S film. This electrostatic repulsion may also have kept AA at a sufficient distance from the polymer interface to prevent it from reacting with DOQ. Thus, the reduction of DOQ back to DA could occur, during the reduction cycle of the cyclic voltammogram, with little or no catalytic regeneration of DA.

These observations highlight the importance of electrostatic interactions for the mode of sensing. However, they do not account completely for the high selectivity of the sensor. According to Equation 5.13, a significant proportion of AA, 38%, remained neutral. To explain the lack of interference from neutral AA we must consider the hydrophilic nature of this molecule. In its neutral form, AA contains

four hydroxyl (OH) groups. These highly polar groups are spread relatively evenly throughout the molecule. Given that polypyrrole is known to be hydrophobic^{53, 54}, it is unlikely that any significant interaction could have formed between AA and the polymer surface. Similarly, it is unlikely that AA could be included into the hydrophobic cavity of C4S. Arena *et al.* studied the inclusion of a range of amino acids by water soluble calix[4]arenes⁴⁵. Specifically, they found that phenylalanine was included into the cavity of C4S via its aromatic ring while tyrosine could not form any interaction with C4S. It can be seen from Figure 5.13 that these two amino acids differ by only a single OH group. Arena *et al.* attributed the failure of tyrosine to be included into the apolar cavity of C4S to the presence of the polar OH group on its aromatic ring⁴⁵. Therefore, it is likely that the lack of interference from neutral AA can be accounted for by its inability to interact with both C4S and the PPy film.

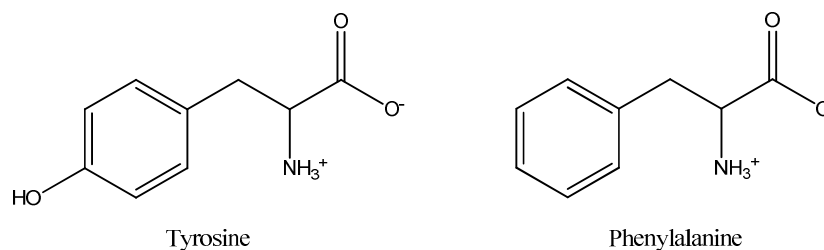
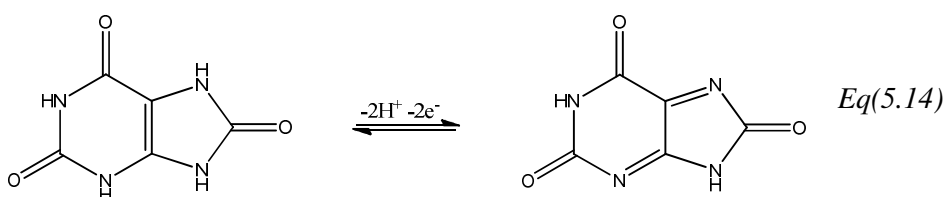


Figure 5.13: The structures of the amino acids tyrosine and phenylalanine.

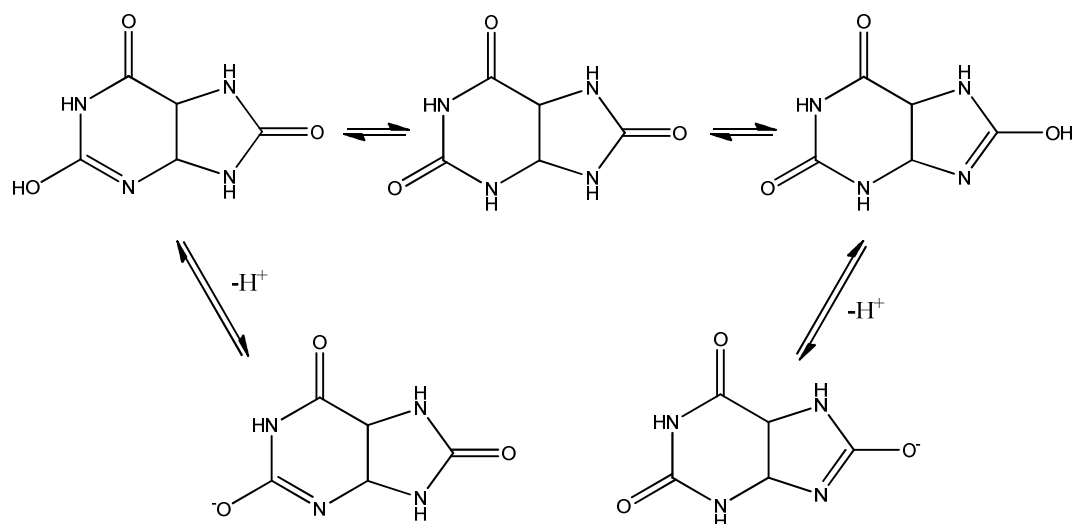
5.2.3 (ii) Uric Acid (UA)

Uric acid (UA) is the primary end product of purine metabolism in the body. Abnormal levels of UA are associated with several diseases such as gout, hyperuricemia, pneumonia, kidney damage, cardiovascular disease and Lesch-Nyhan syndrome^{11, 21}. UA can also interfere in the electrochemical detection of DA due to its electroactivity. UA is oxidised at most solid electrodes with $E_{1/2}$ values between 300 and 400 mV vs. SCE⁵¹. Consequently, the oxidation waves of UA and DA often overlap at conventional electrodes. This difficulty is made more significant by the fact that UA coexists with DA, in most natural samples, at concentrations 100-1000 times higher than that of DA⁷. As a result, UA is considered an important interferent in the electrochemical detection of DA.

Due to solubility issues, UA has a low solubility in water, the highest concentration of UA that could be studied was $1.0 \times 10^{-4} \text{ mol dm}^{-3}$. Figure 5.14 shows cyclic voltammograms of a bare Pt electrode in the presence and absence of UA. The oxidation of UA is evident from the higher currents recorded in the UA solution than in the solution containing no UA. Interestingly, it was found that UA could also be oxidised at the PPy-C4S film. The electrochemical response of UA at the PPy-C4S film is shown in Figure 5.15. A small oxidation peak was observed at 0.580 V vs. SCE. This can be seen more clearly in the inset of Figure 5.15. No corresponding reduction peak was observed. It is believed that this peak was due to the reaction shown in Equation 5.14⁵⁵.



In aqueous solution UA exhibits keto-enol tautomerism⁵⁶. Jiménez *et al.* studied the possible tautomers of UA and determined that the most abundant would be those presented in Scheme 5.3⁵⁶. Of these three, the triketone was shown to be the most stable. UA is known to have an acidic proton with a pK_a of approximately 5.4⁵⁶. Jiménez *et al.* found that the two most likely deprotonation sites were those shown in Scheme 5.3⁵⁶. Thus, according to Equation 5.13, at the pH of the experiment, pH 5.2, approximately 40% of the UA in solution would have been in the form of these anions. However, due to the same electrostatic repulsion that was outlined for AA, it was unlikely that the anionic UA would have been oxidised at the PPy-C4S film. Consequently, the oxidation peak observed was attributed to the oxidation of neutral UA, Equation 5.14. This was supported by the lack of any observable reduction peak. While this reaction is electrochemically reversible, Dryhurst *et al.* found that the oxidation product was unstable and was susceptible to rapid nucleophilic attack from water⁵⁵. Therefore, the oxidation of UA is often irreversible.



Scheme 5.3: Keto-enol tautomerism and deprotonation of UA⁵⁶.

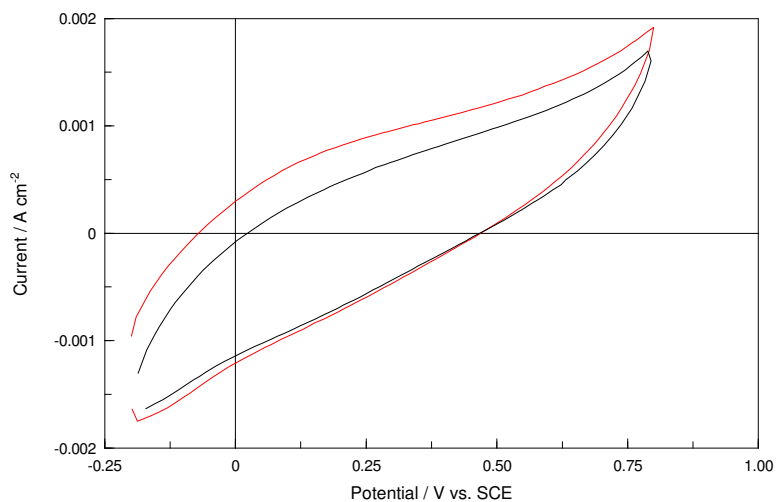


Figure 5.14: Cyclic voltammograms recorded in a 0.10 mol dm⁻³ Na₂SO₄ (—) and a 1.0 × 10⁻⁴ mol dm⁻³ UA / 0.10 mol dm⁻³ Na₂SO₄ solution (—) for a bare Pt electrode. The scan rate of the experiment was 100 mV s⁻¹.

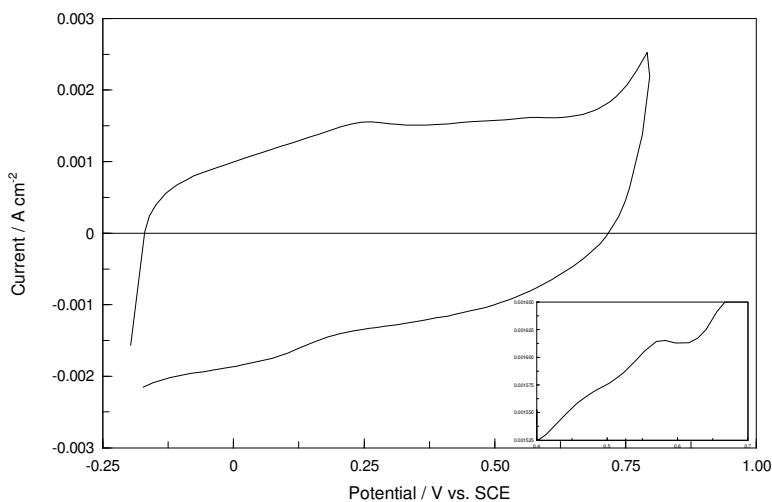


Figure 5.15: Cyclic voltammogram recorded in a $1.0 \times 10^{-4} \text{ mol dm}^{-3}$ UA / 0.10 mol dm^{-3} Na_2SO_4 solution for the PPy-C4S modified electrode. The inset shows the expanded potential region where UA was oxidized. The scan rate was 100 mV s^{-1} .

The influence of UA on the oxidation of DA at the PPy-C4S film was also investigated. The peak potentials for the oxidation of DA in the presence and absence of $1.0 \times 10^{-4} \text{ mol dm}^{-3}$ UA are compared in Figure 5.16. The presence of UA had no significant effect on the oxidation potential for DA. The peak currents for the oxidation of DA in the presence and absence of UA were also compared (Figure 5.17). It is clear that the DA signal was affected by the presence of UA. The DA oxidation currents were consistently lower when UA was present in solution with an average reduction of 14%. This indicated that UA could interfere, if only slightly, with the detection of DA at the PPy-C4S film. However, this interference was not due to overlap between the oxidation peaks for DA and UA. Figure 5.18 shows a cyclic voltammogram for the PPy-C4S electrode recorded in a solution containing $1.0 \times 10^{-4} \text{ mol dm}^{-3}$ DA and UA. It can be seen from the inset of Figure 5.18 that no significant overlap between the two peaks occurred. Therefore, it was proposed that the interference from UA was the result of an interaction between UA and the C4S incorporated within the PPy-C4S film. In this way, UA could have hindered the interaction of DA with the film, causing a reduction in the oxidation currents for DA.

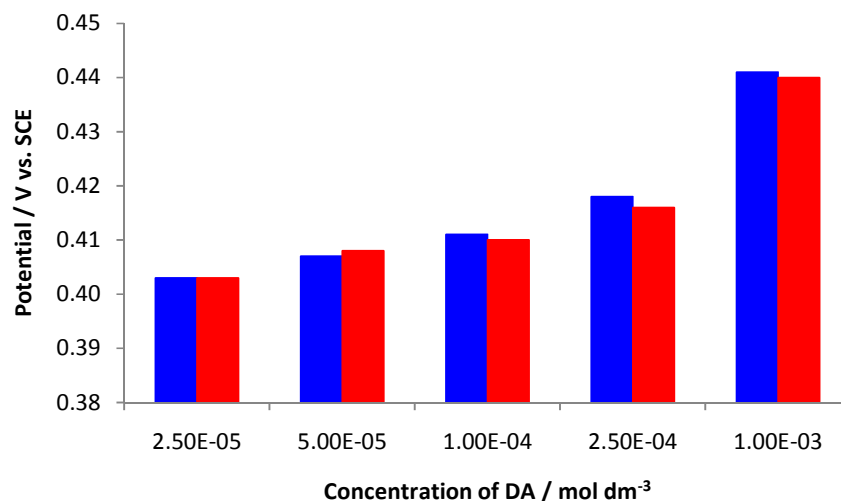


Figure 5.16: Peak oxidation potentials for a range of DA concentrations from 2.5×10^{-5} to 1.0×10^{-3} mol dm⁻³, obtained using cyclic voltammetry, in the absence ■ and presence ■ of 1.0×10^{-4} mol dm⁻³ UA in a 0.10 mol dm⁻³ Na₂SO₄ solution, pH ~5.2 (n = 3).

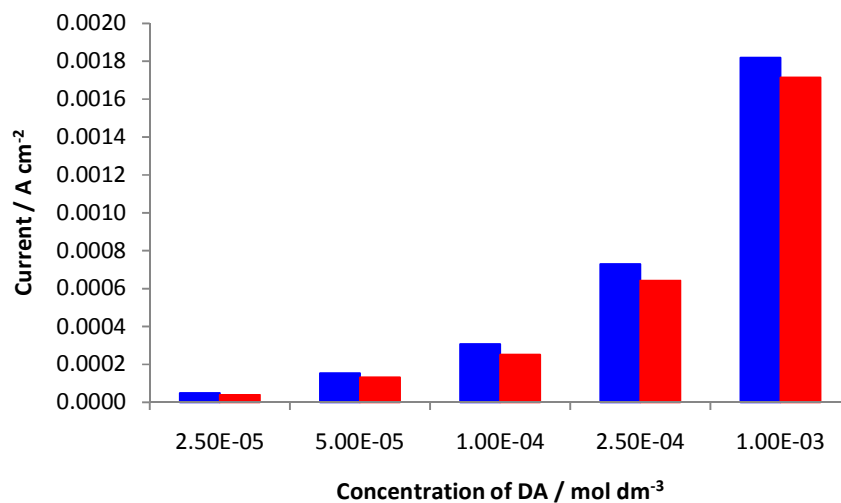


Figure 5.17: Peak oxidation currents for a range of DA concentrations from 2.5×10^{-5} to 1.0×10^{-3} mol dm⁻³, obtained using cyclic voltammetry, in the absence ■ and presence ■ of 1.0×10^{-4} mol dm⁻³ UA in a 0.10 mol dm⁻³ Na₂SO₄ solution, pH ~5.2 (n = 3). The currents shown have been corrected for background currents.

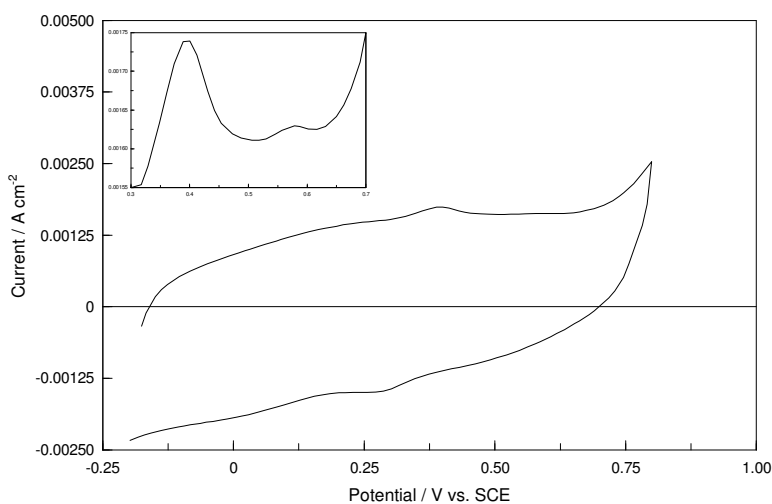


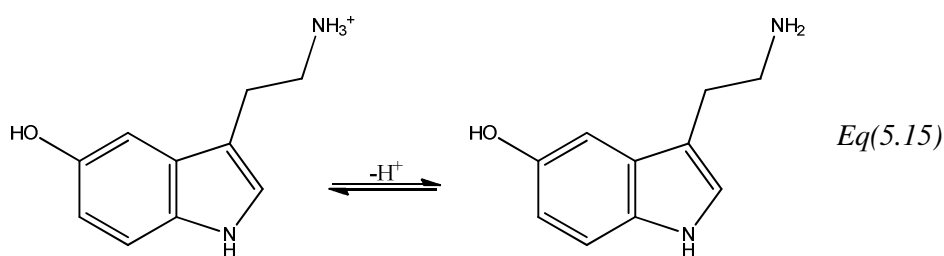
Figure 5.18: Cyclic voltammogram recorded in a 1.0×10^{-4} mol dm⁻³ DA / 1.0×10^{-4} mol dm⁻³ UA / 0.10 mol dm⁻³ Na₂SO₄ solution, pH 4.5, for the PPy-C4S modified electrode. The inset shows the expanded potential region where DA and UA were oxidised. The scan rate of the experiment was 100 mV s⁻¹.

To the best of our knowledge, there are no reports in the literature of UA being complexed by a calixarene. Indeed, given the hydrophilic nature of UA, due to the abundance of polar NH and carbonyl groups, the formation of an inclusion complex with C4S was unlikely. However, fluorescence spectroscopy would be required to prove this as UA does not contain any protons that are observable by NMR spectroscopy. Nevertheless, the fact that neutral UA was oxidised at the PPy-C4S film and could interfere with the detection of DA provided some insight into the mode of sensing of the film. If the selectivity of the sensor was simply due to electrostatic interactions then it would be reasonable to assume that the interaction of neutral UA and neutral AA with the film would be similar. Clearly, this was not the case. No electrochemical response or interference was observed for AA whereas, UA (most likely in its neutral form) was oxidised at the PPy-C4S film and could interfere with the detection of DA. These contrasting results suggest that the selectivity of the sensor was not simply a result of electrostatic attraction or repulsion but that other types of interactions were also important.

5.2.3 (iii) 5-Hydroxytryptamine (Serotonin, 5-HT)

5-Hydroxytryptamine (5-HT) acts as a neurotransmitter in the central nervous system (CNS). Among the roles of 5-HT are the regulation of body temperature, sleep, and certain emotional states^{19, 57}. In particular, 5-HT has been implicated in the development of mental illnesses such as schizophrenia and depression⁵⁷. 5-HT is also a major interfering compound in the electrochemical detection of DA. Like AA and UA, 5-HT coexists with DA in biological systems and is electroactive over a similar potential range to DA^{19, 58}. Accordingly, the accurate determination of DA at bare electrodes can be complicated by an overlapping voltammetric response for 5-HT. Moreover, 5-HT and DA have been shown to influence each other in their respective releases⁵⁸.

The electrochemical response of $1.0 \times 10^{-3} \text{ mol dm}^{-3}$ 5-HT at a bare Pt electrode is shown in Figure 5.19. It is clear from the voltammetric wave, at 0.550 V vs. SCE, that 5-HT was oxidized at the bare electrode. Figure 5.20 shows the electrochemical response of 5-HT at the PPy-C4S modified electrode. It is clear from the peak observed at 0.510 V vs. SCE (inset of Figure 5.20) that 5-HT was also oxidized at the PPy-C4S film. This was unsurprising as 5-HT has a pKa of 9.97⁵⁹. So, at the pH of these experiments (pH 4.5) 5-HT would have been predominantly cationic (Equation 5.15) and capable of interacting electrostatically with the PPy-C4S film.



According to Dryhurst *et al.*, the initial oxidation of 5-HT proceeds *via* the reversible process depicted in Equation 5.16^{57, 60}. They found that the radical species formed was unstable and rapidly reacted with 5-HT and water to form several monomeric and dimeric compounds. Therefore, the oxidation of 5-HT tends to be irreversible^{57, 60, 61}. This would account for the lack of a corresponding reduction wave for 5-HT at the PPy-C4S film.

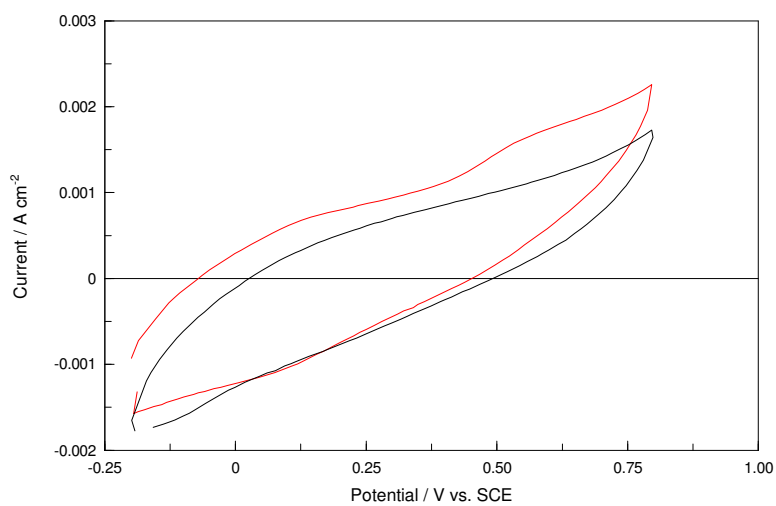
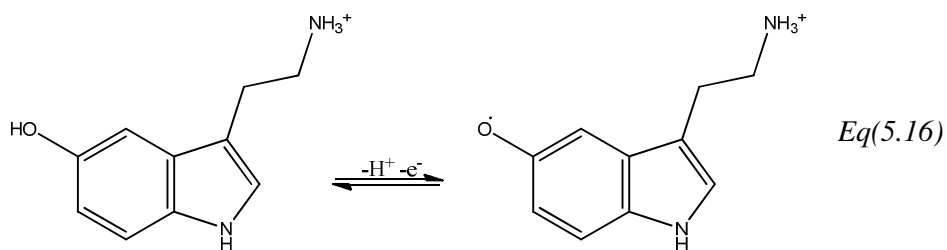


Figure 5.19: Cyclic voltammograms recorded in a $0.10 \text{ mol dm}^{-3} \text{ Na}_2\text{SO}_4$ (—) and a $1.0 \times 10^{-4} \text{ mol dm}^{-3} \text{ 5-HT} / 0.10 \text{ mol dm}^{-3} \text{ Na}_2\text{SO}_4$ (—) solution, pH ~ 4.5 , for a bare Pt electrode. The scan rate used was 100 mV s^{-1} .

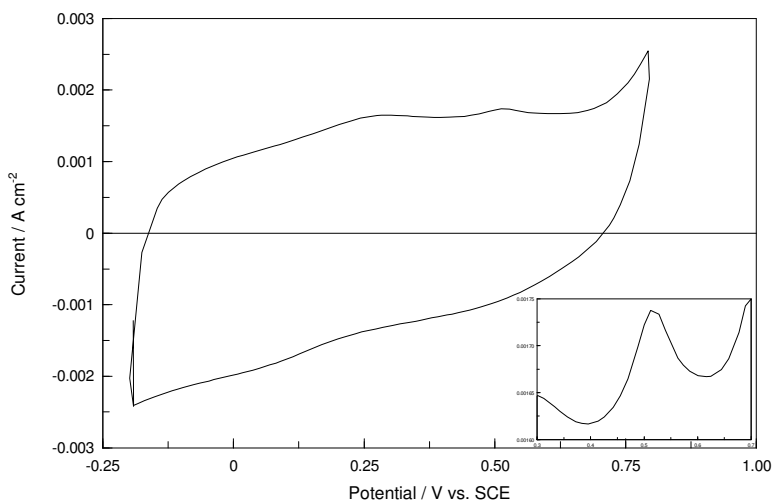


Figure 5.20: Cyclic voltammogram recorded in a $1.0 \times 10^{-3} \text{ mol dm}^{-3}$ 5-HT / 0.10 mol dm^{-3} Na_2SO_4 solution, pH ~4.5, for the PPy-C4S modified electrode. The inset shows the expanded potential region where 5-HT was oxidized. The scan rate used was 100 mV s^{-1} .

The ability of 5-HT to interfere with the detection of DA at the PPy-C4S film was also considered. In Figure 5.21, the peak potentials for the oxidation of DA in the presence and absence of $1.0 \times 10^{-3} \text{ mol dm}^{-3}$ 5-HT are compared. It can be seen from Figure 5.21, that the presence of 5-HT did not affect the potential at which DA was oxidised. On the other hand, there was a significant difference in the peak currents for the oxidation of DA. Figure 5.22 compares the peak currents for the oxidation of DA in the presence and absence of 5-HT. It was found that the currents recorded for the oxidation of DA were considerably lower for the solution containing 5-HT. In fact, the DA oxidation currents were reduced by an average of 60% when 5-HT was present in solution. As was the case for UA, overlapping voltammetric responses could not account for this interference. Figure 5.23 shows a cyclic voltammogram for the PPy-C4S electrode recorded in a solution containing $1.0 \times 10^{-4} \text{ mol dm}^{-3}$ DA and $1.0 \times 10^{-3} \text{ mol dm}^{-3}$ 5-HT. While there was some overlap between the two peaks, it was not significant enough to account for the substantial difference in the DA oxidation currents. Instead, it was more likely that this sizeable reduction in current was due to competition between 5-HT and DA to interact with C4S.

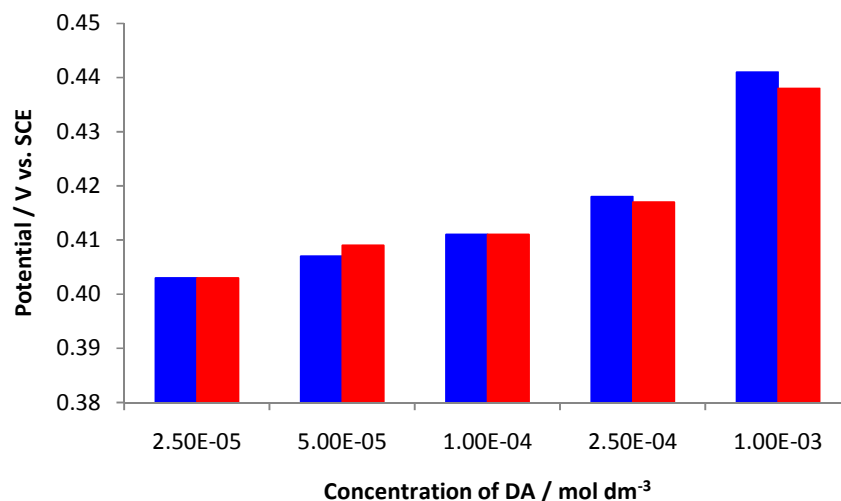


Figure 5.21: Peak oxidation potentials for a range of DA concentrations from 2.5×10^{-5} to 1.0×10^{-3} mol dm⁻³, obtained using cyclic voltammetry, in the absence ■ and presence ■ of 1.0×10^{-3} mol dm⁻³ 5-HT in a 0.10 mol dm⁻³ Na₂SO₄ solution, pH ~4.5 (n = 3).

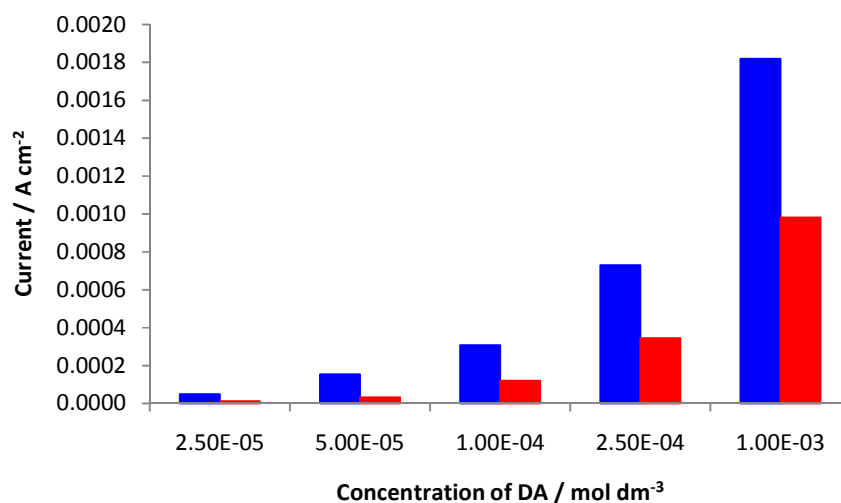


Figure 5.22: Peak oxidation currents for a range of DA concentrations from 2.5×10^{-5} to 1.0×10^{-3} mol dm⁻³, obtained using cyclic voltammetry, in the absence ■ and presence ■ of 1.0×10^{-3} mol dm⁻³ 5-HT in a 0.10 mol dm⁻³ Na₂SO₄ solution, pH ~4.5 (n = 3). The currents shown have been corrected for background currents.

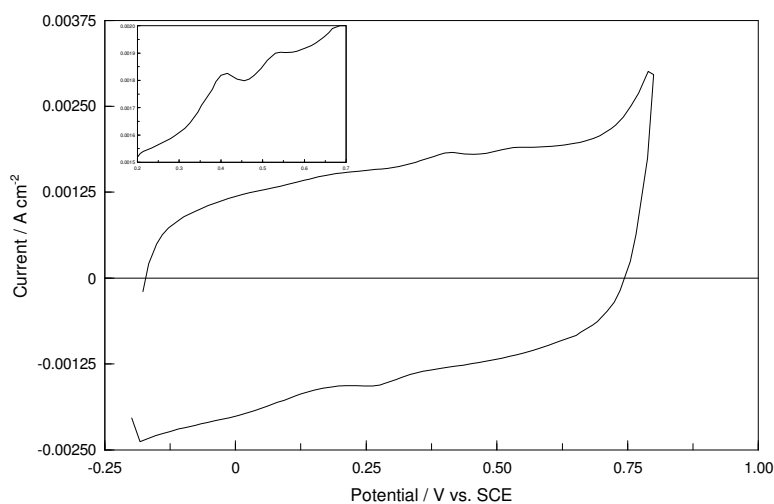


Figure 5.23: Cyclic voltammogram recorded in a $1.0 \times 10^{-4} \text{ mol dm}^{-3}$ DA / $1.0 \times 10^{-3} \text{ mol dm}^{-3}$ 5-HT / 0.10 mol dm^{-3} Na_2SO_4 solution, pH 4.5, for the PPY-C4S modified electrode. The inset shows the expanded potential region where DA and 5-HT were oxidised. The scan rate of the experiment was 100 mV s^{-1} .

By comparing the interference from 5-HT with that from UA it was clear that 5-HT was better able to interact with the PPy-C4S film. The presence of $1.0 \times 10^{-3} \text{ mol dm}^{-3}$ 5-HT in solution caused a 60% reduction in the oxidation currents for DA, whereas, these currents were reduced by only 14% in the presence of $1.0 \times 10^{-4} \text{ mol dm}^{-3}$ UA. Although it is likely that this difference can, to some degree, be accounted for by the higher concentration of 5-HT, there were also significant differences in the manner in which 5-HT and UA could interact with C4S. For a start, it was possible that the increased interference from cationic 5-HT was simply due to its electrostatic attraction to the negatively charged calixarene, an interaction that was not possible for the neutral UA. However, the results from the study of UA suggested that the selectivity of the sensor was not solely due to electrostatic contributions. So, in an effort to better account for this interference, the ability of 5-HT to form an inclusion complex with C4S was investigated. Figure 5.24 shows the ^1H NMR spectra obtained for 5-HT in the absence and presence of a two molar equivalent of C4S. Clearly, each 5-HT proton signal shifted upfield in the presence of C4S. The CH_2 groups of the aliphatic amine moiety, H_a and H_b , exhibited the largest change in chemical shift, $\Delta\delta \sim 0.6 \text{ ppm}$, followed closely by the

signal for H_c , $\Delta\delta \sim 0.5$ ppm, while the aromatic proton signals, H_d , H_e and H_f , were affected the least by the presence of C4S in solution, $\Delta\delta \sim 0.1$ ppm. The upfield shifts of these proton signals indicated that 5-HT could form an inclusion complex with C4S. Moreover, the relative magnitude of these shifts indicated that 5-HT was included into the calixarene cavity in the same way as DA, via its aliphatic amine moiety. Therefore, it was proposed that the substantial interference from 5-HT was due to its ability to compete with DA in terms of both electrostatic and inclusion interactions with the C4S incorporated within the PPy-C4S film.

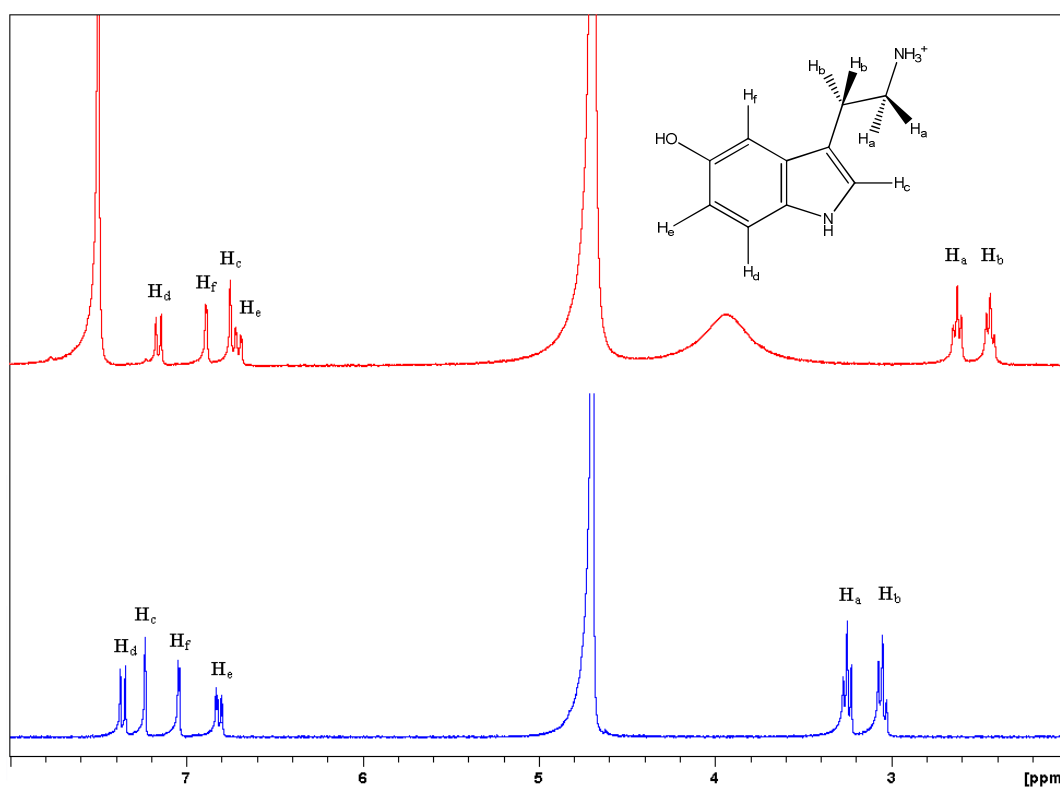


Figure 5.24: ^1H NMR spectra of 5-HT in the absence (—) and presence (—) of a two molar equivalent of C4S. The structure of DA is also shown with the appropriate protons labeled.

5.2.3 (iv) Acetylcholine (Ach)

Acetylcholine (Ach) is a neurotransmitter with roles in both the peripheral nervous system and the central nervous system^{62, 63}. In the peripheral nervous system, Ach is involved in muscle activation, in the central nervous system it participates in learning and memory formation, and the development and maintenance of addiction. Like AA, UA and 5-HT, Ach coexists with DA in the body and so could interfere with the detection of DA. However, unlike these compounds, Ach is not electroactive. This is illustrated clearly in Figure 5.25. No electrochemical response was observed at the bare Pt and PPy-C4S modified electrodes for a 1.0×10^{-3} mol dm⁻³ solution of Ach. Therefore, any interference from Ach in the electrochemical detection of DA could be directly attributed its interaction with the PPy-C4S film.

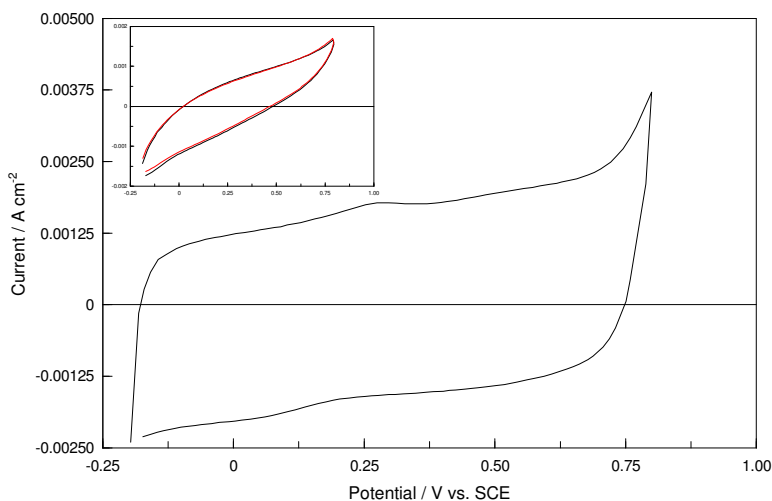


Figure 5.25: Cyclic voltammogram recorded in a 1.0×10^{-3} mol dm⁻³ Ach / 0.10 mol dm⁻³ Na₂SO₄ solution for the PPy-C4S modified electrode. The inset shows cyclic voltammograms recorded for a bare Pt electrode in the absence (—) and presence (—) of 1.0×10^{-3} mol dm⁻³ Ach.

Indeed, the potential for Ach to form such an interaction was the reason it was chosen for study in the first place. It can be seen from the structure of Ach shown in Figure 5.26 that Ach contains a quaternary ammonium group ($pK_a > 14$) and so remained positively charged at the experimental pH (pH 5.5). In this way, Ach could

be electrostatically attracted to the negatively charged calixarene. Equally, Ach could be included into the cavity of C4S. The formation of a strong inclusion complex between C4S and Ach, with a K_a value of approximately $3.2 \times 10^4 \text{ mol}^{-1}$, has been reported in the literature^{46, 49}. This complex was examined here using NMR spectroscopy. The ^1H NMR spectra obtained for Ach in the absence and presence of a two molar equivalent of C4S are shown in Figure 5.26. Each Ach proton signal shifted upfield in the presence of C4S confirming the inclusion of Ach into the cavity of C4S. The mode of inclusion was also deduced from the relative magnitude of these shifts. The methyl groups of the quaternary ammonium moiety, labeled $\text{N}(\text{CH}_3)_3$, exhibited the largest change in chemical shift, $\Delta\delta \sim 2.0 \text{ ppm}$, indicating that this group experienced the greatest shielding effect from the calixarene aromatic π -system. These results are consistent with reports that the quaternary ammonium group of Ach inserts into the cavity of C4S. For these reasons, Ach was expected to compete with the interaction of DA at the PPy-C4S film. Therefore, based on the results obtained for 5-HT, Ach should interfere significantly with the detection of DA.

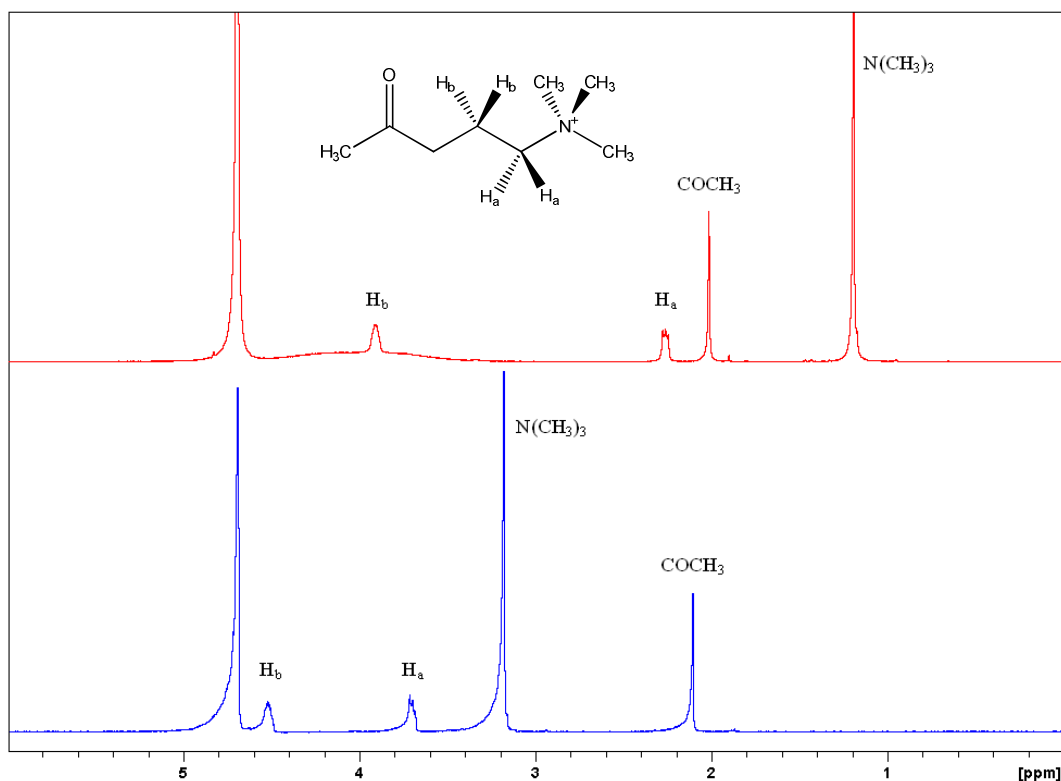


Figure 5.26: ^1H NMR spectra of Ach in the absence (—) and presence (—) of a two molar equivalent of C4S. The structure of DA is also shown with the appropriate protons labeled.

With this in mind, the effect of Ach on the electrochemical detection of DA was investigated at the PPy-C4S electrode. The peak potentials for the oxidation of DA in the presence and absence of $1.0 \times 10^{-3} \text{ mol dm}^{-3}$ Ach are compared in Figure 5.27. Clearly, the presence of Ach had no significant effect on the oxidation potentials for DA. In contrast, the peak currents for the oxidation of DA were altered considerably when Ach was present in solution. Figure 5.28 compares the peak currents for the oxidation of DA in the presence and absence of Ach. The oxidation currents for DA were considerably lower for the solution containing Ach, with an average reduction in current of 48%. These results confirm the idea that significant interference is observed for compounds that can compete with the interaction of DA at the PPy-C4S film.

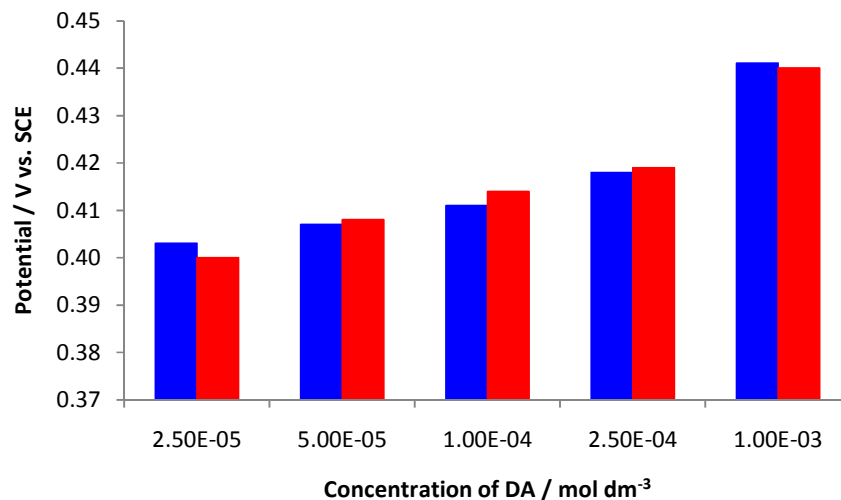


Figure 5.27: Peak oxidation potentials for a range of DA concentrations from 2.5×10^{-5} to $1.0 \times 10^{-3} \text{ mol dm}^{-3}$, obtained using cyclic voltammetry, in the absence ■ and presence ■ of $1.0 \times 10^{-3} \text{ mol dm}^{-3}$ Ach in a $0.10 \text{ mol dm}^{-3} \text{ Na}_2\text{SO}_4$ solution, pH ~5.5 (n = 3).

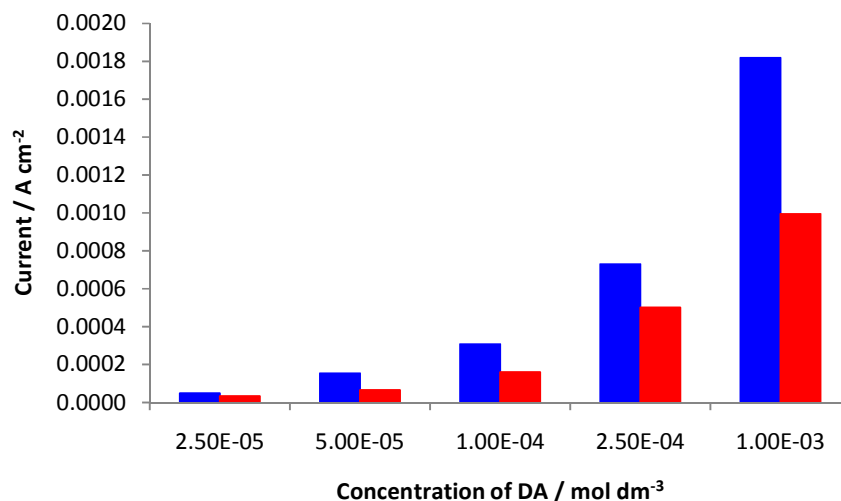


Figure 5.28: Peak oxidation currents for a range of DA concentrations from 2.5×10^{-5} to 1.0×10^{-3} mol dm⁻³, obtained using cyclic voltammetry, in the absence ■ and presence ■ of 1.0×10^{-3} mol dm⁻³ Ach in a 0.10 mol dm⁻³ Na₂SO₄ solution, pH ~5.4 (n = 3). The currents shown have been corrected for background currents.

At this stage it is helpful to compare the selectivity of the PPy-C4S modified electrode with the PPy-SCD modified electrode studied previously in our laboratory³. In studying the selectivity of PPy-SCD film towards DA it was observed that 5-HT was only a very weak interferent in the electrochemical detection of DA and that Ach did not interfere at all³. Conversely, both of these compounds are significant interferents in the detection of DA at the PPy-C4S film. From this observation, the mode of sensing of the PPy-C4S film can be inferred. If the interaction of DA with both of these polymers was based solely on electrostatic attraction then their selectivity should have been similar. Since this clearly was not the case, it is probable that inclusion of DA into C4S was a significant factor in the mode of sensing of the PPy-C4S film. Consequently, the fact that 5-HT and Ach could both form inclusion complexes with C4S can account for the significant interference observed for these compounds.

However, this mode of interaction does not explain the difference in the level of interference from these compounds. 5-HT was found to be the greater interferent, reducing the DA oxidation currents by 60% compared to the 48% reduction recorded for Ach. Yet, the relative magnitudes of the NMR chemical shift changes for 5-HT and Ach suggest that Ach formed the stronger inclusion complex with C4S. The

proton signals for the Ach quaternary amine methyl groups ($\text{N}(\text{CH}_3)_3$) were found to shift by approximately 2.0 ppm, while, the change in shift for the CH_2 protons of 5-HT was just 0.6 ppm. Considering only inclusion components, Ach should have been the more significant interferent. That said, it is unlikely that all the C4S present in the PPy-C4S film would have been capable of forming inclusion complexes. It is more probable that some proportion of DA would also interact with the lower rim of C4S. This could occur through hydrogen bonding between the DA ammonium moiety and the oxide anion on the lower rim of C4S. It is by considering this hydrogen bonding interaction that the difference in the level of interference from 5-HT and Ach can be rationalized. Hydrogen bonding interactions could also occur between the ammonium moiety of 5-HT and the lower rim of C4S, but no such interaction would be possible for the quaternary ammonium of Ach. Thus, two modes of interference exist for 5-HT, inclusion and hydrogen bonding, whereas Ach can only interfere with the interaction of DA at the PPy-C4S film through inclusion. So, even though Ach forms the stronger inclusion complex with C4S, 5-HT is the more significant interferent.

5.3 Conclusion

At the beginning of this chapter, it was proposed that the interaction of DA at the PPy-C4S film was specific to C4S. The superior ability of the PPy-C4S film to sense DA, in comparison to the PPy-SO₄ and PPy-SDS films, indicated that the calixarene played an important role in the sensing of DA. This was supported by the fact that DA was found to adsorb to the polymer film. Moreover, changing the charge on the C4S incorporated within the PPy-C4S film was shown to have a significant effect on this adsorption interaction.

Building on this, the complex formed between DA and C4S in solution was studied using NMR spectroscopy. It was shown that DA could be included into the cavity of C4S through its ammonium moiety. The possible formation of such an inclusion complex within the PPy-C4S film could explain the weaker adsorption of DA observed at low pH. This was accounted for by the fact that the π -system of C4S would be less electron rich when its lower rim was protonated, reducing the strength of the cation- π interaction with the protonated amine of DA. Thus, it was proposed that inclusion was a significant contributor to the mode of sensing of the PPy-C4S modified electrode.

This hypothesis was further substantiated by studies on the selectivity of the sensor. Using cyclic voltammetry, it was found that compounds with the potential to be included into C4S (5-HT and Ach) were significant interferents in the electrochemical detection of DA, whereas compounds with little or no affinity for C4S interfered to a lesser extent (UA) or did not cause any interference (AA). These studies also highlighted the contribution of other types of interactions to the mode of sensing. Using NMR spectroscopy it was shown that Ach formed the strongest inclusion complex with C4S. However, 5-HT was the most significant interferent. This was attributed to the fact that 5-HT could also form hydrogen bonds with the lower rim of C4S, whereas Ach could not. In spite of this, Ach was still a significant interferent in the electrochemical detection of DA, implying that inclusion played an important role in the mode of sensing of the PPy-C4S modified electrode.

Finally, the results of these studies showed that the PPy-C4S modified electrode was highly selective towards DA in the presence of AA, suffering none of the fouling or

catalytic effects observed at bare electrodes. In addition, the low level of interference caused by UA, especially considering that the concentration of UA studied here was higher than most biological concentrations, suggested that the PPy-C4S modified electrode could also be useful for the detection of DA in the presence of UA.

5.4 Bibliography

- (1) Jo, S.; Jeong, H.; Bae, S. R.; Jeon, S. *Microchem. J.* **2008**, *88*, 1-6.
- (2) Ali, S. R.; Parajuli, R. R.; Balogun, Y.; Ma, Y.; He, H. *Sensors* **2008**, *8*, 8423-8452.
- (3) Harley, C. C., PhD Thesis, NUI Maynooth, 2009.
- (4) Henstridge, M. C.; Dickinson, E. J. F.; Aslanoglu, M.; Batchelor-McAuley, C.; Compton, R. G. *Sensors and Actuators B: Chemical* **2010**, *145*, 417-427.
- (5) Hosseinzadeh, R.; Sabzi, R. E.; Ghasemlu, K. *Colloids Surf., B* **2009**, *68*, 213-217.
- (6) Hou, S.; Zheng, N.; Feng, H.; Li, X.; Yuan, Z. *Anal. Biochem.* **2008**, *381*, 179-184.
- (7) Huang, J.; Liu, Y.; Hou, H.; You, T. *Biosens. Bioelectron.* **2008**, *24*, 632-637.
- (8) Ke, N. J.; Lu, S.-S.; Cheng, S.-H. *Electrochem. Commun.* **2006**, *8*, 1514-1520.
- (9) Keeley, G. P.; Lyons, M. E. G. *Int. J. Electrochem. Sci.* **2009**, *4*, 794-809.
- (10) Lai, G.-S.; Zhang, H.-L.; Han, D.-Y. *Microchim. Acta* **2008**, *160*, 233-239.
- (11) Lin, X.; Zhang, Y.; Chen, W.; Wu, P. *Sensors and Actuators B: Chemical* **2007**, *122*, 309-314.
- (12) Majewska, U. E.; Chmurski, K.; Biesiada, K.; Olszyna, A. R.; Bilewicz, R. *Electroanalysis* **2006**, *18*, 1463-1470.
- (13) Nikolelis, D. P.; Petropoulou, S.-S. E.; Pergel, E.; Toth, K. *Electroanalysis* **2002**, *14*, 783-789.
- (14) Raoof, J.-B.; Ojani, R.; Rashid-Nadimi, S. *Electrochim. Acta* **2005**, *50*, 4694-4698.
- (15) Rubianes, M. D.; Rivas, G. A. *Anal. Chim. Acta* **2001**, *440*, 99-108.
- (16) Song, S.; Gao, Q.; Xia, K.; Gao, L. *Electroanalysis* **2008**, *20*, 1159-1166.
- (17) Wang, J.; Wang, Y.; Lv, H.; Hui, F.; Ma, Y.; Lu, S.; Sha, Q.; Wang, E. *J. Electroanal. Chem.* **2006**, *594*, 59-64.
- (18) Wang, Q.; Dong, D.; Li, N. *Bioelectrochemistry* **2001**, *54*, 169-175.
- (19) Wu, K.; Fei, J.; Hu, S. *Anal. Biochem.* **2003**, *318*, 100-106.
- (20) Zhang, H.-M.; Li, N.-Q.; Zhu, Z. *Microchem. J.* **2000**, *64*, 277-282.

- (21) Zhang, R.; Jin, G.-D.; Chen, D.; Hu, X.-Y. *Sensors and Actuators B: Chemical* **2009**, *138*, 174-181.
- (22) Zhang, Y.; Jin, G.; Wang, Y.; Yang, Z. *Sensors* **2003**, *3*, 443-450.
- (23) Zhao, H.; Zhang, Y.; Yuan, Z. *Anal. Chim. Acta* **2001**, *441*, 117-122.
- (24) Zheng, J.; Zhou, X. *Bioelectrochemistry* **2007**, *70*, 408-415.
- (25) Zhou, Y. Z.; Zhang, L. J.; Chen, S. L.; Dong, S. Y.; Zheng, X. H. *Chin. Chem. Lett.* **2009**, *20*, 217-220.
- (26) Harley, C. C.; Rooney, A. D.; Breslin, C. B. *Sensors and Actuators B: Chemical, In Press*.
- (27) Wang, X.; Yang, N.; Wan, Q.; Wang, X. *Sensors and Actuators B: Chemical* **2007**, *128*, 83-90.
- (28) Guo, D.-S.; Wang, K.; Liu, Y. *J. Inclusion Phenom. Macrocyclic Chem.* **2008**, *62*, 1-21.
- (29) Shinkai, S.; Araki, K.; Kubota, M.; Arimura, T.; Matsuda, T. *J. Org. Chem.* **1991**, *56*, 295-300.
- (30) Shinkai, S. *Tetrahedron* **1993**, *49*, 8933-8968.
- (31) Zhou, Y.; Liu, C.; Yu, H.; Xu, H.; Lu, Q.; Wang, L. *Spectrosc. Lett.* **2006**, *39*, 409-420.
- (32) Gal, Y.-S.; Lee, W.-C.; Lyoo, W. S.; Jin, S.-H.; Lim, K. T.; Park, Y.-I.; Park, J.-W. *Int. J. Photoenergy* **2008**, No pp. given.
- (33) Kim, Y.; Kwon, Y.; Lee, K.; Park, J.; Seo, H.; Kim, T. *Mol. Cryst. Liq. Cryst.* **2004**, *424*, 153-158.
- (34) Ko, J. M.; Rhee, H. W.; Park, S. M.; Kim, C. Y. *J. Electrochem. Soc.* **1990**, *137*, 905-909.
- (35) Streeter, I.; Wildgoose, G. G.; Shao, L.; Compton, R. G. *Sensors and Actuators B: Chemical* **2008**, *133*, 462-466.
- (36) Arena, G.; Cali, R.; Lombardo, G. G.; Rizzarelli, E.; Sciotto, D.; Ungaro, R.; Casnati, A. *Supramol. Chem.* **1992**, *1*, 19-24.
- (37) Suga, K.; Ohzono, T.; Negishi, M.; Deuchi, K.; Morita, Y. *Supramol. Sci.* **1998**, *5*, 9-14.
- (38) Yoshida, I.; Yamamoto, N.; Sagara, F.; Ishii, D.; Ueno, K.; Shinkai, S. *Bull. Chem. Soc. Jpn.* **1992**, *65*, 1012-1015.
- (39) Shinkai, S.; Araki, K.; Matsuda, T.; Nishiyama, N.; Ikeda, H.; Takasu, I.; Iwamoto, M. *J. Am. Chem. Soc.* **1990**, *112*, 9053-9058.

- (40) Ma, J. C.; Dougherty, D. A. *Chem. Rev. (Washington, D. C.)* **1997**, *97*, 1303-1324.
- (41) Macomber, R. S. *J. Chem. Educ.* **1992**, *69*, 375-378.
- (42) Fielding, L. *Tetrahedron* **2000**, *56*, 6151-6170.
- (43) Tsukube, H.; Furuta, H.; Odani, A.; Takeda, Y.; Kudo, Y.; Inoue, Y.; Liu, Y.; Sakamoto, H.; Kimura, K. 1996; Elsevier; 425-482.
- (44) McDermott, S., NUI Maynooth, 2010.
- (45) Arena, G.; Casnati, A.; Contino, A.; Magri, A.; Sansone, F.; Sciotto, D.; Ungaro, R. *Org. Biomol. Chem.* **2006**, *4*, 243-249.
- (46) Lehn, J.-M.; Meric, R.; Vigneron, J.-P.; Cesario, M.; Guilhem, J.; Pascard, C.; Asfari, Z.; Vicens, J. *Supramol. Chem.* **1995**, *5*, 97-103.
- (47) Claridge, T.; Editor *High-Resolution NMR Techniques in Organic Chemistry*; Pergamon, 2000.
- (48) Neuhaus, D.; Williamson, M. P. *The Nuclear Overhauser Effect in Structural and Conformational Analysis, Second Edition*; Wiley-VCH, 2000.
- (49) Wang, L.-H.; Guo, D.-S.; Chen, Y.; Liu, Y. *Thermochim. Acta* **2006**, *443*, 132-135.
- (50) Bidan, G.; Niel, M.-A. *Synth. Met.* **1997**, *85*, 1387-1388.
- (51) Lowry, J. P.; O'Neill, R. D. 2006; American Scientific Publishers; 501-523.
- (52) Zhang, L.; Jiang, X. *J. Electroanal. Chem.* **2005**, *583*, 292-299.
- (53) Habermueller, K.; Reiter, S.; Buck, H.; Meier, T.; Staepels, J.; Schuhmann, W. *Microchim. Acta* **2003**, *143*, 113-121.
- (54) Khan, G. F.; Kobatake, E.; Shinohara, H.; Ikariyama, Y.; Aizawa, M. *J. Am. Chem. Soc.* **1996**, *118*, 1824-1830.
- (55) Dryhurst, G. *Bioelectrochem. Bioenerg.* **1985**, *14*, 251-274.
- (56) Jimenez, V.; Alderete, J. B. *J. Mol. Struct.: THEOCHEM* **2005**, *755*, 209-214.
- (57) Dryhurst, G. *Chem. Rev.* **1990**, *90*, 795-811.
- (58) Li, J.; Lin, X. *Sensors and Actuators B: Chemical* **2007**, *124*, 486-493.
- (59) Pratuangdejkul, J.; Nosoongnoen, W.; Guérin, G.-A.; Loric, S.; Conti, M.; Launay, J.-M.; Manivet, P. *Chemical Physics Letters* **2006**, *420*, 538-544.
- (60) Wrona, M. Z.; Dryhurst, G. *J. Org. Chem.* **1987**, *52*, 2817-2825.
- (61) Sarada, B. V.; Rao, T. N.; Tryk, D. A.; Fujishima, A. *Anal. Chem.* **2000**, *72*, 1632-1638.

- (62) Lin, S.; Liu, C.-C.; Chou, T.-C. *Biosensors and Bioelectronics* **2004**, *20*, 9-14.
- (63) Yang, M.; Yang, Y.; Yang, Y.; Shen, G.; Yu, R. *Analytica Chimica Acta* **2005**, *530*, 205-211.

CHAPTER 6

Conclusions

6.1 Conclusions

In this work, a *p*-sulfonatocalix[4]arene (C4S) doped polypyrrole (PPy-C4S) modified electrode was characterized and applied as an electrochemical sensor for dopamine (DA). The sensitivity and selectivity of this sensor were investigated and the mode in which the PPy-C4S modified electrode could detect DA was explored.

The PPy-C4S film was fabricated on a platinum (Pt) electrode from a solution of pyrrole and *p*-sulfonatocalix[4]arene using a potentiostatic mode of electropolymerisation. In general, an oxidation potential of 0.500 V vs. SCE was applied to the Pt electrode until a charge of 0.24 C cm⁻² was consumed. EDX analysis performed on the resulting PPy-C4S film showed a characteristic peak for sulphur ($K_{\alpha} = 2.3075$ keV), indicating that C4S had been successfully incorporated into the PPy matrix. This analysis also showed that the film was doped solely by the calixarene. The C4S used to prepare the PPy-C4S films contained some Ca²⁺ ions, which are known to form a strong outer sphere complex with C4S¹. However, the EDX spectra contained no peaks for Ca²⁺ ($K_{\alpha} = 2.3075$ keV) suggesting that these ions were not incorporated into the film with the calixarene.

SEM images were recorded for PPy-C4S films electropolymerised at two different potentials, 0.500 V and 0.800 V vs. SCE. The images for these films exhibited the typical 'cauliflower' morphology widely observed for PPy films². However, the film grown at 0.800 V vs. SCE was noticeably rougher than the film grown at the lower potential. This was in agreement with literature reports that the surface roughness of PPy films increases with increasing applied potential³⁻⁵. The thickness of the PPy-C4S film was measured using a Tencor profilometer. While reproducible thickness measurements proved difficult to obtain, a definite relationship between the film thickness and the charge consumed during the growth of the film was observed. The thickness of the PPy-C4S film increased as the charge was increased. This was consistent with literature reports^{6, 7}. These results indicated that the PPy-C4S film was deposited on the electrode surface in a manner that was typical of PPy films.

The redox properties of the PPy-C4S film were investigated using cyclic voltammetry. The oxidation of PPy was observed at -0.214 V vs. SCE and the

corresponding reduction of the film occurred at -0.455 V vs. SCE. The relative shape of these voltammetric waves suggested that the PPy-C4S film could act as a cation exchange polymer. The reduction wave was plainly sharper in appearance than the oxidation wave, indicating that this process was accompanied by an influx of high mobility Na^+ cations from the electrolyte solution rather than the expulsion of the bulky C4S anions. EIS studies on the charge transport processes occurring in the PPy-C4S film supported this deduction. The ionic resistance (R_{ion}) of the film was measured over a range of potentials and was found to decrease as the potential became more reducing. Ren and Pickup^{8,9} reported similar behaviour for the cation exchange polymer, PPy-polystyrenesulfonate. They attributed the observed decrease in R_{ion} to the influx of mobile cations associated with the reduction of the film. The electronic resistance (R_e) of the PPy-C4S film was negligible, in accordance with the high electronic conductivity of oxidised PPy films^{8, 10-12}, and only became apparent when the film was highly reduced.

The capacitance of the PPy-C4S film was measured using cyclic voltammetry and EIS. The results obtained from these techniques were in agreement and suggested that the capacitance of the PPy-C4S film arose from the charge separation between the positively charged PPy backbone and the anionic C4S. Using cyclic voltammetry, the capacitance was found to increase with film thickness, *i.e.* with increasing quantities of PPy and C4S. The EIS measurements were obtained over a range of potentials and the capacitance was observed to increase with potential, reaching a maximum near the peak oxidation potential of the film. The specific values determined for the capacitance of the fully oxidised film were 9.4 and 10.4 mF cm^{-2} using cyclic voltammetry and EIS, respectively. These values were typical of the high charge storage capacity expected for PPy films¹³⁻¹⁷.

However, not all of the electrochemical properties of the PPy-C4S film were typical. The presence of C4S in the film was found to bestow novel electrochemical activity on the PPy-C4S film. Cyclic voltammetry revealed a second redox couple, centred at 0.230 V vs. SCE, which was not associated with the electrochemistry of PPy. This novel electrochemical activity was attributed to the oxidation and reduction of a calixquinone. Calixquinones could be generated within the PPy-C4S film at potentials sufficient to oxidise C4S. The oxidation product of C4S was susceptible to nucleophilic attack from water, resulting in the formation of a calixquinone¹⁸⁻²¹. This

novel electrochemistry was characteristic of the PPy-C4S film and provided further proof that C4S had been successfully incorporated into the PPy matrix.

The ability of the PPy-C4S modified electrode to sense DA was examined using cyclic voltammetry. While it was found that DA could indeed be oxidised at the modified electrode the generation of the calixquinone proved to be problematic. The oxidation peak for the calixquinone overlapped with the oxidation peak for DA. Moreover, excessive production of the calixquinone destabilised the PPy-C4S film. This was most likely due the generation of radicals within the polymer that could react with the PPy chains. Therefore, optimising the PPy-C4S film for the electrochemical detection of DA involved a compromise between the experimental parameters that would maximise the oxidation current for DA and those that would minimise the generation of the calixquinone. The optimised PPy-C4S modified electrode was then calibrated for the detection of DA using cyclic voltammetry and constant potential amperometry. The limits of detection were determined as 2.50×10^{-5} and 4.11×10^{-6} mol dm⁻³ DA, respectively.

Unfortunately, doping the PPy film with C4S did not result in the increased sensitivity that we had aimed for. The amperometric detection limit for the sulfonated β -cyclodextrin based sensor studied previously in our laboratory²² was 3.36×10^{-6} mol dm⁻³. However, the results for the PPy-C4S modified electrode were still promising. Constant potential amperometry not only improved the sensitivity of the sensor, compared with cyclic voltammetry, but its performance in general. The lower potential used in the amperometry experiments (0.650 V vs. SCE) minimised the generation of the calixquinone. Consequently, the amperometric detection of DA was significantly more reproducible than the detection of DA using cyclic voltammetry.

An interesting observation to come out of the sensor optimisation experiments was that DA could interact specifically with the C4S incorporated within the PPy-C4S film. By comparison with PPy films doped with other anions²³, such as sulfate and dodecylsulfate anions, the PPy-C4S modified electrode was shown to produce significantly larger currents for the oxidation of DA. This superior performance by the PPy-C4S film indicated that the calixarene played an important role in the sensing of DA. This was supported by the fact that DA was found to adsorb to the

polymer film. Moreover, protonating the lower rim of the C4S incorporated within the PPy-C4S film was found to weaken the adsorption of DA to the film.

These findings prompted a more in depth study of the interaction between DA and C4S. Two approaches were taken: the strength of the interaction and the structure of the complex formed between DA and C4S in solution were investigated using NMR spectroscopy, and the selectivity of the PPy-C4S modified electrode towards DA in the presence of different potential interferents was explored. The NMR spectroscopic studies indicated that the inclusion of DA into C4S occurred *via* its ammonium cation. The driving force for the formation of this complex was attributed to cation- π interactions with the π -system of C4S^{24, 25}. This mode of inclusion provided a possible explanation for the weaker adsorption of DA at low pH. Protonating the oxide anion on the lower rim of C4S reduces the electron richness of the π -system. Thus, at low pH where the lower rim would be fully protonated, the cation- π interactions would be weaker. Consequently, it was proposed that the mode of sensing of the PPy-C4S modified electrode involved the inclusion of DA into the C4S incorporated within the film.

The chosen interferent compounds for the selectivity studies were ascorbic acid (AA), uric acid (UA), 5-hydroxytryptamine (5-HT) and acetylcholine (Ach). It was found that compounds with the potential to be included into C4S (5-HT and Ach) were significant interferents in the electrochemical detection of DA, whereas compounds with little or no affinity for C4S interfered to a lesser extent (UA) or did not cause any interference (AA). These findings indicated that inclusion interactions were certainly important for the mode of sensing of the PPy-C4S modified electrode. However, these studies also highlighted the contribution of other types of interactions to the mode of sensing. ¹H NMR spectra recorded for 5-HT and Ach in the presence and absence of C4S implied that Ach formed the strongest inclusion complex with C4S. Yet, 5-HT was the most significant interferent. This anomaly was rationalized in the following terms. The incorporation of C4S into the PPy film is likely to leave some of the cavities inaccessible. In this situation, primary ammonium cations, such as DA and 5-HT, would retain the ability to interact with C4S by forming hydrogen-bonds with its lower rim. In contrast, this mode of interaction is not open to Ach as it does not contain any polar hydrogen atoms. Therefore, 5-HT can compete with DA for two sites of interaction with C4S whereas

Ach can only compete for one site of interaction. In spite of this, Ach was still a significant interferent in the electrochemical detection of DA, implying that the contribution of inclusion interactions to the mode of sensing of the PPy-C4S modified electrode was considerable.

In summary, the incorporation of C4S into PPy produced a film with cation exchange properties, high charge storage capacity and good electrical conductivity. Interestingly, the cyclic voltammetric profile of the PPy-C4S film is characterized by a calixquinone redox couple which only becomes apparent if a potential of 0.700 V vs. SCE is exceeded. The PPy-C4S modified electrode demonstrated good sensitivity for the electrochemical detection of DA. Moreover, the easy assembly and excellent reproducibility of this sensor make it worthy of further study. In addition, The PPy-C4S modified electrode is highly selective towards DA in the presence of AA, suffering none of the fouling or catalytic effects observed at bare electrodes. Finally, the mode in which the PPy-C4S modified electrode can detect DA is due to a combination of interactions, the most influential being inclusion complexation.

6.2 Bibliography

- (1) Guo, D.-S.; Wang, K.; Liu, Y. *J. Inclusion Phenom. Macrocyclic Chem.* **2008**, *62*, 1-21.
- (2) Wallace, G. G.; Spinks, G. M.; Kane-Maguire, L. A. P. *Conductive Electroactive Polymers: Intelligent Materials Systems, Second Edition*; CRC Press, **2002**.
- (3) Ingram, M. D.; Staesche, H.; Ryder, K. S. *Solid State Ionics* **2004**, *169*, 51-57.
- (4) Reyes, D. C. J. I.; Cavalieri, R. P.; Powers, J. R. *Synth. Met.* **2004**, *142*, 71-79.
- (5) Zhu, R. L.; Li, G. X.; Zheng, J. H.; Jiang, J. W.; Zeng, H. B. *Surf. Eng.* **2009**, *25*, 156-162.
- (6) Diaz, A. F.; Castillo, J. I.; Logan, J. A.; Lee, W. Y. *J. Electroanal. Chem. Interfacial Electrochem.* **1981**, *129*, 115-132.
- (7) Fonner, J. M.; Forciniti, L.; Nguyen, H.; Byrne, J. D.; Kou, Y.-F.; Syeda-Nawaz, J.; Schmidt, C. E. *Biomed Mater* **2008**, *3*, 034124.
- (8) Ren, X.; Pickup, P. G. *J. Phys. Chem.* **1993**, *97*, 5356-5362.
- (9) Ren, X.; Pickup, P. G. *Electrochim. Acta* **1996**, *41*, 1877-1882.
- (10) Mao, H.; Pickup, P. G. *J. Am. Chem. Soc.* **1990**, *112*, 1776-1782.
- (11) Ren, X.; Pickup, P. G. *J. Electrochem. Soc.* **1992**, *139*, 2097-2105.
- (12) Ren, X.; Pickup, P. G. *Journal of Electroanalytical Chemistry* **1997**, *420*, 251-257.
- (13) Bull, R. A.; Fan, F. R. F.; Bard, A. J. *J. Electrochem. Soc.* **1982**, *129*, 1009-1015.
- (14) Duffitt, G. L.; Pickup, P. G. *J. Chem. Soc., Faraday Trans.* **1992**, *88*, 1417-1423.
- (15) Ko, J. M.; Rhee, H. W.; Park, S. M.; Kim, C. Y. *J. Electrochem. Soc.* **1990**, *137*, 905-909.
- (16) Tanguy, J.; Mermilliod, N.; Hoclet, M. *J. Electrochem. Soc.* **1987**, *134*, 795-802.
- (17) Yeu, T.; Yin, K. M.; Carbajal, J.; White, R. E. *J. Electrochem. Soc.* **1991**, *138*, 2869-2877.

- (18) Louati, A.; Spraula, J.; Gabelica, V.; Kuhn, P.; Matt, D. *Electrochem. Commun.* **2006**, *8*, 761-766.
- (19) Ronlan, A.; Parker, V. D. *J. Chem. Soc. C* **1971**, 3214-3218.
- (20) Vataj, R.; Louati, A.; Jeunesse, C.; Matt, D. *Electrochem. Commun.* **2000**, *2*, 769-775.
- (21) Vataj, R.; Louati, A.; Jeunesse, C.; Matt, D. *J. Electroanal. Chem.* **2004**, *565*, 295-299.
- (22) Harley, C. C. Ph.D Thesis, NUI Maynooth, **2009**.
- (23) Harley, C. C.; Rooney, A. D.; Breslin, C. B. *Sensors and Actuators B: Chemical* **2010**, *150*, 498-504.
- (24) Ma, J. C.; Dougherty, D. A. *Chem. Rev. (Washington, D. C.)* **1997**, *97*, 1303-1324.
- (25) Shinkai, S.; Araki, K.; Kubota, M.; Arimura, T.; Matsuda, T. *J. Org. Chem.* **1991**, *56*, 295-300.